Environmental controls on marine methane oxidation

From deep-sea brines to shallow coastal systems

Inauguraldissertation
zur Erlangung der Würde eines Doktors der Philisophie
vorgelegt der
Philosophisch-Naturwissenschaftlichen Fakultät
der Universität Basel

von

Lea Irina Steinle

Basel, 2016

Genehmigt von der Philosophisch-Naturwissenschaftlichen Fakultät auf Antrag von

Prof. Dr. Moritz Lehmann
PD Dr. Helge Niemann
Prof. Dr. Tina Treude
Prof. Dr. Gregor Rehder

Basel, den 19. April 2016

Prof. Dr. Jörg Schibler
Dekan

Summary

Methane is the most abundant greenhouse gas after carbon dioxide and accounts for ~25% of atmospheric warming since the onset of industrialization. Large amounts of methane are stored in the ocean seafloor as solid gas hydrates, gaseous reservoirs or dissolved in pore water. At cold seeps, various physical, chemical, and geological processes force subsurface methane to ascend along pathways of structural weakness to the sea floor. Additionally, methane can be produced in situ within organic-rich sediments. Increasing evidence suggests that ocean bottom water warming is leading to enhanced methane fluxes into the water column, for instance by dissociation of gas hydrates or by enhanced methane production in coastal ecosystems. Previous investigations showed that a large portion (~80%) of ascending methane in ocean sediments is utilised by anaerobic and aerobic methanotrophic microbes, but future elevated methane fluxes might not be counterbalanced by this sedimentary methane filter. Today, about 0.02 Gt yr^{-1} (3-3.5% of the atmospheric budget) of methane bypasses the benthic filter system on a global scale, and subsequently escapes into ocean bottom waters. In the water column, it can be oxidised aerobically (aerobic oxidation of methane - MOx), or less commonly where the water column is anoxic, anaerobically. Water column MOx is the final sink for methane before its release to the atmosphere. However, little is known on the efficiency of this pelagic microbial filter and its ability to adjust to a (rapidly) changing environment. In order to predict future changes, it is thus crucial to understand the efficiency of current water-column MOx, to identify the key organisms mediating MOx, and - most importantly - to determine environmental parameters controlling MOx.

In this dissertation, I investigated the pelagic MOx filter in contrasting ocean environments using a multidisciplinary approach. Systems studied included a deep-sea brine, two gas seep systems, and a shallow, organic-rich coastal environment. The main goals were to determine hot spots of MOx, identify bacteria mediating this process, and to estimate the efficiency of the pelagic methane filter. Furthermore, one important aim was to identify environmental factors controlling the activity and distribution of MOx, which could help in predicting changes of MOx in a future (warmer) ocean. My investigations revealed the following:

1. In the water column above methane gas seeps at the West Spitsbergen margin, MOx rate measurements together with CARD-FISH analysis of the methanotrophic community revealed rapid changes in the abundance of methanotrophs. Simultaneous measurements of physico-chemical water mass properties showed that the change in methanotrophic abundance correlated with changes in the water mass present above the seep system. This water mass exchange was caused by short-term variations in the position (i.e., offshore or nearshore) of the warm-water core of the West Spitsbergen Current: In its offshore mode, methanotroph-rich bottom waters above the methane seeps showed a high MOx capacity. A shift of the warm-water core towards the shelf break during the nearshore mode of the current displaced this cold bottom water with warm surface water containing a much smaller standing stock of methanotrophs, and led to a drop in MOx capacity of ~60%. This water mass exchange, caused by short-term variations of the West Spitsbergen Current, thus constitutes an oceanographic switch severely reducing methanotrophic activity in the water column. Since fluctuating currents are widespread oceanographic features common at many methane seep systems, it follows that the variability of physical water mass transport is a globally important control on the distribution and abundance of methanotrophs and, as a consequence, on the efficiency of methane oxidation above point sources.

2. At a Blowout in the North Sea resulting from an accident during industrial drilling activities, vigorous bubble emanation from the seafloor and strongly elevated methane concentrations in the water column (up to 42 μM) indicated that a substantial fraction of methane bypassed the highly active (up to ~2920 nmol cm^{-3} d^{-1}) AOM zone in sediments. In the water column, we measured MOx rates that were among the highest ever measured in a marine environment ((up to 498 nM d^{-1}) and, under stratified conditions, have the potential to remove a significant part of the released methane prior to evasion to the atmosphere. We speculate, however, that the MOx filter is intermittently inhibited when the water column is fully mixed conditions, so that the Blowout is a source of methane to the atmosphere. An unusual dominance of the water-column methanotrophic

community by Type II methanotrophs is partially supported by recruitment of sedimentary methanotrophs, which are entrained together with sediment particles in the methane bubble plume. Hence, our study demonstrates that gas ebullition not only provides ample methane substrate to fuel MOx in the water column, it also serves as an important transport vector for sediment-borne microbial inocula that aid in the establishment/proliferation of a water-column methanotrophic community at high-flux colds seeps.

3. We investigated MOx in the water column above gassy coastal sediments on quarterly basis over a time-period of two years. At the Boknis Eck study site, which is located in the coastal inlet Eckernförde Bay in the southwestern Baltic Sea, the water column is seasonally stratified with bottom waters becoming hypoxic over the course of the stratification period. We found that MOx rates exhibited a seasonal pattern with maximum rates (up to 11.6 nmol l^{-1} d^{-1}) during the summer months when oxygen concentrations were lowest and bottom water temperatures highest. Overall, MOx consumed between 70 – 95% of methane under stratified conditions, but only 40 – 60% under mixed conditions. Additional laboratory-based experiments with adjusted oxygen concentrations in the range of 0.2 - 220 μmol l^{-1} confirmed a sub-micromolar MOx oxygen optimum. In contrast, the percentage of methane-carbon incorporation into biomass was reduced at sub-micromolar oxygen concentrations, suggesting a different partitioning of catabolic and anabolic processes at saturated and sub-micromolar oxygen concentrations. Additional laboratory experiments verified the above-described mesophilic behaviour of the MOx communities of both surface and bottom waters. Our results highlight the importance of MOx in mitigating methane emission from coastal waters and indicate the existence of an adaptation to hypoxic conditions on the organismic level of the water column methanotrophs.

4. Life in the deep-sea brine basin Kryos in the Eastern Mediterranean Sea faces extreme challenges since the brine is almost saturated in bischofite ($MgCl_2$ - 3.9 mol kg^{-1}). Due to the strong density difference between the anoxic brine and the

overlying Mediterranean seawater, mixing is impeded and a shallow (<3 m) interface has formed. Our ex situ measurements of microbial activity revealed highly active MOx (up to 60 nmol kg^{-1} d^{-1}) at micro-oxic conditions within the interface. In line with elevated MOx rates, the residual methane within the interface was ^{13}C-enriched when compared to the brine, and we found diagnostic, ^{13}C-depleted lipid biomarkers (e.g., diplopterol, -46.6‰), which can be attributed to aerobic methanotrophs. Additionally, we detected relatively $\delta^{13}C$-enriched fatty acids (up to -18‰) in the lower interface and in the brine, which are an indication for a different carbon fixation pathway than the Calvin Benson Cycle, such as the reverse tri-carboxylic acid carbon-fixation pathway found in sulfur-oxidizing Epsilonproteobacteria. Within the brine, we could not find evidence for AOM, despite of thermodynamically favorable conditions for this process. In contrast, we found high rates of sulfate reduction within the brine (up to 430 μmol kg^{-1} d^{-1}) providing evidence that sulfate reducers are active under nearly Mg^{2+} saturated concentrations. Our results emphasize the adaptation of microbial life to the extremely harsh conditions below the chaotropicity limits of life in $MgCl_2$-rich environments.

Table of contents

Introduction

Introduction

This Chapter outlines the global context for the role of marine methane oxidation in controlling ocean methane emissions, and hence the relevance of this dissertation. First, a brief introduction to the general physical and chemical properties of methane and its role as greenhouse gas will be given. The sources of marine methane, its distribution and transport mechanisms, and the consumption in both the sediments and the water column will then be discussed. In the last part, the main objectives, and my contribution to the different Chapters of this thesis will be specified.

1.1 Physical and chemical properties of methane

Methane (CH_4) is the simplest organic compound and the most reduced form of carbon. With a single carbon covalently bound to four hydrogen atoms (Fig. 1.1), it belongs to the group of hydrocarbons. Methane, together with additional small and variable amounts of ethane, propane, butane, carbon dioxide, nitrogen and/or sulfide, is also referred to as "natural gas". Under standard conditions (273 K, 0.1 MPa), methane is a colorless, flammable gas, which shows only slight solubility in water due to its apolar characteristics (ca. 1.4 mM in seawater at atmospheric pressure; Yamamoto et al., 1976)). Salinity and temperature are negatively correlated with the solubility of methane (Wiesenburg and Guinasso Jr, 1979; Siedler and Peters, 1986; Jähne et al., 1987), however, with increasing pressure, solubility of methane increases (Henry's law). Under low temperature and high pressure conditions, methane can also form ice-like structures together with water molecules, commonly referred to as methane hydrates (see section 1.3.2).

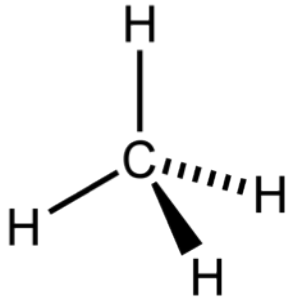

Figure 1.1: Schematic representation of a methane molecule.

The isotopic composition of methane carbon and its four hydrogen atoms can be used to date methane, as well as to distinguish different sources. Two stable carbon isotopes (^{12}C, ^{13}C) and one radioactive isotope (^{14}C) exist. This means that only methane produced from modern carbon (i.e., <35,000 years) contains ^{14}C (Kvenvolden and Rogers, 2005). Similarly, hydrogen has two stable isotopes ($^{1}H \triangleq H$ and $^{2}H \triangleq D$) and one radioactive isotope (^{3}H). The isotopic ratios are expressed relative to the Vienna Pee Dee Belemnite (VPDB) for $^{13}C/^{12}C$, and Vienna Standard Mean Ocean Water (VSMW) for D/H, in ‰ (per mill) notation (*Eq. 1.1*, *1.2*; Whiticar, 1999).

$$R = \frac{^{13}C}{^{12}C} \quad \text{or} \quad R = \frac{D}{H} \qquad \textit{(Eq. 1.1)}$$

$$\delta R = \left(\frac{R_{sample}}{R_{standard}} - 1 \right) \times 1000 [‰] \qquad \text{(Eq. 1.2)}$$

During (bio-)chemical reactions, the higher energy of the chemical bond of the heavier isotope and the resulting lower reactivity leads to a discrimination against the heavier isotope (i.e., ^{13}C-/D-CH_4), which results in an enrichment in ^{13}C-/D-CH_4 in the left-over substrate pool (see e.g., (Mariotti et al., 1981)). This effect is referred to as "kinetic isotope fractionation" and varies between different (bio-)chemical reactions, providing the ability to distinguish between different sources and/or microbial transformations.

1.2 Methane - an important greenhouse gas

The earth's climate depends mainly on the radiative balance of the atmosphere, which is influenced by solar radiation, as well as the abundance of clouds, aerosols and greenhouse gases (GHGs) in the atmosphere (, 2013). In light of understanding the earth's climate system, it is crucial to understand how the radiative balance changed in the past, what factors are controlling it in the present, and how it might change in the future. GHGs are an important part of the radiative balance since they absorb the long wave solar energy, which is reflected back to the atmosphere from the earth's surface (Fig. 1.2). This natural GHG effect leads to the lower atmosphere and earth's surface being 32°C warmer than without GHGs (IPCC, 2013).

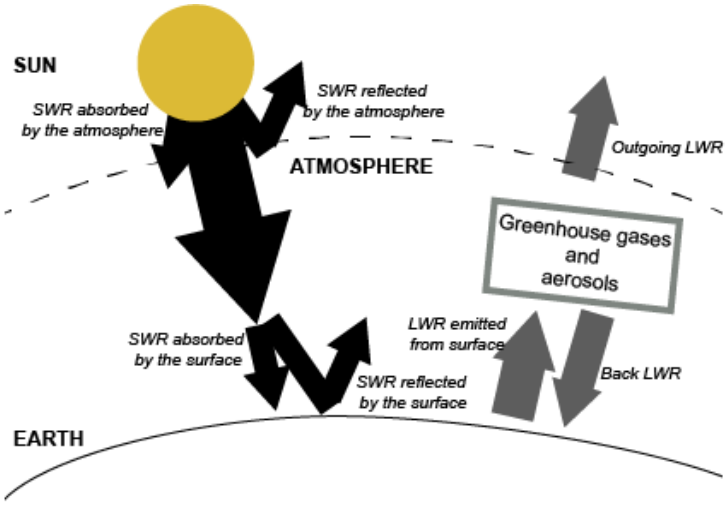

Figure 1.2: Schematic representation of the greenhouse gas effect. SWR: short-wave radiation; LWR: long-wave radiation. Adapted from Cubasch et al. (2013).

Methane is the second most important GHG after CO_2 due to its longevity and high concentrations in the atmosphere but also because of its high energy trapping efficiency, which is about 25 times higher than the one of CO_2 (Hartmann et al., 2013). For the sake of comparison, GHGs are assigned a global warming potential relative to CO_2, which allows comparing the integrated radiative forcing over a specific time interval of one molecule of a certain GHG compared to one molecule of CO_2 (Archer et al., 2009; Hartmann et al., 2013). The global warming potential of methane relative to CO_2 is for instance about 85 over 20 years and 29 over 100 years (Myhre 2013).

Global climate change, considered one of the largest challenges humanity is facing over the coming centuries, is largely caused by the increase in GHG concentrations since the onset of the industrial revolution (IPCC, 2013). These increased concentrations are mainly explained by the increase in anthropogenic-, but also by changes in the strength of natural emissions. In order to distinguish between the origins of atmospheric methane and understand past and possible future changes, the careful evaluation of natural sources is critical. After a brief overview of global sources and sinks of methane, I will focus on the role of the ocean in methane production, storage, consumption, and emission.

1.2.1 Methane concentrations in the atmosphere

Methane concentrations fluctuated between 320 and 790 ppb in the last 420,000 years before the onset of industrialization in ~1750 (Chappellaz et al., 1993; Petit et al., 1999; Wuebbles and Hayhoe, 2002). Past atmospheric methane concentrations and stable isotope values thereof were inferred from ice-core records from Greenland and Antarctica, which go back ~40,000 years before present, covering the last four glacial cycles (Fig. 1.3a; Chappellaz et al., 1993; Wuebbles and Hayhoe, 2002; Ciais et al., 2013; Möller et al., 2013). These records showed that methane concentrations were twice as high during warm interstadials than during glacial cold periods (Dlugokencky et al., 2011). We can infer from this that natural methane concentrations are linked to global average temperature and different hypotheses were brought forward to explain this link. For instance, the clathrate gun hypothesis postulates that large-scale methane release into the atmosphere from temperature-induced gas hydrate destabilization could provide a positive climate feedback (e.g., (Kennett et al., 2000; Nisbet, 2002; O'Hara, 2008). However, whether enough methane would be released from dissociating methane hydrates and also reaches the atmosphere to provide a positive climate feedback is still a matter of debate (see e.g., Graves et al., 2015). Other studies have proposed that variable methane emissions from boreal sources and/or wetlands could have caused the concentration changes (e.g., Chappellaz et al., 1993; Brook et al., 2000; Baumgartner et al., 2012).

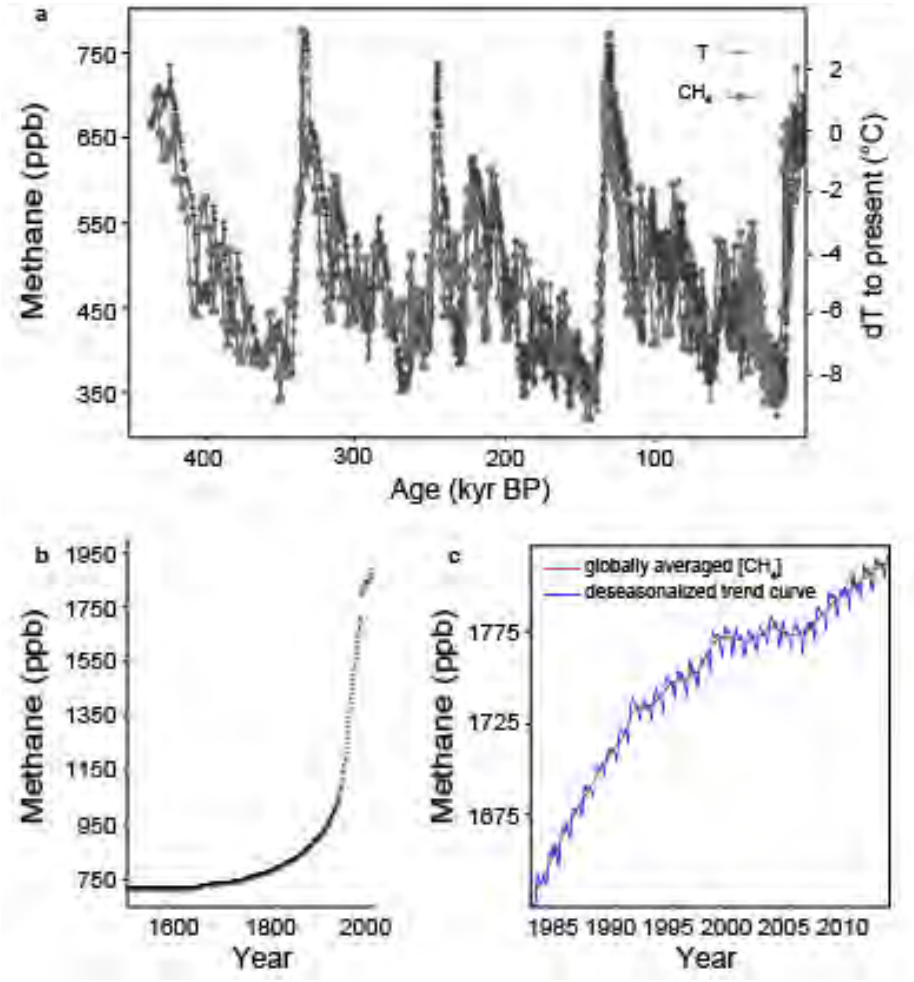

Figure 1.3: Atmospheric methane concentrations. a) Vostok ice core records of atmospheric temperature and methane concentration (volume mixing ratio) from 420,000 years BP to present. b) Ice core and atmospheric records of the increase in atmospheric methane from pre-industrial times to the present. c) Globally averaged atmospheric methane concentrations until 2014. Methane concentration increase almost stopped from 1999 - 2006, but resumed again in 2007. a) and b) are adapted from Wuebbles and Hayhoe (2002) and c) from Nisbet et al (2014).

Next to these natural variations, we are now observing a steady increase of atmospheric methane concentrations, which was initiated with the onset of industrial times (Fig. 1.3b; IPCC, 2013). Globally averaged atmospheric concentrations reached 1803 parts per billion (ppb) in 2011 (Hartmann et al., 2013), which constitutes an increase of about 200% compared to pre-industrial values (Fig. 1.3a; Chappellaz et al., 1993; Kirschke et al., 2013). This increase is the result from a surplus of source- over sink-strength. However, this increase has slowed after 1990 with the concentration of atmospheric methane remaining almost constant from 1999 to 2006 (Fig. 1.3b, c; Hartmann et al., 2013). Concentrations began to increase again in 2007, but what caused these observations is only poorly understood, demonstrating the need to further investigate sink and source strength (Fig. 1.3c; Nisbet et al., 2014). The estimated relative importance of methane sources to the atmosphere over the recent decade

(2000-2009) is summarized in Table 1-1 (Kirschke et al., 2013). About 50% of all emissions are anthropogenic and include emissions from agricultural activity (e.g., cattle farming, rice production), biomass burning and the use of fossil fuels. As for natural sources, wetlands are the biggest source of atmospheric methane, followed by fresh water systems and marine emissions (Fig. 1.4; EPA, 2010; Kirschke et al., 2013).

Table 1.1: Sources of atmospheric methane for the time-period 2000 - 2009. Top-down values estimates employ inversion models to fit atmospheric observations, while bottom-up estimates are based on models of specific processes using global datasets (Ciais et al., 2013; Kirschke et al., 2013). Numbers in square brackets indicate minimum and maximum values.

	Tg CH_4 yr^{-1}	
	Top-down	**Bottom-up**
Natural sources	**218 [179 – 273]**	**347 [238 – 484]**
Natural wetlands	175 [142 – 208]	217 [177 – 284]
Other sources	43 [37 – 65]	130 [61 – 200]
Lakes and rivers		40 [8 – 73]
Wild animals		15 [15 – 16]
Wildfires		3 [1 – 3]
Termites		11 [2 – 11]
Geological (including oceans)		54 [33 – 75]
Hydrates		6 [2 – 9]
Permafrost (excluding lakes and wetlands)		1 [0 – 1]
Anthropogenic sources	**335 [273 – 409]**	**331 [304 – 368]**
Agriculture and water	209 [180 – 241]	200 [187 – 224]
Biomass burning	30 [24 – 45]	35 [32 – 39]
Fossil fuels	96 [77 – 123]	96 [84 – 105]
Total	**548 [526 – 569]**	**678 [542 – 852]**
Growth rate	**6**	

While the sources to the atmospheric methane pool are many, only three major sinks are known. The largest sink of methane (~86%) is the oxidation of methane by the hydroxyl radical in the atmosphere (HO*; Myhre 2013). The rate of atmospheric methane removal is hence dependent on the concentration of this oxidant. Since not only methane but also other atmospheric species are involved in the production and removal of this radical, the estimates of atmospheric life-time of methane contain a high uncertainty (Holmes et al., 2013). One of the main products of this methane oxidation is CO2, which continues to act as a greenhouse gas. The other major sinks are loss of methane to the troposphere and oxidation in soils by methanotrophic bacteria, which account for ~7 and 5% of total methane removal, respectively (Wuebbles and Hayhoe, 2002).

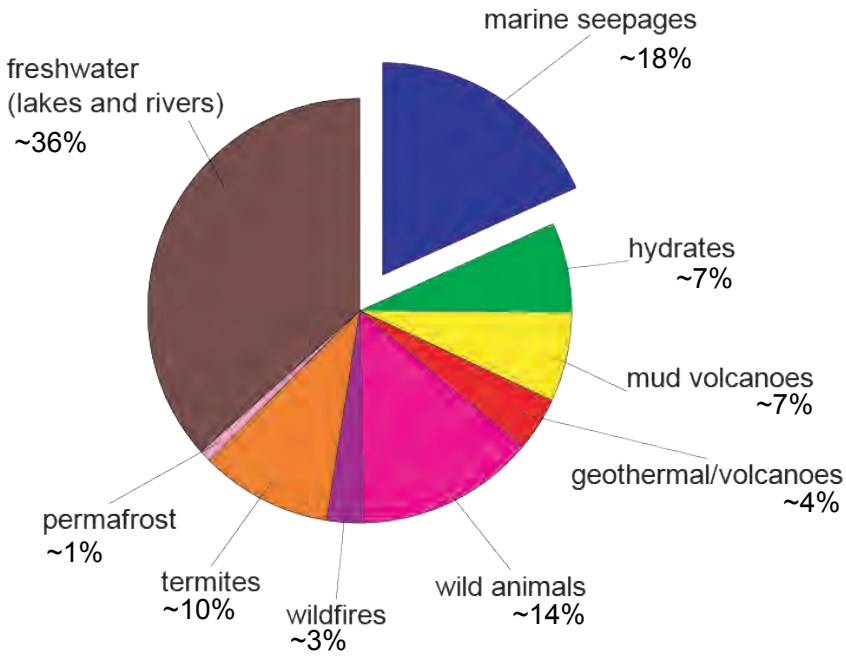

Figure 1.4: Natural sources of methane to the atmosphere excluding wetlands, which contribute about 70% to all natural emissions. Values are taken from bottom-up estimates for the time-period 2000 - 2009 {EPA 2010}{Kirschke 2013}.

1.2.2 Marine emissions into the atmosphere

Ocean sediments store the largest reservoir of methane on earth as gas hydrates, free gas, or dissolved in pore waters (Milkov et al., 2004; Reeburgh, 2007). However, marine methane emissions account only for ~5-10% of natural methane emissions (EPA, 2010; Kirschke et al., 2013). The main reason why oceans are a relatively small source of atmospheric methane are the sedimentary (see section 1.3.4) and pelagic (see section 1.4.4) microbial methane filter (Reeburgh, 2007; Knittel and Boetius, 2009).

A recent estimate of global sea-air methane flux ranges between 0.6 to 1.2 Tg CH_4 yr^{-1} (Rhee et al., 2009). However, seafloor associated seepage on the East Siberian Shelf is estimated to be much higher (> 10 Tg CH_4 yr^{-1}; Shakhova et al., 2014). The large variation in current ocean methane flux estimates shows the need to further investigate marine methane emissions, especially for studies with a higher temporal coverage and in large variety of ocean environments (Bange, 2006; Bange et al., 2010; Bakker et al., 2014). The latter point is important since specific ocean environments can show large differences in organic matter and nutrient input, water depth, mixing dynamics, and salinity, etc., all of which are factors potentially controlling methane production (see section 1.3.1) and the microbial filter systems (see sections 1.3.4 and 1.4.4). As a result, methane emissions are highly variable between these environments (EPA, 2010). Most methane is emitted at continental shelves (~60-75%; Bange et al., 1994; EPA, 2010), even though they cover only about 15% of the global ocean

area (Bakker et al., 2014). The open ocean, in contrast, is overall still a net source of methane to the atmosphere, but emissions never reach values as high as on the shallower continental shelf (Bange et al., 1994; Reeburgh, 2007).

1.3 Methane in ocean sediments - sources, storage, transport and sinks

1.3.1 Methane formation in marine sediments - sources

Methane in marine sediments can originate from biogenic, thermogenic, or abiogenic methanogenesis (Whiticar, 1999). Thermogenic methane is formed by thermal degradation of organic matter, buried to depths where temperatures are >~100°C and pressure is high (Pape et al., 2010). Abiogenic methane is produced from serpentinization of peridotite rocks or from carbonate reduction of magma (Horita and Berndt, 1999; Sherwood Lollar et al., 2002; Judd et al., 2002; Judd and Hovland, 2007). The third methane production pathway, microbial methanogenesis, will be discussed in more detail below. All three processes produce methane within a characteristic range of $\delta^{13}C$- and δD-values (Fig. 1.5), as well as with different proportions of co-occurring higher hydrocarbons (C_2 and up) and associated characteristic isotopic compositions (Whiticar, 1999; Sherwood Lollar et al., 2005). While higher hydrocarbons are making up a very small part of biogenic methane, their concentrations can reach high values in thermogenic and abiogenic methane production (Bernard et al., 1978; Whiticar, 1999).

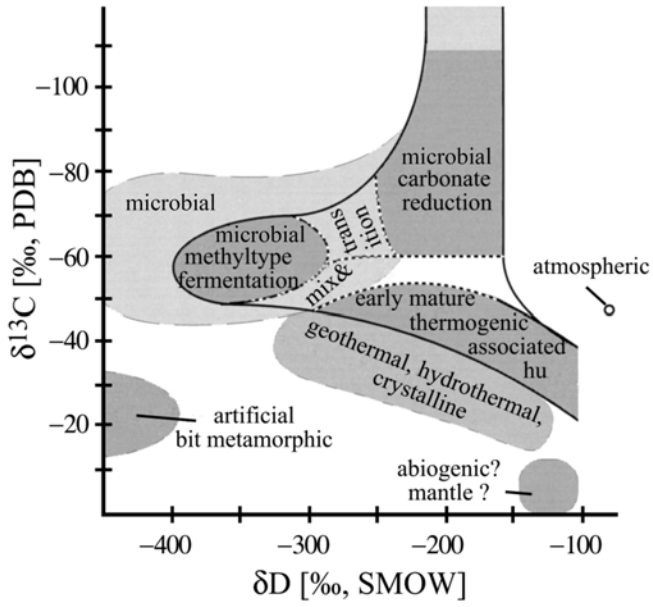

Figure 1.5: CD-diagram of methane. Adapted from Whiticar (1999).

Microbial methanogenesis

Microbial methanogenesis (hereafter "methanogenesis") occurs in sediments characterized by high sedimentation rates and organic matter concentrations (Reeburgh, 2007). Methanogenesis is the last step in the degradation of organic matter. Degradation is initiated by microbially-mediated hydrolysis of complex organic matter into smaller molecules, which are then fermented to H_2, CO_2, alcohols, methylated compounds, and low molecular weight fatty acids (Reeburgh, 2007). Methanogens can only use these small organic molecules and are thus dependent on other fermenters to break down the larger organic molecules (Cicerone and Oremland, 1988). Based on the type of carbon precursor to methane (i.e., CO_2, acetate or methylated compounds), three different groups of methanogenic catabolism exist: hydrogenotrophic (*Eq. 1.3*), acetoclastic (*Eq. 1.4*) and methylotrophic, respectively (e.g., *Eq. 1.5*; Thauer et al., 1977):

$$4H_{2(aq)} + CO_{2(aq)} \rightarrow CH_{4(aq)} + 2H_2O_{(l)}, \Delta G^0 = -131 \text{ kJ mol}^{-1} \qquad (Eq.\ 1.3)$$

$$CH_3COO^-_{(aq)} + H_2O_{(aq)} \rightarrow CH_{4(aq)} + HCO_3^-{}_{(aq)}, \Delta G^0 = -31 \text{ kJ mol}^{-1} \qquad (Eq.\ 1.4)$$

$$CH_3OH_{(aq)} + H_{2(aq)} \rightarrow CH_{4(aq)} + H_2O_{(l)}, \Delta G^0 = -113 \text{ kJ mol}^{-1} \qquad (Eq.\ 1.5)$$

In general, the degradation of organic matter can be coupled to a variety of electron acceptors, resulting in different thermodynamic yields (Fig. 1.6; Emerson and Hedges, 2003). As a result of these thermodynamic constraints, but also because sulfate reducers (see section 1.3.4) outcompete methanogens due to their faster uptake of acetate and H_2, the major part of methanogenesis is restricted to zones where sulfate is exhausted (Whiticar, 1999). In organic rich sediments, however, methylotrophic methanogenesis can take place in the presence of sulfate since it involves the use of non-competitive (with respect to sulfate reduction) methylated substrates (Cicerone and Oremland, 1988; Maltby et al., 2016; Maltby et al., in prep.).

For all three pathways, methanogenesis is a sequence of distinct enzyme-mediated reactions, of which the last step is always mediated by the key enzyme Methyl-coenzyme M reductase (MRC; Thauer, 1998). The detection of the gene encoding the alpha subunit of this key enzyme (*mcr*A) is often used for environmental detection of (unknown) methanogens (e.g., Yakimov et al., 2015).

Microbial methanogenesis is almost exclusively (see section 1.4.2) mediated by autotrophic or fermentative, methanogenic archaea (methanogens) of the orders *Methanobacteriales, Methanococcales, Methanomicrobiales, Methanosarcinales* and *Methanopyrales* (Boone et al., 1993; Jørgensen, 2006; Madigan et al., 2015). They are all strict anaerobes and require highly reducing conditions, i.e., a redox potential below -200 to -400 mV (Zehnder and

Brock, 1979; Reeburgh, 1983; Madigan et al., 2015). However, some species were found to endure oxygen exposure for several hours before cell death occurred (Zinde, 1993). Methanogens were found to be adapted to a broad range of environments, spanning a temperature range from 2-100°C, a pH from 3-9, and a wide range of salinities from freshwater to hypersaline habitats (Zinde, 1993).

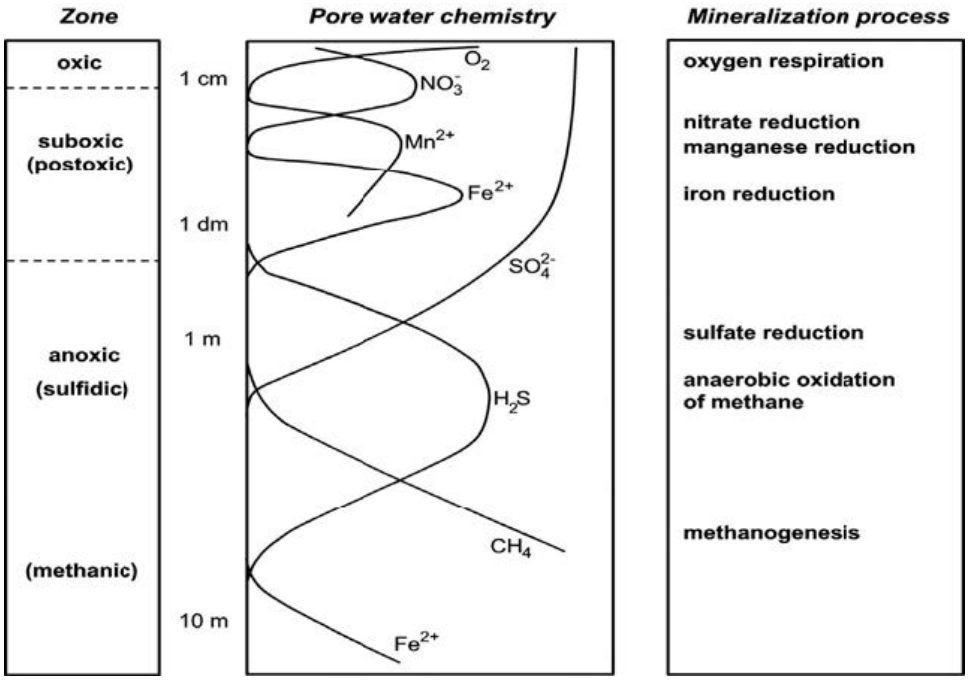

Figure 1.6: Schematic representation of the biogeochemical zonation in marine sediments. Electron acceptors are sequentially used for organic matter remineralization. Adapted from Jørgensen (2006).

1.3.2 Methane reservoirs in sediments - storage

After methanogenesis, buoyancy-driven methane migration towards the seafloor is observed (Judd and Hovland, 2007; Boudreau, 2012). Methane dissolved in porewater or as free gas is transported through high-permeability paths (faults, fractures) and permeable sediment layers (Judd and Hovland, 2007) by diffusive and advective processes. It accumulates where migration is limited and thus forms shallow and deep gas reservoirs. It can then be mobilized by different ways, e.g., by pressure in case of mud volcanoes (see section 1.3.3). In case of high concentrations and under the right temperature and pressure conditions, methane hydrate can form. Methane hydrates can also constitute a (incomplete) barrier to fluid and gas seepage (Naudts et al., 2006).

Methane hydrate

Methane hydrate (or clathrate) is a non-stochiometric ice-like solid, containing cages of water with enclosed methane molecules and possibly other molecules (Sloan Jr and Koh, 2008; Hester and Brewer, 2009). Upon dissociation of 1 L of hydrate more than 160 L of gas are liberated at standard conditions (Kvenvolden, 1993). No fractionation of methane occurs upon formation of hydrates, and their geochemical composition thus reflects the original source of natural gas (Lapham et al., 2012). Different original compositions of natural gas (i.e., amount of heavier hydrocarbons) are also reflected in the size and arrangements of water molecule cages: Structure I hydrates are defined by smaller cages including only methane (and small amounts of ethane), whereas structure II and H hydrates contain larger cages, which are stabilized by higher hydrocarbons (Sloan, 2003). Hydrates are only stable under relatively low temperatures and high pressure, and form naturally within this stability field from methane-saturated water (Clennell et al., 1999; Xu and Ruppel, 1999; Hester and Brewer, 2009). This stability field, referred to as the gas hydrate stability zone, is generally met in sediments of continental margins at water depths greater than 300 - 600 m (Hester and Brewer, 2009). The geothermal gradient determines the lower boundary of methane hydrates in sediments, below which no hydrate can be formed and methane is present as free gas (Kvenvolden, 1993). This phase change from solid to gas is the cause of the geophysically detectable signal, referred to as bottom simulating reflector (BSR; Haacke et al., 2007). The detection of such BSRs is hence often used to infer gas hydrate deposits. Additionally, the presence of gas hydrates can be inferred from geochemical evidence, such as the freshening of pore water upon hydrate destabilization following core recovery (Hesse and Harrison, 1981; Hesse, 2003). Methane hydrates have been detected in sediments all over the world in terrestrial and marine sediments (Milkov, 2005), but the size of the global hydrate inventory is still a matter of debate. Most estimates fall between 450 - 3,000 Gt (Milkov et al., 2004; Burwicz et al., 2011; Archer, 2007; Wallmann et al., 2012; Piñero et al., 2013), which makes hydrates one of the largest methane reservoir on earth. For comparison, fossil fuels (coal included) are estimated at 5,000 Gt (Krey et al., 2009).

At shallower water depths (300 - 600 m), hydrate-stability depends strongly on temperature (Hester and Brewer, 2009). An increase of ocean water temperatures may thus lead to dissociation of part of the hydrate-bound methane, which could further accelerate climate change if the released methane reaches the seawater-atmosphere interface (e.g., Biastoch et al., 2011). In case of a bottom water temperature increase of 3°C, Archer and Buffet (Archer et al., 2009) predicted that over 85% of hydrate-bound methane could be released. More information is provided in the subsection "*Gas seeps including hydrate-associated gas seeps*" of section 1.3.3.

1.3.3 Methane migration and methane-rich environments - transport

Methane is present in various types of habitats in marine environments, fueled either by in situ (biogenic) methanogenesis and/or fossil methane from deeper reservoirs, or by abiogenic production. Fossil methane can either be of biogenic or thermogenic origin, or a combination of both. If methane-rich gasses or fluids are advected from the sediments into the hydrosphere, these systems are referred to as 'cold seeps'. Different types of cold seeps have been discovered all over the world (Fig. 1.7), and are often oasis of life, supporting a large chemosynthetic community, which in turn supports an associated food web (Jørgensen and Boetius, 2007; Dubilier et al., 2008; Bernardino et al., 2012; Niemann et al., 2013). Anaerobic oxidation of methane in the sediments can induce precipitation of authigenic carbonates (see section 1.3.4; Peckmann et al., 2001), which serve as settling ground for sessile fauna, e.g., sponges {. In addition to cold seeps, ebullition or diffusive methane flux from organic- and methane-rich (coastal) sediments contribute significantly to global methane emissions (Bange, 2006; Kirschke et al., 2013).

These habitats are varying in their rate and type of methane production, the rate of methane transport via advection or diffusion, and the temperature of the released gas/fluids. In the following sections, the systems studied in this thesis (gas seeps, blowouts, gassy coastal sediments, brine basins) are presented first, followed by the description of other important methane-rich environments.

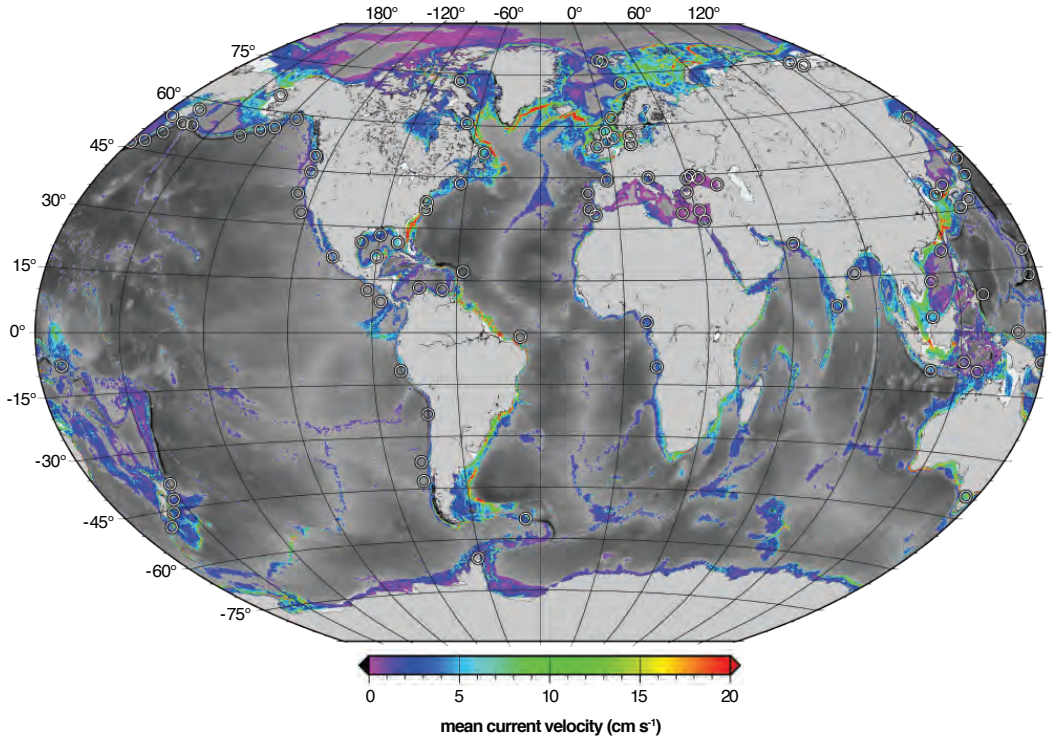

Figure 1.7: Global distribution of seeps (black circles). Colors represent average current velocities (see Chapter 2).

Gas seeps including hydrate-associated gas seeps

Gas seeps are characterized by gas leakage and associated fluid seepage. The gas originates from shallow gas accumulations, subsurface gas reservoirs, or from dissociation of submerged permafrost and gas hydrates (Judd et al., 2002; Shakhova et al., 2010). Well-studied non-hydrate associated gas seeps include the Black Sea seeps (Reeburgh et al., 1991) and the Tommeliten area (Hovland and Judd, 1988). Next to longer known hydrate-associated gas seeps (Hydrate Ridge, Oregon, Suess et al., 1999; Eel River Basin, California, Hinrichs et al., 1999; Gulf of Mexico, Joye et al., 2004), several seep areas were recently discovered (W-Svalbard margin (Westbrook et al., 2009); Beaufort margin, USA (Phrampus et al., 2014); N-Atlantic margin, USA (Skarke et al., 2014). The recently discovered seeps are all located along the gas-hydrate stability limit. This observation led to the hypothesis of bottom water warming induced dissociation of gas hydrates caused by climate change (e.g, Westbrook et al., 2009). However, studies at the W-Svalbard margin showed that methane seepage is not recent, but already proceeded >23 k BP years ago at the gas hydrate stability limit (Berndt et al., 2014). Warming bottom temperatures may lead to hydrate dissocation to some extent, but a catastrophic release of methane is not as likely as previously thought (Graves et al., 2015).

Gas seeps are significant contributors of methane to the hydrosphere, mostly because the high advective fluxes of dissolved and free gas lead to an incomplete oxidation of methane by the sediment filter system (Knittel and Boetius, 2009). In Chapter 2 of this thesis, the water column above the hydrate-associated Svalbard seeps will be the focus of the study.

Pockmarks and blowouts

Pockmarks were observed in a variety of oceanographic settings and are crater-like structures caused by the removal of sediments by ascending gas/fluids (Hovland and Judd, 1988). Formation processes range from groundwater seepage (e.g., Eckernförde Bay, Whiticar, 2002), a sudden escape of pressurized gas and/or fluids (e.g., North Sea (Hovland et al., 1984; Fox, 1995), to gas hydrate destabilization (Judd et al., 2002). Pockmarks may also be referred to as “blowouts” if they were formed by a sudden escape of gas (Judd and Hovland, 2007). The release of methane from these structures varies widely with regard to the amount and duration of released methane, which makes release estimates difficult (Judd and Hovland, 2007). In Chapter 3 of this thesis, methanotrophy at a blowout in the North Sea will be discussed.

Gassy coastal sediments - zones of high organic matter input

In coastal systems, elevated organic matter input leads to very high rates of benthic methanogenesis, which may cause surface sediments to be over-saturated in methane and even lead to bubble formation (Martens et al., 1986; Jackson et al., 1998; Whiticar, 2002). These “foamy”, organic-rich sediments are likely to occur in estuaries, fjords and river

plumes. Generally, not all the methane can be consumed within the sediments, leading to elevated methane concentrations within the overlying water column (e.g., Bange et al., 2010). Eckernförde Bay, which will be discussed in Chapter 4, is a well-studied example for gassy coastal sediments.

Brine basins

Brine basins were discovered at the seafloor of the Gulf of Mexico, the Red-, Black- and Eastern Mediterranean Sea (see Stock et al., 2013, for a review). These brines formed upon re-dissolution of ancient salt deposits that were re-exposed to seawater and migrated to the seafloor where they accumulated in depressions (Boetius and Joye, 2009). The brines are stable, anoxic habitats since mixing with the overlying seawater is strongly limited by the strong density difference. Due to the isolation and extreme conditions, brines are interesting environments to study selection and adaptation mechanisms (Stock et al., 2013), and they can be regarded as an analogue to potential habitats on other planets (Hansen et al., 2006; McEwen et al., 2014; Martín-Torres et al., 2015; Hsu et al., 2015). In the Mediterranean Sea, the brines originate from the re-dissolution of ancient salt deposited during the Messinian salinity crisis (5-6 million years ago). During that time period, the Eastern Mediterranean Sea evaporated almost completely on several occasions (Hsü et al., 1973; Camerlenghi, 1990). After being buried by newly formed sediment, tectonic activity re-exposed these salt layers to seawater, which lead to the above described re-dissolution (Camerlenghi, 1990). In general, brines often contain high amounts of methane but are probably not large sources of methane to the overlying seawater (e.g., van der Wielen, 2005). In Chapter 5, results from an investigation on methane oxidation and the sulfur cycle of the Mediterranean Kryos brine basin will be presented.

Hydrothermal vents

Methane can also be emitted together with hydrothermal fluids at spreading zones of oceanic plates at hydrothermal vents such as black smokers (Von Damm, 1990). The emitted methane is predominantly of abiogenic origin, produced by water-rock reactions, and partly of biogenic origin by pyrolysis of complex organic (Teske et al., 2002; Kelley et al., 2005) A large field of black smokers was recently discovered in the Gulf of California, which is not located over a spreading zone (pers. comm., C. Berndt). The formation of these hydrothermal vents may be the result of a temporary splitting of the oceanic crust.

Mud volcanoes

Mud volcanoes are topographically elevated structures, built up by vertically ascending fluidized mud (Niemann, 2010). Mud volcanism is caused by diverse geolocial processes, such as fluid emissions from mineral dehydration, slope failures, tectonic accretion and faulting, and/or rapid burial of sediments. The resulting abnormally high pore fluid pressure leads to the extrusion of mud and fluids through a central conduit up to the seafloor, which is

often accompanied by elevated release of methane and higher hydrocarbons (Niemann, 2010). Extreme spatial heterogeneity in fluid flow and associated (methanotrophic) microbial communities has been detected in these environments (e.g., Niemann et al., 2006). Methane emission into the hydrosphere is significant in these systems, but due to unknown number and varying rates of methane discharge by submarine mud volcanoes, estimates are difficult (Niemann et al., 2006).

Diffusive systems

Diffusive systems are present in a variety of sediments, ranging from coastal to deep-sea settings (e.g., Iversen and Jørgensen, 1985; Niewöhner et al., 1998). In these settings, methane is only transported by diffusion, and advective processes are absent. Most methane in these systems originates from in situ methanogenesis and is generally almost completely consumed by AOM several meters below the seafloor (e.g., Iversen and Blackburn, 1981; Fossing et al., 2000; Treude et al., 2005). As a result, these systems are not a source of methane to the overlying seawater.

Anoxic basins

Although anoxic marine basins are not located within the sediments but in the overlying water column, they are included in this section because the microbial processes occurring in these systems are similar to those occurring in anoxic sediment. Anoxic basins such as the Cariaco basin (Ward et al., 1987), the Black Sea (Reeburgh et al., 1991), and the Central Baltic Sea (Schmale et al., 2010) are (almost) permanently anoxic and contain high amounts of methane and hydrogen sulfide from sedimentary sources. AOM was detected in several basins, e.g., in the Black Sea (Reeburgh et al., 1991; Schubert et al., 2006), but methanogenesis is generally absent due to the high sulfate concentrations (Reeburgh, 2007).

1.3.4 Sedimentary methane filter (AOM) - microbial sink

In sediments, a large fraction (~80% on average; Knittel and Boetius, 2009) of uprising methane is oxidized through sulfate-dependent anaerobic oxidation of methane (AOM, *Eq. 1.6*). This process leads to hydrogen sulfide production and to an increase in alkalinity (Barnes and Goldberg, 1976), which in turn can cause carbonate precipitation (Peckmann et al., 2001).

$$CH_{4(aq)} + SO_4^{2-}{}_{(aq)} \rightarrow HCO_3^{-}{}_{(aq)} + HS^{-}{}_{(aq)} + H_2O_{(l)}, \Delta G^0 = -16 \text{ kJ mol}^{-1} \qquad \textit{(Eq. 1.6)}$$

The occurrence of this process was first inferred on observations of porewater profiles, where sulfate and methane were depleted in the same zone, sulfate diffusing downwards from the seawater and methane diffusing upwards through the sediments (Martens and Berner, 1974). This zone is referred to as the sulfate-methane transition zone (SMTZ; Fig. 1.8), and is

often found in low-porosity sediments and/or diffusive flux settings (e.g., (Treude et al., 2003; Knittel and Boetius, 2009; Niemann et al., 2006). Sandy sediments or sediments with a high advective flux of methane often do not show such clear profiles (Niemann et al., 2005; Knittel and Boetius, 2009; Treude and Ziebis, 2010).

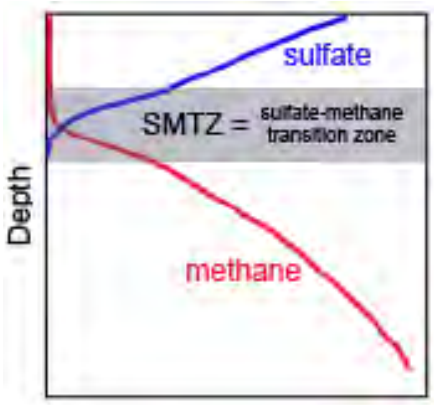

Figure 1.8: Schematic representation of the sulfate-methane transition zone (SMTZ). Methane is indicated in red and sulfate in blue.

AOM is typically mediated by consortia of anaerobic methanotrophic archaea (ANME) and sulfate-reducing bacteria (SRB; Boetius et al., 2000; Orphan et al., 2001; Niemann et al., 2006). The physical association of ANMEs and SRB, thermodynamic constraints of the AOM reaction (Boetius et al., 2000; Orphan et al., 2001; Treude et al., 2003), and molecular indications for direct electron transfer from ANMEs to SRB (McGlynn et al., 2015; Wegener et al., 2015) suggests that ANMEs carry out CH_4-oxidation with the SRB as a syntrophic partner. In this reaction, SRB mediate the reduction of sulfate as the terminal electron acceptor (Knittel and Boetius, 2009). However, recent findings showed that ANME may possibly also mediate AOM without partner bacteria (Milucka et al., 2012). Observations of solitary ANME cells and aggregates supports putative evidence from natural environments that AOM can indeed be performed independent of an obligate SRB partner (Orphan et al., 2002; Niemann et al., 2005; Maignien et al., 2013). Recent evidence suggest that AOM can also be coupled to reduction of alternative electron acceptors, i.e., iron or manganese (Beal et al., 2009; Wankel et al., 2012; Egger et al., 2015) and nitrate (Haroon et al., 2013), but the environmental importance of these processes is still not well constrained.

Phylogenetically, ANME are divided in three major groups, i.e., ANME-1, ANME-2 and ANME-3. They all belong to the Euryarchaeota, and are most closely related to the methanogenic groups *Methanosarcinales* and *Methanomicrobiales* (Knittel and Boetius, 2009). Similar to methanogens, all ANME groups contain gene homologues to the *mcr*A gene encoding the alpha subunit of the Methyl-coenzyme M reductase (MCR; Knittel and Boetius, 2009). ANME are strictly aneraobic and do not tolerate oxygen (Treude et al., 2005;

Knittel and Boetius, 2009). Due to the low energy yield of AOM (*Eq. 1.6*), the doubling time is very long, 4-7 months in incubation experiments (Nauhaus et al., 2007).

ANME were found to be ubiquitous and cosmopolitan in almost all methane-rich environments on earth including anoxic basins (Knittel and Boetius, 2009). ANME were even detected in some hypersaline environments (Wankel et al., 2010; Lazar et al., 2011; Lazar et al., 2011; Avrahamov et al., 2014), but were found to be absent or inhibited in other hypersaline environments (e.g., van der Wielen, 2005; Joye et al., 2009; Maignien et al., 2013). Other habitats of ANMEs include authigenic carbonates (Marlow et al., 2014), or living in close association to gas hydrates (Orcutt et al., 2004).

Sulfate reduction

In the marine system, sulfate reduction (SR) is the most common electron acceptor used for degradation of organic matter (Jørgensen, 1982). This is largely due to the high concentration of sulfate compared to other energetically more favorable electron acceptors (Fig. 1.6; D'Hondt et al., 2002). Next to methane dependent sulfate reduction, i.e., during AOM, sulfate is reduced via organoclastic sulfate reduction, i.e. based directly on the reduction of organic matter (*Eq. 1.7*).

$$SO_4^{2-}{}_{(aq)} + 2CH_2O_{(l)} \rightarrow 2HCO_3^{-}{}_{(aq)} + HS^{-}{}_{(aq)} + H^{+}{}_{(aq)}; \Delta G^\circ =< 100 \text{ kJ mol}^{-1} \quad (Eq.\ 1.7)$$

Sulfate reduction is mostly mediated by Deltaproteobacteria (Madigan et al., 2015). They are either heterotrophic or autotrophic (use of CO_2 as sole carbon source with H_2 as electron donor). SRB involved in AOM either belong to the *Desulfoarcina, Desulfococcus* or *Desulfobulbus* (Knittel and Boetius, 2009). These SRB involved in AOM do not tolerate oxygen, similar to ANMEs (Knittel and Boetius, 2009). Most other SRB are also obligate anaerobes but some can tolerate oxygen to a small extent (Cypionka, 2000; Madigan et al., 2015). Additionally, sulfate reduction was also reported in some archaeal groups (Dahl and Friedrich, 2008), which probably acquired the necessary enzymes by horizontal gene transfer (Mussmann et al., 2005).

Efficiency of the sedimentary microbial methane filter

In the uppermost part of sediments, where oxygen is still available, methane can also be oxidized aerobically (Boetius and Wenzhöfer, 2013; see section 1.4.4). AOM and aerobic methane oxidation together act as a biological filter hindering the methane from seeping into the water column. The efficiency of the sedimentary filter system is strongly dependent on the type and velocity of methane transport (Knittel and Boetius, 2009). In case of diffusive systems, methane is almost completely oxidized by AOM. However, the benthic microbial filter was found to be less effective in systems characterized by elevated advective fluxes of CH_4 (Treude et al., 2003; Niemann et al., 2006; Knittel and Boetius, 2009; Steeb et al., 2014).

AOM and aerobic oxidation of methane act as a sedimentary methane filter in basically all systems described in section 1.3.3. Globally, 0.02 Gt yr^{-1} (3-3.5% of the atmospheric budget; Kirschke et al., 2013) of methane was estimated to bypass the benthic filter systems and to be released into the ocean water column (Boetius and Wenzhöfer, 2013). The fate of methane in the ocean water column will be discussed in the following section.

1.4 Methane in the ocean water column - sources, transport and sinks

1.4.1 Physical processes - transport and dilution

Methane dissolved in seawater is subjected to horizontal and lateral transport away from the methane point source by diffusion, dilution and advection with ocean currents. These physical processes are not final sinks as methane is not removed from the water column, just diluted. Together with methane oxidation, these physical transport processes reduce methane to background ocean concentrations of ~3 nM (Rehder et al., 1998; Yoshikawa et al., 2014). There are a few studies that considered fate of methane in the ocean by modeling methane concentrations and isotopic composition, oxidation rates, and current speeds (e.g., Heeschen et al., 2005). However, most studies concentrated on the immediate seep area and knowledge on down-stream fate of methane remains sparse.

1.4.2 Methane production in the oxic water column - sources

Methane supersaturation with respect to atmospheric concentrations is genrally observed in surface waters of the oxic open ocean, and concentration profiles show a clear increase in methane at the pycnocline compared to the water column below, a phenomenon referred to as the “Ocean Methane Paradox”. (Reeburgh, 2007). In the absence of lateral input from coastal methane sources, explanations for this observations range from methanogenesis in anoxic micro-niches (e.g., in particles, Karl and Tilbrook, 1994; Holmes, 2000; or inside of plankton, de Angelis and Lee, 1994), to breakdown of methylated substrate under oxic conditions (e.g., Karl et al., 2008). The latter has recently been demonstrated to be mediated by bacteria and archaea, as a de-methylation reaction from either methylphosphonates (Karl et al., 2008; Metcalf et al., 2012; Carini et al., 2014), or dimethyl-sulfoniopropionate (Damm et al., 2010). The importance of these processes is as of yet poorly quantified.

1.4.3 Seawater-atmosphere exchange - sink

There is a continuous exchange of gases dissolved in the surface mixed layer of the ocean and the overlying atmosphere (see section 1.2.2). This exchange depends on the concentration difference between methane concentrations in surface waters and the equilibrium concentration, which depends on temperature, salinity, and the atmospheric

methane concentration (Wiesenburg and Guinasso Jr, 1979). Additionally, the gas transfer velocity, which is mostly dependent on wind speed, is determining the velocity of the gas exchange (Wanninkhof et al., 2009). If surface methane concentrations are higher than equilibrium concentrations, and the ocean acts as a net source of methane to the atmosphere, as described in section 1.2.2. In general, surface waters are slightly supersaturated in the open oceans (Reeburgh, 2007) and can reach extremely high values on the continental shelf (Bange, 2006), in coastal ecosystem (e.g., 7000% in Eckernförde Bay, Bussmann and Suess, 1998), and in systems with high local seafloor seepage (e.g., Shakhova et al., 2010; Solomon et al., 2009).

1.4.4 Aerobic oxidation of methane (MOx) - microbial sink

In the water column, the main sink of methane is aerobic oxidation of methane (MOx; *Eq. 1.8*; Reeburgh, 2007):

$$CH_{4(aq)} + 2O_{2(aq)} \rightarrow CO_{2(aq)} + 2H_2O_{(l)}, \Delta G^0 = -842 \text{ kJ mol}^{-1} \qquad (Eq.\ 1.8)$$

In the rare case of ocean water column anoxia, methane can also be oxidized anaerobically (see section 1.3.4). MOx is mediated by methane oxidizing bacteria (MOB), which are generally members of the Alpha- or Gammaproteobacteria. Methanotrophs are unique in their ability to use methane as their sole carbon and energy source, and form a subgroup of the methylotrophs, which use a larger variety of C_1 substrates (Murrell, 2010). MOB are divided into two groups, Type I and Type II, whose members use different carbon assimilation pathways (Hanson and Hanson, 1996). Type I MOB utilise the ribulose monophosphate (RuMP) pathway, whereas Type II MOB fix carbon via the serine pathway. Historically, a subgroup of Type I MOB was referred to as Type X since it showed physiological traits of both other groups, but it is now reclassified as Type I MOB based on biochemical and molecular analyses (Bowman et al., 1993; Semrau et al., 2010). Both Type I and the 'historical' Type X MOB belong to the Gammaproteobacteria, specifically to the family *Methylococcaceae*. Type II MOB belong to the order Rhizobiales within the class Alphaproteobacteria and therein to two genera of the family *Methylocystacea* (Hanson and Hanson, 1996). However, additional methanotrophic bacteria were discovered not included within these groups. For instance, members of two additional genera (*Methylocella* and *Methylocapsa*) within the order Rhizobiales were recently identified as obligate methanotrophs, but are not considered traditional Type II MOB as they belong to the family *Beijerinckiacea* and not to *Methylocystacea* (Marín and Ruiz Arahal, 2014). Other authors, however, include them in the Type II group (e.g., Murrell, 2010).

The first step of MOx from methane to methanol is catalyzed by the enzyme particulate or soluble methane mono-oxygenase (pMMO or sMMO, respectively; Semrau et al., 2010) and references therein). The functional centre of pMMO contains copper, whereas sMMO has a di-iron centre (Semrau et al., 2010). The soluble form, sMMO, is not as ubiquitous in Type II MOB, but present in most Type I MOB (Semrau et al., 2010). The gene encoding the alpha subunit of the membrane-bound pMMO (*pmo*A) is present in most known methanotrophs and is used as a marker gene (Costello and Lidstrom, 1999). However, strongly diverging *pmo*A genes, e.g., closely related to *amo*A of ammonia oxidizers (Tavormina et al., 2008; Tavormina et al., 2010), as well as the occurrence of *pmo*A in non-methanotrophic bacteria highlights the importance of a careful interpretation of *pmo*A libraries (Knief, 2015).

MOB were detected in a wide range of environments from terrestrial and limnic to marine environments as free-living cells or as intracellular symbionts in invertebrates (Hanson and Hanson, 1996; Murrell, 2010). They have relatively low specific growth rates and estimates for doubling times in the environment are up to several days (Kessler et al., 2011; Murrell, 2010).

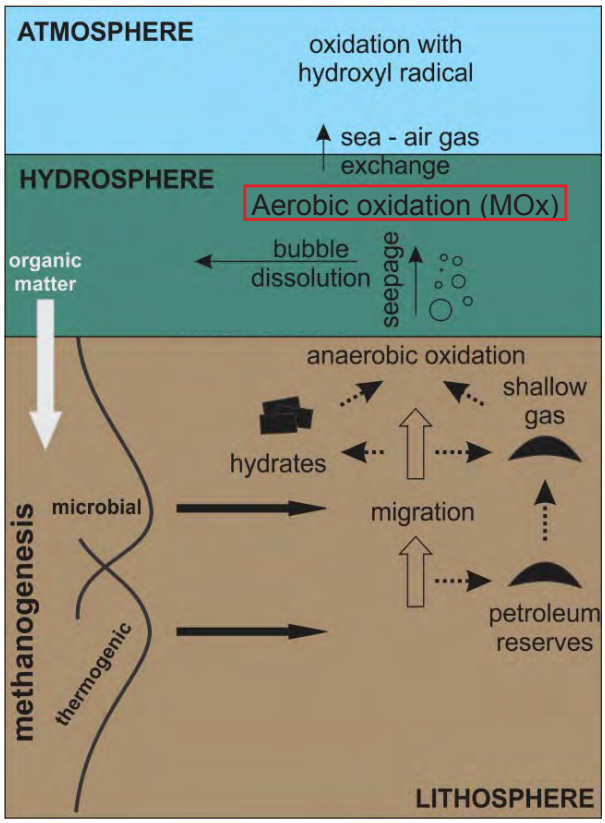

Figure 1.9: Schematic of principal sources, storage and transport types and sinks of methane in the marine system. Modified from Judd (2004).

Next to MOx, sulfate-independent anaerobic oxidation of methane with nitrite as an electron acceptor is mediated by the bacterium Candidatus *Methylomirabilis oxyfera* (Raghoebarsing et al., 2006; Hu et al., 2009; Ettwig et al., 2008). In contrast to AOM, oxygen is generated intracellulary from NOx (Ettwig et al., 2010) and the subsequent biochemical pathway is similar to MOx (Raghoebarsing et al., 2006; Ettwig et al., 2008). A similar pathway was recently discovered in *Methylomonas denitrificans*, a type I MOB, where methane can be oxidized with nitrate as electron acceptor producing NO_2 under oxygen-limited conditions (Kits et al., 2015). However, both *M. oxyfera* and *M. denitrificans* were isolated from freshwater environments, and their importance in marine methane oxidation is unclear. Additionally, methane can be oxidized aerobically by thermoacidophilic methanotrophs or the bacterial phylum Verrucomicrobia, which are only distantly related to Proteobacteria, and were only found in highly acidic environments (pH ~2; Dunfield et al., 2007; Islam et al., 2008; Pol et al., 2007). The carbon assimilation pathway of these organisms is different from MOB and *M. oxyfera,* but is not yet understood (reviewed in Semrau et al., 2008).

1.4.5 Environmental controls on aerobic methane oxidation

MOx is the final sink for methane before its potential release to the atmosphere (see Fig. 1.9), but little is known about environmental factors controlling the spatio-temporal distribution and activity of pelagic MOB (Tavormina et al., 2010; Kessler et al., 2011; Mau et al., 2013; Crespo-Medina et al., 2014). Previous studies showed that MOx, and the distribution of Type I and Type II MOB in the oceans are controlled by methane (Kessler et al., 2011; Mau et al., 2013; Crespo-Medina et al., 2014) and oxygen concentrations (Sansone and Martens, 1978; Ward et al., 1993), as well as by trace metal availability (e.g., iron and copper; Semrau et al., 2010; Crespo-Medina et al., 2014). The relative importance of these controls is, however, unknown.

Physiologically, hydrostatic pressure and (elevated) methane concentrations were both found to have a positive effect on MOx rates (de Angelis et al., 1991), but studies are sparse. Methane availability was proposed as a predictor for turnover time in marine settings (Nauw et al., 2015) since a general inverse relationship between methane turnover times and methane concentrations exists. Since the variation between and within environments is rather large, methane concentration can likely not the be used as the sole parameter in predicting MOx rates.

In anoxic basins, MOB were detected at oxic/anoxic interfaces where both methane and oxygen are present (Schubert et al., 2006; Jakobs et al., 2013). Most interestingly, recent studies showed that aquatic and terrestrial methanotrophs coped with low oxygen concentrations by using several mechanisms: A switch of methanotrophic metabolism to a

fermentative mode was observed (Vecherskaya et al., 2009; Kalyuzhnaya et al., 2013), and *M. denitrificans* was found to use nitrate as electron acceptor (Kits et al., 2015). However, *Methylomonas sp.* have not yet been detected in marine environments but only in freshwater systems (Knief, 2015). In two lake-based studies, photosynthetic algae provided enough oxygen for MOx to proceed in anoxic parts of the water column (Milucka et al., 2015; Oswald et al., 2015). In contrast, MOx was often found to be very low in highly oxic surface waters (e.g., Schubert et al., 2006), which could be due to competition with other heterotrophs (van Bodegom et al., 2001) or due to grazing, as shown in a recent study in a shallow Finnish lake (Devlin et al., 2015). However, most studies were conducted in freshwater systems, which often harbour a distinctly different MOB community than marine settings (Knief, 2015), and the effect of low oxygen concentration on MOx is largely unknown in the ocean, with the exception of anoxic basins (Schubert et al., 2006; Jakobs et al., 2013).

Very little is known about factors selecting for specific groups of MOB in marine environments: MOB almost exclusively belong to the Type I group in oceanic waters and sediments (Elsaied et al., 2004; Tavormina et al., 2008; Tavormina et al., 2010; Reed et al., 2009; Håvelsrud et al., 2011; Kessler et al., 2011). In some marine studies, Type II MOB were observed in sediments, but in all cases they constituted only a small part of the methanotrophic community (Wang et al., 2004; McDonald et al., 2005; Hamdan et al., 2011), and no Type II were detected in the water column as of now. The reason for the absence of Type II MOB is unknown.

In general, the efficiency and environmental controls of MOx in oceanic systems is poorly constrained compared to the sedimentary filter system, mainly due to a limited number of rate measurements (Reeburgh, 2007) and the much larger volume of the water column compared to surface sediments. Additionally, the low spatio-temporal coverage of direct observations together with the high spatio-temporal variation of all processes involved (i.e., physical transport, MOx, and environmental controls thereof) adds further uncertainty to current estimates.

1.5 Rationale and PhD project objectives

Increasing evidence suggests that ocean bottom water warming is leading to enhanced methane fluxes into the water column, for instance by dissociation of gas hydrates or by enhanced methane production in coastal ecosystems. Elevated methane fluxes into seawater can potentially lead to increased methane emissions from the ocean into the atmosphere, where it acts as a potent greenhouse gas and thus contributes to further global warming. Water-column MOx is the final sink for methane before its release to the atmosphere. However, little is known on the efficiency of this microbial filter and its ability to adjust to a (rapidly) changing environment. In order to predict future changes, it is thus extremely important to understand the efficiency of methanotrophic communities, to identify the key players in these communities, and to determine environmental parameters controlling MOx. This dissertation presents a biochemical, microbiological, and molecular approach to the investigation of methane oxidation in contrasting ocean environments. In all of the studied methane-rich habitats, water-column methane oxidation had not previously been investigated. Studied environments span the $MgCl_2$-rich deep-sea brine basins Kryos in the Eastern Mediterranean, the continental slope gas-hydrate associated gas seeps offshore Svalbard, a man-made highly active gas Blowout in the North Sea and a shallow organic-rich coastal site in the southern Baltic Sea.

For each study site, I was interested in the following questions:

- What is the magnitude of methane oxidation rates?
- What are the dominant pathways of methane consumption?
- What is the effect of different methane flux rates on the methanotrophic community?
- What are other key environmental parameters controlling methanotrophy?
- What microbial key players are present and how abundant are they?
- What is the relationship between methane oxidation rates and MOB cell numbers?
- What is the overall efficiency of the pelagic MOx filter system?
- Can we predict how MOx will change in these systems in a future (warmer) ocean?

In addition, we aimed to further develop current methods of methane oxidation rate measurements. Since the central goal of this dissertation was a systematic study of aerobic methane oxidation, collaborations with researchers of other disciplines (i.e., geophysicists and modelers) were also initiated to allow for a more thorough understanding of the investigated systems.

1.6 Chapters and publication outline

This thesis includes four manuscripts, of which one is already published in *Nature Geoscience*, one is under review for publication in *Limnology & Oceanography*, and two are in preparation and will be submitted within three month after thesis submission. My contribution to the publications is detailed below.

1. Water column methanotrophy controlled by a rapid oceanographic switch

Lea Steinle, Carolyn A. Graves, Tina Treude, Bénédicte Ferré, Arne Biastoch, Ingeborg Bussmann, Christian Berndt, Sebastian Krastel, Rachael H. James, Erik Behrens, Claus W. Böning, Jens Greinert, Célia-Julia Sapart, Markus Scheinert, Stefan Sommer, Moritz F. Lehmann and Helge Niemann

Published as: *Nature Geoscience* (2015), **8**: 378–382.

This study will be presented in Chapter 2. It includes the results of an investigation of MOx in the water column above the recently discovered gas-hydrate associated cold seeps at the continental margin offshore Svalbard. Most data for this paper were collected on a cruise in 2012 with R/V Maria S. Merian with a few additional data points from a cruise in 2011 with R/V Poseidon. In 2012, rate measurements of aerobic water column methanotrophy were performed by Helge Niemann and myself, and methane concentrations were measured by Carolyn A. Graves. I performed CARD-FISH analyses and initiated the collaboration with the modelling group led by Arne Biastoch and coordinated this exchange together with Helge Niemann. I wrote the paper with input form all co-authors.

2. Linked sediment and water-column methanotrophy at a man-made gas blowout in the North Sea: Implications for methane budgeting in seasonally stratified shallow seas

Lea Steinle, Mark Schmidt, Lee Bryant, Matthias Haeckel, Peter Linke, Stefan Sommer, Jakob Zopfi, Moritz F. Lehmann, Tina Treude, and Helge Niemann

Under review in: *Limnology & Oceanography*

All rate measurements and microbial analyses were performed by myself, except for sedimentary CARD-FISH counts, which were analysed by Gabi Schüssler. I also extracted DNA and DGGE and subsequent phylogenetic analyses. Mark Schmidt measured methane concentrations and stable isotopes, and Matthias Haeckel measured sediment geochemistry. I wrote the paper with input from all co-authors.

3. Environmental controls on aerobic methane oxidation in seasonally hypoxic coastal waters

Lea Steinle, Johanna Maltby, Tina Treude, Annette Kock, Hermann W. Bange, Moritz F. Lehmann, and Helge Niemann

In preparation for: *Biogeosciences*

Samples were collected by Johanna Maltby and myself. I measured methane oxidation rates and conducted all experimental work. I wrote the paper with input from all co-authors.

4. Micro-aerophilic methanotrophy at the interface between Mediterranean seawater and the $MgCl_2$-dominated Kryos brine basin and evidence for microbial activity at 4 M $MgCl_2$.

Lea Steinle, Nicole Felber, Claudia Casalino, Chiara Tessarolo, Gert de Lange, Alina Stadniskaia, Jaap S. Sinninghe Damste, Moritz Lehmann, Tina Treude and Helge Niemann

In preparation for: *Environmental Microbiology*

Samples were collected by all members of the Ristretto & Lungo cruise of the Mocca project with R/V Pelagia in 2011/2012. Helge Niemann and myself measured microbial rates, Nicole Felber and myself extracted lipid biomarkers and analysed them with help from Helge Niemann. The rest of the data analysis was performed by myself. I wrote the paper with input from all co-authors.

References

de Angelis, M.A., and Lee, C. (1994). Methane production during zooplankton grazing on marine phytoplankton. *Limnology and Oceanography* 39: 1298-1308.

de Angelis, M.A., Baross, J.A., and Lilley, M.D. (1991). Enhanced microbial methane oxidation in water from a deep-sea hydrothermal vent field at simulated in situ hydrostatic pressures. *Limnology and Oceanography* 3: 565-570.

Archer, D. (2007). Methane hydrate stability and anthropogenic climate change. *Biogeosciences Discussions* 4: 993-1057.

Archer, D., Buffett, B., and Brovkin, V. (2009). Ocean methane hydrates as a slow tipping point in the global carbon cycle. *Proceedings of the National Academy of Sciences* 106: 20596-20601.

Archer, D., Eby, M., Brovkin, V., Ridgwell, A., Cao, L., Mikolajewicz, U., et al. (2009). Atmospheric lifetime of fossil fuel carbon dioxide. *Annual Review of Earth and Planetary Sciences* 37: 117.

Avrahamov, N., Antler, G., Yechieli, Y., Gavrieli, I., Joye, S.B., Saxton, M., et al. (2014). Anaerobic oxidation of methane by sulfate in hypersaline groundwater of the Dead Sea aquifer. *Geobiology* 12: 511-528.

Bakker, D.C., Bange, H.W., Gruber, N., Johannessen, T., Upstill-Goddard, R.C., Borges, A.V., et al. (2014). Air-sea interactions of natural long-lived greenhouse gases (CO2, N2O, CH4). in a changing climate, In *Ocean-Atmosphere Interactions of Gases and Particles*. Liss, P.S., and Johnson, M.T. (eds) Heidelberg: Springer Verlag, pp. 113-169.

Bange, H.W. (2006). Nitrous oxide and methane in European coastal waters. *Estuarine, Coastal and Shelf Science* 70: 361-374.

Bange, H.W., Bartell, U.H., Rapsomanikis, S., and Andreae, M.O. (1994). Methane in the Baltic and North Seas and a reassessment of the marine emissions of methane. *Global Biogeochemical Cycles* 8: 465-480.

Bange, H.W., Bergmann, K., Hansen, H.P., Kock, A., Koppe, R., Malien, F., and Ostrau, C. (2010). Dissolved methane during hypoxic events at the Boknis Eck time series station (Eckernförde Bay, SW Baltic Sea). *Biogeosciences (BG)*. 7: 1279-1284.

Barnes, R.O., and Goldberg, E.D. (1976). Methane production and consumption in anoxic marine sediments. *Geology* 4: 297-300.

Baumgartner, M., Schilt, A., Eicher, O., Schmitt, J., Schwander, J., Spahni, R., et al. (2012). High-resolution interpolar difference of atmospheric methane around the Last Glacial Maximum. *Biogeosciences* 9: 3961-3977.

Beal, E.J., House, C.H., and Orphan, V.J. (2009). Manganese- and iron-dependent marine methane oxidation. *Science (New York, N.Y.)*. 325: 184-187.

Bernard, B.B., Brooks, J.M., and Sackett, W.M. (1978). Light hydrocarbons in recent Texas continental shelf and slope sediments. *Journal of Geophysical Research: Oceans* 83: 4053-4061.

Bernardino, A.F., Levin, L.A., Thurber, A.R., and Smith, C.R. (2012). Comparative composition, diversity and trophic ecology of sediment macrofauna at vents, seeps and organic falls. *PLoS One* 7: e33515.

Berndt, C., Feseker, T., Treude, T., Krastel, S., Liebetrau, V., Niemann, H., et al. (2014). Temporal Constraints on Hydrate-Controlled Methane Seepage off Svalbard. *Science* 343: 284-287.

Biastoch, A., Treude, T., Rüpke, L.H., Riebesell, U., Roth, C., Burwicz, E.B., et al. (2011). Rising Arctic Ocean temperatures cause gas hydrate destabilization and ocean acidification. *Geophysical Research Letters* 38: n/a-n/a.

Boetius, A., and Joye, S. (2009). Thriving in salt. *Science* 324: 1523-1525.

Boetius, A., and Wenzhöfer, F. (2013). Seafloor oxygen consumption fuelled by methane from cold seeps. *Nature Geoscience* 6: 725-734.

Boetius, A., Ravenschlag, K., Schubert, C.J., Rickert, D., Widdel, F., Gieseke, A., et al. (2000). A marine microbial consortium apparently mediating anaerobic oxidation of methane. *Nature* 407: 623-626.

Boone, D.R., Whitman, W.B., and Rouvière, P. (1993). Diversity and Taxonomy of Methanogens, In *Methanogenesis*. Ferry, J.G. (eds) Boston, MA: Springer US.

Boudreau, B.P. (2012). The physics of bubbles in surficial, soft, cohesive sediments. *Marine and Petroleum Geology* 38: 1-18.

Bowman, J.P., Sly, L.I., Nichols, P.D., and Hayward, A.C. (1993). Revised taxonomy of the methanotrophs: description of Methylobacter gen. nov., emendation of Methylococcus, validation of Methylosinus and Methylocystis species, and a proposal that the family Methylococcaceae includes only the group I methanotrophs. *International Journal of Systematic and Evolutionary Microbiology* 43: 735-753.

Brook, E.J., Harder, S., Severinghaus, J., Steig, E.J., and Sucher, C.M. (2000). On the origin and timing of rapid changes in atmospheric methane during the last glacial period. *Global Biogeochemical Cycles* 14: 559-572.

Burwicz, E.B., Rüpke, L.H., and Wallmann, K. (2011). Estimation of the global amount of submarine gas hydrates formed via microbial methane formation based on numerical reaction-transport modeling and a novel parameterization of Holocene sedimentation. *Geochimica et Cosmochimica Acta* 75: 4562-4576.

Bussmann, I., and Suess, E. (1998). Groundwater seepage in Eckernförde Bay (Western Baltic Sea): Effect on methane and salinity distribution of the water column. *Continental Shelf Research* 18: 1795-1806.

Camerlenghi, A. (1990). Anoxic basins of the eastern Mediterranean: geological framework. *Marine chemistry* 31: 1-19.

Carini, P., White, A.E., Campbell, E.O., and Giovannoni, S.J. (2014). Methane production by phosphate-starved SAR11 chemoheterotrophic marine bacteria. *Nat Commun* 5: 4346.

Chappellaz, J., Bluniert, T., Raynaud, D., Barnola, J.M., Schwander, J., and Stauffert, B. (1993). Synchronous changes in atmospheric CH4 and Greenland climate between 40 and 8 kyr BP. *Nature* 366: 443-445.

Ciais, H., Sabine, c., Govndasamy, B., Bopp, L., Brovkin, V., Canadell, J., et al. (2013). Carbon and other biogeochemical cyles, In *Climate Change 2013 - The Physical Science Basis. Contribution of Working Group I to the Fifth Assessment Report of the Intergovernmental Panel on Climate Change*. Stocker, T.F., Q.D., Qin, D., Plattner, G., Tignor, M., Allen, S., Boschung, J., et al. (eds) Cambridge: Cambridge University Press.

Cicerone, R.J., and Oremland, R.S. (1988). Biogeochemical aspects of atmospheric methane. *Global biogeochemical cycles* 2: 299-327.

Clennell, M.B., Hovland, M., Booth, J.S., Henry, P., and Winters, W.J. (1999). Formation of natural gas hydrates in marine sediments: 1. Conceptual model of gas hydrate growth conditioned by host sediment properties. *Journal of Geophysical Research: Solid Earth* 104: 22985-23003.

Costello, A.M., and Lidstrom, M.E. (1999). Molecular characterization of functional and phylogenetic genes from natural populations of methanotrophs in lake sediments. *Appl Environ Microbiol* 65: 5066-5074.

Crespo-Medina, M., Meile, C.D., Hunter, K.S., Diercks, A., Asper, V.L., Orphan, V.J., et al. (2014). The rise and fall of methanotrophy following a deepwater oil-well blowout. *Nature Geoscience* 7: 423-427.

Cypionka, H. (2000). Oxygen Respiration by Desulfovibrio Species 1. *Annual Reviews in Microbiology* 54: 827-848.

Dahl, C., and Friedrich, C.G. (2008). *Microbial sulfur metabolism*. Springer.

Damm, E., Helmke, E., Thoms, S., Schauer, U., Nöthig, E., Bakker, K., and Kiene, R.P. (2010). Methane production in aerobic oligotrophic surface water in the central Arctic Ocean. *Biogeosciences* 7: 1099-1108.

Devlin, S.P., Saarenheimo, J., Syväranta, J., and Jones, R.I. (2015). Top consumer abundance influences lake methane efflux. *Nat Commun* 6: 8787.

D'Hondt, S., Rutherford, S., and Spivack, A.J. (2002). Metabolic activity of subsurface life in deep-sea sediments. *Science* 295: 2067-2070.

Dlugokencky, E.J., Nisbet, E.G., Fisher, R., and Lowry, D. (2011). Global atmospheric methane: budget, changes and dangers. *Philosophical transactions. Series A, Mathematical, physical, and engineering sciences* 369: 2058-2072.

Dubilier, N., Bergin, C., and Lott, C. (2008). Symbiotic diversity in marine animals: the art of harnessing chemosynthesis. *Nat Rev Microbiol* 6: 725-740.

Dunfield, P.F., Yuryev, A., Senin, P., Smirnova, A.V., Stott, M.B., Hou, S., et al. (2007). Methane oxidation by an extremely acidophilic bacterium of the phylum Verrucomicrobia. *Nature* 450: 879-882.

Egger, M., Rasigraf, O., Sapart, C.J., Jilbert, T., Jetten, M.S., Röckmann, T., et al. (2015). Iron-mediated anaerobic oxidation of methane in brackish coastal sediments. *Environ Sci Technol* 49: 277-283.

Elsaied, H.E., Hayashi, T., and Naganuma, T. (2004). Molecular analysis of deep-sea hydrothermal vent aerobic methanotrophs by targeting genes of 16S rRNA and particulate methane monooxygenase. *Marine Biotechnology* 6: 503-509.

Emerson, S., and Hedges, J. (2003). Sediment diagenesis and benthic flux. *Treatise on Geochemistry* 6: 625.

EPA, and 2010, I. (2010). *Methane and nitrous oxide emissions from natural sources*. *EPA* papers2://publication/uuid/D7772781-A95C-4753-B53D-F12E25DD263D: 12-17.

Ettwig, K.F., Butler, M.K., Le Paslier, D., Pelletier, E., Mangenot, S., Kuypers, M.M., et al. (2010). Nitrite-driven anaerobic methane oxidation by oxygenic bacteria. *Nature* 464: 543-548.

Ettwig, K.F., Shima, S., van de Pas-Schoonen, K.T., Kahnt, J., Medema, M.H., Op den Camp, H.J., et al. (2008). Denitrifying bacteria anaerobically oxidize methane in the absence of Archaea. *Environ Microbiol* 10: 3164-3173.

Fossing, H., Ferdelman, T.G., and Berg, P. (2000). Sulfate reduction and methane oxidation in continental margin sediments influenced by irrigation (South-East Atlantic off Namibia). *Geochimica et Cosmochimica Acta* 64: 897-910.

Graves, C.A., Steinle, L., Rehder, G., Niemann, H., Connelly, D.P., Lowry, D., et al. (2015). Fluxes and fate of dissolved methane released at the seafloor at the landward limit of the gas hydrate stability zone offshore western Svalbard. *Journal of Geophysical Research: Oceans* 120: 6185-6201.

Haacke, R.R., Westbrook, G.K., and Hyndman, R.D. (2007). Gas hydrate, fluid flow and free gas: Formation of the bottom-simulating reflector. *Earth and Planetary Science Letters* 261: 407-420.

Hamdan, L.J., Gillevet, P.M., Pohlman, J.W., Sikaroodi, M., Greinert, J., and Coffin, R.B. (2011). Diversity and biogeochemical structuring of bacterial communities across the Porangahau ridge accretionary prism, New Zealand. *FEMS microbiology ecology* 77: 518-532.

Hansen, C.J., Esposito, L., Stewart, A.I., Colwell, J., Hendrix, A., Pryor, W., et al. (2006). Enceladus' water vapor plume. *Science* 311: 1422-1425.

Hanson, R.S., and Hanson, T.E. (1996). Methanotrophic bacteria. *Microbiological reviews* 60: 439-471.

Haroon, M.F., Hu, S., Shi, Y., Imelfort, M., Keller, J., Hugenholtz, P., et al. (2013). Anaerobic oxidation of methane coupled to nitrate reduction in a novel archaeal lineage. *Nature* 500: 567-570.

Hartmann, D.L., Tank, A.M.G.K., Rusticucci, M., Alexander, L.V., Brönnimann S, Charabi, Y., et al. (2013). Observations: Atmosphere and surface, In *Climate Change 2013 - The Physical Science Basis. Contribution of Working Group I to the Fifth Assessment Report of the Intergovernmental Panel on Climate Change*. Stocker, T.F., Q.D., Qin,

D., Plattner, G., Tignor, M., Allen, S., Boschung, J., et al. (eds) Cambridge: Cambridge University Press.

Håvelsrud, O., Haverkamp, T.H., Kristensen, T., Jakobsen, K.S., and Rike, A. (2011). A metagenomic study of methanotrophic microorganisms in Coal Oil Point seep sediments. *BMC Microbiology* 11: 221.

Heeschen, K.U., Collier, R.W., de Angelis, M.A., Suess, E., Rehder, G., Linke, P., and Klinkhammer, G.P. (2005). Methane sources, distributions, and fluxes from cold vent sites at Hydrate Ridge, Cascadia Margin. *Global Biogeochemical Cycles* 19.

Hesse, R. (2003). Pore water anomalies of submarine gas-hydrate zones as tool to assess hydrate abundance and distribution in the subsurface: What have we learned in the past decade? *Earth-Science Reviews* 61: 149-179.

Hesse, R., and Harrison, W.E. (1981). Gas hydrates (clathrates). causing pore-water freshening and oxygen isotope fractionation in deep-water sedimentary sections of terrigenous continental margins. *Earth and Planetary Science Letters* 55: 453-462.

Hester, K.C., and Brewer, P.G. (2009). Clathrate hydrates in nature. *Annual review of marine science* 1: 303-327.

Hinrichs, K., Hayes, J.M., and Sylva, S.P. (1999). Methane-consuming archaebacteria in marine sediments. 398: 802-805.

Holmes, C.D., Prather, M.J., Søvde, O.A., and Myhre, G. (2013). Future methane, hydroxyl, and their uncertainties: key climate and emission parameters for future predictions. *Atmospheric Chemistry and Physics* 13: 285-302.

Holmes, M.E. (2000). Methane production, consumption, and air-sea exchange in the open ocean: An evaluation based on carbon isotopic ratios M. Elizabeth Holmes, 1 Francis J. Sansone, Terri M. Rust, and Brian N. Popp. *Global Biogeochemical Cycles* 14: 1-10.

Horita, J., and Berndt, M.E. (1999). Abiogenic methane formation and isotopic fractionation under hydrothermal conditions. *Science* 285: 1055-1057.

Hovland, M., and Judd, A. (1988). Seabed pockmarks and seepages: impact on geology, biology, and the marine environment. Springer.

Hovland, M., Judd, A.G., and King, L.H. (1984). Characteristic features of pockmarks on the North Sea Floor and Scotian Shelf. *Sedimentology* 31: 471-480.

Hsu, H.W., Postberg, F., Sekine, Y., Shibuya, T., Kempf, S., Horányi, M., et al. (2015). Ongoing hydrothermal activities within Enceladus. *Nature* 519: 207-210.

Hsü, K.J., Ryan, W.B.F., and Cita, M.B. (1973). Late Miocene desiccation of the Mediterranean. *Nature* 242: 240-244.

Hu, S., Zeng, R.J., Burow, L.C., Lant, P., Keller, J., and Yuan, Z. (2009). Enrichment of denitrifying anaerobic methane oxidizing microorganisms. *Environ Microbiol Rep* 1: 377-384.

IPCC, 2013. Stocker, T.F., Qin, D., Plattner, G., Tignor, M., Allen, S., Boschung, J., et al. (eds). Climate Change 2013 - The Physical Science Basis. Contribution of Working

Group I to the Fifth Assessment Report of the Intergovernmental Panel on Climate Change. Cambridge University Press.

Islam, T., Jensen, S., Reigstad, L.J., Larsen, and Birkeland, N.-K. (2008). Methane oxidation at 55 C and pH 2 by a thermoacidophilic bacterium belonging to the Verrucomicrobia phylum. *Proceedings of the National Academy of Sciences* 105: 300-304.

Iversen, N., and Blackburn, T.H. (1981). Seasonal Rates of Methane Oxidation in Anoxic Marine Sediments. *Applied & Environmental Microbiology* 41: 1295-1300.

Iversen, N., and Jørgensen, B.B. (1985). Anaerobic methane oxidation rates at the sulfate-methane transition in marine sediments from Kattegat and Skagerrak (Denmark). *Limnol. Oceanogr* 30: 944-955.

Jackson, D.R., Williams, K.L., Wever, T.F., Friedrichs, C.T., and Wright, L.D. (1998). Sonar evidence for methane ebullition in Eckernförde Bay. *Continental Shelf Research* 18: 1893-1915.

Jakobs, G., Rehder, G., Jost, G., Kießlich, K., Labrenz, M., and Schmale, O. (2013). Comparative studies of pelagic microbial methane oxidation within the redox zones of the Gotland Deep and Landsort Deep (central Baltic Sea). *Biogeosciences* 10: 7863-7875.

Jähne, B., Heinz, G., and Dietrich, W. (1987). Measurement of the diffusion coefficients of sparingly soluble gases in water. *Journal of Geophysical Research: Oceans* 92: 10767-10776.

Jørgensen, B.B. (2006). Bacteria and marine biogeochemistry, In *Marine geochemistry*. Zabel, M., and Schulz, H.D. (eds) Berlin/Heidelberg: Springer, pp. 173-207.

Jørgensen, B.B., and Boetius, A. (2007). Feast and famine--microbial life in the deep-sea bed. *Nat Rev Microbiol* 5: 770-781.

Joye, S.B., Boetius, A., Orcutt, B.N., Montoya, J.P., Schulz, H.N., Erickson, M.J., and Lugo, S.K. (2004). The anaerobic oxidation of methane and sulfate reduction in sediments from Gulf of Mexico cold seeps. *Chemical Geology* 205: 219-238.

Joye, S.B., Samarkin, V.A., Orcutt, B.N., MacDonald, I.R., Hinrichs, K., Elvert, M., et al. (2009). Metabolic variability in seafloor brines revealed by carbon and sulphur dynamics. *Nature Geoscience* 2: 349-354.

Judd, A., and Hovland, M. (2007). Seabed Fluid Flow: The impact of geology, biology and the marine environment. Cambridge University Press.

Judd, A.G., Hovland, M., Dimitrov, L.I., Garcia Gil, S., and Jukes, V. (2002). The geological methane budget at continental margins and its influence on climate change. *Geofluids* 2: 109-126.

Jørgensen, B.B. (1982). Mineralization of organic matter in the sea bed-the role of sulphate reduction. *Nature* 296: 643-645.

Kalyuzhnaya, M.G., Yang, S., Rozova, O.N., Smalley, N.E., Clubb, J., Lamb, A., et al. (2013). Highly efficient methane biocatalysis revealed in a methanotrophic bacterium. *Nat Commun* 4: 2785.

Karl, D.M., and Tilbrook, B.D. (1994). Production and transport of methane in oceanic particulate organic matter. .

Karl, D.M., Beversdorf, L., Björkman, K.M., Church, M.J., Martinez, A., and Delong, E.F. (2008). Aerobic production of methane in the sea. *Nature Geoscience* 1: 473-478.

Kelley D. S., Karson J. A., Früh-Green G., and Yoerger D. R. (2005) A Serpentinite-Hosted Ecosystem: The Lost City Hydrothermal Field. *Science* 307, 1428-1434.

Kennett, J.P., Cannariato, K.G., Hendy, I.L., and Behl, R.J. (2000). Carbon isotopic evidence for methane hydrate instability during quaternary interstadials. *Science* 288: 128-133.

Kessler, J.D., Valentine, D.L., Redmond, M.C., Du, M., Chan, E.W., Mendes, S.D., et al. (2011). A persisten Oxygen Anomaly Reveals the Fate of Spilled Methane in the Deep Gulf of Mexico. *Science (New York, N.Y.)*. 331: 312-315.

Kirschke, S., Bousquet, P., Ciais, P., Saunois, M., Canadell, J.G., Dlugokencky, E.J., et al. (2013). Three decades of global methane sources and sinks. *Nature Geoscience* 6: 813-823.

Kits, K.D., Klotz, M.G., and Stein, L.Y. (2015). Methane oxidation coupled to nitrate reduction under hypoxia by the Gammaproteobacterium Methylomonas denitrificans, sp. nov. type strain FJG1. *Environ Microbiol* 17: 3219-3232.

Knief, C. (2015). Diversity and habitat preferences of cultivated and uncultivated aerobic methanotrophic bacteria evaluated based on pmoA as molecular marker. *Frontiers in microbiology* 6.

Knittel, K., and Boetius, A. (2009). Anaerobic Oxidation of Methane: Progress with an Unknown Process. *Annual Review of Microbiology* 63: 311-334.

Krey, V., Canadell, J.G., Nakicenovic, N., Abe, Y., Andruleit, H., Archer, D., et al. (2009). Gas hydrates: entrance to a methane age or climate threat? *Environmental Research Letters* 4: 034007.

Kvenvolden, K.A. (1993). Gas hydrates-geological perspective and global change. *REVIEWS OF GEOPHYSICS-RICHMOND VIRGINIA then Washington-* 31: 173-173.

Kvenvolden, K.A., and Rogers, B.W. (2005). Gaia's breathglobal methane exhalations. *Marine and Petroleum Geology* 22: 579-590.

Lapham, L.L., Wilson, R.M., and Chanton, J.P. (2012). Pressurized laboratory experiments show no stable carbon isotope fractionation of methane during gas hydrate dissolution and dissociation. *Rapid Commun Mass Spectrom* 26: 32-36.

Lazar, C.S., Parkes, R.J., Cragg, B.A., L'Haridon, S., and Toffin, L. (2011). Methanogenic diversity and activity in hypersaline sediments of the centre of the Napoli mud volcano, Eastern Mediterranean Sea. *Environ Microbiol* 13: 2078-2091.

Lazar, C.S., Parkes, R.J., Cragg, B.A., L'Haridon, S., and Toffin, L. (2011). Methanogenic diversity and activity in hypersaline sediments of the centre of the Napoli mud volcano, Eastern Mediterranean Sea. *Environ Microbiol* 13: 2078-2091.

Madigan, Q.D., Martinko, J., Bender, K., Buckley, D., and Stahl, D. (2015). *Brock Biology of Microorganisms*. Person: Boston.

Maignien, L., Parkes, R.J., Cragg, B., Niemann, H., Knittel, K., Coulon, S., et al. (2013). Anaerobic oxidation of methane in hypersaline cold seep sediments. *FEMS Microbiol Ecol* 83: 214-231.

Maltby, J., Steinle, L., Bange, H.W., Löscher, C.R., Fischer, M.A., Schmidt, M., and Treude, T. Microbial methanogenesis in the sulfate-reducing zone in sediments from Eckernförde Bay, SW Baltic Sea. *Geochmica Cosmochimica et Acta:* **in preparation.**

Mariotti, A., Germon, J.C., Hubert, P., Kaiser, P., Letolle, R., Tardieux, A., and Tardieux, P. (1981). Experimental determination of nitrogen kinetic isotope fractionation: Some principles; illustration for the denitrification and nitrification processes. *Plant and Soil* 62: 413-430.

Marín, I., and Ruiz Arahal, D. (2014). The Family Beijerinckiaceae, In *4*. Rosenberg, E., DeLong, E.F., Lory, S., Stackebrandt, E., and Thompson, F. (eds) Springer Berlin Heidelberg, pp. 263-282.

Marlow, J.J., Steele, J.A., Case, D.H., Connon, S.A., Levin, L.A., and Orphan, V.J. (2014). Microbial abundance and diversity patterns associated with sediments and carbonates from the methane seep environments of Hydrate Ridge, OR. *Frontiers in Marine Science* 1: 1-16.

Martens, C.S., and Berner, R.A. (1974). Methane production in the interstitial waters of sulfate-depleted marine sediments. *Science* 185: 1167-1169.

Martens, C.S., Blair, N.E., Green, C.D., and Des Marais, D.J. (1986). Seasonal variations in the stable carbon isotopic signature of biogenic methane in a coastal sediment. *Science* 233: 1300-1303.

Martín-Torres, F.J., Zorzano, M.-P., Valentín-Serrano, P., Harri, A.-M., Genzer, M., Kemppinen, O., et al. (2015). Transient liquid water and water activity at Gale crater on Mars. *Nature Geoscience* .

Mau, S., Blees, J., Helmke, E., Niemann, H., and Damm, E. (2013). Vertical distribution of methane oxidation and methanotrophic response to elevated methane concentrations in stratified waters of the Arctic fjord Storfjorden (Svalbard, Norway). *Biogeosciences* 10: 6267-6278.

McDonald, I.R., Smith, K., and Lidstrom, M.E. (2005). Methanotrophic populations in estuarine sediment from Newport Bay, California. *FEMS Microbiol Lett* 250: 287-293.

McEwen, A.S., Dundas, C.M., Mattson, S.S., Toigo, A.D., Ojha, L., Wray, J.J., et al. (2014). Recurring slope lineae in equatorial regions of Mars. *Nature Geoscience* 7: 53-58.

McGlynn, S.E., Chadwick, G.L., Kempes, C.P., and Orphan, V.J. (2015). Single cell activity reveals direct electron transfer in methanotrophic consortia. *Nature* 526: 531-535.

Fox, M. A. (1995). Memoradum 22/4b-4 well site hazards. MOBIL North Sea Ltd.

Metcalf, W.W., Griffin, B.M., Cicchillo, R.M., Gao, J., Janga, S.C., Cooke, H.A., et al. (2012). Synthesis of methylphosphonic acid by marine microbes: a source for methane in the aerobic ocean. *Science* 337: 1104-1107.

Milkov, A.V. (2005). Molecular and stable isotope compositions of natural gas hydrates: a revised global dataset and basic interpretations in the context of geological settings. *Organic Geochemistry* 36: 681-702.

Milkov, A.V., Vogt, P.R., Crane, K., Lein, A.Y., Sassen, R., and Cherkashev, G.A. (2004). Geological, geochemical, and microbial processes at the hydrate-bearing Håkon Mosby mud volcano: a review. *Chemical Geology* 205: 347-366.

Milucka, J., Ferdelman, T.G., Polerecky, L., Franzke, D., Wegener, G., Schmid, M., et al. (2012). Zero-valent sulphur is a key intermediate in marine methane oxidation. *Nature* 491: 541-546.

Milucka, J., Kirf, M., Lu, L., Krupke, A., Lam, P., Littmann, S., et al. (2015). Methane oxidation coupled to oxygenic photosynthesis in anoxic waters. *ISME J* 9: 1991-2002.

Möller, L., Sowers, T., Bock, M., Spahni, R., Behrens, M., Schmitt, J., et al. (2013). Independent variations of CH4 emissions and isotopic composition over the past 160,000 years. *Nature Geoscience* 6: 885-890.

Murrell, J.C. (2010). The Aerobic Methane Oxidizing Bacteria (Methanotrophs), In *3.26*. Timmis, K.N. (eds) Berlin, Heidelberg: Springer Berlin Heidelberg, pp. 1953-1966.

Mussmann, M., Richter, M., Lombardot, T., Meyerdierks, A., Kuever, J., Kube, M., et al. (2005). Clustered genes related to sulfate respiration in uncultured prokaryotes support the theory of their concomitant horizontal transfer. *J Bacteriol* 187: 7126-7137.

Myhre, G., Shindell, D., Bréon, F.-M., Collins, W., Fuglestvedt, J., Huang, et al. (2013). Anthropogenic and natural radiative forcing. In *Climate Change 2013 - The Physical Science Basis. Contribution of Working Group I to the Fifth Assessment Report of the Intergovernmental Panel on Climate Change*. Stocker, T.F., Q.D., Qin, D., Plattner, G., Tignor, M., Allen, S., Boschung, J., et al. (eds) Cambridge: Cambridge University Press.

Naudts, L., Greinert, J., Artemov, Y., Staelens, P., Poort, J., Van Rensbergen, P., and De Batist, M. (2006). Geological and morphological setting of 2778 methane seeps in the Dnepr paleo-delta, northwestern Black Sea. *Marine Geology* 227: 177-199.

Nauhaus, K., Albrecht, M., Elvert, M., Boetius, A., and Widdel, F. (2007). In vitro cell growth of marine archaeal-bacterial consortia during anaerobic oxidation of methane with sulfate. *Environmental Microbiology* 9: 187-196.

Nauw, J., Haas, H.D., and Rehder, G. (2015). A review of oceanographic and meteorological controls on the North Sea circulation and hydrodynamics with a view to the fate of North Sea methane from well site 22 / 4b and other seabed sources. *Marine and Petroleum Geology* 68: 861-882.

Niemann, H. (2010). Handbook of Hydrocarbon and Lipid Microbiology. .

Niemann, H., Elvert, M., Hovland, M., Orcutt, B., Judd, A., Suck, I., et al. (2005). Methane emission and consumption at a North Sea gas seep (Tommeliten area). *Biogeosciences* 2: 335-351.

Niemann, H., Linke, P., Knittel, K., MacPherson, E., Boetius, A., Brückmann, W., et al. (2013). Methane-carbon flow into the benthic food web at cold seeps--a case study from the Costa Rica subduction zone. *PLoS One* 8: e74894.

Niemann, H., Lösekann, T., de Beer, D., Elvert, M., Nadalig, T., Knittel, K., et al. (2006). Novel microbial communities of the Haakon Mosby mud volcano and their role as a methane sink. *Nature* 443: 854-858.

Niewöhner, C., Hensen, C., Kasten, S., Zabel, M., and Schulz, H.D. (1998). Deep sulfate reduction completely mediated by anaerobic methane oxidation in sediments of the upwelling area off Namibia. *Geochimica et Cosmochimica Acta* 62: 455-464.

Nisbet, E.G. (2002). Have sudden large releases of methane from geological reservoirs occurred since the Last Glacial Maximum, and could such releases occur again? *Philos Trans A Math Phys Eng Sci* 360: 581-607.

Nisbet, E.G., Dlugokencky, E.J., and Bousquet, P. (2014). Methane on the riseagain. *Science* 343: 493-495.

O'Hara, K.D. (2008). A model for late quaternary methane ice core signals: wetlands versus a shallow marine source. *Geophysical Research Letters* 35.

Orcutt, B.N., Boetius, A., Lugo, S.K., MacDonald, I.R., Samarkin, V.A., and Joye, S.B. (2004). Life at the edge of methane ice: microbial cycling of carbon and sulfur in Gulf of Mexico gas hydrates. *Chemical Geology* 205: 239-251.

Orphan, V.J., House, C.H., Hinrichs, K., McKeegan, K.D., and DeLong, E.F. (2002). Multiple archaeal groups mediate methane oxidation in anoxic cold seep sediments. *Proceedings of the National Academy of Sciences of the United States of America* 99: 7663-7668.

Orphan, V.J., Sylva, S.P., Hayes, J.M., and Delong, E.F. (2001). Comparative Analysis of Methane-Oxidizing Archaea and Sulfate-Reducing Bacteria in Anoxic Marine Sediments Comparative Analysis of Methane-Oxidizing Archaea and Sulfate-Reducing Bacteria in Anoxic Marine Sediments. *Applied and environmental microbiology* 67: 1922 - 1934.

Oswald, K., Milucka, J., Brand, A., Littmann, S., Wehrli, B., Kuypers, M.M., and Schubert, C.J. (2015). Light-Dependent Aerobic Methane Oxidation Reduces Methane Emissions from Seasonally Stratified Lakes. *PLoS One* 10: e0132574.

Pape, T., Bahr, A., Rethemeyer, J., Kessler, J.D., Sahling, H., Hinrichs, K.-U., et al. (2010). Molecular and isotopic partitioning of low-molecular-weight hydrocarbons during migration and gas hydrate precipitation in deposits of a high-flux seepage site. *Chemical Geology* 269: 350-363.

Peckmann, J., Reimer, A., Luth, U., Luth, C., Hansen, B.T., Heinicke, C., et al. (2001). Methane-derived carbonates and authigenic pyrite from the northwestern Black Sea. *Marine Geology* 177: 129-150.

Petit, J.-R., Jouzel, J., Raynaud, D., Barkov, N.I., Barnola, J.-M., Basile, I., et al. (1999). Climate and atmospheric history of the past 420,000 years from the Vostok ice core, Antarctica. *Nature* 399: 429-436.

Phrampus, B.J., Hornbach, M.J., Ruppel, C.D., and Hart, P.E. (2014). Widespread gas hydrate instability on the upper US Beaufort margin. *Journal of Geophysical Research: Solid Earth* 119: 8594-8609.

Piñero, E., Marquardt, M., Hensen, C., Haeckel, M., and Wallmann, K. (2013). Estimation of the global inventory of methane hydrates in marine sediments using transfer functions. *Biogeosciences* 10: 959-975.

Pol, A., Heijmans, K., Harhangi, H.R., Tedesco, D., Jetten, M.S., and den Camp, H.J.O. (2007). Methanotrophy below pH 1 by a new Verrucomicrobia species. *Nature* 450: 874-878.

Raghoebarsing, A.A., Pol, A., van de Pas-Schoonen, K.T., Smolders, A.J., Ettwig, K.F., Rijpstra, W.I., et al. (2006). A microbial consortium couples anaerobic methane oxidation to denitrification. *Nature* 440: 918-921.

Reeburgh, W. (2007). Oceanic methane biogeochemistry. *Chemical Reviews* 107: 486-513.

Reeburgh, W.S. (1983). Rates of Biogeochemical Processes in Anoxic Sediments. *Annual Review of Earth and Planetary Sciences* 11: 269-298.

Reeburgh, W.S., Ward, B.B., Whalen, S.C., Sandbeck, K.A., Kilpatrickt, K.A., and Kerkhof, L.J. (1991). Black Sea methane geochemistry. *Deep Sea Research Part A. Oceanographic Research Papers* 38: S1189-S1210.

Reed, A.J., Dorn, R., Van Dover, C.L., Lutz, R.A., and Vetriani, C. (2009). Phylogenetic diversity of methanogenic, sulfate-reducing and methanotrophic prokaryotes from deep-sea hydrothermal vents and cold seeps. *Deep Sea Research Part II: Topical Studies in Oceanography* 56: 1665-1674.

Rehder, G., Keir, R.S., Suess, E., and Pohlmann, T. (1998). The multiple sources and patterns of methane in North Sea waters. *Aquatic Geochemistry* 4: 403-427.

Rhee, T.S., Kettle, A.J., and Andreae, M.O. (2009). Methane and nitrous oxide emissions from the ocean: A reassessment using basin-wide observations in the Atlantic. *Journal of Geophysical Research: Atmospheres* 114.

Sansone, F.J., and Martens, C.S. (1978). Methane oxidation in Cape Lookout Bight, North Carolina. *Limnology and Oceanography* 23: 349-355.

Schmale, O., Schneider von Deimling, J., Gülzow, W., Nausch, G., Waniek, J.J., and Rehder, G. (2010). Distribution of methane in the water column of the Baltic Sea. *Geophysical Research Letters* 37.

Schubert, C.J., Coolen, M.J., Neretin, L.N., Schippers, A., Abbas, B., Durisch-Kaiser, E., et al. (2006). Aerobic and anaerobic methanotrophs in the Black Sea water column. *Environmental microbiology* 8: 1844-1856.

Semrau, J.D., Dispirito, A.A., and Murrell, J.C. (2008). Life in the extreme: thermoacidophilic methanotrophy. *Trends Microbiol* 16: 190-193.

Semrau, J.D., DiSpirito, A.A., and Yoon, S. (2010). Methanotrophs and copper. *FEMS Microbiology Reviews* 34: 496-531.

Shakhova, N., Semiletov, I., Leifer, I., Sergienko, V., Salyuk, A., Kosmach, D., et al. (2014). Ebullition and storm-induced methane release from the East Siberian Arctic Shelf. *Nature Geoscience* 7: 64-70.

Shakhova, N., Semiletov, I., Salyuk, A., Yusupov, V., Kosmach, D., and Gustafsson, O. (2010). Extensive methane venting to the atmosphere from sediments of the East Siberian Arctic Shelf. *Science* 327: 1246-1250.

Sherwood Lollar, B., Telling, J., Lacrampe-Couloume, G., Fu, Q., Seyfried Jr, W., Horita, J., and McCollom, T.M. (2005). Carbon and hydrogen isotope measurements in abiogenic hydrocarbon synthesis. *Geochimica et Cosmochimica Acta Supplement* 69: A557.

Sherwood Lollar, B., Westgate, T.D., Ward, J.A., Slater, G.F., and Lacrampe-Couloume, G. (2002). Abiogenic formation of alkanes in the Earth's crust as a minor source for global hydrocarbon reservoirs. *Nature* 416: 522-524.

Siedler, P., and Peters, H. (1986). Properties of sea water, Physical properties (general), In *LANDOLT-BÖRNSTEIN, Numerical Data and Functional Relationships in Science and Technology, New Series, Oceanography*. Sündermann, J. (eds) Berlin: Springer Verlag, pp. 233-264.

Skarke, A., Ruppel, C., Kodis, M., Brothers, D., and Lobecker, E. (2014). Widespread methane leakage from the sea floor on the northern US Atlantic margin. *Nature Geoscience* 7: 657-661.

Sloan, E.D. (2003). Fundamental principles and applications of natural gas hydrates. *Nature* 426: 353-363.

Sloan Jr, E.D., and Koh, C. (2008). *Clathrate hydrates of natural gases*. Boca Rotan, FL: CRC press, Taylor and Francis Group.

Solomon, E.A., Kastner, M., MacDonald, I.R., and Leifer, I. (2009). Considerable methane fluxes to the atmosphere from hydrocarbon seeps in the Gulf of Mexico. *Nature Geoscience* 2: 561-565.

Steeb, P., Linke, P., and Treude, T. (2014). A sediment flow-through system to study the impact of shifting fluid and methane flow regimes on the efficiency of the benthic methane filter. *Limnology and Oceanography: Methods* 12: 25-45.

Stock, A., Filker, S., Yakimov, M., and Stoeck, T. (2013). Deep Hypersaline Anoxic Basins as Model Systems For Enivronmental Selection Of Microbial Plankton. *Polyextremophiles Life Under Multiple Forms of Stress Series* : 501-515.

Suess, E., Torres, M.E., Bohrmann, G., Collier, R.W., Greinert, J., Linke, P., et al. (1999). Gas hydrate destabilization: enhanced dewatering, benthic material turnover and large methane plumes at the Cascadia convergent margin. *Earth and Planetary Science Letters* 170: 1-15.

Tavormina, P.L., Ussler, W., and Orphan, V.J. (2008). Planktonic and Sediment-Associated Aerobic Methanotrophs in Two Seep Systems along the North American Margin. *Applied and Environmental Microbiology* 74: 3985-3995.

Tavormina, P.L., Ussler, W., Joye, S.B., Harrison, B.K., and Orphan, V.J. (2010). Distributions of putative aerobic methanotrophs in diverse pelagic marine environments. *The ISME journal* 4: 700-710.

Teske, A., Hinrichs, K.U., Edgcomb, V., de Vera Gomez, A., Kysela, D., Sylva, S.P., et al. (2002). Microbial diversity of hydrothermal sediments in the Guaymas Basin: evidence for anaerobic methanotrophic communities. *Appl Environ Microbiol* 68: 1994-2007.

Thauer, R.K. (1998). Biochemistry of methanogenesis: a tribute to Marjory Stephenson. 1998 Marjory Stephenson Prize Lecture. *Microbiology* 144 (Pt 9): 2377-2406.

Thauer, R.K., Jungermann, K., and Decker, K. (1977). Energy conservation in chemotrophic anaerobic bacteria. *Bacteriological reviews* 41: 100.

Treude, T., and Ziebis, W. (2010). Methane oxidation in permeable sediments at hydrocarbon seeps in the Santa Barbara Channel, California. *Biogeosciences* 7: 3095-3108.

Treude, T., Boetius, A., Knittel, K., Wallmann, K., and Barker Jørgensen, B. (2003). Anaerobic oxidation of methane above gas hydrates at Hydrate Ridge, NE Pacific Ocean. *Marine Ecology Progress Series* 264: 1-14.

Treude, T., Krüger, K., Boetius, A., and Jørgensen, B.B. (2005). Environmental control on anaerobic oxidation of methane in gassy sediments of Eckernförde Bay (German Baltic) *Limnology and oceanography* 50: 1771-1786.

Treude, T., Niggemann, J., Kallmeyer, J., Wintersteller, P., Schubert, C.J., Boetius, A., and Jørgensen, B.B. (2005). Anaerobic oxidation of methane and sulfate reduction along the Chilean continental margin. *Geochimica et Cosmochimica Acta* 69: 2767-2779.

van Bodegom, P., Stams, F., Mollema, L., Boeke, S., and Leffelaar, P. (2001). Methane oxidation and the competition for oxygen in the rice rhizosphere. *Appl Environ Microbiol* 67: 3586-3597.

van der Wielen, P.W.J.J. (2005). The Enigma of Prokaryotic Life in Deep Hypersaline Anoxic Basins. *Science* 307: 121-123.

Vecherskaya, M., Dijkema, C., Saad, H.R., and Stams, A.J. (2009). Microaerobic and anaerobic metabolism of a Methylocystis parvus strain isolated from a denitrifying bioreactor. *Environ Microbiol Rep* 1: 442-449.

Von Damm, K.L. (1990). Seafloor hydrothermal activity: black smoker chemistry and chimneys. *Annual Review of Earth and Planetary Sciences* 18: 173.

Wallmann, K., Piñero, E., Burwicz, E., Haeckel, M., Hensen, C., Dale, A., and Ruepke, L. (2012). The global inventory of methane hydrate in marine sediments: A theoretical approach. *Energies* 5: 2449-2498.

Wang, P., Wang, F., Xu, M., and Xiao, X. (2004). Molecular phylogeny of methylotrophs in a deep-sea sediment from a tropical west Pacific Warm Pool. *FEMS microbiology ecology* 47: 77-84.

Wankel, S.D., Adams, M.M., Johnston, D.T., Hansel, C.M., Joye, S.B., and Girguis, P.R. (2012). Anaerobic methane oxidation in metalliferous hydrothermal sediments:

influence on carbon flux and decoupling from sulfate reduction. *Environ Microbiol* 14: 2726-2740.

Wankel, S.D., Joye, S.B., Samarkin, V.A., Shah, S.R., Friederich, G., Melas-Kyriazi, J., and Girguis, P.R. (2010). New constraints on methane fluxes and rates of anaerobic methane oxidation in a Gulf of Mexico brine pool via in situ mass spectrometry. *Deep Sea Research Part II: Topical Studies in Oceanography* 57: 2022-2029.

Wanninkhof, R., Asher, W.E., Ho, D.T., Sweeney, C., and McGillis, W.R. (2009). Advances in quantifying air-sea gas exchange and environmental forcing. *Ann Rev Mar Sci* 1: 213-244.

Ward, B.B., Kilpatrick, K.A., Novelli, P.C., and Scranton, M.I. (1987). Methane oxidation and methane fluxes in the ocean surface layer and deep anoxic waters. *Nature* 327: 226-229.

Ward, G.M., Doxtader, K.G., Miller, W.C., and Johnson, D.E. (1993). Effects of intensification of agricultural practices on emission of greenhouse gases. *Chemosphere* 26: 87-93.

Wegener, G., Krukenberg, V., Riedel, D., Tegetmeyer, H.E., and Boetius, A. (2015). Intercellular wiring enables electron transfer between methanotrophic archaea and bacteria. *Nature* 526: 587-590.

Westbrook, G.K., Thatcher, K.E., Rohling, E.J., Piotrowski, A.M., Pälike, H., Osborne, A.H., et al. (2009). Escape of methane gas from the seabed along the West Spitsbergen continental margin. *Geophysical Research Letters* 36: 0-4.

Whiticar, M.J. (1999). Carbon and hydrogen isotope systematics of bacterial formation and oxidation of methane. *Chemical Geology* 161: 291-314.

Whiticar, M.J. (2002). Diagenetic relationships of methanogenesis, nutrients, acoustic turbidity, pockmarks and freshwater seepages in Eckernförde Bay. *Marine Geology* 182: 29-53.

Wiesenburg, D.A., and Guinasso Jr, N.L. (1979). Equilibrium solubilities of methane, carbon monoxide, and hydrogen in water and sea water. *Journal of Chemical and Engineering Data* 24: 356-360.

Wuebbles, D.J., and Hayhoe, K. (2002). Atmospheric methane and global change. *Earth-Science Reviews* 57: 177-210.

Xu, W., and Ruppel, C. (1999). Predicting the occurrence, distribution, and evolution of methane gas hydrate in porous marine sediments. *Journal of Geophysical Research: Solid Earth* 104: 5081-5095.

Yakimov, M.M., La Cono, V., Spada, G.L., Bortoluzzi, G., Messina, E., Smedile, F., et al. (2015). Microbial community of the deep-sea brine Lake Kryos seawater-brine interface is active below the chaotropicity limit of life as revealed by recovery of mRNA. *Environ Microbiol* 17: 364-382.

Yamamoto, S., Alcauskas, J.B., and Crozier, T.E. (1976). Solubility of methane in distilled water and seawater. *Journal of Chemical and Engineering Data* 21: 78-80.

Yoshikawa, C., Hayashi, E., Yamada, K., Yoshida, O., Toyoda, S., and Yoshida, N. (2014). Methane sources and sinks in the subtropical South Pacific along 17 S as traced by stable isotope ratios. *Chemical Geology* 382: 24-31.

Zehnder, A.J., and Brock, T.D. (1979). Methane formation and methane oxidation by methanogenic bacteria. *J Bacteriol* 137: 420-432.

Zinde, S.H. (1993). Physiological ecology of methanogen, In *Methanogenesis*. Ferry, J.G. (eds) Boston, MA: Springer US.

Water column methanotrophy controlled by a rapid oceanographic switch

Lea Steinle[1,2,*], Carolyn A. Graves[3], Tina Treude[2,4], Bénédicte Ferré[5], Arne Biastoch[2], Ingeborg Bussmann[6], Christian Berndt[2], Sebastian Krastel[7], Rachael H. James[3], Erik Behrens[2,8], Claus W. Böning[2], Jens Greinert[2,4,9], Célia-Julia Sapart[10,11], Markus Scheinert[2], Stefan Sommer[2], Moritz F. Lehmann[1] and Helge Niemann[1,*]

published as: Published in: *Nature Geoscience* (2015), **8**: 378–382.

*Correspondence to: lea.steinle@unibas.ch, helge.niemann@unibas.ch

[1] Department of Environmental Sciences, University of Basel, 4056 Basel, Switzerland

[2] GEOMAR, Helmholtz Centre for Ocean Research Kiel, 24148 Kiel, Germany

[3] Ocean and Earth Science, National Oceanography Centre Southampton, Southampton SO14 3ZH, U.K.

[4] Present address: University of California, Los Angeles, Department of Earth, Planetary & Space Sciences and Atmospheric & Oceanic Sciences, Los Angeles CA 90095, USA

[5] CAGE-Centre for Arctic Gas Hydrate, Environment and Climate, Department of Geology, University of Tromsø, 9037 Tromsø, Norway

[6] Alfred Wegener Institute, Marine Station Helgoland, 27498 Helgoland, Germany

[7] Institute of Geosciences, University of Kiel, 24118 Kiel, Germany

[8] National Institute of Water and Atmospheric Research, Wellington 6021, New Zealand

[9] Royal Netherlands Institute for Sea Research NIOZ, Texel, The Netherlands

[10] Laboratoire de Glaciologie, Université Libre de Bruxelles, 1050 Brussels, Belgium

[11] Institute for Marine and Atmospheric Research, Utrecht University, 3584CC Utrecht, The Netherlands

Large amounts of the greenhouse gas methane are released from the seabed to the water column[1] where it may be consumed by aerobic methanotrophic bacteria[2]. This microbial filter is consequently the last marine sink for methane before its liberation to the atmosphere. The size and activity of methanotrophic communities, which determine the capacity of the water column methane filter, are thought to be mainly controlled by nutrient and redox dynamics[3-7], but little is known about the effects of ocean currents. Here, we assessed methane oxidation rates and methanotrophic cell numbers and compared the results to measured and modelled physical water mass properties. We show that cold bottom water at methane seeps west of Svalbard, containing a large number of aerobic methanotrophs, was rapidly displaced by warmer water with a considerably smaller methanotrophic community. This water mass exchange, caused by short-term variations of the West Spitsbergen Current, constitutes an oceanographic switch severely reducing methanotrophic activity in the water column. Our ocean model shows that strong and fluctuating currents are widespread oceanographic features common at many methane seep systems and are thus likely to globally affect methane oxidation in the ocean water column.

Large amounts of methane are stored in the subsurface of continental margins as solid gas hydrates, gaseous reservoirs or dissolved in pore water[8]. At cold seeps, various physical, chemical, and geological processes force subsurface methane to ascend along pathways of structural weakness to the sea floor where a portion of this methane is utilised by anaerobic and aerobic methanotrophic microbes[1,9]. On a global scale, about 0.02 Gt yr^{-1} (3-3.5% of the atmospheric budget[10]) of methane bypasses the benthic filter system and is liberated to the ocean water column[1] where some of it is oxidised aerobically (aerobic oxidation of methane - MOx) (ref 2), or less commonly where the water column is anoxic, anaerobically (anaerobic oxidation of methane – AOM) (refs 2, 11). MOx is performed by methanotrophic bacteria (MOB) typically belonging to the Gamma- (type I) or Alphaproteobacteria (type II) (refs 12, 13):

$$CH_4 + 2\ O_2 \rightarrow CO_2 + 2\ H_2O$$

Water column MOx is consequently the final sink for methane before its release to the atmosphere, where it acts as a potent greenhouse gas. The water column MOx filter could become more important in the future because environmental change may induce bottom water warming, which in turn may accelerate release of methane from the seafloor[14], in particular along the Arctic continental margins[15]. Despite the paramount importance of MOx for mitigating the release of methane to the atmosphere, little is known about environmental controls on the efficiency of the water column filter system. Known important factors determining the structure, activity and size of MOx communities are the availability of

methane[5-7] and oxygen[3], or the abundance of trace metals (e.g. iron and copper) (refs 4, 7). Moreover, evolutionary adaptations to specific environmental conditions select for certain types of methanotrophs[13]. In addition to environmental selection, the physical transport of water masses harbouring distinct microbial communities has been identified as an important factor in shaping the biogeography of prokaryotic communities[16]. However, the potential effects of advective processes on the distribution of methanotrophs and the efficiency of the water column MOx filter system remain unconstrained[11,17,18].

During two research cruises to the Svalbard continental margin with R/V Poseidon (cruise POS419) and R/V Maria S. Merian (cruise MSM21/4) in August 2011 and 2012, respectively, we investigated methane dynamics and the activity levels and size of the water column MOx community in relation to water mass properties (Fig. 1). The Svalbard margin hosts an extensive, elongated (~22 km) cold seep system that is influenced by gas hydrates (Fig. 1a) (ref 19). Numerous gas flares emanate from the sea floor between the 350 and 400 m isobath[19,20], which corresponds to the landward termination of the gas hydrate stability zone. Seep sites have also been mapped on the shelf[19-21], and elevated methane levels have been observed in several of the fjords in the Svalbard archipelago[6,22,23].

The hydrodynamics west of Svalbard are governed by the West Spitsbergen Current (WSC), a 100 km-wide branch of the Norwegian Atlantic Current, which transports large amounts (up to 10 Sv) of warm and salty Atlantic Water (AW; >1°C, >35 psu) northward into the Fram Strait[24]. The WSC flows above cold Arctic Intermediate Water (AIW; <1°C, ~34.9 psu) (ref 25). It is steered topographically, and its eastern extension is constrained by the shelf break[26]. East of the WSC on the shelf, the comparably slow East Spitsbergen Current transports cold and relatively fresh Arctic Water (ArW; <3°C, <34.8 psu) to the north[27]. During two sampling surveys in late August 2012, we measured methane concentrations, MOx activity and MOx biomass, as well as temperature, salinity and oxygen along a transect perpendicular to the line of the methane flares.

The two mid-transect stations were at the MASOX site (named after the MASOX observatory[19]), which is located at 380 m water depth in the centre of the gas flare area both along slope and down slope. During both surveys, methane concentrations were highest in bottom waters, frequently exceeding 100 nmol L^{-1} (Fig. 1b). Surface water methane concentrations (9 nmol CH_4 L^{-1} on average) were ~3-fold supersaturated with respect to the local atmospheric equilibrium, indicating methane efflux to the atmosphere from this seep system[19]. Methane dissolved in the water column apparently originates from gas bubbles, which we observed visually during dives with the submersible *Jago*, and which were detected as flares in the middle of the transect with hydroacoustic single-beam systems[19].

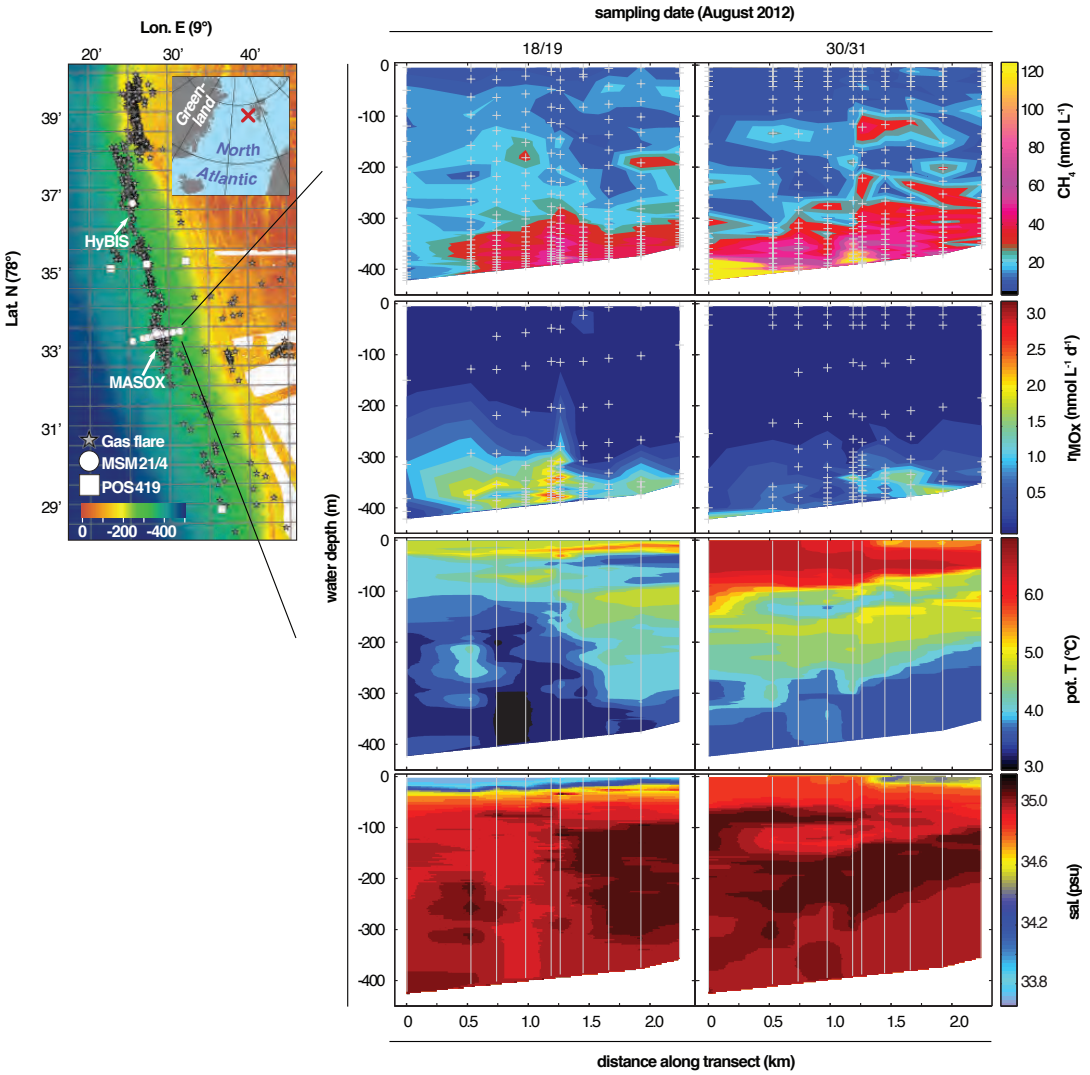

Figure 1: Study area and distribution of aerobic methanotrophy and physicochemical parameters above methane seeps at the Svalbard continental margin. a, Map of the seep system with numerous methane flares (grey stars) emanating from the sea floor around the depth of the landward termination of the gas hydrate stability zone. Sampling locations are indicated (squares: POS419, 2011; circles: MSM21/4, 2012). Distribution of b, methane, c, aerobic methane oxidation rates (rMOx), d, temperature and e, salinity measured during two sampling surveys along the same transect crossing the MASOX site19. b-e, Positions of discrete samples (crosses) and continuous measurements (lines) are indicated.

Despite the constant supply of methane from the sea floor, we found considerable spatial and temporal variability in MOx activity (Fig. 1c Supplementary Fig. 1). MOx was highest in bottom waters (>300 m water depth) during the first survey (Aug. 18/19) with methane turnover rates of up to 3.2 nmol L^{-1} d^{-1} (Fig. 1c, Tab. 1). These rates were similar to maximum rates detected at seeps on the Svalbard shelf[21] and in a nearby fjord[6]. In contrast, overall MOx activity was strongly reduced during the second survey (Aug. 30/31, Fig. 1c, Tab. 1). Consistent with the MOx activity measurements, cell enumeration conducted in the mid-transect region revealed a maximum in type I MOB cells on August 18/19 (up to 3.0 ×

10^7 cells L^{-1}; Tab. 1, Supplementary Fig. 1), but ~75% lower cell numbers during the second survey (up to 7.6×10^6 type I MOx cells L^{-1}). The distributions of MOx activity and cell numbers translate to relatively constant, although low[12,28], cell-specific MOx rates of 1.54 to 1.66×10^{-2} fmol h^{-1} during the two sampling campaigns (Tab. 1). This constancy suggests that the efficiency of the methanotrophic filter system in the water column was controlled by the size of the MOx community rather than by an environmental stimulus or suppression mechanism of MOx activity at the organismic level (Supplementary Fig. 2a, b).

Tab. 1: Comparison of methane consumption and methanotrophic cell numbers between the two transect sampling campaigns in 2012. Total CH_4 oxidised in the seep area was calculated by extrapolation of average MOx rates calculated for each sampling date to the total seep-affected water mass volume (3 km width × 22 km length × 0.388 km average water depth). Highest MOB cell numbers and fraction (in %) of total cell numbers are indicated. Cell-specific MOx rates represent the average of all samples counted on the respective transects (±standard error. n=12, Aug. 18/19; n=15, Aug. 30/31).

	sampling date (August 2012)	
	18/19	**30/31**
bottom water	cAW	wAW
mode	offshore	nearshore
max. MOx activity	3.2 nmol L^{-1} d^{-1}	2.1 nmol L^{-1} d^{-1}
CH_4 oxidised in seep area	17.82 kmol d^{-1} (0.28 t d^{-1})	5.57 kmol d^{-1} (0.09 t d^{-1})
max. MOx cells	29.7×10^6 L^{-1}	3.65×10^6 L^{-1}
max. MOx cells (% of tot. cells)	8.3	2.5
cell specific MOx activity	$1.54 \pm 0.34 \times 10^{-2}$ fmol h^{-1} ($0.22 – 5.74 \times 10^{-2}$ fmol h^{-1})	$1.66 \pm 0.37 \times 10^{-2}$ fmol h^{-1} ($0.06 – 5.66 \times 10^{-2}$ fmol h^{-1})

Together with the reduction in MOx activity and community size, we observed a strong spatiotemporal change in the distribution of water mass properties. During the August 18/19 survey, bottom waters consisted of cold AW with admixture of AIW and ArW (Fig. 1d, e), which we subsequently refer to as cold AW (cAW). The cAW has water mass properties (temperature and salinity) akin to those of bottom waters found on the shelf[21]. By August 30/31, the cAW at the bottom was replaced by warmer Atlantic water (wAW, Fig. 1d, e). As the standing stock of methanotrophs in wAW was much lower compared to the cAW, rapid water mass exchange constitutes an oceanographic switch, causing a system-wide reduction of the efficiency of water column MOx. This apparent mechanistic link between MOx activity and the presence of either cAW or wAW is reflected in all water column profiles measured in 2012, as well as 2011 (Supplementary Figs. 1n, 2c).

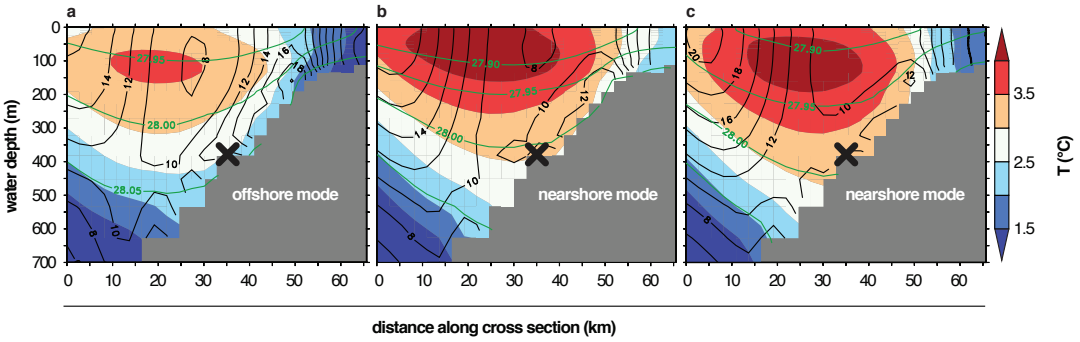

Fig. 2: Modelled cross-slope distribution of water column temperature and current velocity in the West Spitsbergen Current. Modelled time-averaged water column temperature (°C), sigma-t (green contours, kg m^{-3}-1000) and current velocity (black contours, cm s^{-1}) for a, cold temperature anomalies, b, mean temperature and c, warm temperature anomalies. Anomalies were defined as one standard deviation below or above the seasonally and interannually varying temperature mean in bottom waters at the MASOX site (cross mark; cf. Supplementary Fig. 3c). During times of cold temperature anomalies, the WSC is in its offshore mode, with a cold undercurrent along the slope.

We simulated the observed hydrodynamics using the high-resolution (1/20°, ~2.5 km grid space) VIKING20 model, which is nested in the global ocean/sea-ice model ORCA025 and represents ocean circulation variability in the northern North Atlantic at great verisimilitude[29] (Supplementary Fig. 3). For the WSC, the model yields two modes (offshore and nearshore) with respect to the meandering of the main, warm core of the WSC (Fig. 2, Supplementary Fig. 3d, e). During the offshore mode, the WSC separates into a warm offshore component and a cold undercurrent, which flows closely along the shelf break. The increase of the undercurrent causes stronger tilts of the isotherms and results in comparably cold bottom water temperatures. As a consequence, bottom waters at the shelf break and on the shelf are of similar density. The ArW on the shelf and fjord waters, both of which are characterised by a high MOx capacity[6,21], can thus be entrained downslope and contribute to the cAW, a situation that we observed during the August 18/19 survey. As a result, it is plausible that the high standing stock of methanotrophs in cAW partly originates from the shelf. The slow-flowing East Spitsbergen Current and the sheltered fjords lead to comparably long water mass residence times, ensuring continuity of methane supply and supporting MOx community development in the shelf waters. During the nearshore mode, which is representative of the situation that we encountered during the August 30/31 survey, the warm core of the WSC flows closely along the shelf break, replacing the cAW with wAW and separating shelf and deeper AIW. The open-ocean origin of the WSC[24] makes an exposure to elevated methane concentrations in the history of the wAW unlikely, and could therefore explain the low standing stock of methanotrophs in this water mass.

The dynamics and magnitudes of bottom water temperatures and current velocities simulated by our model correspond well to recorded long-term measurements at the shelf break of the Svalbard margin[19,24]. Modelled and observational data indicate a transition time of 5-10 days between the two described modes. The meandering of the WSC appears to be associated with far-field variations and internal variability of the WSC, but this causality is non-linear so that the exact timing of the observed switch between the off- and nearshore mode cannot be predicted. Yet, both our model results as well as measured data from previous work[19,24] indicate that the WSC predominantly flows along the shelf break, whereas the offshore mode, with cAW at the bottom and a high MOx capacity in the water column, occurs only 15 % of the time.

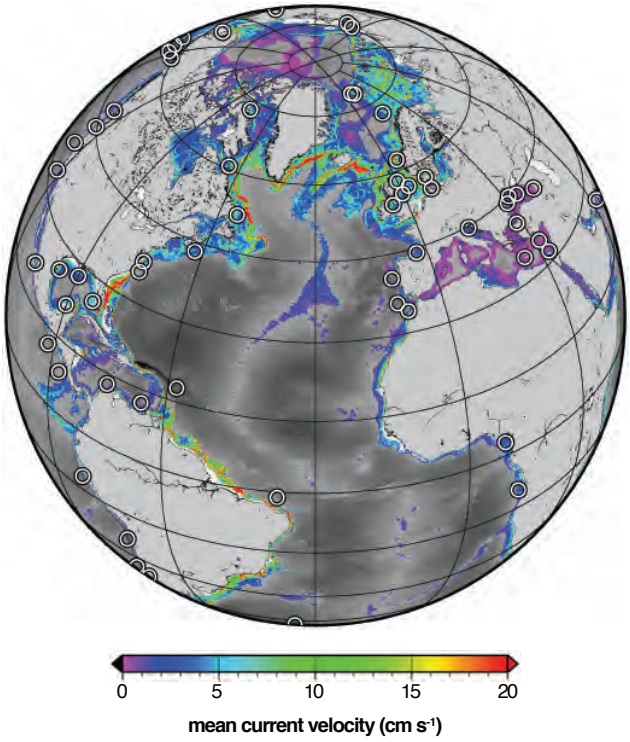

Fig. 3: Modelled bottom current velocity at methane seeps. Modelled (1/12° resolution) mean annual (year 2000) bottom water current velocities for bottom depths between 100 and 2500 m. Current velocities at continental margins, where most methane seeps are located, frequently exceed 10 cm s^{-1} and can be highly variable (cf. Supplementary Fig. 4). White circles indicate locations of selected methane seeps.

At the Svalbard margin, methane flares were observed along a 22 km-long stretch of the upper slope at around 390 m water depth[19,20]. Our model results, together with the measurements of MOx activity and water mass properties, indicate that the entire area is similarly affected by water mass exchange. When spatially extrapolating MOx rate measurements from the transect samplings to the whole seep area (66 km^2), total MOx amounted to 0.28 t CH_4 d^{-1} on August 18/19, and was reduced by 66 % on August 30/31

(Tab. 1). Based on the maximum measurements, the capacity of the MOx filter in the studied seep area could well exceed 100 t CH_4 yr^{-1}, but this potential remains largely unexploited because the predominant nearshore mode of the WSC reduces MOx capacity to 45 t CH_4 yr^{-1}. Similar to our measurements, varying MOx activities were detected in systems affected by differential circulation patterns and water mass mixing (Black Sea[11]; Santa Monica Basin[18]), and only low water column MOx activities were found at highly active methane seeps influenced by strong bottom currents (Hydrate Ridge[17]; Haakon Mosby Mud Volcano[30]). Currents result in relatively short water mass residence times above methane point sources, so that not enough time and continuity is provided for the development of large methanotrophic communities. Similarly, a well-established MOx community will be swept away from the methane source with the onset of water mass exchange. Dissolved methane, together with the methanotrophic community, will be dispersed leeward where ongoing MOx activity reduces methane concentrations further[7], most probably at rates controlled by the size of the MOx community. With respect to methane emission to the atmosphere, the impact of currents on water column MOx thus seems strongest in shallow-water cold seep environments, where the spatiotemporal distance between seafloor methane venting, water column methane consumption and methane evasion to the atmosphere is short. Most methane seeps are located along continental margins, where bottom water currents are commonly strong and fluctuating, as shown by our results from a global, high-resolution circulation model (ORCA12; Fig. 3, Supplementary Fig. 4). We thus argue that the variability of physical water mass transport is a globally important control on the distribution and abundance of methanotrophs and, as a consequence, on the efficiency of methane oxidation above point sources.

Data Availability:

All data presented in this paper are available in the PANGAEA data library (www.pangaea.de). In-depth information on the ORCA12 and VIKING20 models (data and code) will be provided on request.

References

1. Boetius, A. & Wenzhofer, F. Seafloor oxygen consumption fuelled by methane from cold seeps. *Nat. Geosci.* **6,** 725-734 (2013).
2. Reeburgh, W. S. Oceanic methane biogeochemistry. *Chem. Rev.* **107,** 486-513 (2007).
3. Sansone, F. J. & Martens, C. S. Methane oxidation in Cape Lookout Bight, North Carolin. *Limnol. and Oceanogr.* **23,** 349-355 (1978).
4. Semrau, J. D., DiSpirito, A. A. & Yoon, S. Methanotrophs and copper. *FEMS Microbiol. Rev.* **34,** 496-531 (2010).
5. Kessler, J. D., Valentine, D. L., Redmond, M. C., Du, M. R., *et al.* A Persistent Oxygen Anomaly Reveals the Fate of Spilled Methane in the Deep Gulf of Mexico. *Science* **331,** 312-315 (2011).
6. Mau, S., Blees, J., Helmke, E., Niemann, H. & Damm, E. Vertical distribution of methane oxidation and methanotrophic response to elevated methane concentrations in stratified waters of the Arctic fjord Storfjorden (Svalbard, Norway). *Biogeosciences* **10,** 6267-6278 (2013).
7. Crespo-Medina, M., Meile, C. D., Hunter, K. S., Diercks, A. -R., *et al.* The rise and fall of methanotrophy following a deepwater oil-well blowout. *Nat. Geosci.* **7,** 423-427 (2014).
8. Wallmann, K., Pinero, E., Burwicz, E., Haeckel, M., *et al.* The Global Inventory of Methane Hydrate in Marine Sediments: A Theoretical Approach. *Energies* **5,** 2449-2498 (2012).
9. Knittel, K. & Boetius, A. Anaerobic Oxidation of Methane: Progress with an Unknown Process. *Annu. Rev. of Microbiol.* **63,** 311-334 (2009).
10. Kirschke, S., Bousquet, P., Ciais, P., Saunois, M., *et al.* Three decades of global methane sources and sinks. *Nat. Geosci.* **6,** 813-823 (2013).
11. Reeburgh, W. S., Ward, B. B., Whalen, S. C., Sandbeck, K. A., *et al.* Black-Sea Methane Geochemistry. *Deep-Sea Res. Pt. I* **38,** 1189-1210 (1991).
12. Hanson, R. S. & Hanson, T. E. Methanotrophic bacteria. *Microbiol. Rev.* **60,** 439-471 (1996).
13. Murrell, J. C. in *Handbook of Hydrocarbon and Lipid Microbiology* (eds Timmis, K. N.) 1953-1966 (Springer, Berlin, 2010).
14. Ferré, B., Mienert, J. & Feseker, T. Ocean temperature variability for the past 60 years on the Norwegian-Svalbard margin influences gas hydrate stability on human time scales. *J. Geophy. Res.-Oceans* **117,** 10.1029/2012JC008300 (2012).
15. Biastoch, A., Treude, T., Rüpke, L. H., Riebesell, U., *et al.* Rising Arctic Ocean temperatures cause gas hydrate destabilization and ocean acidification. *Geophys. Res. Lett.* **38,** DOI: 10.1029/2011GL047222 (2011).
16. Wilkins, D., van Sebille, E., Rintoul, S. R., Lauro, F. M. & Cavicchioli, R. Advection shapes Southern Ocean microbial assemblages independent of distance and environment effects. *Nat. Commun.* **4,** (2013).
17. Heeschen, K. U., Collier, R. W., de Angelis, M. A., Suess, E., *et al.* Methane sources, distributions, and fluxes from cold vent sites at Hydrate Ridge, Cascadia Margin. *Glob. Biogeochem. Cy.* **19,** (2005).
18. Heintz, M. B., Mau, S. & Valentine, D. L. Physical control on methanotrophic potential in waters of the Santa Monica Basin, Southern California. *Limnol. Oceanogr.* **57,** 420-432 (2012).
19. Berndt, C., Feseker, T., Treude, T., Krastel, S., *et al.* Temporal Constraints on Hydrate-Controlled Methane Seepage off Svalbard. *Science* **343,** 284-287 (2014).
20. Westbrook, G. K., Thatcher, K. E., Rohling, E. J., Piotrowski, A. M., *et al.* Escape of methane gas from the seabed along the West Spitsbergen continental margin. *Geophys. Res. Lett.* **36,** (2009).

21. Gentz, T., Damm, E., Schneider von Deimling, J., Mau, S., *et al*. A water column study of methane around gas flares located at the West Spitsbergen continental margin. *Cont. Shelf Res*. **72,** 107-118 (2014).
22. Damm, E., Mackensen, A., Budéus, G., Faber, E. & Hanfland, C. Pathways of methane in seawater: Plume spreading in an Arctic shelf environment (SW-Spitsbergen). *Cont. Shelf Res*. **25,** 1453-1472 (2005).
23. Damm, E., Kiene, R. P., Schwarz, J., Falck, E. & Dieckmann, G. Methane cycling in Arctic shelf water and its relationship with phytoplankton biomass and DMSP. *Mar. Chem*. **109,** 45-59 (2008).
24. Schauer, U., Fahrbach, E., Osterhus, S. & Rohardt, G. Arctic warming through the Fram Strait: Oceanic heat transport from 3 years of measurements. *J. Geophy. Res.-Oceans* **109,** 14 (2004).
25. Blindheim, J. Arctic intermediate water in the Norwegian sea. *Deep-Sea Res. Pt. I* **37,** 1475-1489 (1990).
26. Bourke, R. H., Weigel, A. M. & Paquette, R. G. The westward turning branch of the West Spitsbergen Current. *J. Geophy. Res.-Oceans* **93,** 14065-14077 (1988).
27. Loeng, H. Features of the physical oceanographic conditions of the Barents Sea. *Polar Res*. **10,** 5-18 (1991).
28. Carini, S., Bano, N., LeCleir, G. & Joye, S. B. Aerobic methane oxidation and methanotroph community composition during seasonal stratification in Mono Lake, California (USA). *Environ. Microbiol*. **7,** 1127-1138 (2005).
29. Fischer, J., Karstensen, J., Zantopp, R., Visbeck, M., *et al*. Intra-seasonal variability of the DWBC in the western subpolar North Atlantic. *Prog. Oceanogr*. 10.1016/j.pocean.2014.04.002 (2014).
30. Sauter, E. J., Muyakshin, S. I., Charlou, J. L., Schluter, M., *et al*. Methane discharge from a deep-sea submarine mud volcano into the upper water column by gas hydrate-coated methane bubbles. *Earth Planet. Sc. Lett*. **243,** 354-365 (2006).

Correspondence and requests for materials should be addressed to helge.niemann@unibas.ch and lea.steinle@unibas.ch.

Acknowledgements

We thank the Captains, crews and shipboard scientific parties of R/V Poseidon and R/V Maria S. Merian for their help at sea. This work received financial support through a D-A-CH project funded by the Swiss National Science Foundation and German Research foundation (grant no. 200021L_138057). Further support was provided through the EU COST Action PERGAMON (ESSEM 0902), a Postgraduate Scholarship of the National Research Council of Canada, the Centre of Excellence "CAGE" funded by the Norwegian Research Council (grant no. 223259) and the Cluster of Excellence "The Future Ocean" funded by the German Research Foundation.

Author Contributions

L.S., C.G., T.T., I.B., J.G., C.J.S. S.S. and H.N. collected the samples and performed measurements of biogeochemical rates and/or physicochemical parameters. L.S. carried out enumeration of microbial cells. A.B., B.F., J.G., E.B., C.W.B. and M.S. conducted oceanographic modelling, interpretation and/or graphical representation. C.B. and S.K. were responsible for acoustic measurements. H.N., T.T., R.H.J. and M.F.L supervised research. L.S. and H.N led the development of the manuscript and all co-authors contributed to data interpretation and writing of manuscript.

The authors declare no competing financial interests.

Supplementary Information

1. Physiochemical and biogeochemical water column parameters

1.1 Temperature and salinity

Temperature and salinity were measured with a Seabird SBE911 CTD (CTD: conductivity/temperature/density probe; Seabird-Electronics, USA) equipped with dual temperature and conductivity sensors. For monitoring sensor performance, we conducted several CTD casts with a third set of temperature and conductivity sensors (SAIV A/S SN363, Norway, calibrated by SAIV A/S directly before the cruise). The offsets between the Seabird and SAIV were ≤0.01°C and ≤0.04 psu. During the MSM21/4 cruise, most CTD casts were taken at the MASOX site (78°33.3'N, 9°28.6'E; ~380 m water depth; ref 1) and/or along a transect crossing this site. One additional CTD cast was performed ~6.4 km further north at the HyBIS site (78°36.68'N, 009°25.50'E; cf. Fig. 1a; ref 1). During the POS419 cruise, CTD casts were also performed using a Seabird SBE911 device at three stations between the MASOX and HyBIS site and at one station ~8.8 km south of the MASOX site (Fig. 1a). For a complete station list see Supplementary Tab. 1.

1.2 Methane concentrations

For analysis of methane concentrations and MOx rates at discrete water depths, we sampled the water column with 24 × 10 L PTFE-lined Niskin bottles mounted on a CTD/Rosette sampler and sub-samples were taken immediately upon recovery of the sampler[1]. During the MSM21/4 cruise, methane was analysed with a headspace technique and gas chromatography with flame ionisation detection[1]. Briefly, ~ 600 mL seawater was subsampled bubble-free into triple-layer Evarex Barrier Bags (Oxford Nutrition, U.K.) followed by the addition of a headspace (20 mL N_2) and equilibration for several hours. Methane concentrations were determined by gas chromatography (Agilent 7890A GC; 80/100 mesh HayeSep Q packed stainless steel column, 1.83 m length, 2 mm i.d.; flame ionization detector set at 250 °C; oven operated isocratically at 60 °C; N_2 carrier gas at 33 mL min^{-1}) from a 2 mL aliquot of the headspace. The GC system was calibrated with external standards (20 ppm methane standard, Air Liquide, Germany), and reproducibility (determined by 3 replicate analyses of an individual sample) was < ± 5 %. During the POS419 cruise, methane concentrations were analysed with a slightly modified headspace method with respect to sampling vials (120 mL glass vials, 5 mL N_2 headspace, fixed with 0.5 mL saturated aqueous $HgCl_2$ solution) and manufacturers of analytical instruments (Thermo Scientific FOCUS GC, direct injection; Resteck packed column HayeSep Q 80/100, 2 m length, 2 mm i.d.; flame ionization detector

set at 170 °C; oven temperature was ramped from 40 to 120 °C in steps, H_2 carrier gas at 33 mL min^{-1}). Seawater methane concentrations and the degree of saturation with respect to the atmospheric equilibrium were calculated with consideration of sample and headspace volume, temperature, salinity, atmospheric pressure and atmospheric CH_4 mixing ratio[2,3].

1.3 Methane oxidation rates

MOx rates were determined at sea from *ex situ* incubations with trace amounts of tritium-labelled methane (^3H-CH_4) similarly to published methods[4,5] with some modifications[6]. For each depth, four crimp-top vials (20 mL) were filled bubble-free and closed with bromobutyl stoppers (Helvoet Pharme, Belgium), amended with 10 μl gaseous ^3H-CH_4/N_2 mixture (~25 kBq, <50 pmol CH_4, American Radiolabeled Chemicals, USA) and incubated for 72 h at *in situ* temperature in the dark. Linearity of MOx during the incubation time period (~72 h) was confirmed by replicate incubations at 24, 48 and 72 h. MOx rates were corrected for (insubstantial) tracer turnover in killed controls (addition of 100 μL, saturated aqueous $HgCl_2$ solution). Rates on the POS419 cruise were measured analogously, but instead of 20 mL we incubated in 120 mL bromobutyl-sealed (Ochs, Germany) crimp top vials with an amendment of 100 μl tracer gas. Single or triplicate incubations were conducted for each depth. MOx rates were calculated from the fractional turnover of labelled CH_4 and water column CH_4 concentration assuming first order kinetics[5]. Average standard deviation between replicates was ±20.4 % for MSM21/4 incubations and ±38 % for POS419 incubations.

1.4 Biomass estimation of methanotrophs

The identity and abundance of aerobic methanotrophic bacteria (MOB) was investigated by catalysed reporter deposition fluorescence *in situ* hybridisation (CARD-FISH; refs 7,8) from samples collected during the MSM 21/4 cruise. A 100 mL seawater aliquot was fixed for ~4 h with formaldehyde (1.5 % final concentration) at 4 °C. The fixed sample was filtered through a polycarbonate filter (Whatman Nuclepore black track-etched polycarbonate membrane filter, 25 mm diameter, 0.2 μm pore size) with a gentle vacuum-pressure of 0.5 bar. Filters were air-dried and stored at -20 °C until further analyses. Cells embedded on the filter were permeabilised with lysozyme[7], followed by inactivation of endogenous peroxidases in a 0.15 % H_2O_2/methanol solution for 30 min at room temperature. Filters were then washed successively in sterile MilliQ (1 min) and aqueous ethanol solution (96 %, v/v; 2 min) and finally air-dried. Filters were hybridised with ~300 μl hybridisation buffer for 3 h at 46 °C. The buffer contained either a mix of probes Mγ705-HRP and Mγ84-HRP (0.3 ng μL^{-1} each), or probe Mα450-HRP (0.6 ng μL^{-1}) for the detection of Type I and Type II MOx communities, respectively[9]. Negative controls (sulphide-oxidizing mixed culture, enriched

from a freshwater lake) were used to ensure specificity of probe binding with our hybridisation conditions.

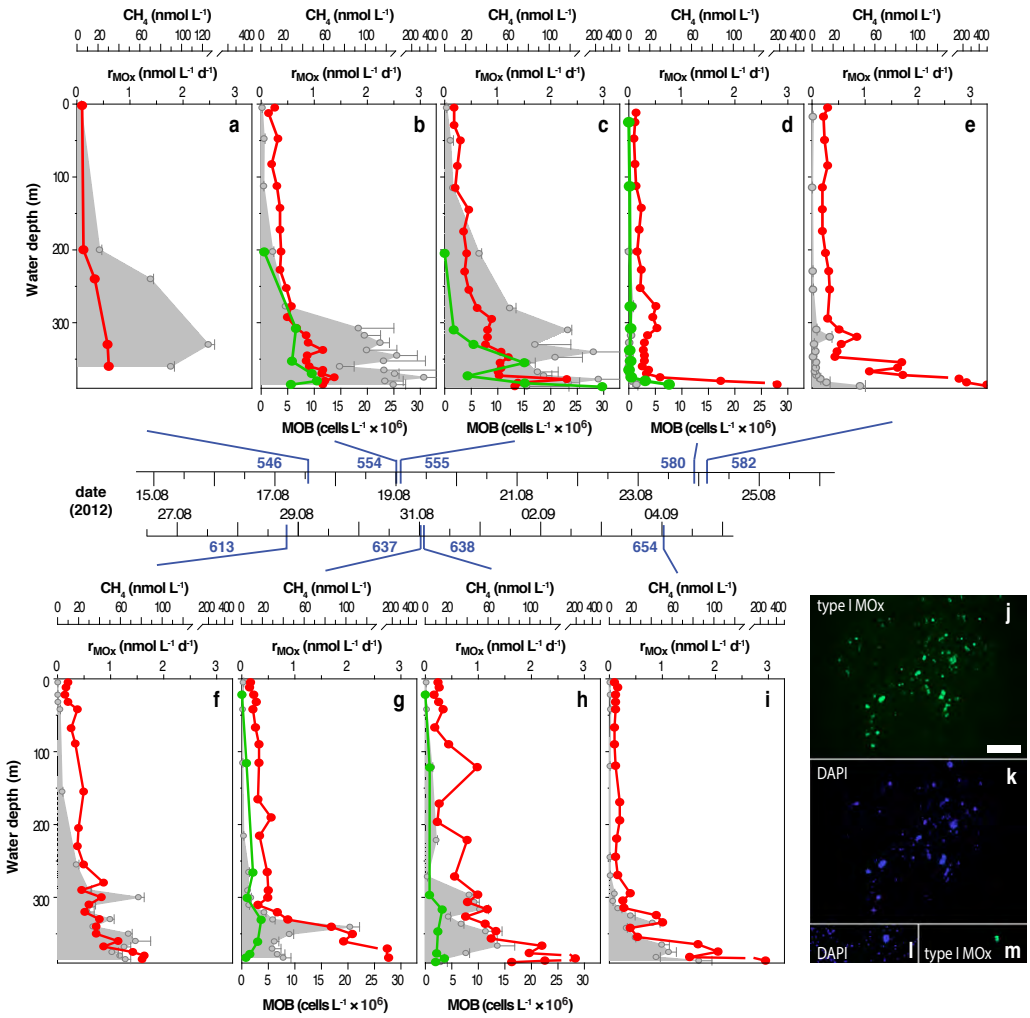

n					MOx	
Date (2012)	Stat. no.	Site	BW conditions	WSC mode	max (nmol L^{-1} d^{-1})	depth integr. (μmol m^{-2} d^{-1})
17 Aug.	546	MASOX	cAW	offshore	2.5	349
19 Aug.	554	MASOX	cAW	offshore	3.1	251
19 Aug.	555	MASOX	cAW	offshore	2.9	314
23 Aug.	580	MASOX	wAW	onshore	0.2	7
24 Aug.	582	MASOX	wAW	onshore	0.9	16
28 Aug.	613	MASOX	wAW/cAW	on-/offshore	1.5	147
31 Aug.	637	MASOX	wAW	onshore	2.0	72
31 Aug.	638	MASOX	wAW	onshore	1.4	121
04 Sep.	654	MASOX	wAW	onshore	1.7	61

Supplementary Figure 1: Methane concentrations, methane oxidation rates and methanotrophic cell numbers from repeated sampling campaigns at the MASOX site. a-i, Methane concentration (red), methane oxidation rates (grey), and b, c, d, g, h, cell numbers of type I aerobic methanotrophic bacteria (MOB; green), at the MASOX site measured during the MSM21/4 cruise at different dates (chronological station numbers are indicated in blue). Error bars of MOx represent standard deviation (n=4). j-m, Micrographs of water column microbes from samples collected at 380 m water depth at the MASOX site (station 554).

Type I MOB cells were quantified by CARD-FISH (j, m; in green; mixture of probes Mγ705-HRP and Mγ84-HRP) and DAPI (=total cells; k, l, in blue) staining, followed by epifluorescence microscopy. The scale bar represents 10 μm. Type I MOB cells occurred as m, single/double cells, or j, as loose 'aggregates'. Stations 554/555 and 637/638 were sampled during transect samplings on Aug. 18/19 and Aug. 30/31, respectively. n, Maximum and depth integrated MOx rates at the MASOX site (cf. a-g) in relation to the presence of cAW or wAW at the sea floor. Together with the MOx community size, the MOx filter capacity was only elevated in relatively cold and saline bottom waters (<4 °C, >34.9 psu; cf. Supplementary Fig. 2a), which were solely present during the offshore mode of the WSC.

Catalysed reporter deposition and DAPI staining was carried out according to published recommendations[8] with an amplification time of 20 min at 37 °C in a buffer containing 1 μL of the labelled tyramide (Alexa488: Invitrogen A20000, lot 1252193; USA). Filters were finally washed for 10 min in PBS. We used Citifluor AF1 (Citifluor Ltd., U.K.) as mountant for fluorescence microscopy. CARD-FISH- and DAPI-stained samples were examined with an epifluorescence microscope (Leica DM2500 equipped with the external ultraviolet light source, EL6000) at a 1000-fold magnification. For each sample, ~1000 DAPI-stained cells in ≥ 10 microscopic fields were counted. Total cell numbers in the lowest 200 m of the water column were similar between sampling dates ($2.09 \pm 0.14 \times 10^8$ cells L^{-1}), while surface water generally contained higher cell numbers (up to 10.8×10^8 cells L^{-1}) with higher variations between sampling dates (data not shown).

Type I MOB cells occurred as single/double cells (Supplementary Fig. 1m) or as loose 'aggregates' (Supplementary Fig. 1j). To account for the heterogeneous distribution of the aggregates, we counted 70 microscopic fields for each sample (average StDev. of MOB cell numbers between grids for one sample: ± 37%). Type II MOB cells accounted for less than 1 % of all MOB cells (data not shown), and were thus of minor importance for the water column MOx filter capacity.

Water samples collected at the MASOX site during the MSM21/4 cruise concomitantly showed elevated type I MOB cell numbers and MOx rates (Supplementary Fig. 1). Vice versa, water samples characterised by low MOx rates generally contained low numbers of MOB cells. Although MOx was maximal in bottom waters with elevated methane concentrations (Fig. 1c, Supplementary Fig. 1), we frequently encountered low levels of MOx activity (and methanotrophic biomass) in bottom water samples with high methane concentrations. MOx activity was thus determined by MOx biomass rather than methane substrate availability (Supplementary Figs. 2a, b). Furthermore, together with the MOx community size, the MOx filter capacity (see MOx rates in Supplementary Fig. 1) was only elevated in relatively cold and saline bottom waters (<4 °C, >34.9 psu, Supplementary Fig. 2c), which were only present during the offshore mode of the West Spitsbergen Current (WSC).

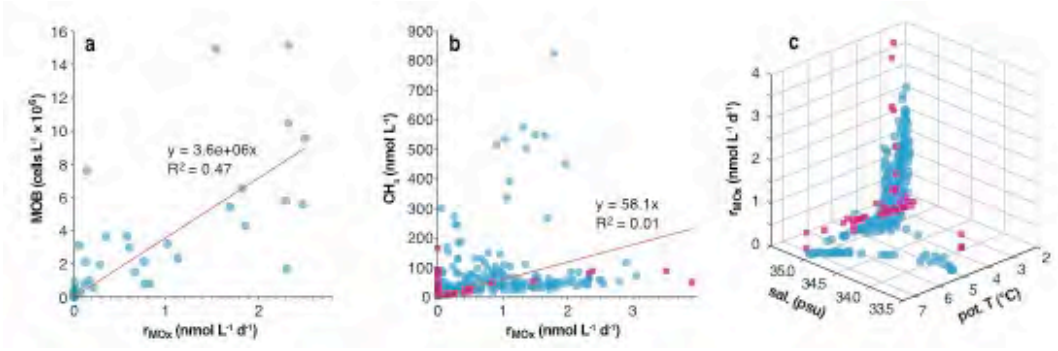

Supplementary Figure 2: Aerobic methane oxidation in relation to bottom water properties. Methane oxidation rates (r_{MOX}) in relation to a, cell numbers of type I aerobic methane oxidising bacteria, b methane concentration and, c salinity and temperature, measured during the MSM21/4 (cyan dots) and POS419 (pink squares) cruise. Note that MOB cell numbers were only determined from selected samples from the MASOX site collected during the MSM21/4 cruise, while methane concentration, salinity and temperature were determined for all samples designated for MOx rate measurements. Linear correlation for b, includes all samples from MSM21/4 and POS419.

1.5 Interpolation and extrapolation of physiochemical and biogeochemical water column parameters.

Values of physiochemical and biogeochemical water column parameters were measured at discrete stations, and, in case of methane concentration and MOx activity, in discrete water depths, during the transect sampling campaigns (Aug. 18/19 and 30/31). Depth-integrated areal MOx rates were determined by linear interpolation between measured rates and extrapolation to a water column of 1 m^2. For representation as contour plots (Fig 1b-e), discrete values were linearly interpolated by using the Matlab software package. For extrapolating MOx rates to the known seep area, we first calculated weighted averages from the interpolated MOx rates (Fig. 1c) for the two sampling campaigns. These averages (0.7 and 0.2 nmol L^{-1} d^{-1} for Aug. 18/19 and 30/31, respectively) were then extrapolated to the whole water volume in the seep area (3 km width × 22 km length × 0.388 km average water depth).

2. Regional hydrographic changes in a wider oceanographic context

For a deeper understanding of the hydrographic changes west off the Svalbard shelf and the interplay with the large-scale circulation, we utilised 5-daily output from the VIKING20 model, a high-resolution ocean/sea-ice simulation[10,11]. Based on the NEMO code[12], VIKING20 has a 1/20° grid cell size of the subpolar/subarctic North Atlantic (32°N - 85°N) (ref 10) and is two-way nested[13] in a global 1/4° configuration (ORCA025 grid; ref 11). It is forced by atmospheric data covering synoptic (6-hourly to daily), seasonal, interannual to

decadal timescales of the years 1948-2007 (ref 11). With a ~2.5 km grid space off West-Spitsbergen and 46 vertical levels (20 in the upper 500 m), VIKING20 realistically captures both the large-scale circulation and the mesoscale variability in the subpolar/subarctic North Atlantic by great verisimilitude[14], both with detailed mean flow characteristics[15] and temporal variability on short-term to decadal time scales[16]. The circulation in the Fram Strait, for instance, shows the same variability along the eastern boundary, with northward velocities up to 40 cm s^{-1} and beyond, as observed by Schauer et al., 2004 (ref 17). Modelled bottom current velocity (Fig. 2) agrees well with measurement data from the MASOX observatory (10 cm s^{-1} on average; ref 1).

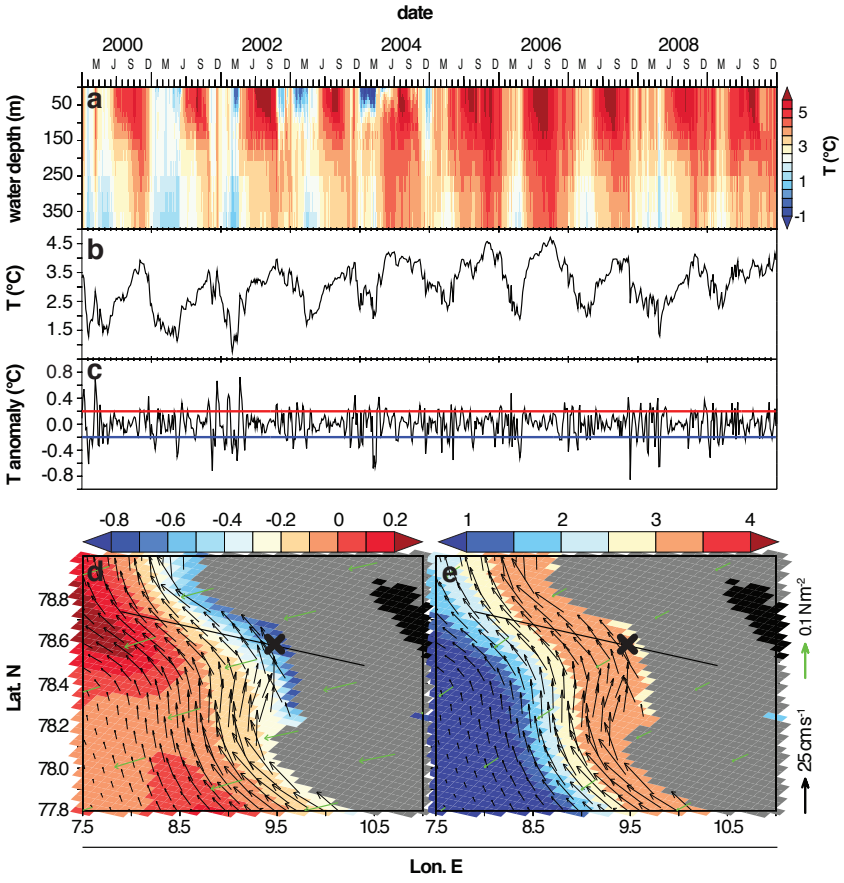

Supplementary Figure 3: Modelled temporal progression of water temperature and circulation patterns of the WSC. Temperature distribution in a, the entire water column (surface to bottom), and b, bottom waters (300 m water depth), as well as c, bottom water temperature corrected for seasonal and interannual temperature variations at the MASOX site. d, Time-averaged circulation patterns of the WSC at 300 m water depth during the offshore mode (temperature anomaly against long-term average, colour-coded, °C), and e, the nearshore mode (long-term averaged temperature, colour-coded, °C). The MASOX position is indicated with a cross mark. Current velocities are indicated as black arrows and wind forcing as green arrows. The vertical distribution of time-averaged temperature, density and current velocity, respectively, along a cross-section over the MASOX site (black line) is shown in Fig. 2.

Water column temperatures at the MASOX site (Supplementary Fig. 3a, b) greatly vary on seasonal and interannual timescales, but also show distinct minima and maxima (Supplementary Fig. 3c) strongly deviating from the (seasonally and interannually varying) temperature mean. These minima and maxima are caused by the variable position of the main, warm core of the WSC. Supplementary Fig. 3d shows time-averaged circulation patterns of the WSC along the offshore flank of the study area at 300 m water depth. The geographical position of the MASOX site is indicated with a cross mark. During time periods of cold bottom water temperature anomalies (i.e., greater than one standard deviation below the seasonally and interannually varying temperature mean; blue line in Supplementary Fig. 3c), the main core of the WSC is located offshore, giving rise to a cold undercurrent at the shelf break (Supplementary Fig. 3d), and thus to the observed and modelled cold bottom water temperatures at the shelf break. The comparably strong northward tilting of the flares that we observed during hydroacoustic surveys just before our samplings on August 17 and 18/19 (data not shown) indicates the presence of this fast undercurrent. In contrast, when the main core is meandering to the shore, the warm water of the WSC replaces the cold bottom water, resulting in the rise of bottom water temperatures. This nearshore mode corresponds to observed and modelled average and anomalously warm bottom water temperatures (i.e., values above one standard deviation above the seasonally and interannually varying temperature mean; red line in Supplementary Fig. 3c). The time-averaged circulation pattern of the nearshore mode is shown in Supplementary Fig. 3e. The meandering of the main core is caused by far-field and internal variations of the WSC, leading to a nonlinear behavior of the current with transition times between offshore- and nearshore mode of 5-10 days.

Global bottom water velocities at continental margins were analyzed using a global variant of the ocean/sea-ice model at 1/12° resolution (ORCA12). Similar to VIKING20, this model has been forced by atmospheric data[14], but over a shorter timeframe (1978-2003). Highly variable near-bottom currents are common along continental slopes and below regions of strong surface currents[18].

Supplementary Figure 4 (next page): Modelled bottom current velocity and standard deviation of current velocities at methane seeps. a, Modelled (1/12° resolution) mean annual (year 2000) bottom water current velocities and, b, standard deviation of bottom current velocities (based on 5-day averages) for bottom depths between 100 and 2500 m. Bottom current velocities at continental margins, where most methane seeps are located, frequently exceed 10 cm s^{-1} and are highly variable. Standard deviations typically exceed 50% of the mean flow. White circles indicate locations of selected methane seeps.

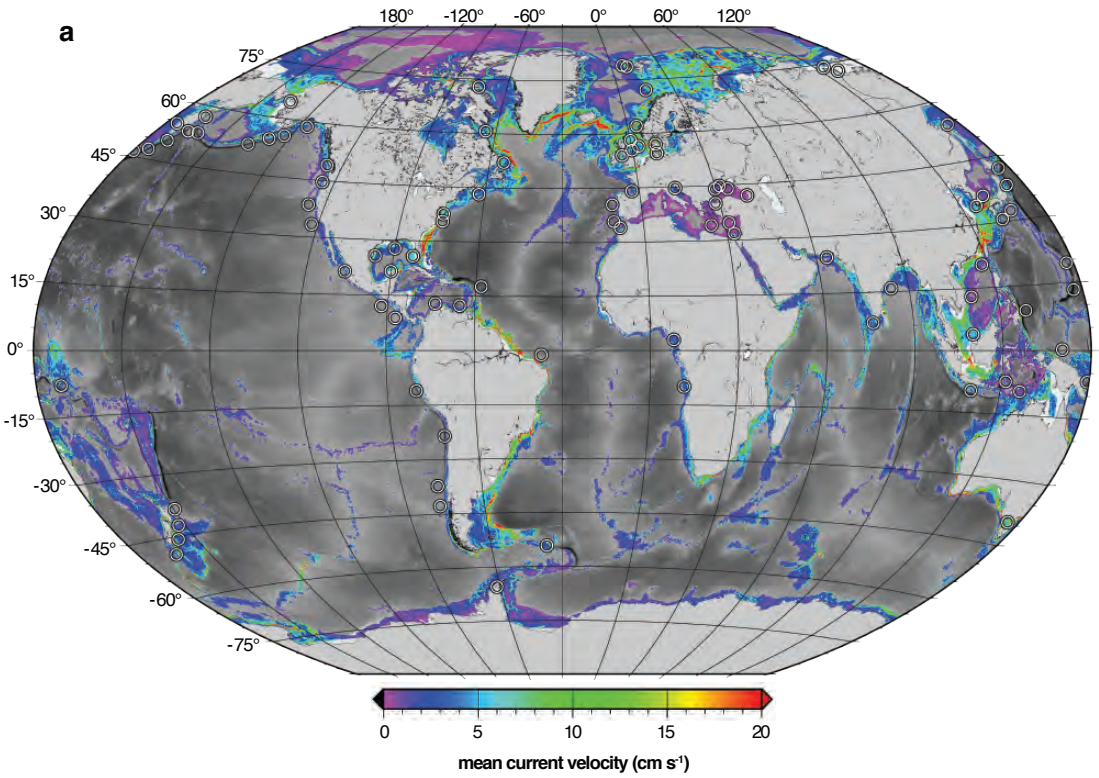
a
180°
-120°
-60°
0°
60°
120°
75°
60°
45°
30°
15°
0°
-15°
-30°
-45°
-60°
-75°
0
5
10
15
20
mean current velocity (cm s-1)

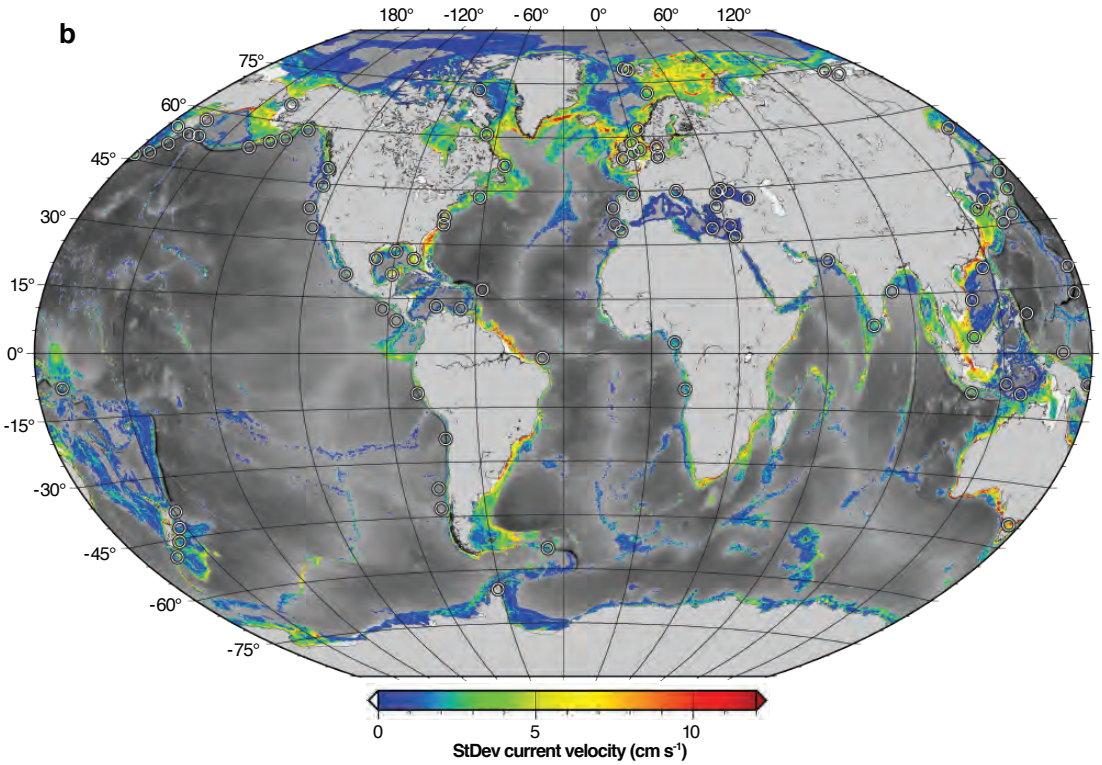
b
180°
-120°
- 60°
0°
60°
120°
75°
60°
45°
30°
15°
0°
-15°
-30°
-45°
-60°
-75°
0
5
10
StDev current velocity (cm s-1)

Supplementary Table 1: List of Stations sampled during the POS419 and MSM21/4 cruises. The numbers of bottles sampled per CTD cast are indicated.

									# niskin bottles sampled		
Cruise	**Station**	**Transect**	**Site**	**Date**	**Lat. (N)**	**Lon. (E)**	**Salinity**	**Temperature**	**CH_4**	**MOx**	**CARD-FISH**
POS419	599	-	CTD-2	13.08.11	78.585	9.458	x	x	12	12	-
POS419	615	-	CTD-9	17.08.11	78.585	9.456	x	x	12	12	-
POS419	654	-	CTD-33	23.08.11	78.585	9.455	x	x	12	12	-
POS419	671	-	CTD-36	27.08.11	78.585	9.456	x	x	12	12	-
MSM21/4	546	-	MASOX	17.08.12	78.555	9.477	x	x	5	5	-
MSM21/4	550	1st	-	18.08.12	78.553	9.423	x	x	24	6	-
MSM21/4	551	1st	-	18.08.12	78.554	9.446	x	x	24	6	-
MSM21/4	552	1st	-	18.08.12	78.554	9.455	x	x	24	10	-
MSM21/4	553	1st	-	19.08.12	78.555	9.466	x	x	24	14	-
MSM21/4	554	1st	MASOX	19.08.12	78.555	9.475	x	x	24	17	6
MSM21/4	555	1st	MASOX	19.08.12	78.555	9.479	x	x	24	17	7
MSM21/4	556	1st	-	19.08.12	78.555	9.487	x	x	24	14	-
MSM21/4	557	1st	-	19.08.12	78.556	9.496	x	x	23	10	-
MSM21/4	558	1st	-	19.08.12	78.556	9.508	x	x	23	6	-
MSM21/4	558	1st	-	19.08.12	78.557	9.522	x	x	23	6	-
MSM21/4	580	-	MASOX	23.08.12	78.556	9.474	x	x	24	16	10
MSM21/4	581	-	-	24.08.12	78.556	9.472	x	x	23	16	-
MSM21/4	582	-	MASOX	24.08.12	78.556	9.476	x	x	23	16	-
MSM21/4	583	-	-	24.08.12	78.555	9.476	x	x	23	16	-
MSM21/4	584	-	-	24.08.12	78.555	9.472	x	x	23	16	-
MSM21/4	613	-	MASOX	28.08.12	78.555	9.476	x	x	24	18	-
MSM21/4	633	2nd	-	30.08.12	78.553	9.423	x	x	24	7	-
MSM21/4	634	2nd	-	30.08.12	78.554	9.446	x	x	24	7	-
MSM21/4	635	2nd	-	30.08.12	78.554	9.456	x	x	23	10	-
MSM21/4	636	2nd	-	31.08.12	78.555	9.466	x	x	24	14	-
MSM21/4	637	2nd	MASOX	31.08.12	78.555	9.476	x	x	24	17	8
MSM21/4	638	2nd	MASOX	31.08.12	78.555	9.479	x	x	24	17	8
MSM21/4	639	2nd	-	31.08.12	78.556	9.487	x	x	24	14	-
MSM21/4	640	2nd	-	31.08.12	78.556	9.497	x	x	24	10	-
MSM21/4	641	2nd	-	31.08.12	78.556	9.508	x	x	24	7	-
MSM21/4	642	2nd	-	31.08.12	78.557	9.523	x	x	23	7	-
MSM21/4	654	-	MASOX	04.09.12	78.556	9.473	x	x	24	17	-
MSM21/4	655	-	HyBIS	04.09.12	78.611	9.425	x	x	24	17	-

Supplementary References

1. Berndt, C., Feseker, T., Treude, T., Krastel, S., *et al*. Temporal Constraints on Hydrate-Controlled Methane Seepage off Svalbard. *Science* **343,** 284-287 (2014).
2. Wiesenburg, D. A. & Guinasso, N. L. Equilibrium solubilities of methane, carbon monoxide, and hydrogen in water and sea water. *J. Chem. Eng. Data* **24,** 356-360 (1979).
3. Fisher, R. E., Sriskantharajah, S., Lowry, D., Lanoisellé, M., *et al*. Arctic methane sources: Isotopic evidence for atmospheric inputs. *Geophys. Res. Lett.* **38,** DOI: 10.1029/2011GL049319 (2011).
4. Valentine, D. L., Blanton, D. C., Reeburgh, W. S. & Kastner, M. Water column methane oxidation adjacent to an area of active hydrate dissociation, Eel River Basin. *Geochim. Cosmochim. Ac.* **65,** 2633-2640 (2001).
5. Reeburgh, W. S. Oceanic methane biogeochemistry. *Chem. Rev.* **107,** 486-513 (2007).
6. Niemann, H., Steinle, L., Blees, J. H., Krause, S., *et al*. Toxic effects of butyl elastomers on aerobic methane oxidation. *Limnolog and Oceanography: Methods*. **13**: 40-52 (2015).
7. Pernthaler, A., Pernthaler, J. & Amann, R. Fluorescence In Situ Hybridization and Catalyzed Reporter Deposition for the Identification of Marine Bacteria. *Appl. Env. Microb.* **68,** 3094-3101 (2002).
8. Pernthaler, A. & Pernthaler, J. Fluorescence in situ hybridization for the identification of environmental microbes. *Methods Mol. Biol.* **353,** 153-164 (2007).
9. Eller, G., Stubner, S. & Frenzel, P. Group-specific 16S rRNA targeted probes for the detection of type I and type II methanotrophs by fluorescence in situ hybridisation. *FEMS Microbiol. Lett.* **198,** 91-97 (2001).
10. Behrens, E. The oceanic response to Greenland melting: the effect of increasing model resolution (Christian Albrechts University, Kiel , Germany, 2013).
11. Behrens, E., Biastoch, A. & Böning, C. W. Spurious AMOC trends in global ocean sea-ice models related to subarctic freshwater forcing. *Ocean Model.* **69,** 39-49 (2013).
12. Madec, G. Nemo ocean engine, Note du Pole de modélisation, Institut Pierre-Simon Laplace (IPSL) No 27, France 2008).
13. Debreu, L., Vouland, C. & Blayo AGRIF: Adaptive Grid Refinement in Fortran. *Comput. Geosci.* **34,** 8-13 (2008).
14. Large, W. G. & Yeager, S. G. The global climatology of an interannually varying air–sea flux data set. *Clim. Dynam.* **33,** 341-364 (2009).
15. Mertens, C., Rhein, M., Walter, M., Böning, C. W., *et al*. Circulation and transports in the Newfoundland Basin, western subpolar North Atlantic. *J. Geophys. Res.-Oceans* **119,** 7772-7793 (2014).
16. Fischer, J., Karstensen, J., Zantopp, R., Visbeck, M., *et al*. Intra-seasonal variability of the DWBC in the western subpolar North Atlantic. *Prog. Oceanogr.* 10.1016/j.pocean.2014.04.002 (2014).
17. Schauer, U., Fahrbach, E., Osterhus, S. & Rohardt, G. Arctic warming through the Fram Strait: Oceanic heat transport from 3 years of measurements. *J. Geophys. Res.-Oceans* **109,** 14 (2004).
18. Cronin, M. F., Tozuka, T., Biastoch, A., Durgadoo, J. V. & Beal, L. M. Prevalence of strong bottom currents in the greater Agulhas system. *Geophys. Res. Lett.* **40,** 1772-1776 (2013)

.

Linked sediment and water-column methanotrophy at a man-made gas blowout in the North Sea: Implications for methane budgeting in seasonally stratified shallow seas

Lea Steinle[1,2,*], Mark Schmidt[2], Lee Bryant[2,a], Matthias Haeckel[2], Peter Linke[2], Stefan Sommer[2], Jakob Zopfi[1], Moritz F. Lehmann[1], Tina Treude[2,b], and Helge Niemann[1,3]

submitted to *Limnology & Oceanography* (currently under review)

[1] Department of Environmental Sciences, University of Basel, Basel, Switzerland

[2] GEOMAR, Helmholtz Centre for Ocean Research, Kiel, Germany

[3] CAGE – Centre for Arctic Gas Hydrate, Environment and Climate, Department of Geology, UiT the Arctic University of Norway, 9037 Tromsø, Norway

[a] Present address: Department of Architecture and Civil Engineering, University of Bath, Bath, UK

[b] Present address: Department of Earth, Planetary & Space Sciences and Atmospheric & Oceanic Sciences, University of Los Angeles, Los Angeles, California, USA

*Corresponding author: lea.steinle@unibas.ch

Abstract

Large quantities of the greenhouse gas methane (CH_4) are stored in the seafloor. The flux of CH_4 from the sediments into the water column and finally to the atmosphere is mitigated by a series of microbial methanotrophic filter systems of unknown efficiency at highly active CH_4-release sites in shallow marine settings. Here, we studied CH_4-oxidation and the methanotrophic community at a high-CH_4-flux site in the northern North Sea (well 22/4b), where CH_4 is continuously released since a blowout in 1990. Vigorous bubble emanation from the seafloor and strongly elevated CH_4 concentrations in the water column (up to 42 μM) indicated that a substantial fraction of CH_4 bypassed the highly active (up to ~2920 nmol cm^{-3} d^{-1}) anaerobic CH_4-oxidation zone in sediments. In the water column, we measured rates of CH_4-oxidation (up to 498 nM d^{-1}) that were among the highest ever measured in a marine environment and, under stratified conditions, have the potential to remove a significant part of the uprising CH_4 prior to evasion to the atmosphere. An unusual dominance of the water-column methanotrophs by Type II methane-oxidizing bacteria (MOB) is partially supported by recruitment of sedimentary MOB, which are entrained together with sediment particles in the CH_4 bubble plume. Our study thus provides evidence that bubble emission can be an important vector for the transport of sediment-borne microbial inocula, aiding in the rapid colonization of the water column by methanotrophic communities and promoting their persistence close to highly active CH_4 point sources.

Introduction

Even though large quantities of methane (CH_4) are stored in the ocean seafloor as shallow and deep gaseous reservoirs, bound in CH_4 hydrates or dissolved in pore water (Wallmann et al. 2012), most recent estimates suggest that oceans account for only a minor fraction of natural CH_4 emissions to the atmosphere (Kirschke et al. 2013; IPCC 2013). The fact that the marine contribution is rather small can largely be attributed to a series of microbial CH_4-oxidation filter systems preventing large-scale CH_4 evasion into the atmosphere (Reeburgh 2007; Knittel and Boetius 2009; Kessler et al. 2011; Boetius and Wenzhöfer 2013; Graves et al. 2015; Steinle et al. 2015). In sediments, a large fraction (~80% on average, Knittel and Boetius 2009) of uprising CH_4 is oxidized through sulfate-dependent anaerobic oxidation of CH_4 (AOM, *Eq. 1*).

$$CH_4 + SO_4^{2-} \rightarrow HCO_3^- + HS^- + H_2O \qquad (Eq.\ 1)$$

AOM is typically mediated by consortia of anaerobic methanotrophic archaea (ANME) and sulfate-reducing bacteria (SRB; Boetius et al. 2000; Orphan et al. 2001; Niemann et al. 2006)

though ANME may possibly mediate AOM without partner bacteria (Milucka et al. 2012). Furthermore, aerobic methane-oxidizing bacteria (MOB) consume part of the CH_4 flux in oxygenated surface sediments (aerobic oxidation of CH_4 – MOx; *Eq. 2*) and represent a second sedimentary filter (Niemann et al. 2006; Boetius and Wenzhöfer 2013).

$$CH_4 + 2O_2 \rightarrow CO_2 + 2H_2O \qquad (Eq.\ 2)$$

These sedimentary filters, however, are less effective in systems characterized by elevated advective fluxes of CH_4 (Treude et al. 2003; Niemann et al. 2006; Knittel and Boetius 2009; Steeb et al. 2014). Globally, 0.02 Gt yr^{-1} (3-3.5% of the atmospheric budget; Kirschke et al. 2013) of CH_4 is estimated to bypass the benthic filter systems and to be released into the ocean water column (Boetius and Wenzhöfer 2013). Within the water column, CH_4 can be oxidized aerobically, or anaerobically in the rare case of ocean water column anoxia (Reeburgh 2007).

MOx is performed by MOB, generally belonging to the Gamma- (Type I) or Alphaproteobacteria (Type II) (Hanson and Hanson 1996; Murrell 2010). In oceanic waters, MOB typically belong to the Type I group (Elsaied et al. 2004; Tavormina et al. 2008, 2010; Reed et al. 2009; Håvelsrud et al. 2011; Kessler et al. 2011; Steinle et al. 2015). The first step of MOx is catalyzed by the enzyme particulate or soluble methane mono-oxygenase (pMMO or sMMO, respectively; Semrau et al. 2010, and references therein).

Water-column MOx is the final sink for CH_4 before its release to the atmosphere, where it acts as a potent greenhouse gas; however, relatively little is known about the mechanisms and environmental factors controlling the spatio-temporal distribution and activity of pelagic MOB (Tavormina et al. 2010; Kessler et al. 2011; Mau et al. 2013; Crespo-Medina et al. 2014; Steinle et al. 2015). Previous studies showed that MOx, and the distribution of Type I and Type II MOB in the oceans, are controlled by CH_4 and O_2 concentrations (Kessler et al. 2011; Mau et al. 2013; Crespo-Medina et al. 2014) and trace metal availability (Semrau et al. 2010; Crespo-Medina et al. 2014). Furthermore, advection of water masses harboring distinct microbial communities can constrain prokaryote-biogeographic patterns (Wilkins et al. 2013). Current-induced water mass exchange at CH_4 seeps, for example, has been shown to control the distribution of water column MOx communities, thereby modulating the microbial CH_4 filter capacity in the water column (Steinle et al. 2015).

Knowledge of the physical and biogeochemical controls on the activity and distribution of MOB is particularly important for our understanding of the role of shallow water environments (e.g., shelf and coastal seas) in the global marine CH_4 budget. In contrast to deep-sea environments, the distance between the seafloor and the atmosphere is short in shallow-water settings, leaving limited time/space for quantitative CH_4 consumption to occur

prior to its release to the atmosphere (Graves et al. 2015). This effect is amplified when benthic CH_4 flux rates are particularly high. Accidents during oil and gas exploration, for example, can lead to the release of excessive amounts of CH_4 (and other hydrocarbons) to the ocean water column (Kessler et al. 2011; Sommer et al. 2015). Elevated CH_4 evasion is also expected as a result of intensified CH_4 hydrate destabilization and permafrost degradation in Arctic shelf environments in the future (Shakhova et al. 2010; Biastoch et al. 2011; Ferré et al. 2012; Berndt et al. 2014); yet it is unknown to which extent the sediment- and water-column methanotrophic filter systems will be able to adapt to high CH_4 fluxes, and hence to hinder excessive CH_4 liberation to the atmosphere. In support of evaluating future CH_4 seepage scenarios at high-latitude shelf environments, present-day CH_4 release sites in other shelf seas, such as those initiated or enhanced by drilling activities, provide a "natural" laboratory for studying the distribution and activity of methanotrophs, and thus the efficiency of the microbial CH_4 filter in sediment and the water column in high CH_4 flux settings.

Extensive shallow gas accumulations occur in North Sea sediments (Judd and Hovland 2007), and one of the gas pockets at well 22/4b (hereafter referred to as the "Blowout", Figure 1) was accidentally tapped during drilling operations in November 1990. This caused a massive blowout (Fox 1995), which left a 60-m wide crater behind (see below), with extensive amounts of CH_4 being released from its center until today (Schneider Von Deimling et al. 2015). In this study, we assessed the impact of the persistent and vigorous seabed CH_4 release from the Blowout on the methanotrophic community in sediments and the water column. In an interdisciplinary approach combining biogeochemical and molecular tools, we confirm that a stable and highly active AOM community may establish in ocean sediments within ~20 years after seepage onset (Wilfert et al. 2015). We further demonstrate that the aerobic methanotrophic communities in sediments and in the water column are linked. High water-column MOx rates are supported by the bubble-plume- associated entrainment of sediment-borne MOB, which restock the water-column methanotrophic community and thus help to maintain a highly efficient aerobic water-column CH_4 filter.

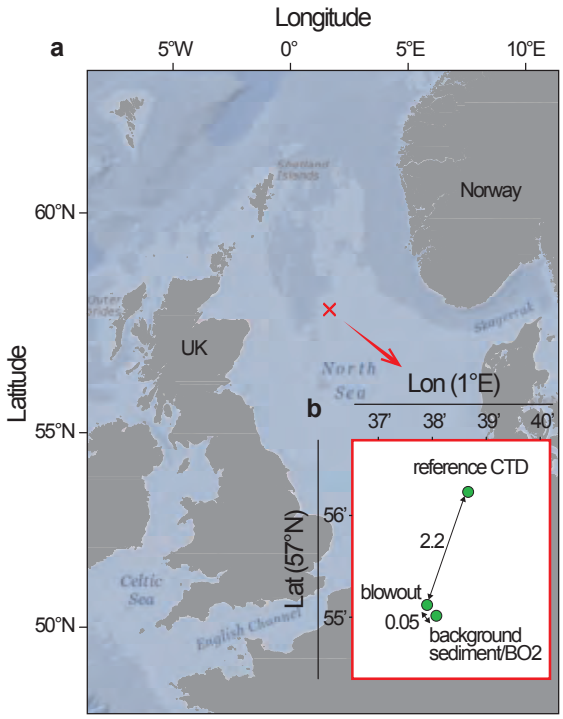

Figure 1. a, Location of the Blowout area (red cross) in the northern North Sea (sources: Esri, GEBCO, NOAA, and other contributors). b, sectional enlargement showing the relative location and distance (in km) of the different sampling sites.

Material and methods

Site description

The Blowout (57°55.41'N and 1°37.95'E, Fig. 1) is located in the northern North Sea at a water depth of 98 m (Fig. 2a) and consists of a ~60 m wide and ~20 m deep crater (for details see e.g., Schneider Von Deimling et al. 2007). Although the vigorousness of the gas release has declined since the accident, the Blowout still releases more CH_4 (mostly as bubbles, building spiral vortexes, Fig. 2b, Schneider Von Deimling et al. 2015) than any other natural seep in the North Sea (Rehder et al. 1998; Judd 2015). Based on stable carbon isotope analyses, the Blowout emits CH_4 of biogenic origin ($\delta^{13}C$-CH_4, ca. -75‰; Sommer et al. 2015). The water column above the Blowout is seasonally stratified, with a well-developed thermocline lasting from approx. April until October/November when deep mixing is induced by the first fall storms (Nauw et al. 2015). Throughout the duration of our study (July/Aug 2012), the water column above the Blowout was stratified with a well-developed thermocline at approx. 30 m water depth (Fig. 3b). In this area, hydrographic processes are highly dynamic with strong tidal currents changing direction approximately every six hours (Nauw et al. 2015, and references therein).

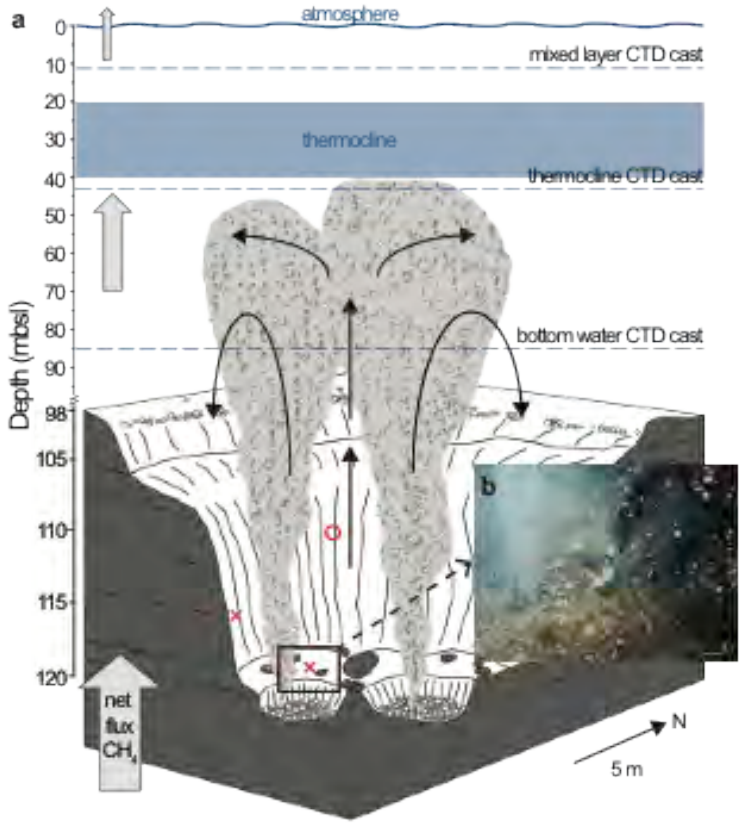

Figure 2. a, Schematic representation of the Blowout crater. Isopycnal surfaces for water-column sampling with the CTD are indicated at 11 mbsl (mixed layer), 42 mbsl (thermocline), and 85 mbsl (bottom water grid), respectively. Sediment sampling locations at the crater bottom and the crater wall are indicated with a red cross. Crater water sampling location is indicated with a red circle. b, Photograph of sediment sampling at the crater bottom next to a bubble jet.

Sediment sampling

Undisturbed surface sediments were recovered by push-coring with the remotely operated vehicle (ROV) KIEL 6000 (GEOMAR, Kiel). Biogeochemical and microbiological investigations were conducted at three different sites on parallel push cores sampled in close proximity (~10 cm) to each other (Tab. 1). At the Blowout, we sampled sediments in the center of the crater (Fig. 2a,b), in close vicinity (~0.5 m) to the emanation point of one of the two main bubble jets, and sediments from the Blowout crater wall (Fig. 2a). Finally, we retrieved push cores at a background site 50 m to the southeast of the Blowout crater at a water depth of 99 m. Parameters measured at each sampling site are summarized in Tab. 1.

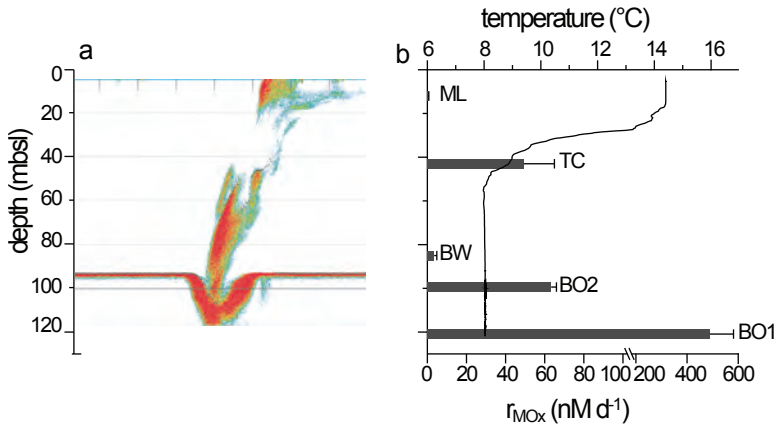

Figure 3. a, Sonar image of the Blowout gas flare (Simrad ER60, 38 kHz). b, Temperature profile from the ROV-CTD and average water column MOx rates, calculated from all replicates recovered from a specific depth. Niskin bottle or CTD cast grids are indicated (mixed layer (ML): n=40, thermocline (TC): n=43, bottom water grid (BW): n=48, BO2: n=4, BO1: n=4). Error bars represent standard errors.

Water column sampling

Water samples were recovered with a video-guided rosette sampler equipped with twelve 10-L Niskin bottles and probes for continuous measurements of conductivity, temperature and pressure/depth (CTD; Linke et al. 2015; Tab. 2). The water within the crater and close to the seafloor was sampled with two 5-L Niskin bottles mounted to the ROV. At the Blowout, samples were collected along three surfaces with a grid size of about 200 × 200 m (Fig. 2) were sampled: (i) bottom waters at 85 meters below sea level (mbsl), (ii) the lower part of the thermocline at 42 mbsl, and (iii) the upper mixed layer at 11 mbsl above the thermocline. In the following, the different will be referred to as (i) bottom water grid, (ii) thermocline, and (iii) mixed layer. We recovered 11 (mixed layer) to 12 (bottom water grid and thermocline) discrete water samples from each isopycnal surface. Within the Blowout crater, we sampled crater waters ~1m away from the bubble stream at 110 mbsl with the ROV (bottle 1=BO1). One additional water sample (bottle 2=BO2, 50 cm above the seafloor; 98 mbsl) was recovered 50 m away from the crater (i.e., above the sediment background site). A reference CTD cast with samples recovered from 11, 41 and 85 mbsl was conducted 2.2 km NNE of the Blowout crater. CH_4 concentrations, $\delta^{13}C$-CH_4 signatures and MOx rates were measured in all samples. For Catalyzed Reporter Deposition-Fluorescence In Situ Hybridization (CARD-FISH) analyses, we fixed four discrete samples from each CTD grid (Tab. 2, Fig. 6g-i). For DNA analysis, we combined ~20 L of water from 4 different Niskin bottles (5 L each) from each grid, which was filtered through a single Whatman GF/F Glass Microfiber filter (4.7 cm ⌀, Tab. 2, Fig. 6g-i). The filters were wrapped in aluminum foil and stored at -20°C until further analyses.

Table 1. List of sediment sampling locations and parameters measured during cruise CE12010.

location	IDs	position	#PC length	geochemistry	rates/microbiology	sediment characteristics
blowout centre	BOC	57°55.293'N 1°37.859'E	3(2) 12-16cm	CH_4, SO_4^{2-}, H_2S, por.	AOM, SRR, CARD-FISH, DNA	clay, layer of shells at ca. 8cm
blowout wall	BOW	57°55.291'N 1°37.856'E	4(3) 17-18cm	CH_4, SO_4^{2-},H_2S, por.	AOM, SRR, CARD-FISH, DNA	clay, black layer between 4-9cm
background site	-	57°55.270'N 1°37.888'E	3(2) 18-20cm	CH_4, SO_4^{2-}, H_2S, por.	AOM, SRR, CARD-FISH	clay, no colour change

#PCs denotes the number of total push cores taken at a sampling location. The number of push cores used for rate measurements or microbiological analyses are given in brackets. por. = porosity.

Table 2. List of water-column sampling locations parameters sampled during cruise CE12010.

location	IDs	position	#Niskin bottles	depth (mbsl)	geochemistry	rates/microbiology
crater water	BO1	57°55.29'N 1°37.85'E	1 (ROV)	~110	CH_4(1), $\delta^{13}C$- CH_4(1)	MOx(1), CARD-FISH(1)
0.5 m above sediment*	BO2	57°55.27'N 1°37.89'E	1 (ROV)	97.5	CH_4(1), $\delta^{13}C$- CH_4(1)	MOx(1), CARD-FISH(1)
upper mixed layer	ML	57°55.29'N 1°37.85'E	11 (CTD)	10.9	CH_4(11), $\delta^{13}C$- CH_4(11)	MOx(11), CARD-FISH(4), DNA(1)
lower thermocline	TC	57°55.29'N 1°37.85'E	12 (CTD)	41.5	CH_4(12), $\delta^{13}C$- CH_4(12)	MOx(12), CARD-FISH(4), DNA(1)
bottom water grid	BW	57°55.29'N 1°37.85'E	12 (CTD)	84.5	CH_4(12), $\delta^{13}C$- CH_4(12)	MOx(12), CARD-FISH(4), DNA(1)
reference CTD	refCTD	57°56.41'N 1°38.62'E	3 (CTD)	10.6/40.6/85.0	CH_4(3), $\delta^{13}C$- CH_4(3)	MOx(3), CARD-FISH(3), DNA(1)

*sampled 50 m away from the crater above the background sediment site

Numbers in brackets (geochemistry, rates/geochemistry) indicate number of samples taken per parameter.

Sediment Biogeochemistry

Sediments were subsampled for concentration measurements of dissolved CH_4, SO_4^{2-}, H_2S, and porosity. Immediately after recovery, 2 cm slices of push-core sediments were extruded with a plunger, and 3 mL were subsampled with a cut-off syringe and fixed in NaCl solution for head-space CH_4 concentration measurements by gas chromatography with flame ionization detection (GC-FID) according to Sommer et al. (2009). 5 mL of wet sediment was sampled for porosity determination by weight difference before and after freeze-drying and the remaining sediment-slice (~50 mL) was transferred to a low pressure-squeezer for porewater extraction. Porewater samples were filtered through 0.45 µm regenerated cellulose filters (Whatman) and aliquots were used for onboard analyses of sulfide (photometry of methylene blue; Grasshoff 1999). Dissolved SO_4^{2-} concentrations were determined by ion chromatography in our home laboratory. Analytical details are described in Wallmann et al. (2006) and Haffert et al. (2013).

Water column CH4 concentrations and isotopic composition

Immediately after CTD/ROV recovery, water samples for CH_4 concentration measurements were transferred into 100 mL serum vials and closed bubble-free with butyl rubber septa. Dissolved CH_4 concentrations were determined using headspace extraction (Linke 2012). Briefly, we replaced 10 mL of water sample by argon and fixed the remaining water sample

with 50 μl of saturated $HgCl_2$-solution. CH_4 concentrations were determined by GC-FID measurements onboard (Linke 2012). Serum vials were then stored at 4°C for subsequent stable carbon isotope measurements at GEOMAR by using continuous flow GC combustion-Isotope Ratio Mass Spectrometry (Thermo, MAT253; Linke 2012). All isotope ratios presented here are reported in the conventional δ-notation (i.e., $\delta^{13}C\text{-}CH_4$) and normalized against the Vienna Pee Dee Belemnite (VPDB) standard. Analytical precision of the reported concentrations and isotopic composition is ± 3% and ± 0.3‰, respectively

Methane-oxidation and sulfate-reduction rate measurements

CH_4-oxidation (AOM and MOx) and sulfate-reduction (SR) rates in sediments were measured by ex situ whole-core incubation (Jørgensen 1977): small push cores were subsampled from the push cores amended with trace amounts of ^{14}C-labelled aqueous CH_4 solution (10 μl, 4 kBq, ~150 nmol CH_4, American Radiolabeled Chemicals, USA) and ^{35}S-labelled sulfate (25 μl, 20 kBq, American Radiolabeled Chemicals, USA), respectively (Jørgensen 1977). All incubations were conducted in triplicates for 24 h at in situ temperature (7 - 9 °C) in the dark. Incubations were either stopped by fixing extruded sediment slices (1-3 cm) in 20 mL 2.5% sodium hydroxide (MOx/AOM) or in 20 mL 20% zinc acetate (sulfate reduction). CH_4-oxidation rates were assessed by $^{14}CH_4$ combustion (Treude et al. 2005), $^{14}CO_2$-acidification and determination of rest activity in the remaining sample (Blees et al. 2014). The first order rate constant (k) was calculated from the fractional tracer turnover with consideration of ^{14}C-label transfer into biomass:

$$k_{AOM/MOx} = \frac{(A_{CO_2} + A_R)}{(A_{CH_4} + A_{CO_2} + A_R)} \times \frac{1}{t} \qquad (Eq.\ 3)$$

where A_{CH_4} is the activity of remaining ^{14}C-CH_4 after incubation, A_{CO_2} is the activity of the generated CO_2, A_R is the rest activity (biomass and non-carbonate intermediates), and t is the incubation time.

SR rates were determined with the cold-chromium distillation method (Kallmeyer et al. 2004) to separate total reduced inorganic sulfur species (TRIS) from unreacted SO_4^{2-}. Similar to AOM, the first order rate constant of SR (k_{SR}) was then determined from the fractional tracer turnover:

$$k_{SR} = \frac{A_{TRIS}}{\left(A_{TRIS} + A_{SO_4^{2-}}\right)} \times \frac{1}{t} \times 1.06 \qquad (Eq.\ 4)$$

where $A_{SO_4^{2-}}$ is the remaining activity in the sulfate pool after incubation, A_{TRIS} is the activity of the generated sulfide and associated sulfur species, t is the incubation time and 1.06 the correction factor for the expected ^{35}S-isotope discrimination (Jørgensen and Fenchel 1974).

Samples for SR rates were not kept frozen until rates were measured, which may lead to an underestimate of the SR rates (Røy et al. 2014).

For water-column MOx measurements, water samples were transferred bubble-free into ~22 mL crimp-top vials and sealed with bromobutyl stoppers (Helvoet Pharma, Belgium), which have been tested not to impede MOx activity (Niemann et al. 2015). Samples were amended with 6 μl of a ^{14}C-CH_4:N_2 gas mixture (~0.25 kBq, ~100 nmol CH_4, American Radiolabeled Chemicals, USA) and incubated for 2 days at in situ temperature in the dark. Incubations were terminated by fixing the sample in butyl rubber sealed glass bottles with ~1 g of solid NaOH, and bottles were stored at room temperature until determination of A_{CH_4}, A_{CO_2}, and A_R onshore. First order rate constants were determined analogously as for AOM in the sediments.

Rates of AOM/MOx and SR were then calculated as

$$r_{AOM/MOx} = k \times [CH_4] \qquad (Eq.\ 5)$$

$$SRR = k_{SRR} \times [SO_4^{2-}] \times p \qquad (Eq.\ 6)$$

where $[CH_4]$ is the concentration of CH_4 in sediments or the water column, respectively, at the beginning of the incubation (plus the CH_4 added by ^{14}C-CH_4 tracer injection), $[SO_4^{2-}]$ is the sulfate concentration in the porewater, and p is the porosity of the sediment. All rate measurements were corrected for abiotic tracer turnover in killed controls.

CARD-FISH

Type I and II MOB in the water column were enumerated by CARD-FISH (Pernthaler et al. 2002). In addition, we tested for the presence of Type I and II MOB in surface sediment layers (0-1 cm sediment depth (cmsd)) in the Blowout center- and the background sediment cores, and for the presence of ANME in sediment layers with maximal AOM rates (6-10 cmsd) of the core from the Blowout center. Fixation of water-column samples was carried out as described in Steinle (2015) and references therein. CARD-FISH was performed as described by Schmale et al. (2015), except that Type I MOB were detected with a mixture of probes Mγ705-HRP (-horseradish peroxidase) and Mγ84-HRP (0.3 ng μl^{-1} each), and probe Mα450-HRP (0.6 ng μl^{-1}) was used for detecting Type II MOB (Eller et al. 2001). CARD-FISH in sediments was conducted according to Wilfert and colleagues (Wilfert et al. 2015). Further treatment for CARD-FISH of ANME-1, -2, and -3 was performed as described by Wilfert et al. (2015). CARD-FISH staining of benthic Type I- and II MOB was done as for water-column samples.

Molecular analyses

DNA was extracted from one quarter of a GF/F filter (water-column samples) or ~0.5 g of wet sediment (Tab. 1, Tab. 2) with the FastDNA® SPIN Kit for soil (MP Biomedicals) using a Precellys24® (Bertin Technologies) cell homogenizer. Partial 16S rRNA gene sequences of Type I and Type II MOB were amplified by PCR with the primer pairs MethT1dF/MethT1bR and 27F/MetT2R, respectively (Lane 1991; Murray et al. 1996; Costello and Lidstrom 1999; Wise et al. 1999). DNA extracts and amplification products were verified by electrophoresis in 0.8% - 2% (wt/vol) agarose gels with 0.001% (vol/vol) Midori Green DNA stain (Nippon Genetics) and quantified fluorometrically using Qubit® (Invitrogen). The community structure of surface sediments and the water column was investigated by denaturing gradient gel electrophoresis (DGGE) following the approach of Tsutsumi et al. (2011). GC-clamped PCR products were separated on a 9% polyacrylamide gel with a linear denaturing gradient of a 40%-70% (with 100% denaturants corresponding to 7 M urea and 40% (v/v) deionized formamide). Migration was done in a phorU-2 DGGE system (Ingeny International) at a constant temperature of 62 °C and a voltage of 130 V for 1 h, followed by 16 h at 75 V. The gel was stained in 300 mL TAE (Tris-acetate-EDTA buffer) containing 25 μl SYBR®Safe (Invitrogen) for 30 min. Dominant bands were excised and DNA was extracted from gel slices with sterile, nuclease-free water at 4 °C overnight. Extracted DNA was re-amplified, cleaned (Wizard® SV Gel and PCR Clean-up System, Promega) and finally cloned in E. coli JM109 using the pGEM®-T Easy Vector System (Promega). Inserts were verified by direct clone colony PCR using KAPA2G Robust Polymerase (KAPA Biosystems) and primers SP6/T7. Purified amplicons were sent out for sequencing. Partial 16S rRNA gene sequences have been deposited in the ENA-EBI database under the study accession number PRJEB12646.

Phylogenetic analysis

Phylogenetic analysis of the partial 16S rRNA gene sequences from isolated DGGE bands was performed in MEGA6 (Tamura et al. 2013). 16S rRNA gene sequences of the nearest uncultivated neighbors were identified and downloaded using SINA (Pruesse et al. 2012), completed by additional sequences of closely related cultivated bacteria as well as outgroup representatives. The sequences were aligned using the Muscle implementation of MEGA. The phylogenetic relationship was inferred using the Maximum Likelihood method based on the Kimura 2-parameter model (Kimura 1980). Initial Neighbor-Joining tree(s) for the heuristic search were based on a pairwise distances matrix calculated with the Maximum Composite Likelihood method. The phylogenetic analysis involved 35 (Type I) / 34 (Type II)

sequences. Positions with less than 95% site coverage were eliminated from the analysis, resulting in 159 (Type I) / 135 (Type II) positions in the final dataset.

Results

Sediments

In the center of the Blowout, sedimentary CH_4 concentrations (after retrieval) were saturated at ambient pressure without any clear downcore trends (Fig. 4a). Similarly, porewater sulfate concentrations were high (~29.5 mM) and did not change substantially as a function of depth. No sulfide was detected. AOM and SR rates both peaked between 6-11 cmsd with rates of up to 2920 and 2380 nmol cm^{-3} d^{-1}, respectively (Fig. 4b,c). At 6 cmsd, CARD-FISH analyses revealed the presence of large aggregates, which only contained ANME-2 cells (6.6×10^7 cells cm^{-3}); however, potentially associated SRB could not be observed (Fig. 5a,d). Additionally, some single cells of ANME-1 and -3, and some cell-chains of ANME-1 were detected (all together $<0.3 \times 10^7$ cells cm^{-3}). In surface sediments (0-1 cmsd), both Type I and II MOB were detectable by CARD-FISH (8.0 and 8.4×10^7 cells cm^{-3}, respectively, Fig. 5b,c,e,f), while ANMEs were not detected in this layer.

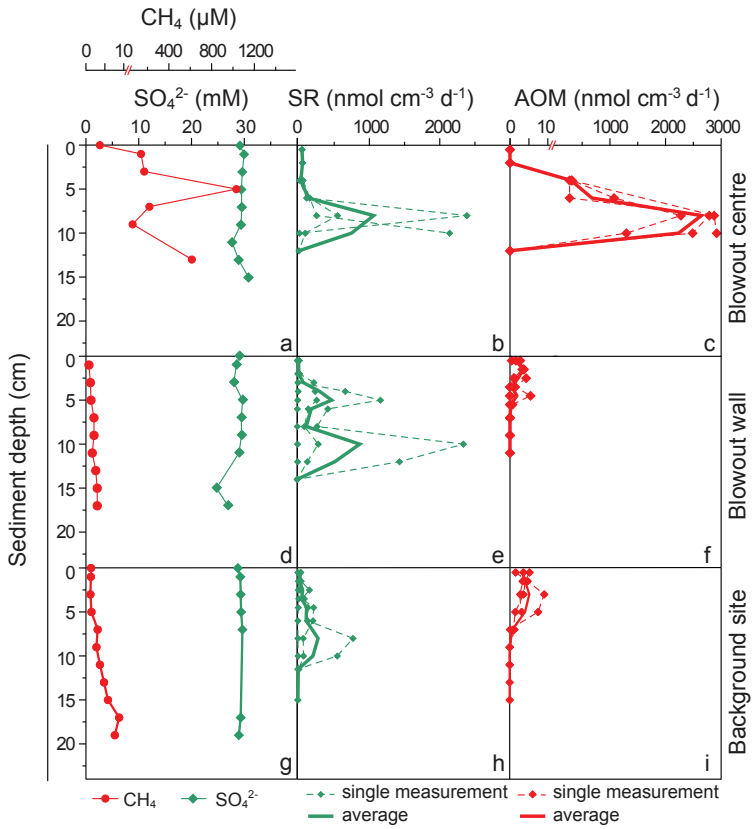

Figure 4. Sediment geochemical profiles and rate measurements from the bottom of the blowout crater (a-c), blowout wall (d-f), and background site 50 m away from the blowout (g-i). Replicate rate measurements are shown individually (dashed lines) and the average value is indicated as a thick, solid line.

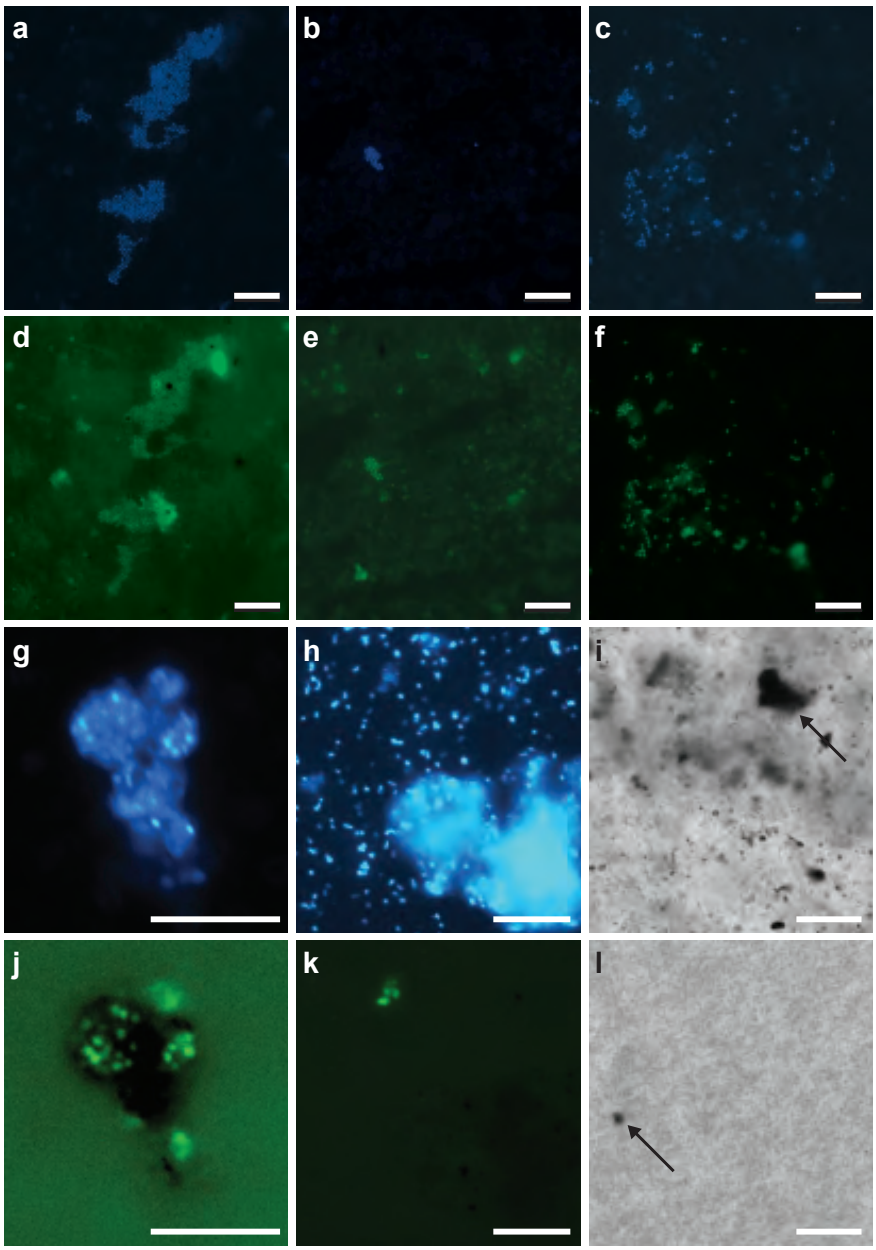

Figure 5. Micrographs of sediment samples from the Blowout crater bottom and from water samples. a-f, Epifluorescence micrographs from crater bottom sediments and g-k from the bottom water grid (85 mbsl). Images a-c, g, h are stained with DAPI for total cell counts, and d-f, j, k with Alexa488 for CARD-FISH using probe ANME-2-538 targeting ANME-2 (d), Mγ705 and Mγ84 targeting Type I MOB (e), or Mα450 targeting Type II MOB (f, j, k). a, d image of sediment sample from 6-10 cmsd, and b, c, e, f from 0-1 cmsd. i, l Unstained transmitted light micrographs from i, within the Blowout crater (BO1) and l, from the bottom water grid (85 mbsl) above the Blowout. Arrows indicate sediment particles. Scale bars represent 10 μm.

In the Blowout wall sediment, CH_4 concentrations generally increased with sediment depth (i.e., horizontal penetration depth) reaching ~3 μM at 17 cmsd; yet they were still ~1000 times lower than in sediment cores retrieved from the crater bottom (Fig. 4d). Sulfate

concentrations decreased slightly from seawater concentrations (~29.5 mM) to about 25 mM at 15 cmsd (Fig. 4d). Sulfide could not be detected. We measured only very low CH_4-oxidation rates in the upper section of the sediment core (~6 nmol cm^{-3} d^{-1} at 5 cmsd, Fig. 4e). In contrast, SR rates were three orders of magnitude higher and showed a double-peak with maximum values of ~1300 and ~2400 nmol cm^{-3} d^{-1} at 5 and 10 cmsd, respectively (Fig. 4f). Note that slumping probably disturbed crater wall sediments, which complicates further interpretation of this data.

At the background site 50 m away from the crater, downcore CH_4 concentrations increased only slightly, reaching ~8 μM at the bottom of the core (17 cmsd, Fig. 4g), and were thus much lower than in nearby crater bottom sediments. Sulfate concentrations were essentially invariant throughout the core and sulfide could not be detected (Fig. 4g). Methanotrophic activity was comparatively low (max. 9 nmol cm^{-3} d^{-1}, Fig. 4h) and similar to what was observed for the crater wall sediments. Compared to the other sediment sampling sites, SR rates were relatively low, with values of <500 nmol cm^{-3} d^{-1} (Fig. 4i). Both Type I and Type II MOB were detected in the upper 0-1 cm of the sediment core by CARD-FISH.

Water column

Spatial variations of CH_4 concentrations and $\delta^{13}C$-CH_4

We detected the highest CH_4 concentration of ~42,000 nM within the Blowout crater, just adjacent to the main bubble stream (BO1, Tab. 3). However, even higher concentrations can be expected closer to the bubble jets. Somewhat lower CH_4 concentrations were found in the bottom water grid (>500 nM and up to 37,000 nM; Fig. 6c, Tab. 3) and within the thermocline (> 50 nM and up to 13,500 nM; Fig 6b, Tab. 3). While we also found elevated CH_4 concentrations (~1,800 nM) in waters sampled ~0.5 m above the sediment background site (BO2, Tab. 3), we did not find indications for active CH_4 seepage at this site (e.g., gas ebullition). In the mixed layer above the thermocline, CH_4 concentrations were comparably low (<20 nM), but even here they were at supersaturation levels (up to 8-fold) with respect to the atmospheric equilibrium (~2.5 nM). $\delta^{13}C$-CH_4 values as low as -71.1‰ were detected in crater waters next to the plume (BO1) and similarly negative δ-values were measured in the bottom water grid (Tab. 3, Fig. 6f). More variable and more positive $\delta^{13}C$-CH_4 values (up to -67.5‰) were detected within the thermocline, particularly in samples with values at the lower end of the CH_4 concentration range (Fig. 6e). Samples collected further away from the crater (sample BO2) also showed a slight enrichment in ^{13}C (-69.3‰; Tab. 3) when compared to BO1. CH_4 concentrations at the reference CTD site were highest at 85 mbsl (221 nM) and decreased to 88 nM within the thermocline (Tab. 3).

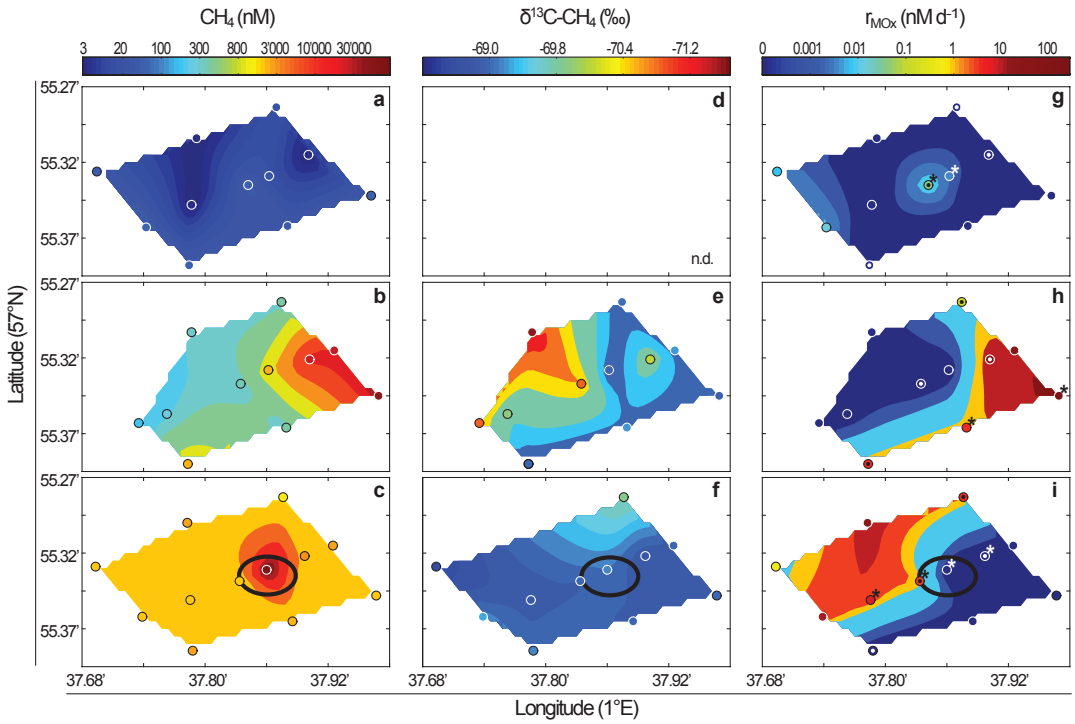

Figure 6. a-c, Water column CH_4 concentrations, d-f, $\delta^{13}C$-CH_4 values and g-i, MOx rates in the bottom water grid (c, f, i), within the thermocline (b, e, h), and in the mixed layer (a, d, g). Isolines were calculated from triangulation-based linear interpolation of measured values (indicated as circles). Locations, for which rate samples and parallel CARD-FISH samples were recovered are indicated with a dot in the center of the circles (g, h, i). Locations additionally sampled for DGGE analysis are indicated with a star (g, h, i). The position of the crater is indicated by a black oval in the bottom water plots. Relatively low CH_4 concentrations in the mixed layer (6a) precluded $\delta^{13}C$-CH_4 measurements (detection limit ~20 nM).

Methane oxidation rates

The vertical distribution of MOx in the water column displayed two maxima: One within the Blowout crater (BO1; 498 nM d^{-1}), and a second one at the thermocline (up to 262 nM d^{-1}; 49 nM d^{-1} on average; Fig. 3b, Tab. 3). In sample BO2, MOx rates were also elevated (up to 63 nM d^{-1}) while samples from the bottom water grid showed substantially lower rates with values <19 nM d^{-1} (3.5 nM d^{-1} on average; Fig. 3b, Fig. 4i). MOx rates in the mixed layer were low (<0.03 nM d^{-1}). Nevertheless, it has to be noted that, despite generally high CH_4 concentrations measured in the bottom water grid and the thermocline, rates were variable, and below detection limit in several samples (Fig. 6, detection limit of k = 0.001 d^{-1}). All rates from the reference CTD were below detection limit.

MOB communities in the water column

The water-column MOB community within the crater, in the bottom water grid and the thermocline was mainly composed of Type II MOB (76 – 95% of all MOB, Fig. 5j,k). Highest cell counts of Type II MOB were observed within the crater (44.8×10^3 cells mL^{-1}; BO1; Tab. 3) and in the sample taken 50 m away from the crater (29.3×10^3 cells mL^{-1}; BO2; Tab. 3). In both the bottom water grid and the thermocline, average Type II cell numbers were ~0.5×10^3 cells mL^{-1} (Tab. 3), but ~100-fold lower than within the crater. In contrast, average Type I MOB counts differed between the bottom water grid and the thermocline, with higher average cell numbers in the bottom water grid (0.15×10^3 cells mL^{-1}) compared to the thermocline (0.03×10^3 cells mL^{-1}; Tab. 3). No Type II MOB and only few Type I MOB (max. 0.02×10^3 cells mL^{-1}) were observed in the mixed layer (Tab. 3). MOB contributed up to 29% of total DAPI cell counts in the water column at the Blowout (29% - BO1; 7.3% - BO2; <0.3% - bottom water grid and thermocline; <0.01% - mixed layer). We observed abundant sediment particles on the filters of the BO1 (Fig. 5i) and BO2 samples, whereas only a few particles were present on filters from the bottom water grid (Fig. 5l) and none on filters from the thermocline.

In the reference CTD samples, no MOB were present, except for sporadic Type I MOB cells at the thermocline, where they constituted <1% of total DAPI cell counts (0.01×10^3 MOB cells mL^{-1}, Tab. 3).

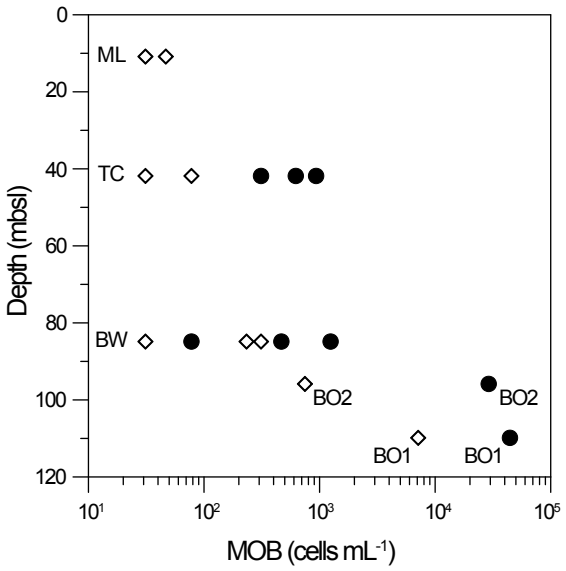

Figure 7. CARD-FISH cell counts of Type I (open diamonds) and Type II (filled circles) MOB in the water column. Niskin bottle or CTD cast grids are indicated (BW = bottom water grid, TC = thermocline, ML = mixed layer). Samples without any detectable Type I or Type II MOB are not shown.

DGGE and phylogenetic analysis of methanotrophs

Community fingerprints of Type I MOB and other Gammaproteobacteria from the Blowout crater surface sediments (BOC 0-1, 1-2 cm and BOW 0-1 cm) were very similar to the one from the bottom-water sample (Fig. 8a). In contrast, the upper water column (thermocline and mixed layer) and waters from the reference CTD were characterized by DGGE band patterns that were distinct from the sediments and the bottom-water sample. However, while the mixed layer sample showed some similarity to the reference CTD sample, the band pattern of the thermocline sample was unique. Phylogenetic analysis of cloned bands (Fig. 8b) revealed that the sequences BW_3 and BOC_3 were identical to a clone from the Haakon Mosby Mud Volcano (HMMVBeg-1; AJ704654; Lösekann et al. 2007). The BW_3/BOC_3 and the BOC_1 sequences grouped into the 'Marine Methanotrophic Group I' or 'deep sea-clade 1' (Fig. 8b; Ruff et al. 2013; Tavormina et al. 2015). Sequences of BOW_1 and TC_2 also grouped within the Type I MOB, while all other sequences were more closely related to potentially methanotroph-related clones originating from the water column above cold seeps at the E-Atlantic continental margin (Tavormina et al. 2008). Among these, the sequences of BW_2 and BOC_2 were identical, as were BOC_3 and BW_3.

Figure 8. (next page). a, DGGE community fingerprints of Type I MOB and other Gammaproteobacteria at the different sampling sites. Sample names are indicated (BOC = Blowout crater push core, BOW = Blowout wall push core, BW = bottom water grid, TC = thermocline, ML = mixed layer, refCTD = reference CTD). b, Maximum Likelihood tree based on partial 16S rRNA gene sequences showing the phylogenetic affiliation of sequenced DGGE bands (indicated with a star and a label on the DGGE gels) with closely related cultivated MOB and sequences of uncultivated close relatives from comparable environments. Bootstrap values are based on 2000 sub-samplings.

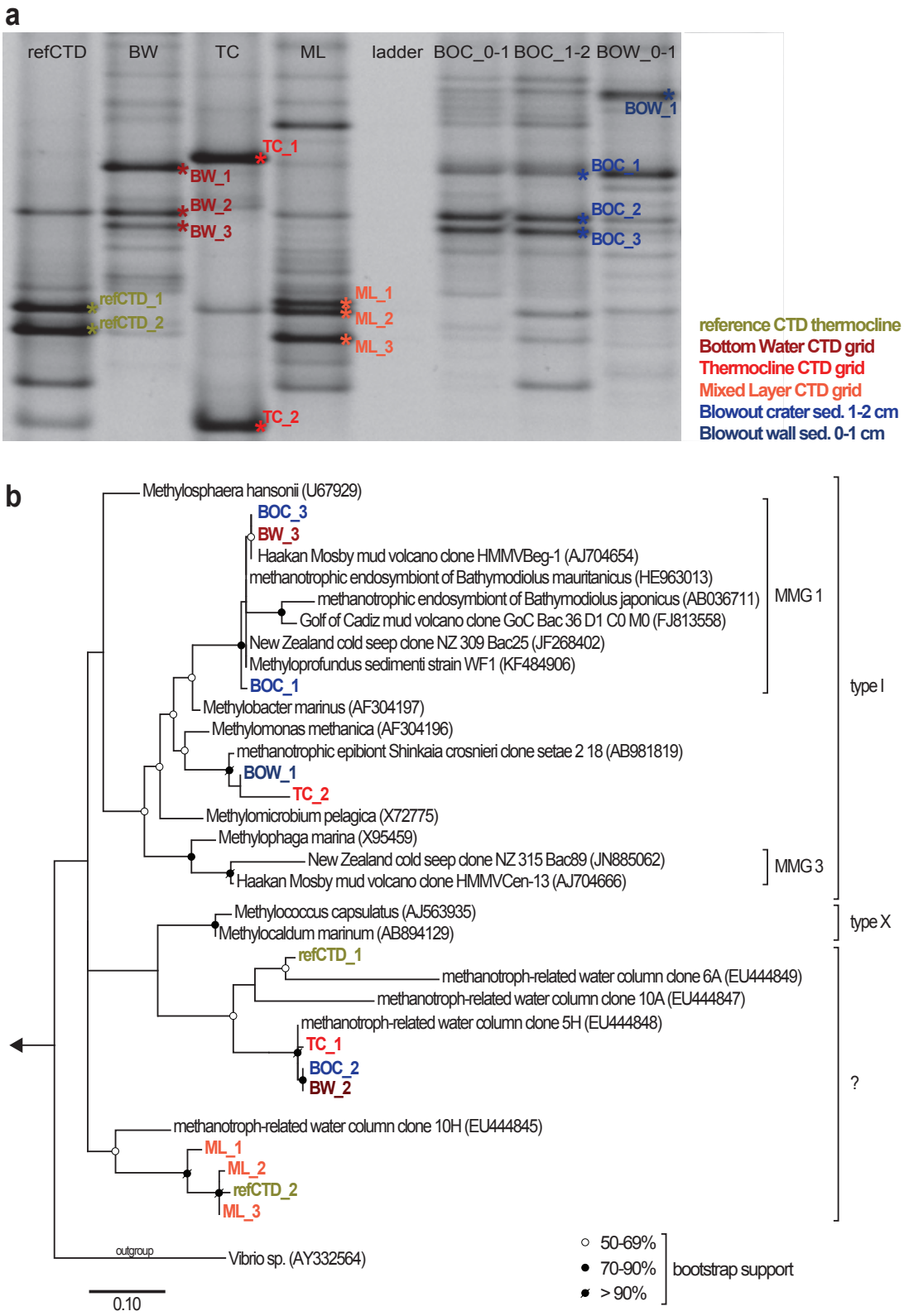
a
refCTD
BW
TC
ML
ladder
BOC_0-1
BOC_1-2
BOW_0-1
BOW_1
TC_1
BW_1
BOC_1
BW_2
BOC_2
BW_3
BOC_3
refCTD_1
refCTD_2
ML_1
ML_2
ML_3
TC_2
reference CTD thermocline
Bottom Water CTD grid
Thermocline CTD grid
Mixed Layer CTD grid
Blowout crater sed. 1-2 cm
Blowout wall sed. 0-1 cm
b
Methylosphaera hansonii (U67929)
BOC_3
BW_3
Haakan Mosby mud volcano clone HMMVBeg-1 (AJ704654)
methanotrophic endosymbiont of Bathymodiolus mauritanicus (HE963013)
methanotrophic endosymbiont of Bathymodiolus japonicus (AB036711)
Golf of Cadiz mud volcano clone GoC Bac 36 D1 C0 M0 (FJ813558)
New Zealand cold seep clone NZ 309 Bac25 (JF268402)
Methyloprofundus sedimenti strain WF1 (KF484906)
BOC_1
MMG 1
Methylobacter marinus (AF304197)
Methylomonas methanica (AF304196)
methanotrophic epibiont Shinkaia crosnieri clone setae 2 18 (AB981819)
BOW_1
TC_2
Methylomicrobium pelagica (X72775)
Methylophaga marina (X95459)
New Zealand cold seep clone NZ 315 Bac89 (JN885062)
Haakan Mosby mud volcano clone HMMVCen-13 (AJ704666)
MMG 3
type I
Methylococcus capsulatus (AJ563935)
Methylocaldum marinum (AB894129)
type X
refCTD_1
methanotroph-related water column clone 6A (EU444849)
methanotroph-related water column clone 10A (EU444847)
methanotroph-related water column clone 5H (EU444848)
TC_1
BOC_2
BW_2
?
methanotroph-related water column clone 10H (EU444845)
ML_1
ML_2
refCTD_2
ML_3
outgroup
Vibrio sp. (AY332564)
0.10
50-69%
70-90%
> 90%
bootstrap support

DGGE band patterns of Type II MOB and other Alphaproteobacteria were similar for both Blowout sediment samples (Fig. 9a). In contrast to the Type I DGGE gels, there was only one strong band in the water-column samples from the bottom water grid and the mixed layer (BW_6, ML_4, respectively) with the same migration distance as a band from the sediments (BOC_6). With this exception, the band patterns of water-column samples differed from those of the sediment samples. Additionally, the band pattern of all water-column samples did not show a substantial degree of similarity. Sequencing of excised bands and subsequent phylogenetic analyses grouped most sediment and water-column sequences into either the Sphingomonadales or Rhodobacterales clade (Fig. 9b). No sequences were related to the groups conventionally defined as Type II MOB (including only the genus *Methylosinus* and *Methylocystis*). However, the sequences from the thermocline (TC_3, TC_4) were closely related to known (obligate) MOB (*Methylocapsa sp.*) belonging to the family *Beijerinckiaceae* (Marín and Ruiz Arahal 2014). BOC_5 grouped with uncultivated bacterial clones from gas-hydrate-influenced areas; furthermore, sequences of bands BW_6 and TC_4 showed a relatively high degree of similarity (~99%) when compared to a clone sequence from the water column found in the Gulf of Mexico after the Deepwater Horizon oil spill (S2-8-036; KF786955). The sequences obtained from the faint bands of the bottom water grid (BW_7) and the Blowout sediment sample (BOC_7) were identical, and grouped in the Sphingomonodales clade.

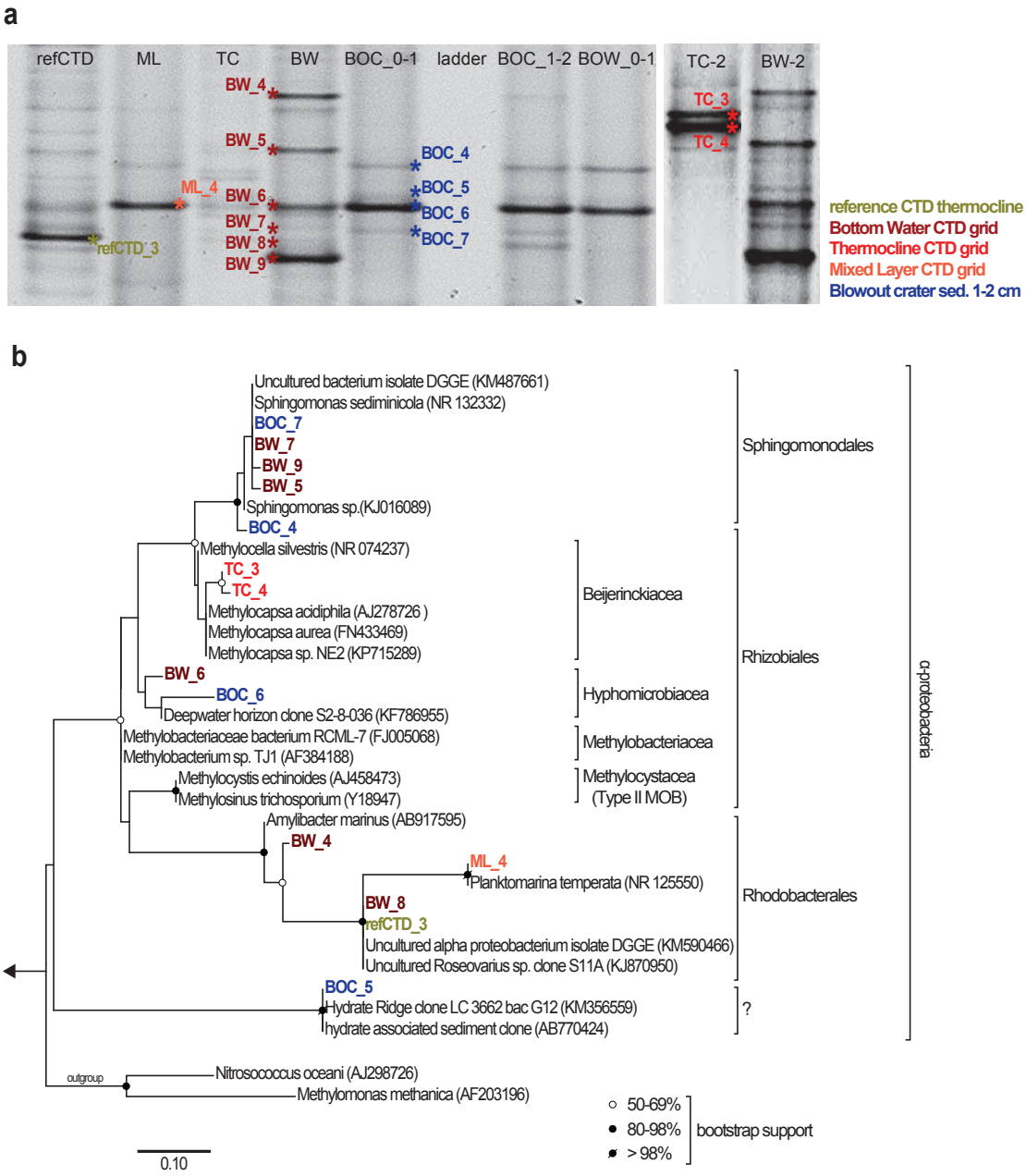

Figure 9. a, DGGE community fingerprints of Type II MOB and other Alphaproteobacteria at the different sampling sites. Sample names are indicated (BOC = Blowout crater push core, BOW = Blowout wall push core, BW = bottom water grid, TC = thermocline, ML = mixed layer, refCTD = reference CTD). The bands for the thermocline sample (TC_3, TC_4) are from a second DGGE-gel. b, Maximum Likelihood tree based on partial 16S rRNA gene sequences showing the phylogenetic affiliation of sequenced DGGE bands (indicated with a star and a label on the DGGE gels) with closely related cultivated MOB and sequences of uncultivated close relatives from comparable environments. Bootstrap values are based on 2000 sub-samplings.

Discussion

CH_4 seepage at the Blowout was triggered as a result of a drilling accident in 1990, during which a shallow gas pocket was tapped. This caused an explosion-like release of gas and the mobilization of sediments, leaving behind a crater of ~60 m diameter and ~20 m depth. Vigorous seepage mainly in the form of CH_4-bubble plumes emanating from the crater's center has been observed during every investigation of the Blowout (Fox 1995; Rehder et al. 1998; Schneider Von Deimling et al. 2007; Schneider Von Deimling et al. 2015), suggesting uninterrupted seepage since the early 1990s. The Blowout is thus an ideal model system to study the developmental state and activity of CH_4-oxidizing communities, as well as the spatial distribution of microbial CH_4-oxidation (AOM and MOx) at highly active CH_4 point sources in shallow shelf seas.

AOM in sediments

Two decades after the onset of seepage, our investigations revealed a distinct AOM horizon between 5 and 10 cm sediment depth at the Blowout crater bottom with ex situ rates that are comparable to the highest known AOM activities in the marine environment (e.g., Hydrate Ridge: Boetius et al. 2000; Treude et al. 2003; Black Sea: Treude et al. 2007). Wilfert et al. (2015) found similar (though potential) AOM rates in an in vitro slurry experiment from Blowout crater sediments recovered in 2011. Our ex situ observations thus confirm the development of a highly active AOM community within only two decades after the onset of gas seepage (Wilfert et al. 2015). Despite the highly active AOM community at the Blowout, only a small fraction of CH_4 is retained by the sediment CH_4 filter, as becomes obvious when looking at the high dissolved CH_4 concentrations at the sediment water interface and in the water column (Fig. 4, Fig. 6, Table 3). The role of SRB in AOM at the Blowout, however, remains unclear. SR and AOM rates displayed similar trends and were of the same order of magnitude, indicating that SR was most likely AOM-dependent (Knittel and Boetius 2009). Yet, we only found large ANME-2 aggregates without any obvious association with SRB, which is rather atypical for sediments characterized by high rates of AOM (Boetius et al. 2000; Michaelis et al. 2002; Niemann et al. 2006). The physical association of ANMEs and SRB, thermodynamic constraints of the AOM reaction (Boetius 2000; Orphan 2001; Treude et al. 2003), and molecular indications for direct electron transfer from ANMEs to SRB (McGlynn et al. 2015) suggests that ANMEs carry out CH_4-oxidation with the SRB as a syntrophic partner in which the SRB mediate the reduction of sulfate as the terminal electron acceptor (Knittel and Boetius 2009). On the other hand, a study on an AOM enrichment culture showed that ANMEs may perform AOM by themselves (Milucka et al. 2012). Our observations of solitary ANME cells and aggregates supports putative evidence from natural environments that AOM can indeed be performed independent of an obligate SRB partner

(see also Orphan et al. 2002; Niemann et al. 2005; Maignien et al. 2013). In contrast to sediments of the Blowout center, the Blowout-wall and background-site sediments were only moderately effected from CH_4 bubble emanations and dissolved CH_4 seepage (i.e., low CH_4 concentrations, and low CH_4-oxidation rates restricted to the uppermost ~5 cm, Fig. 4), underscoring that CH_4 flow is very much focused within the Blowout crater bottom sediments (Schneider Von Deimling et al. 2015, and references therein).

Methane oxidation in the water column

CH_4 concentrations in the water column above the Blowout (up to 42,000 nM), were comparable to other catastrophic CH_4-release sites, such as the Deepwater Horizon oil spill site (Kessler et al. 2011; Crespo-Medina et al. 2014; Sommer et al. 2015), or anoxic marine basins (Reeburgh et al. 1991). Water-column CH_4 concentrations at other highly active marine seeps, e.g., hydrothermal vents at the Juan de Fuca Ridge (deAngelis et al. 1993), cold seeps in the Santa Monica basin (Mau et al. 2012), at Hydrate Ridge (Heeschen et al. 2005), and at the Svalbard continental margin (Steinle et al. 2015) are generally about 1-2 orders of magnitude lower. The highest CH_4 concentrations at the Blowout (i.e., $[CH_4] > 5{,}000$ nM, Fig. 6b,c) seem to be constrained to waters most directly influenced by the main bubble plume (Schneider Von Deimling et al. 2015; Sommer et al. 2015). The horizontal extension of the plume can be estimated from the highest CH_4 concentrations located in the eastern part of the CTD grid (Fig. 6b,c). In line with results from data from 2011 (Sommer et al. 2015), bottom water grid samples (Fig. 6c) showed ubiquitously high CH_4 concentrations (~900 nM), and thus a strong lateral influence of the plume, possibly driven by density-driven recirculation of CH_4-rich waters ascending with the main bubble plume (Schneider Von Deimling et al. 2015; Wilson et al. 2015). At the thermocline, the impact of the bubble plume on CH_4-concentrations seems reduced and less constant (CH_4-concentrations as low as 50 nM; Fig. 6b). See Sommer et al. (2015) and Schneider Von Deimling et al. (2015) for a detailed discussion on lateral plume extension.

At the Blowout, >95% of the uprising CH_4 seems to be trapped below the thermocline (Schneider Von Deimling et al. 2015; Sommer et al. 2015), so that relatively little CH_4 reaches the mixed layer (see Fig. 6a). Yet, the fate of the uprising CH_4 is not completely certain. The relative enrichment of ^{13}C of thermocline CH_4 relative to the source CH_4 (Tab. 3, Fig. 4d-f) is consistent with C-isotope fractionation during partial CH_4-consumption by MOx (Whiticar 1999), and implies that a fraction of seep-derived CH_4 is oxidized in the water column. However, the rather subtle increase in $\delta^{13}C$ suggests that ^{13}C-enrichment during MOx is counteracted by the continuous resupply of CH_4 with a low $\delta^{13}C$-signature. In light of the very high water-column CH_4 concentrations, mixing with atmospheric CH_4 (about -47‰; NOAA-ESRL network) can be excluded to cause the observed ^{13}C-isotopic enrichment in the

residual CH_4 pool, leaving, indeed, partial consumption by water-column MOx as the most likely explanation for the elevated methane $\delta^{13}C$ within the thermocline.

Table 3. Overview of water depth, CH_4 concentrations, $\delta^{13}C$-CH_4 values, MOx rates, MOx rate constants, and Type I and II MOB cell numbers in the water column.

parameter: site:	crater water (BO1)	0.5m above sediment (BO2)	bottom water grid	thermocline	upper mixed layer	refCTD
water depth (mbsl)	110	97.5	85	42	11	11/41/85
max. CH_4 (nM)	42,097	1,794	37,233	13,526	21	221
min. CH_4 (nM)	-	-	523	57	<5	88
source $\delta^{13}C$ CH_4 (gas bubble) (‰)	-74.8	-	-	-	-	-
max. $\delta^{13}C$ dissolved CH_4 (‰)	-71.1	-69.3	-69.9	-67.5	NA	-
max. MOx rate (nM d^{-1})	498.4 (±159.6)	63.3 (±5.4)	17.5 (±18.1)	261.7 (±18.7)	0.03 (±0.01)	0
average MOx rate (nM d^{-1})	-	-	3.5	49	0.006	-
max. k (*10^2)	1.2 (±0.4)	3.5 (±0.3)	1.9 (±2.0)	2.9 (±2.5)	0.2 (±0.1)	0
average k (*10^2)	-	-	0.5 (±0.7)	1.1 (±1.3)	0.04 (±0.06)	0
max. Type I MOB (*10^3 cells mL^{-1})	0.7	0.8	0.3	0.08	0.05	0.01
max. Type II MOB (*10^3 cells mL^{-1})	44.8	29.3	1.3	0.9	-	-

The MOx rates in the Blowout water column (Fig. 3b, 6g-i) are among the highest values reported for marine environments (Reeburgh 2007; Mau et al. 2013; Steinle et al. 2015). They lie within the same range as rates detected in the anoxic basin of the Black Sea (Reeburgh et al. 1991) and the Gulf of Mexico water column following the Deepwater Horizon oil spill (Kessler et al. 2011; Crespo-Medina et al. 2014). Two rate maxima were observed within the water column, one within the crater and the second one at the thermocline (Fig. 3b), indicating more favorable conditions for MOx in these water layers. Previous studies found that important factors controlling MOx are (i) CH_4 availability, (ii) trace metal abundance, and/or (iii) changes in the abundance of MOB bacteria caused by water mass exchange (Semrau et al. 2010; Kessler et al. 2011; Mau et al. 2013; Crespo-Medina et al. 2014; Steinle et al. 2015).

(i) CH_4 availability. Low CH_4 concentrations may explain the overall low MOx rates in the mixed layer; and the high variability of MOx rates in the thermocline may to some extent be related to variable CH_4 concentrations (Fig. 6). However, even though very high CH_4 concentrations were observed both in the bottom water grid and in crater waters, MOx rates were much lower in the bottom water grid compared to crater waters. The overall rather poor correlation between CH_4 concentrations and MOx (R^2-values <0.2; data not shown) implies that the ambient CH_4 concentrations are not the major control on MOx activity in these water layers.

(ii) Trace metal abundance. Within the crater and the plume above, it seems plausible that sediment mobilization can increase the concentration of trace metals that are important for

MOB (i.e., Cu, Fe; Semrau et al. 2010) and thus stimulate MOx in the water column (see section below *"Type II MOB in the water column"* for further discussion).

(iii) Water mass transport. Within the Blowout crater, the water is somewhat shielded against tidal influences/currents, providing relatively stable conditions. We also detected a constant supply of MOB from surface sediments to the water column within the crater (see below). Combined, these factors warrant conditions conducive to MOB community development and thus high MOx rates (Steinle et al. 2015). A similar situation seems to apply to thermocline waters, where CH_4 is being trapped during density stratification. Yet, the rather variable CH_4 concentrations (Fig. 6b) suggest a stronger influence by lateral advection (Sommer et al. 2015). At seeps offshore Svalbard, lateral transport of water column MOB away from the CH_4 point source was found to reduce water-column MOx activity (Steinle et al. 2015). In comparison to the crater, the more variable conditions at the Blowout's thermocline may thus explain the fluctuating MOx rates in this water layer (Fig. 6h).

Sediment-borne MOB fuel the water-column MOx filter

Sediment particles on the filter from the Blowout crater water sample (Fig. 5i) and, though less abundant, on filters from the bottom water grid (Fig. 5l) indicate that sediment is entrained in the bubble plume and transported into the water column. Our DGGE and phylogenetic analysis revealed several bottom water sequences (BW_2, BW_3, BW_7), which were identical to sequences from crater surface sediments (BOC_2, BOC_3, BOC_7; Fig. 8,9) providing evidence that mobilized sediments provide a vector for transporting benthic microbes into the water column. The distribution of sediment particles in the water column paired with the identity of pelagic versus benthic microbes thus suggests that MOB, maybe in immediate association with sediment particles, were transported at least ~40 m up into the water column. The elevated MOx rates in the bottom water grid samples are hence likely supported by the ebullition-aided dispersal of pelagic MOB, which seem to continuously re-stock the MOx filter in the water column. A recent study by Schmale et al. (2015) described the entrainment of MOB by bubbles at the Rostocker seep site (Coal Oil Point seep field, California, USA) as 'bubble transport mechanism'; however, the bubble stream containing the entrained microbes was captured only 15 cm above the sediment surface in their study. Here, we confirm that mobilization of sediment microbes into the water column can play an important role for inoculating the water column. In addition, we demonstrate for the first time that 'bubble plumes' can transport pelagic microbes over much larger distances, thereby linking benthic and pelagic bacterial communities. Although other work at cold seeps could not find similar MOB communities in sediments and in bottom waters (Tavormina et al. 2008), our study suggests that transport of benthic microbes far into

the water column may be a globally important mechanism that shapes the regional microbial biogeography (Schmale et al. 2015).

Type II methanotrophs in the water column

Results from earlier studies suggest that aerobic MOB in marine habits almost exclusively belong to Type I MOB (Elsaied et al. 2004; Tavormina et al. 2008, 2010; Reed et al. 2009; Kessler et al. 2011; Håvelsrud et al. 2011; Steinle et al. 2015). In some marine studies, Type II MOB were observed, but in all cases they constituted only a small part of the methanotrophic community (Wang et al. 2004; McDonald et al. 2005; Hamdan et al. 2011). So far, Type II dominated MOB communities seem to be restricted to certain fresh water systems - e.g., some arctic lakes (He et al. 2012), soils (Henckel et al. 2000), and rice fields (Bodelier et al. 2000; Macalady et al. 2002). Our finding of a Type II dominated MOB community in the water column at the Blowout (Fig. 7) is thus unique. The recruitment from the sediments (where both Type I and II MOB were detected, Tab. 3) provides a stock of both types of aerobic MOB to bottom waters, which explains the presence of Type II MOB in the bottom water grid. However, it remains unclear as to why the thermocline MOB community at the Blowout is dominated by Type II MOB. Very little is known about factors selecting for this group of MOB. Hanson and Hanson (1996) suggested that Type II MOB are better adapted to high CH_4 concentrations, which agrees with more recent environmental observations (Bodelier et al. 2000; Henckel et al. 2000; Macalady et al. 2002; Kessler et al. 2011; He et al. 2012). Besides CH_4 concentrations, the availability of copper and iron – which are present in the reaction centers of the soluble and particulate MMO, respectively – may also influence expression, enzyme activity and ultimately the community structure of MOB. For example, pMMO has been found to be less expressed under copper limitation compared to sMMO (Murrell 2000). While Type II MOB often have the ability to express both, pMMO and sMMO, most Type I MOB synthesize only the particulate form of MMO (Semrau et al. 2010, and references therein). We did not measure water-column trace metal concentrations, so that we can only speculate if the water column at the Blowout is depleted in copper, which could potentially limit the expression of pMMO and thus give competitive advantage to Type II MOB over Type I MOB. We propose that elevated levels of CH_4 in the water column paired with potential copper limitation (to be confirmed by future work) constitute important selection mechanisms for Type II MOB at the Blowout.

Diversity of MOB in the Blowout area

Phylogenetic analyses revealed strong differences between the MOB and phylogenetically related communities in the bottom water grid, the thermocline, and the mixed layer. As for Type I MOB, we found several sequences from the bottom water grid (and from the Blowout crater sediment) that were closely related to known MOB of the ‘Marine Methanotrophic

Group I' or 'deep-sea clade 1'. These sequences are thus originating from obligate MOB (Tavormina et al. 2008; Ruff et al. 2013). Similarly, two sequences from the bottom water grid and the thermocline at the Blowout are also likely to originate from bacteria mediating MOx, since they were closely related to a methanotrophic epibiont from a deep-sea crab (Watsuji et al. 2014). In addition to sequences related to known obligate MOB, we found several sequences that were closely related to putatively methanotroph-related bacteria (Tavormina et al. 2008) previously found in the water column at cold seeps offshore the US west coast. Their occurrence at the Blowout, and at two other CH_4-rich environments (Eeel River Basin and Santa Monica Basin; Tavormina et al. 2008) may indicate an involvement of these organisms in hydrocarbon degradation.

The Type II MOB recovered from the water column belong to the order Rhizobiales within the class Alphaproteobacteria and, therein, to two genera of the family *Methylocystacea*: *Methylocystis* or *Methylosinus* (Hanson and Hanson 1996). Two additional genera, *Methlyocella* and *Methylocapsa* within the order Rhizobiales, were recently identified as obligate methanotrophs, but are not considered traditional Type II MOB as they belong to the family *Beijerinckiacea* and not to *Methylocystacea* (Marín and Ruiz Arahal 2014). The identified sequences from the thermocline are closely related to *Methylocapsa sp*. (TC_3 and TC_4) are hence most likely (obligate) methanotrophs. Several other members within the Rhizobiales, belonging to the families *Methylobacteriaceae* and *Hyphomicrobiacea*, were found to be methylotrophic (e.g. Urakami et al. 1995; Vuilleumier et al. 2011; Marx et al. 2012). As a result, the sequences from the BW grid and the Blowout crater sediments (BW_6, BOC_6) clustering with *Hyphomicrobium sp*. and with a clone sequence recovered from the water column after the Deepwater Horizon oil spill (KF786955) could also be involved in hydrocarbon degradation. Similarly, another crater sediment sequence (BOC_2) is closely related to environmental clones from hydrate-influenced areas and an involvement in CH_4 metabolism is hence possible.

Efficiency of the water-column methane filter

At the Blowout, less than 5% of the uprising dissolved CH_4 is estimated to reach the upper mixed layer during stratified conditions (Schneider Von Deimling et al. 2015; Sommer et al. 2015). The thermocline acts as a barrier, which delays diffusive CH_4 emissions into the atmosphere and, thus, enhances the CH_4 availability for water column MOB communities. For the water column where the CH_4 is trapped (i.e., below the upper mixed layer: 20 – 98 mbsl), we calculated a depth-weighted average turnover constant (k) by linear interpolation between the measured k in the thermocline, the bottom water grid and in bottom waters sampled 0.5 m above the seafloor (BO2). The depth-weighted k was 0.01 – 0.03 d^{-1} when considering average and maximum k in the different water layers, respectively (Tab. 3). This

translates to a CH_4 turnover time ($1/k$), of 92 or 31 days (for average and maximum depth-weighted k, respectively). Assuming that first-order rate kinetics applies, MOx has the potential to oxidize only 1 – 3% of the CH_4 in our study area. The only possible sink for the remaining >95% of the emitted CH_4 is lateral advective transport away from the immediate Blowout-seep area. Strong tidal currents will not only transport CH_4 (Sommer et al. 2015) laterally away from the CH_4 point source, but probably also MOB, so that MOx is very likely to proceed outside the immediate Blowout seep area. Indeed, previous work from the Svalbard Continental margin suggests that much of the total CH_4 liberated from a cold seep area is likely consumed downstream of the CH_4 point source (Graves et al. 2015; Steinle et al. 2015). The efficiency of the water-column MOx thus depends strongly on the time scale of turbulent vertical mixing, i.e., the time needed for (CH_4-rich) water to be transported from the sea floor to the sea surface in a MOB-containing water parcel. In the Blowout region, slow vertical mixing during stratified conditions results in a retention time for CH_4 of ~23d (Nauw et al. 2015). Assuming that the range of depth-weighted k values determined above also apply to MOx during lateral transport of the MOB community away from the Blowout, and given typical vertical mixing rates under stratified conditions, we calculate that at least 25% (and up to 74%) of the emitted CH_4 could be oxidized. Importantly, our estimates do not consider that advection-related dilution of the MOB cell density, may act to lower k. On the other hand, they also do not take into account the possibility of MOB community growth during lateral transport away from the Blowout, which would likely lead to higher k values.

During fully mixed conditions, in contrast, rapid vertical transport within the water column leads to a short retention time for CH_4 of ~1 d (Nauw et al. 2015). Even a similarly active MOB community as the one present during stratified conditions could thus only consume <3% of the emitted CH_4. Yet, the development of a highly active MOB community is unlikely under fully mixed conditions due to a lack of environmental stability and continuity (Steinle et al. 2015), resulting in an even less efficient CH_4 removal. Additional investigations of MOx activity in the water column in the wider Blowout area under both stratified and fully mixed conditions are necessary to further constrain the fate of the seep-derived CH_4 and the overall MOx filter capacity.

In conclusion, MOx rates in the water column at the Blowout are among the highest rates ever measured in a marine environment, and effectively consume a significant part of the emitted CH_4, at least during stratified conditions. We speculate, however, that the microbial methane filter is temporarily suspended during fully mixed conditions, so that the Blowout is a source of CH_4 to the atmosphere. The MOB community in the lower water column is – at least in parts – recruited from sedimentary MOB, which are entrained in CH_4-bubble plumes rising from the sediments and transported into the water column. Hence our study demonstrates that gas ebullition not only provides ample CH_4 substrate fueling MOx in the water column, it also serves as an important transport vector for sediment-borne microbial inocula that aid in the establishment/ proliferation of a water-column methanotrophic community at high-flux colds seeps.

Acknowledgements

We thank the Captain and crew of R/V Celtic Explorer, the ROV team (GEOMAR) and the scientific party of cruise CE12010 for the excellent support at sea. Additional thanks go to G. Schüßler, M. Dibbern, B. Domeyer, A. Bleyer, and A. Bodenbinder for technical support. This work received financial support through a D-A-CH project funded by the Swiss National Science Foundation and the German Research foundation (grants 200021L_138057 & 200020_159878/1). Further support was provided through the EU COST Action PERGAMON (ESSEM 0902). The project's ship time and transportation was funded by EUROFLEETS (grant 228344), with work being conducted in the framework of the ECO2 project (FP7, grant 265847). Further support came from the Cluster of Excellence "The Future Ocean" funded by the German Research Foundation.

References

Berndt, C., T. Feseker, T. Treude, and others. 2014. Temporal constraints on hydrate-controlled methane seepage off Svalbard. Science 343: 284-287.

Biastoch, A., T. Treude, L.H. Rüpke, and others. 2011. Rising arctic ocean temperatures cause gas hydrate destabilization and ocean acidification. Geophys. Res. Lett. 38: L08602, doi: 10.1029/2011GL047222.

Blees, J., H. Niemann, and C.B. Wenk, and others. 2014. Micro-aerobic bacterial methane oxidation in the chemocline and anoxic water column of deep south-Alpine Lake Lugano (Switzerland). Limnol. and Oceanogr. 59: 311-324.

Bodelier, P. L., P. Roslev, T. Henckel, and P. Frenzel. 2000. Stimulation by ammonium-based fertilizers of methane oxidation in soil around rice roots. Nature 403: 421-424.

Boetius, A., K. Ravenschlag, C.J. Schubert, and others. 2000. A marine microbial consortium apparently mediating anaerobic oxidation of methane. Nature 407: 623-626.

Boetius, A., and F. Wenzhöfer. 2013. Seafloor oxygen consumption fuelled by methane from cold seeps. Nat. Geosci. 6: 725-734.

Costello, A. M., and M.E. Lidstrom. 1999. Molecular characterization of functional and phylogenetic genes from natural populations of methanotrophs in lake sediments. Appl. Environ. Microb. 65: 5066-5074.

Crespo-Medina, M., C.D. Meile, K.S. Hunter, and others. 2014. The rise and fall of methanotrophy following a deepwater oil-well blowout. Nat. Geosci. 7: 423-427.

deAngelis, M. A., M.D. Lilley, and J.A. Baross. 1993. Methane oxidation in deep-sea hydrothermal plumes of the endeavour segment of the Juan de Fuca Ridge. Deep-sea Res Pt I 40: 1169-1186.

Eller, G., S. Stubner, and P. Frenzel. 2001. Group-specific 16S rRNA targeted probes for the detection of type I and type II methanotrophs by fluorescence in situ hybridisation. FEMS Microbiol. Lett. 198: 91-97.

Elsaied, H. E., T. Hayashi, and T. Naganuma. 2004. Molecular analysis of deep-sea hydrothermal vent aerobic methanotrophs by targeting genes of 16S rRNA and particulate methane monooxygenase. Mar. Biotechnol. 6: 503-509.

Ferré, B., J. Mienert, and T. Feseker. 2012. Ocean temperature variability for the past 60 years on the Norwegian-Svalbard margin influences gas hydrate stability on human time scales. J Geophys. Res. 117: C10017, doi: 10.1029/2012JC008300.

Fox, M. A. 1995. Memoradum 22/4b-4 well site hazards. MOBIL North Sea Ltd.

Grasshoff, K., K. Kremling, and M. Ehrhardt. 1999. Methods of seawater analysis. Wiley.

Graves, C. A., L. Steinle, G. Rehder, and others. 2015. Fluxes and fate of dissolved methane released at the seafloor at the landward limit of the gas hydrate stability zone offshore western Svalbard. J Geophys. Res.-Oceans 120: 6185-6201.

Haffert, L., M. Haeckel, V. Liebetrau, and others. 2013. Fluid evolution and authigenic mineral paragenesis related to salt diapirism – the Mercator mud volcano in the Gulf of Cadiz. Geochim. Cosmochim. Ac. 106: 261-286.

Hamdan, L. J., P.M. Gillevet, J.W. Pohlman, M. Sikaroodi, J. Greinert, and R.B. Coffin. 2011. Diversity and biogeochemical structuring of bacterial communities across the Porangahau ridge accretionary prism, New Zealand. FEMS Microbiol. Ecol. 77: 518-532.

Hanson, R. S., and T.E. Hanson. 1996. Methanotrophic bacteria. Microbiol. Rev. 60: 439-471.

Håvelsrud, O., T.H. Haverkamp, T. Kristensen, K.S. Jakobsen, and A. Rike. 2011. A metagenomic study of methanotrophic microorganisms in Coal Oil Point seep sediments. BMC Microbiol. 11: 221.

He, R., M.J. Wooller, J.W. Pohlman, J. Quensen, J.M. Tiedje, and M.B. Leigh. 2012. Shifts in identity and activity of methanotrophs in arctic lake sediments in response to temperature changes. Appl. Environ. Microbiol. 78: 4715-4723.

Heeschen, K. U., R.W. Collier, M.A. de Angelis, E. Suess, G. Rehder, P. Linke, and G.P. Klinkhammer. 2005. Methane sources, distributions, and fluxes from cold vent sites at Hydrate Ridge, Cascadia Margin. Global Biogeochem. Cy. 19: GB2016, doi:10.1029/2004GB002266.

Henckel, T., P. Roslev, R. Conrad, and Mikrobiologie. 2000. Effects of O2 and CH4 on presence and activity of the indigenous methanotrophic community in rice field soil. Environ. Microbiol. 2: 666-679.

IPCC, 2013. Stocker, T.F., Qin, D., Plattner, G., Tignor, M., Allen, S., Boschung, J., et al. [eds.]. Climate Change 2013 - The Physical Science Basis. Contribution of Working Group I to the Fifth Assessment Report of the Intergovernmental Panel on Climate Change. Cambridge University Press.

Jørgensen, B. B., and T. Fenchel. 1974. The sulfur cycle of a marine sediment model system. Mar. Biol. 24: 189-201.

Jørgensen, B. B. 1977. The sulfur cycle of a coastal marine sediment (Limfjorden, Denmark). Limnol. and Oceanogr. 22: 814-832.

Judd, A., and M. Hovland. 2007. Seabed fluid flow: the impact of geology, biology and the marine environment. Cambridge University Press.

Judd, A. 2015. The significance of the 22/4b blow-out site methane emissions in the context of the North Sea. Mar. Petr. Geol. 68: 836-847.

Kallmeyer, J., T.G. Ferdelman, A. Weber, H. Fossing, and B.B. Jørgensen. 2004. A cold chromium distillation procedure for radiolabeled sulfide applied to sulfate reduction measurements. Limnol. Oceanogr.-Meth. 2: 171-180.

Kessler, J. D., D.L. Valentine, M.C. Redmond, and others. 2011. A persistent oxygen anomaly reveals the fate of spilled methane in the deep Gulf of Mexico. Science 331: 312-315.

Kimura, M. 1980. A simple method for estimating evolutionary rates of base substitutions through comparative studies of nucleotide sequences. J. Mol. Evol. 16: 111-120.

Kirschke, S., P. Bousquet, P. Ciais, and others. 2013. Three decades of global methane sources and sinks. Nat. Geosci. 6: 813-823.

Knittel, K., and A. Boetius. 2009. Anaerobic oxidation of methane: progress with an unknown process. Annu. Rev. Microbiol. 63: 311-334.

Lane, D. J. 1991. 16S/23S rRNA sequencing, p. 125-175. In E. Stackebrandt and M. Goodfellow [eds.], Nucleic acid techniques in bacterial systematics. Wiley.

Linke, P. 2012. RV Celtic Explorer EUROFLEETS cruise report CE12010-ECO2, NorthSea: 20.07.-06.08. 2012, Bremerhaven-Hamburg. GEOMAR Report, N. Ser. 004.

Linke, P., M. Schmidt, M. Rohleder, A. Al-Barakati, and R. Al-Farawati. 2015. Novel online digital video and high-speed data broadcasting via standard coaxial cable onboard marine operating vessels. Mar. Technol. Soc. J. 49: 7-18.

Lösekann, T., K. Knittel, T. Nadalig, B. Fuchs, H. Niemann, A. Boetius, and R. Amann. 2007. Diversity and abundance of aerobic and anaerobic methane oxidizers at the Haakon Mosby mud volcano, Barents Sea. Appl. Environ. Microbiol. 73: 3348-3362.

Macalady, J. L., A.M.S. McMillan, A.F. Dickens, S.C. Tyler, and K.M. Scow. 2002. Population dynamics of type I and II methanotrophic bacteria in rice soils. Env. Microbiol. 4: 148-157.

Leifer, I., and A. Judd. 2015. The UK22/4b blowout 20 years on: investigations of continuing methane emissions from sub-seabed to the atmosphere in a North Sea context. Mar. Petr. Geol. 68: 706-717.

Maignien, L., R.J. Parkes, B. Cragg, H. Niemann, K. Knittel, S. Coulon, A. Akhmetzhanov, and N. Boon. 2013. Anaerobic oxidation of methane in hypersaline cold seep sediments. FEMS Microbiol. Ecol. 83: 214-231.

Marín, I., and D. Ruiz Arahal. 2014. The family Beijerinckiaceae, p. 263-282. In E. Rosenberg, E.F. DeLong, S. Lory, E. Stackebrandt, and F. Thompson [eds.], The Prokaryotes. Springer.

Marx, C. J., F. Bringel, L. Chistoserdova, and others. 2012. Complete genome sequences of six strains of the genus Methylobacterium. J. Bacteriol. 194: 4746-4748.

Mau, S., J. Blees, E. Helmke, H. Niemann, and E. Damm. 2013. Vertical distribution of methane oxidation and methanotrophic response to elevated methane concentrations in stratified waters of the Arctic fjord Storfjorden (Svalbard, Norway). Biogeosciences 10: 6267-6278.

Mau, S., M.B. Heintz, and D.L. Valentine. 2012. Quantification of CH4 loss and transport in dissolved plumes of the Santa Barbara Channel, California. Cont. Shelf Res. 32: 110-120.

McDonald, I. R., K. Smith, and M.E. Lidstrom. 2005. Methanotrophic populations in estuarine sediment from Newport Bay, California. FEMS Microbiol. Lett. 250: 287-293.

McGlynn, S. E., G.L. Chadwick, C.P. Kempes, and V.J. Orphan. 2015. Single cell activity reveals direct electron transfer in methanotrophic consortia. Nature 526: 531-535.

Michaelis, W., R. Seifert, K. Nauhaus, and others. 2002. Microbial reefs in the Black Sea fueled by anaerobic oxidation of methane. Science 297: 1013-1015.

Milucka, J., T.G. Ferdelman, L. Polerecky, and others. 2012. Zero-valent sulphur is a key intermediate in marine methane oxidation. Nature 491: 541-546.

Murray, A. E., J.T. Hollibaugh, and C. Orrego. 1996. Phylogenetic compositions of bacterioplankton from two California estuaries compared by denaturing gradient gel electrophoresis of 16S rDNA fragments. Appl. Environ. Microbiol. 62: 2676-2680.

Murrell, J. C. 2010. The aerobic methane oxidizing bacteria (methanotrophs), p. 1953-1966. In K.N. Timmis [eds.], Handbook of hydrocarbon and lipid microbiology. Springer.

Nauw, J., H.D. Haas, and G. Rehder. 2015. A review of oceanographic and meteorological controls on the North Sea circulation and hydrodynamics with a view to the fate of North Sea methane from well site 22 / 4b and other seabed sources. Mar. Petr. Geol. 68: 861-882.

Niemann, H., M. Elvert, M. Hovland, and others. 2005. Methane emission and consumption at a North Sea gas seep (Tommeliten area). Biogeosciences 2: 335-351.

Niemann, H., T. Lösekann, D. de Beer, and others. 2006. Novel microbial communities of the Haakon Mosby mud volcano and their role as a methane sink. Nature 443: 854-858.

Niemann, H., L.I. Steinle, J. Blees, S. Krause, I. Bussmann, T. Treude, M. Elvert, and M.F.Lehmann. 2015. Toxic effects of butyl elastomers on aerobic methane oxidation. Limnol. Oceanogr.-Meth. 13: 40-52.

Orphan, V. J., C.H. House, K.-U. Hinrichs, K.D. McKeegan, and E.F. Delong. 2001. Methane-consuming archaea revealed by directly coupled isotopic and phylogenetic analysis. Science 293: 484-487.

Orphan, V. J., C.H. House, K.-U. Hinrichs, K.D. McKeegan, and E.F. DeLong. 2002. Multiple archaeal groups mediate methane oxidation in anoxic cold seep sediments. P. Natl. Acad. Sci. USA 99: 7663-7668.

Pernthaler, A., J. Pernthaler, and R. Amann. 2002. Fluorescence In situ hybridization and catalyzed reporter deposition for the identification of marine bacteria. Appl. Environ. Microbiol. 68: 3094-3101.

Pruesse, E., J. Peplies, and F.O. Glockner. 2012. SINA: Accurate high-throughput multiple sequence alignment of ribosomal RNA genes. Bioinformatics 28: 1823-1829.

Reeburgh, W. S., B.B. Ward, S.C. Whalen, K.A. Sandbeck, K.A. Kilpatrickt, and L.J. Kerkhof. 1991. Black Sea methane geochemistry. Deep-sea Res Pt I 38: S1189-S1210.

Reeburgh, W. S. 2007. Oceanic methane biogeochemistry. Chem. Rev. 107: 486-513.

Reed, A. J., R. Dorn, C.L. Van Dover, R.A. Lutz, and C. Vetriani. 2009. Phylogenetic diversity of methanogenic, sulfate-reducing and methanotrophic prokaryotes from deep-sea hydrothermal vents and cold seeps. Deep-sea Res Pt II 56: 1665-1674.

Rehder, G., R.S. Keir, E. Suess, and T. Pohlmann. 1998. The multiple sources and patterns of methane in North Sea waters. Aquat. Geochem. 4: 403-427.

Ruff, S. E., J. Arnds, K. Knittel, R. Amann, G. Wegener, A. Ramette, and A. Boetius. 2013. Microbial communities of deep-sea methane seeps at Hikurangi continental margin (New Zealand). PloS One 8: e72627. doi:10.1371/journal.pone.007262.7

Røy, H., H.S. Weber, I.H. Tarpgaard, T.G. Ferdelman, and B.B. Jørgensen. 2014. Determination of dissimilatory sulfate reduction rates in marine sediment via radioactive 35S tracer. Limnol. Oceanogr.-Meth. 12: 196-211.

Schmale, O., I. Leifer, J.S.V. Deimling, C. Stolle, S. Krause, K. Kießlich, A. Frahm, and T.Treude. 2015. Bubble transport mechanism: indications for a gas bubble-mediated inoculation of benthic methanotrophs into the water column. Cont. Shelf Res. 103: 70-78.

Schneider Von Deimling, J., J. Brockhoff, and J. Greinert. 2007. Flare imaging with multibeam systems: Data processing for bubble detection at seeps. Geochem. Geophy. Geosy. 8: 1-7.

Schneider Von Deimling, J., P. Linke, M. Schmidt, and G. Rehder. 2015. Ongoing methane discharge at well site 22 / 4b (North Sea) and discovery of a spiral vortex bubble plume motion. Mar. Petr. Geol. 68: 718-730.

Semrau, J. D., A.A. DiSpirito, and S. Yoon. 2010. Methanotrophs and copper. FEMS Microbiol. Rev. 34: 496-531.

Shakhova, N., I. Semiletov, A. Salyuk, V. Yusupov, D. Kosmach, and O. Gustafsson. 2010. Extensive methane venting to the atmosphere from sediments of the East Siberian Arctic Shelf. Science 327: 1246-1250.

Sommer, S., P. Linke, O. Pfannkuche, and others. 2009. Seabed methane emissions and the habitat of frenulate tubeworms on the Captain Arutyunov mud volcano (Gulf of Cadiz). Mar. Ecol. Prog. Ser. 382: 69-86.

Sommer, S., M. Schmidt, and P. Linke. 2015. Continuous inline tracking of dissolved methane plume at a blow out site in the North Sea UK - water column stratification impedes immediate methane release into the atmosphere. Mar. Petr. Geol. 68: 766-775.

Steeb, P., P. Linke, and T. Treude. 2014. A sediment flow-through system to study the impact of shifting fluid and methane flow regimes on the efficiency of the benthic methane filter. Limnol. Oceanogr.-Meth. 12: 25-45.

Steinle, L., C.A. Graves, T. Treude, and others. 2015. Water column methanotrophy controlled by a rapid oceanographic switch. Nat. Geosci. 8: 378-382.

Tamura, K., G. Stecher, D. Peterson, A. Filipski, and S. Kumar. 2013. MEGA6: Molecular Evolutionary Genetics Analysis Version 6.0. Mol. Biol. Evol. 30: 2725-2729.

Tavormina, P. L., R. Hatzenpichler, S. McGlynn, G. Chadwick, K.S. Dawson, S.A. Connon, and V.J. Orphan. 2015. Methyloprofundus sedimenti gen. nov., sp. nov., an obligate methanotroph from ocean sediment belonging to the 'deep sea-1' clade of marine methanotrophs. Int. J. Syst. Evol. Micr. 65: 251-259.

Tavormina, P. L., W. Ussler, and V.J. Orphan. 2008. Planktonic and sediment-associated aerobic methanotrophs in two seep systems along the North American margin. Appl. Environ. Microbiol. 74: 3985-3995.

Tavormina, P. L., W. Ussler, S.B. Joye, B.K. Harrison, and V.J. Orphan. 2010. Distributions of putative aerobic methanotrophs in diverse pelagic marine environments. ISME J. 4: 700-710.

Treude, T., A. Boetius, K. Knittel, K. Wallmann, and B. Barker Jørgensen. 2003. Anaerobic oxidation of methane above gas hydrates at Hydrate Ridge, NE Pacific Ocean. Mar. Ecol. Prog. Ser. 264: 1-14.

Treude, T., J. Niggemann, J. Kallmeyer, P. Wintersteller, C.J. Schubert, A. Boetius, and B.B. Jørgensen. 2005. Anaerobic oxidation of methane and sulfate reduction along the Chilean continental margin. Geochim. Cosmochim. Ac. 69: 2767-2779.

Treude, T., V. Orphan, K. Knittel, A. Gieseke, C.H. House, and A. Boetius. 2007. Consumption of methane and CO2 by methanotrophic microbial mats from gas seeps of the anoxic Black Sea. Appl. Environ. Microbiol. 73: 2271-2283.

Tsutsumi, M., T. Iwata, H. Kojima, and M. Fukui. 2011. Spatiotemporal variations in an assemblage of closely related planktonic aerobic methanotrophs. Freshwater Biol. 56: 342-351.

Urakami, T., J. Sasaki, K.-I. Suzuki, and K. Komagata. 1995. Characterization and Description of Hyphomicrobium denitrificans sp. nov. Int. J. Syst. Bacteriol. 45: 528-532.

Vuilleumier, S., T. Nadalig, M.F. Ul Haque, and others. 2011. Complete genome sequence of the chloromethane-degrading Hyphomicrobium sp. strain MC1. J. Bacteriol. 193: 5035-5036.

Wallmann, K., G. Aloisi, M. Haeckel, A. Obzhirov, G. Pavlova, and P. Tishchenko. 2006. Kinetics of organic matter degradation, microbial methane generation, and gas hydrate formation in anoxic marine sediments. Geochim. Cosmochim. Ac. 70: 3905-3927.

Wallmann, K., E. Pinero, E. Burwicz, M. Haeckel, C. Hensen, A. Dale, and L. Ruepke. 2012. The global inventory of methane hydrate in marine sediments: a theoretical approach. Energies 5: 2449-2498.

Wang, P., F. Wang, M. Xu, and X. Xiao. 2004. Molecular phylogeny of methylotrophs in a deep-sea sediment from a tropical west Pacific Warm Pool. FEMS Microbiol. Ecol. 47: 77-84.

Watsuji, T.-O., A. Yamamoto, K. Motoki, K. Ueda, E. Hada, Y. Takaki, S. Kawagucci, and K.Takai. 2014. Molecular evidence of digestion and absorption of epibiotic bacterial community by deep-sea crab Shinkaia crosnieri. ISME J. 9: 1-11.

Whiticar, M. J. 1999. Carbon and hydrogen isotope systematics of bacterial formation and oxidation of methane. Chem. Geol. 161: 291-314.

Wilfert, P., S. Krause, V. Liebetrau, J. Schönfeld, M. Haeckel, P. Linke, and T. Treude. 2015. Response of anaerobic methanotrophs and benthic foraminifera to 20 years of methane emission from a gas blowout in the North Sea. Mar. Petr. Geol. 68: 731-742.

Wilkins, D., E. van Sebille, S.R. Rintoul, F.M. Lauro, and R. Cavicchioli. 2013. Advection shapes Southern Ocean microbial assemblages independent of distance and environment effects. Nat. Comm. 4: 2457, doi:10.1038/ncomms3457.

Wilson, D. S., I. Leifer, and E. Maillard. 2015. Megaplume Bubble Process Visualization by 3D Multibeam Sonar Mapping. Mar. Petr. Geol. 68: 753-765.

Wise, M. G., J.V. McArthur, and L.J. Shimkets. 1999. Methanotroph diversity in landfill soil: isolation of novel type I and type II methanotrophs whose presence was suggested by culture-independent 16S ribosomal DNA analysis. Appl. Environ. Microbiol. 65: 4887-4897.

Environmental controls on aerobic methane oxidation in seasonally hypoxic coastal waters

Lea Steinle[a,b], Johanna Maltby[b], Tina Treude[b,1], Annette Kock[b], Hermann W. Bange[b], Moritz F. Lehmann[a], and Helge Niemann[a,c]

in preparation for *Biogeosciences*.

[a] Department of Environmental Sciences, University of Basel, 4056 Basel, Switzerland

[b] GEOMAR Helmholtz Centre for Ocean Research Kiel, Marine Biogeochemistry Research Division, 24148 Kiel, Germany

[c] CAGE – Centre for Arctic Gas Hydrate, Environment and Climate, Department of Geology, UiT the Arctic University of Norway, 9037 Tromsø, Norway

[1] Present address: Department of Earth, Planetary & Space Sciences and Atmospheric & Oceanic Sciences, University of Los Angeles, Los Angeles, California, USA

Correspondence: lea.steinle@unibas.ch

Abstract

Coastal seas may account for more than 75% of global oceanic methane emissions. In coastal systems, methane is mainly produced microbially in anoxic sediments from where it can be released to the overlying water column. Aerobic methane oxidation (MOx) in the water column acts as a biological filter reducing the amount of methane that eventually escapes into the atmosphere. MOx is potentially controlled by temperature, salinity, dissolved methane and oxygen availability. Since these factors are highly variable in coastal ecosystems, we conducted a two-year time-series study with measurements of methane, MOx, and physico-chemical water column parameters in a seasonally stratified, and hypoxic, coastal inlet in the southwestern Baltic Sea (Eckernförde Bay, Boknis Eck Time Series Station, 54°31.823 N, 10°02.764 E, 28 m water depth). We found that MOx increased toward the seafloor and was not directly linked to methane concentrations. MOx rates exhibited a seasonal behaviour with maximum rates (up to 11.6 nmol l^{-1} d^{-1}) during the summer months when oxygen concentrations were lowest and bottom water temperatures highest. Overall, MOx retained between 70 – 95% of methane under stratified conditions, but only 40 – 60% under mixed conditions. Additional lab-based experiments with adjusted oxygen concentrations in the range of 0.2 – 220 μmol l^{-1} confirmed a sub-micromolar MOx oxygen-optimum. In contrast, the percentage of methane-carbon incorporation into biomass was up to 3800% higher at saturated oxygen concentrations suggesting a different partitioning of catabolic and anabolic processes at saturated and low oxygen concentrations. Our results underscore the importance of MOx in mitigating methane emission from coastal waters and indicate an adaptation on the organismic level of the water column methanotrophs to hypoxic conditions.

1. Introduction

Methane is a potent greenhouse gas, but the contribution of individual natural sources to the atmospheric budget is still not well constrained (Kirschke et al., 2013). Coastal (shelf) seas are estimated to account for more than 75% of global methane oceanic emissions, even though they cover only about 15% of the total oceanic surface area (Bange et al., 1994; Bakker et al., 2014). In coastal systems, methane is mainly produced via degradation of organic matter by methanogenic archaea in anoxic sediments, and to a much smaller extent in the anoxic water column (Bakker et al., 2014). Part of this methane is consumed via anaerobic- or aerobic oxidation of methane within the sediments (Knittel and Boetius, 2009), but the remainder seeps out into the overlying water column (Reeburgh, 2007). In the water column, methane can also be oxidized anaerobically in the rare case of water column anoxia,

but most of it is consumed via aerobic oxidation of methane (MOx; *Eq. 1*), mediated by aerobic methane-oxidizing bacteria (MOB; Reeburgh, 2007).

$$CH_4 + 2O_2 \rightarrow CO_2 + 2H_2O \qquad (Eq.\ 1)$$

MOx is hence an important sink for methane before its release into the atmosphere, but little is known about the efficiency of MOx in coastal ecosystems, where the shallow water depth often provides little time for methane oxidation when compared to deep-sea methane sources. Coastal ecosystems show a high temporal variability with regard to, e.g., temperature, oxygen, salinity, or organic matter (OM) input (e.g., Lennartz et al., 2014). Moreover, coastal ecosystems have globally experienced an increase of seasonally or permanently hypoxic or even anoxic zones over the past decades, generally owing to anthropogenic eutrophication and/or climate change (Diaz and Rosenberg, 2008; HELCOM: 2009; Rhein et al., 2013; Lennartz et al., 2014; Rabalais et al., 2014). Several definitions for water column oxygenation levels were suggested in the literature (Diaz and Rosenberg, 2008; Canfield and Thamdrup, 2009; Middelburg and Levin, 2009; Naqvi et al., 2010). For reasons of simplicity, we adopt in the following the definition of Diaz and Rosenberg (2008), where hypoxia is defined as $[O_2]<90\ \mu mol\ l^{-1}$. Additionally, we consider areas where our oxygen sensor indicated 0 $\mu mol\ l^{-1}$ O_2 not necessarily as anoxic, but as potentially having sub-micromolar oxygen concentrations since the detection limit of the Winkler method applied to calibrate the oxygen sensor is at 1-2 $\mu mol\ l^{-1}$.

Enhanced OM input via the associated oxygen depletion from OM remineralisation is likely to impact MOx, which is an aerobic, and in some cases micro-aerophilic process (Carini et al., 2005; Schubert et al., 2006; Blees et al., 2014). In addition, enhanced OM input can potentially increase methane production rates (Maltby et al., in prep.), which, in turn, could affect MOx rates. Additionally, increasing ocean water temperatures as a result of climate change (Rhein et al., 2013) will not only influence water column stratification and thus oxygenation levels during summer time (Diaz and Rosenberg, 2008), but higher temperatures may also directly impact metabolic rates of microbes, e.g., of methanogens or methanotrophs (Madigan et al., 2015). In order to predict the fate of coastal methane, knowledge on the seasonality of water column methane oxidation, and the environmental controls thereof, will be of great importance in predicting future changes in methane emissions (Bakker et al., 2014). However, to our knowledge no long-term seasonal marine studies of MOx have been previously conducted.

A prime spot to investigate coastal water column MOx at different oxidation/stratification regimes is the Boknis Eck time series station located in Eckernförde Bay (SW-Baltic Sea). Here, we present results from a study over the course of two years, during which we investigated MOx rates, methane concentrations and physicochemical parameters in the water

column at Boknis Eck on a quarterly basis with the aim to investigate seasonal changes in, and the environmental controls on, MOx.

2. Material and methods

2.1 Site description

The time series station Boknis Eck (54°31.15 N, 10°02.18 E; www.bokniseck.de; Fig. 1) is situated at the entrance of the coastal inlet Eckernförde Bay in the SW-Baltic Sea with an approximate water depth of 28 m, (Bange et al., 2011). Physico-chemical water column parameters have been monitored since 1957, making this station one of the longest operated time-series stations worldwide (Lennartz et al., 2014). The hydrography in Eckernförde Bay is characterised by the outflow of low salinity Baltic Sea water and the inflow of higher salinity North Sea water through the Kattegat and the Great Belt (Fig. 1a). From mid-March to mid-September, the two water masses are stratified with a pycnocline at ~15 m water depth (Lennartz et al., 2014). Large phytoplankton blooms generally occur in early spring (Feb/March) and in autumn (Sept – Nov), with a smaller bloom in summer (July/Aug). These blooms result in high sedimentation rates of up to 50% in spring, 75% in autumn, and 25% in summer of total OM produced (Smetacek et al., 1984; Smetacek 1985). The resulting high OM content in the deep layer, and subsequent degradation thereof, leads to a high oxygen demand, often resulting in bottom water hypoxia (March – Sept) and sometimes in anoxia during late summer (Aug/Sept) (Hansen et al., 1999). Similar to the above-described global trends, the frequency of water column hypoxia has increased since the 1960s (Lennartz et al, 2014).

The stratification period ends in fall (Oct/Nov) with the onset of surface-water cooling and fall storms (Bange et al., 2010). Aside from seasonal changes, episodic disturbances of the water column were observed during major saltwater inflows. Such events occur over short time periods (days to weeks) when easterly winds are followed by strong westerly winds, leading to the major inflow of salty oxygen-enriched (fall/winter) or oxygen-poor (summer) bottom water, respectively (Mohrholz et al., 2015). During our two-year study period, inflows occurred twice in fall 2013 (ca. 20-31 Oct. and 5-8 Dec.), and winter 2014 (ca. 3-20 Feb. and 8-19 Mar.; Naumann and Nausch, 2015). As a result of these major inflows and of the regular exchange between North Sea- and Baltic Sea water, bottom water salinity also varied strongly (17-24 psu; Lennartz et al, 2014).

Due to the large OM input to the sediments in Eckernförde Bay, high rates of methanogenesis in the Boknis Eck sediments leads to elevated water column methane concentrations and year-round methane super-saturation of surface waters (with respect to the atmospheric equilibrium; Whiticar 2002; Treude et al., 2005; Bange et al., 2010; Maltby et al., in prep.).

The high loading in OM and fast sedimentation rates lead not only to hypoxia, but also to elevated methanogenesis in the muddy sediment, and to high CH_4 concentrations in the overlying water column (Jackson et al., 1998; Whiticar 2002; Treude et al., 2005; Bange et al., 2010; Maltby et al., in prep.). Results from monthly samplings during the last ten years have revealed year-round methane seepage from the seafloor and methane super-saturation (with respect to the atmospheric equilibrium) of surface waters (Bange et al., 2010).

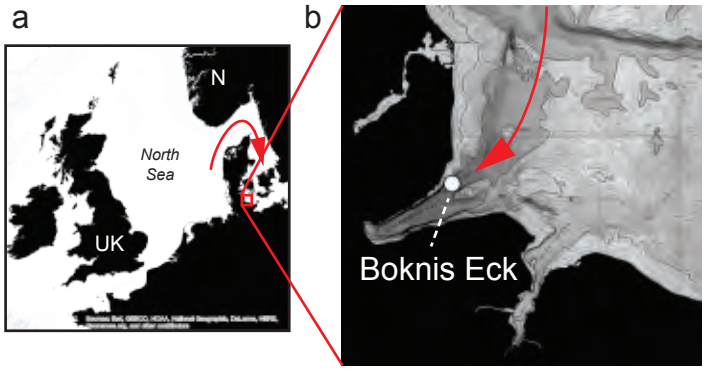

Figure 1. *Map of the Western Baltic Sea and a close-up of the study area*. a, Overview map of the Western Baltic Sea including the Kattegat, Skagerrak and parts of the North Sea. b, close-up of the study area with the sampling site (time-series station Boknis Eck) marked with a red dot. Red arrows indicate sporadic inflow of North Sea water.

2.2 Sampling

Sampling was conducted over a time-period of two years (Oct. 2012 – Sept. 2014) during which the water column was sampled every ~3 months. Sampling was carried out on board the R/V Alkor, RC Littorina or RB Polarfuchs in fall (Oct. 2012/Nov. 2013), winter (Mar. 2013/Feb. 2014), beginning of summer (Jun. 2013/Jun. 2014) and end of summer (Sept. 2013/Sept. 2014). Water samples from 1, 5, 10, 20 and 25 meters below sea level (mbsl) were recovered with a rosette sampler equipped with 6 × 4 L Niskin bottles and probes for continuous measurements of conductivity, temperature, density, and dissolved oxygen (Hydro-Bios, Kiel, Germany; O_2-sensor: RINKO III). In the following the rosette sampler with its sensor phalanx is termed CTD. Water aliquots were sampled for measurements of methane concentration and MOx activity. For an overview of sampling dates and corresponding parameters or incubations see Table 1. In the following, samples from 1 and 5 mbsl will be referred to as 'surface waters', and samples from 20 and 25 mbsl as 'bottom waters'.

Table 1. *Overview of sampling dates and sampled parameters*. Temp. dep. indicates samples used for temperature dependency incubations, O_2 dep. indicates samples used for O_2 incubations with ^{3}H-CH_4 and ^{14}C-MOx for O_2 incubations with ^{14}C-CH_4 and determination of ^{14}C-incorporation into biomass.

sampling	Date	CH_4	r_{MOx}	temp. dep.		O_2 dep.		^{14}C-MOx	
				5 mbsl	20 mbsl	5 mbsl	20 mbsl	5 mbsl	20 mbsl
Oct. '12	17.10.12	x	x						
Mar. '13	13.03.13	x	x						
June '13	27.06.13	x	x						
Sept. '13	05.09.13	x	x		x				
Nov. '13	08.11.13	x	x	x	x		x**		x
Feb. '14	24.02.14	x	x	x	x*	x	x*	x	x*
June '14	18.06.14	x	x	x	x	x	x	x	x
Sept. '14	17.09.14	x	x	x	x				

* because of disturbance of the water column, we used water from 25 mbsl instead of 20 mbsl

** because of disturbance of the water column, we used water from 15 mbsl instead of 20 mbsl

2.3 Dissolved methane concentration

For dissolved methane (methane) determinations, three 25 ml vials per sampling depth were filled bubble-free immediately after CTD-rosette recovery, poisoned with saturated mercury chloride solution and stored at room temperature. Methane concentrations were then determined by gas chromatography and flame ionization detection with a headspace method as described in Bange et al. (2010).

2.4 Methane oxidation rate measurements

MOx rates (r_{MOx}) were determined in quadruplicates from ex situ incubations of water samples with trace amounts of ^{3}H-labeled methane as described in (Steinle et al., 2015) based on a previously described method (Reeburgh et al., 1991). In brief, 25 ml crimp-top vials were filled bubble-free and closed with bromobutyl stoppers (Helvoet Pharma, Belgium; Niemann et al., 2015). Within a few hours after sampling, 6 μl gaseous 3H-CH_4/N_2 mixture (~15 kBq, <30 pmol CH_4, American Radiolabeled Chemicals, USA) was added and samples were incubated for three days in the dark at in situ temperature. The linearity of MOx during a time period up to five days was confirmed by replicate incubations at 24, 48, 72, 96 and 120 hours. At the end of the incubation, we determined the activities from the produced ^{3}H-H_2O (including possible incorporation into biomass; A_{H_2O}) and leftover ^{3}H-CH_4 (A_{CH_4}) by wet scintillation. Activities were corrected for (insubstantial) tracer turnover in killed controls (addition of 100 μl saturated aqueous $HgCl_2$ solution). With these activities we calculated the fractional turnover of methane (first order rate constants; *k*; *Eq. 2*):

$$k = \frac{A_{H_2O}}{(A_{H_2O} + A_{CH_4})} \times \frac{1}{t} \qquad (Eq.\ 2)$$

where t is incubation time.

r_{MOx} was calculated from k and water column [CH_4] at the beginning of the incubation (see 2.4; *Eq. 3*):

$$r_{MO_x} = k \times [CH_4] \qquad (Eq.\ 3)$$

r_{MOx} from incubations with ^{14}C-labelled methane (see 'oxygen dependency experiments) was determined as described in Blees et al. (2014) and Steinle et al. (subm.), which allows to estimate the incorporation of ^{14}C-CH_4 into biomass (Eq. 4):

$$C_{incorp.} = \frac{A_R}{A_{CO_2} + A_R} \qquad (Eq.\ 4)$$

where A_{CO_2} is produced ^{14}C-CO_2 from ^{14}C-CH_4 and A_R is the incorporated ^{14}C.

Oxygen dependency experiments

Oxygen dependency experiments were conducted with water from 20 mbsl depth sampled in Feb. 2014 and Jun. 2014. Until experimentation (~5 days after sampling), the water was stored headspace-free at 0°C. For the incubation experiments, the water was filled into 160 ml glass vials, which were closed with gas-tight bromobutyl rubber stoppers (Helvoet Pharma, Niemann et al., 2015). Before use, the stoppers were boiled in water and stored under N_2, in order to avoid bleeding of oxygen from the rubber matrix into the vials. Subsequently to filling, the vials were purged for 30 min with high-purity N_2 gas, transferred into an anoxic glovebox (N_2 atmosphere), and the N_2 headspace was filled up with N_2-purged Boknis Eck water. For final oxygen concentrations <15 μmol l^{-1} (Fig. 3), we injected 0.1 – 8 ml of Boknis Eck water in the glovebox that was previously equilibrated with ambient air. We then added 12 μl of anoxic Boknis Eck water enriched in methane resulting in a final concentration of ~100 nmol l^{-1} in the incubation vial. For final oxygen concentrations >10 μmol l^{-1}, 10 ml headspace with a predefined gas mixture of 5:95 – 12:88 O_2:N_2 was added and vials were left to equilibrate overnight at 4°C. Additional vials were used to fill up the headspace the next day. We then added 12 μl of CH_4-enriched water (final conc. 100 nmol l^{-1}), as described above. For r_{MOx} determination, we added ^{3}H-CH_4 tracer in the glove box as described in section 2.3. Oxygen concentration was measured with a high-sensitive (detection limit ca. 0.050 μM) OX-500 microsensor (Unisense). Seawater amended with dithionite (final concentration 9 mmol l^{-1}) was used as blank. Oxygen concentrations during incubations were determined by measuring initial and final oxygen concentration in parallel incubations, which were amended with 6 μl N_2 gas instead of ^{3}H-CH_4. Vials were incubated at 20°C in the dark for 6 h ([O_2]>10 μmol l^{-1}) or 10 h (for [O_2]<10 μmol l^{-1}). Incubation times differed because of time-constraints during sample processing. r_{MOx} was determined as described above.

Temperature dependency experiments

Similar to the determination of r_{MOx} at in situ temperature, we incubated water column aliquots in triplicates at temperatures from -0.5 – 37°C in incubators. We determined temperature dependency of MOx from Sept. 2013 – Sept. 2014 with water from 5 and 20 mbsl (Tab. 1, Fig. 5, Supplementary Fig. 2). The MOx temperature optimum is defined here as the temperature, where MOx rates were highest (i.e., not as the optimum for growth).

2.5 Areal MOx rates and methane release to the atmosphere

For each sampling date, we interpolated linearly between the measured rates and extrapolated the rate to an area of 1 m^2 to get a depth-integrated rate for the 28 m-deep water column, and thus the daily flux of methane removed from the system via oxidization (F_{MOx}; in μmol m^{-2} d^{-1}). Methane flux (F_{atm}; in μmol m^{-2} d^{-1}) from surface waters to the atmosphere was calculated according to Bange et al. (2010; *Eq. 5*).

$$F_{atm} = k_w \times 60 \times 60 \times 24 \times (Sc_{CH_4} / 600)^{-0.5} \times ([CH_4] - [CH_4]_{eq}) \qquad (Eq.\ 5)$$

where Sc_{CH_4} is the Schmidt number, which is dependent on temperature and salinity, and is calculated as the ratio of kinematic viscosity of seawater (Siedler and Peters, 1986) and the diffusion of methane in seawater (Jähne et al., 1987). $[CH_4]$ is the measured methane concentration at 1 mbsl, $[CH_4]_{eq}$ is the calculated equilibrium concentration (Wiesenburg and Guinasso, 1979), with respect to average atmospheric pressure at sea-level and the median atmospheric methane concentration in the Northern Hemisphere (Mace Head Station) from 2012 – 2014, and k_w is the gas transfer coefficient. Following Bange et al. (2010), we used 0.65×10^{-5} and 1.51×10^{-5} m s^{-1} as minimum and maximum value for k_w as recommended for coastal systems (Raymond and Cole, 2001), and thus did not include wind strength into our calculations. To determine the strength of stratification, we calculated the Brunt–Väisälä or buoyancy frequency N (*Eq. 6*).

$$N = \sqrt{-\frac{g}{\rho} \times \frac{d\rho}{dz}} \qquad (Eq.\ 6)$$

where g is the gravitational constant, ρ is potential density and z is geometric height.

3. Results

3.1 Seasonal variations in physico-chemical water column properties

In general, physico-chemical water column properties showed large seasonal variations (Fig. 2). Salinity varied strongly in bottom- (18 – 25 psu) and surface waters (13 – 24 psu) with highest salinities observed in Sept.-Nov. (Fig. 2a). Water density at Boknis Eck showed the same seasonal pattern as salinity (data not shown). Bottom water densities varied between 1015 – 1019 kg m^{-3} with the highest densities from June – Nov. Surface water densities were

between 1009 – 1015 kg m^{-3} with the lowest densities in June and Sept. In bottom waters, dissolved oxygen concentration varied from <1 – 450 μmol l^{-1} with the highest concentration during fully mixed conditions (Mar. 2013/Feb. 2014). Bottom waters became hypoxic in June (2013/2014), and reached concentrations ≤1 μmol l^{-1} towards the end of the stratification period (Sept. 2013/2014). In surface waters, dissolved oxygen was always replete (>280 μmol l^{-1}), reaching very high levels in Mar. 2013/Feb. 2014 (>450 μmol l^{-1}; Fig. 2d), when, according to chlorophyll a concentrations, sampling took place during a phytoplankton bloom (data not shown). Temperatures were coldest and constant throughout the water column at the end of winter at 1 - 3°C (Mar. 2013, Feb. 2014; Fig. 2c). Temperatures increased from spring until the end of summer to a maximum of 18°C in surface waters (June 2013, Sept. 2014) and 13°C in bottom waters (Oct. 2012, Sept. 2014). Dissolved methane concentrations reached 466 ± 13 nmol l^{-1} in bottom waters, and were always >30 nmol l^{-1} during the time of our study, without showing a clear seasonal pattern (Fig. 2f). Surface dissolved methane concentrations were lower with 8 – 27 nmol l^{-1}, resulting in a super-saturation of 270 – 870 % with respect to atmospheric equilibrium (2.8 – 4.3 nmol l^{-1}).

3.2 Seasonal variability of MOx

First order rate constants (k) of MOx were always highest in bottom waters (0.003 – 0.084 d^{-1}) with the exception of Nov. 2013 where the highest k was measured at 15 mbsl (Fig. 2g). The same pattern was found for r_{MOx} where rates were always highest in bottom waters (1.0 – 11.6 nmol l^{-1} d^{-1}), again with the exception of Nov. 2013 where the highest rate was measured at 15 mbsl (2.2 ± 0.2 nmol l^{-1} d^{-1}; Fig. 2h). The highest r_{MOx} were detected in summer (June 2013) or fall (Oct. 2012/Sept. 2013/Sept. 2014) when bottom water temperatures were highest and oxygen concentration were lowest, but not when methane concentrations were highest, i.e. in March 2014.

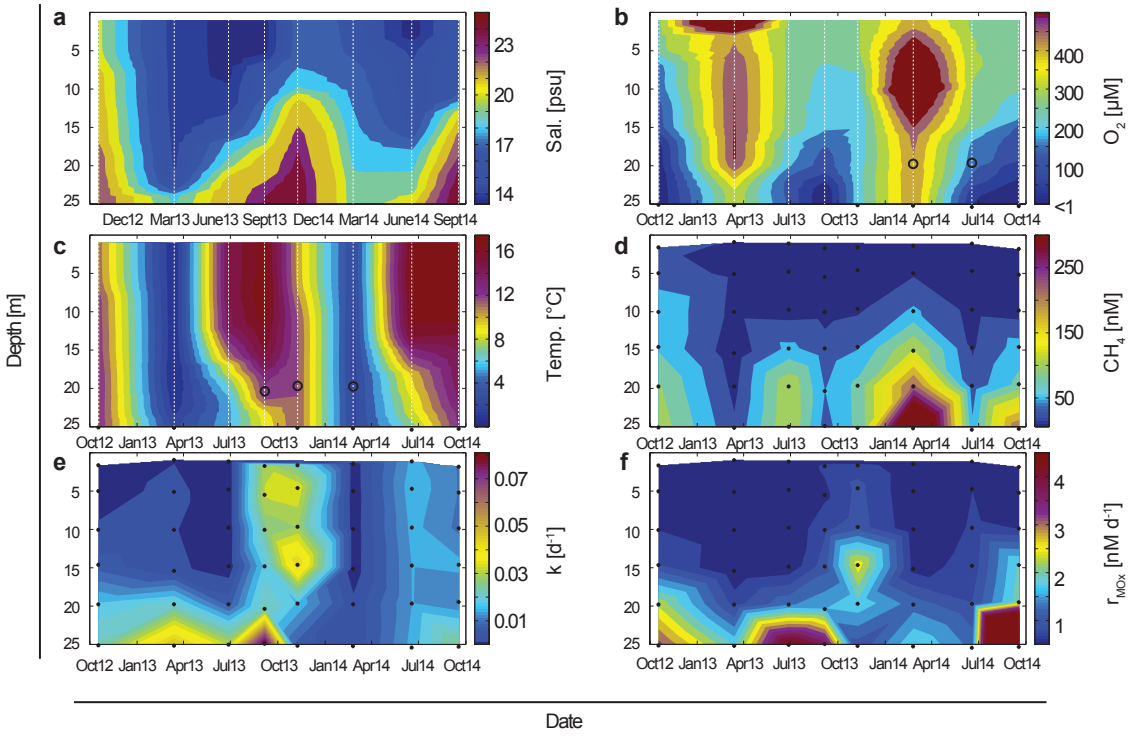

Figure 2. *Seasonal distribution of physico-chemical parameters and aerobic methanotrophy at the Boknis Eck station*. Distribution of salinity (a), oxygen (b), temperature (c), methane (d), first order rate constants of aerobic methane oxidation -*k* (e), and aerobic methane oxidation rates - r_{MOx} (f). Positions of discrete samples (dots) and continuous measurements (dashed lines) are indicated. Depths of water used for oxygen and temperature incubation experiments (Fig. 3, 4 and 5) are indicated with circles in (b) and (c).

3.3 Influence of oxygen concentrations on MOx activity

During our lab-based experiment with adjusted oxygen concentrations, r_{MOx} was highest in incubations with the lowest oxygen concentration independently in both Feb. and June of 2014 (Fig. 3). Rates under nearly saturated oxygen conditions were significantly lower (50% in February, 75% in June) than the rate measured at the lowest initial oxygen concentration. However, while we found that r_{MOx} did not vary strongly at different oxygen concentration <140 μmol l^{-1} (Fig. 3a) in Feb. 2014, the rates measured in June 2014 were more variable but the highest rates were still measured at the two lowest initial oxygen concentration (0.35 ± 0.16 μmol l^{-1} and 0.94 ± 0.05 μmol l^{-1}, Fig. 3b).

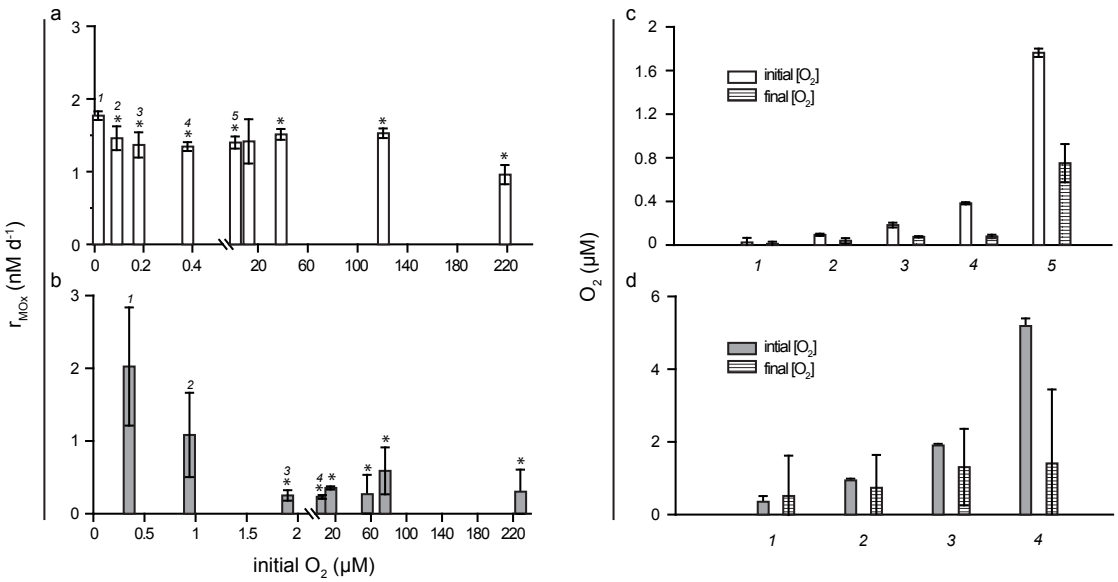

Figure 3. *MOx rates in incubations with adjusted O_2 concentrations*. r_{MOx} determined in incubations of Boknis Eck water (20 mbsl) with ^{3}H-CH_4 in Feb. 2014 (a) and June 2014 (b). * indicates a p-value <0.05 of a two-tailed, two-sample t-test assuming equal variance of the MOx rate compared to the MOx rate of the lowest O_2 concentration. Corresponding oxygen concentrations determined at the beginning and the end of incubations from the Feb. 2014 (c) and June 2014 sampling (b) for incubations with O_2 concentration below 10 μmol l^{-1}. Incubations were performed in triplicates and standard deviations are indicated. For O_2 concentrations > 10 μmol l-1, O_2 concentrations at the end of incubations were 14-40% (Feb. 2014) and 3-8% (June 14) lower than at the beginning (data not shown).

All incubations remained oxic during the incubation time period, even incubations with very low initial oxygen concentrations (Fig. 3c, d). In Feb. 2014, 53 – 79% of oxygen was consumed during incubations with initial [O_2]<10 μmol l^{-1} (Fig. 3c), and 14 – 40% during incubations with initial [O_2]>10 μmol l^{-1}. In June 2014, 22 – 73% of oxygen was consumed during incubations with initial [O_2]<15 μmol l^{-1} (Fig. 3d), and 3 – 8% during incubations with [O_2]>15 μmol l^{-1}.

Similar to incubations with ^{3}H-CH_4, *k* values determined with ^{14}C-CH_4 at saturated oxygen concentration were lower than *k* values measured in incubations with [O_2] <0.5 μmol l^{-1} (32% lower on average; Fig. 4a, Supplementary Fig. 1a, b). In contrast, a higher fraction of the oxidized ^{14}C was incorporated into biomass in incubations at saturated oxygen concentration than at [O_2] <0.5 μmol l^{-1} (108 – 3800% more; Fig. 4b, Supplementary Fig. 1c, d). These patterns were independent of water depth and season (June 2014: Fig.4a; Nov. 2013 and Feb. 2014: Supplementary Fig. 1), but generally more pronounced in bottom- (20 mbsl) than in surface waters (5 mbsl).

In the following, [O_2] < 60 μmol l^{-1} will be referred to as low oxygen concentrations and [O_2] > 60 μmol l^{-1} as high oxygen concentrations.

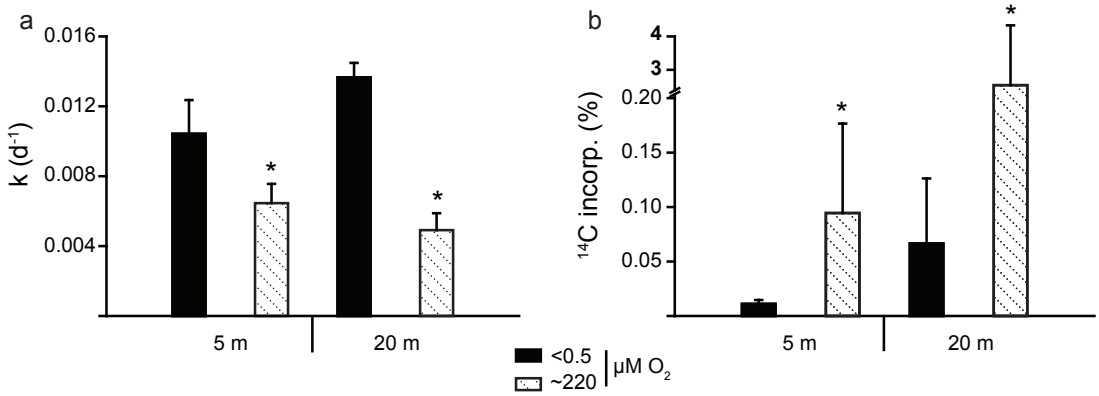

Figure 4. *Methane-carbon assimilation in relation to oxygen concentration*. Methane-carbon assimilation was determined from incubations amended with ^{14}C-CH_4 at saturated (~220 μmol l^{-1}, shaded bars) or low oxygen concentrations (<0.5 μmol l^{-1}, black bars) of water recovered in June 2014 at 5 mbsl and 20 mbsl. Incubations were performed in triplicates and standard deviations are indicated. (a) First-order rate constant (*k*). (b) Fraction of oxidized methane incorporated into biomass. * indicates a p-value <0.05 of a two-tailed, two-sample t-test assuming equal variance between the samples at low and high oxygen concentrations.

3.4 Temperature dependence of MOx

In general, *k* increased with temperature and reached a maximum at 20 – 37°C in waters sampled at 20 mbsl, which corresponds to a mesophilic temperature optimum (Fig. 5a,c; shown are results from Sept. 2013 and Feb. 2014; Tab. 1). Only in Nov. 2013, maximum MOx was detected at 10 – 20°C, consistent with a psychrophilic temperature optimum (Fig. 5b). These patterns were independent of water depth (Fig. 5, Supplementary Fig. 2).

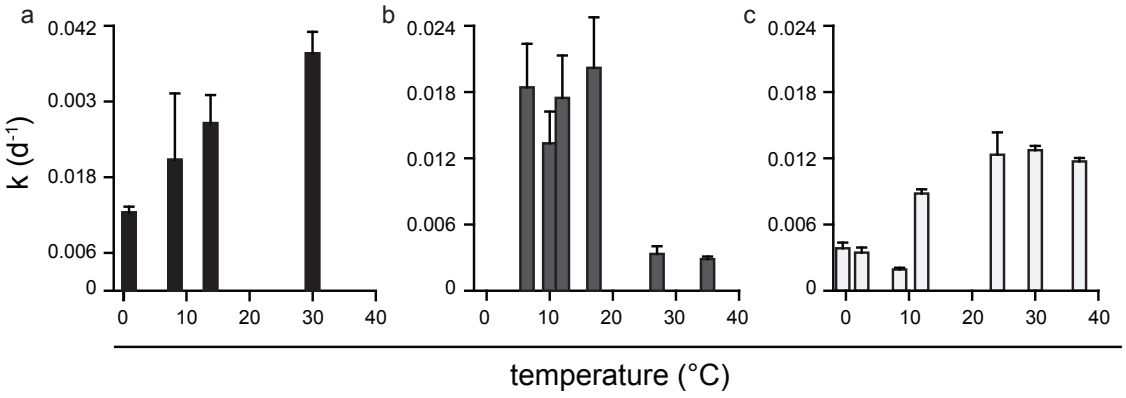

Figure 5. *MOx first order rate constants (k) at different temperatures*. First order rate constants of MOx were determined with ^{3}H-CH_4 amendments in triplicated incubations of water from 20 mbsl recovered in Sept. 2013 (a), Nov. 2013 (b), and Feb. 2014 (c).

3.5 Estimation of water-column methane removal by MOx and methane flux to the atmosphere

Depth-integrated r_{MOx} or F_{MOx} varied between 11.7 (Mar. 2013) and 82.3 (Sept. 2014) μmol m^{-2} d^{-1} (Tab. 2). Estimated average fluxes of methane to the atmosphere were 3.6 – 9.2 μmol m^{-2} d^{-1} during stratified periods, and 10.0 – 25.1 μmol m^{-2} d^{-1} during the mixed period (considering a minimum or maximum piston velocity, respectively; Tab. 2; Raymond and Cole 2001). The water column was only weakly stratified/almost fully mixed in Oct. 2012, Mar. 2013, and Feb. 2014 (i.e., N<120 cph), and strongly stratified during all other sampling times (i.e., N>120 cph; Tab. 2).

4. Discussion

4.1 Seasonal variations

Development of seasonal hypoxia

During the course of our study, oxygen was replete during winter samplings, when the water column was almost fully mixed and phytoplankton blooms were occurring, which is typical for this time period (Bange et al., 2010). During June samplings, we observed significantly lower bottom water oxygen concentrations indicating the onset of hypoxia, which resulted in sub-micromolar oxygen concentrations in Sept. (2013, 2014) below 24 mbsl. This observation is in accordance with a study by Bange et al. (2010) over the time-period 2006 – 2008, during which three hypoxic events took place starting in May/Aug. and lasting until Sept./Nov. Long-term monitoring at Boknis Eck showed that the occurrence and length of hypoxic events has continued to increase in the last twenty years (Lennartz et al., 2014), although nutrient inputs into the Baltic Sea were strongly reduced (HELCOM: 2009). Additionally, bottom water temperatures increased since the 1960s (Lennartz et al., 2014). The reason for the observed ongoing decrease in oxygen concentration is thus most likely related to an earlier onset of the stratification period, which in return, is due to enhanced surface water temperatures, resulting in reduced exchange between bottom and surface waters (Hoppe et al., 2013; Lennartz et al., 2014). Furthermore, a general increase in temperature also enhances mineralisation of OM in bottom waters and thus leads to higher oxygen consumption (Hoppe et al., 2013; Lennartz et al., 2014).

Seasonal dynamics of methane concentrations and MOx

Methane concentrations at Boknis Eck were in a typical range with regard to other shelf seas and coastal ecosystems (e.g., Rehder et al., 1998; Bange, 2006; Upstill-Goddard 2016). However, we could not find clear seasonal methane concentration patterns as observed for oxygen and all other physico-chemical parameters (Fig. 2). Our data are in line with

observations from 2006 – 2008 (Bange et al., 2010) showing that methane concentrations did not follow a bimodial seasonal distribution. Bange et al. (2010) observed that water column methane accumulations were correlated with a 1-month time lag to chlorophyll *a* concentrations indicating that pulses of OM input to the sediments were boosting methanogenesis. A recent study by Maltby et al. (in prep.) found that surface methanogenesis is indeed mostly dependent on the availability and quality of OM. Oxygen concentrations can have a modulating (indirect) effect on methane concentrations: Low water-column oxygen concentrations, for instance, lead to enhanced burial of 'fresh' OM to the sediments, which in turn favours methanogenesis at Boknis Eck (Bange et al., 2010; Maltby et al., in prep). Such a modulating effect of oxygen concentrations on methane concentrations has also been found in other hypoxic ecosystem (see Naqvi et al., 2010 for a review).

MOx rates at Boknis Eck were in the same order of magnitude as the ones measured in other coastal environments (e.g., Abril and Iversen 2002; Mau et al., 2013; Osudar et al., 2015). We could not find a direct stimulus of high methane concentrations on MOx, i.e., k (and r_{MOx}) was not correlated to methane concentrations (R^2=0.01). For example, we found low methane concentrations in Sept. 2013 but high MOx rates, while high methane concentrations in Feb. 2014 were accompanied by only moderately elevated MOx rates. Previous studies suggested an inverse relationship between turnover time (i.e., 1/k) and methane concentrations (Elliott et al., 2011; Nauw et al., 2015; Osudar et al., 2015). Although this relationship might hold true on a larger scale spanning different environmental settings, several studies found that on a smaller, regional scale this is not the case (Heintz et al., 2012; Mau et al., 2012; Steinle et al., 2015; Steinle et al., subm.). Steinle et al (2015) found, for instance, that currents translocating methanotrophic communities exerted a more important control on the magnitude of local MOx rates than methane concentrations at the continental margin offshore Svalbard. MOx measurements in our study showed a seasonal behaviour with lower rates during the winter season featuring a mixed water column (Mar. 2013/Feb. 2014), and highest rates during stratified conditions (June – Oct.). Linear regression and PCA analysis revealed that k was mainly correlated to depth. If depth was removed, k inversely correlated with oxygen concentrations ($p<0.01$), whereas temperature, salinity and methane concentrations showed no significant correlation. In order to investigate these results and our observations during our time-series study further, we conducted laboratory experiments to test the effect of oxygen concentration (section 4.2), and temperature on MOx (section 4.3).

4.2 Aerobic methanotrophy at micro-oxic conditions

In our seasonal study, we detected some of the highest MOx rates in Sept. 2013 and 2014 (Fig. 2f), where bottom water oxygen concentrations were below detection limit of our oxygen sensor (i.e., <1 – 2 μmol l^{-1}). Our incubation experiments with oxygen concentrations

as low as ~0.1 nmol l^{-1} confirmed the occurrence of the highest MOx rates at the lowest oxygen concentration in bottom waters from both in situ oxygen-rich or oxygen-depleted conditions (Fig. 3, 4). It is likely that in situ oxygen concentration fell below the 1 – 2 μmol l^{-1} detection limit of the CTD sensor, but never reached 0 μmol l^{-1} since sulphide was never observed. AOM thus seems unlikely to account for the observed oxidation rates since ANMEs cannot persist if oxygen is present (Treude et al., 2005; Knittel and Boetius, 2009). Three other recent studies in lakes reported the occurrence of aerobic methanotrophy in apparently anoxic environments (Blees et al., 2015; Milucka et al., 2015; Oswald et al., 2015). Two of these studies were carried out in shallow Swiss lakes and showed that under light conditions algae provided enough oxygen through photosynthesis for MOx to proceed under otherwise anoxic conditions (Milucka et al., 2015; Oswald et al., 2015). At Boknis Eck, light intensities at oxygen-limited depths (>20 mbsl) are probably too low to account for the observed high rates. Additionally, in our dark incubations, rates were still highest at the lowest oxygen concentration, making it unlikely that photosynthetic production of oxygen played a role in our incubations. The third study discovered a large active MOx community in clearly anoxic environments at ~200 m water depth, which was too deep for light-dependent MOx (Blees et al., 2014). At in situ oxygen concentrations above 1 μmol l^{-1}, no MOx was detected. It was hypothesized that sporadic oxygen-inflow is sufficient for the MOx community to thrive in hypoxic waters (Blees et al., 2014). At Boknis Eck, it is likely that there were some sporadic oxygen inputs through currents and that truly anoxic waters were rare. Nevertheless, this would still not explain why we detected highest rates at the lowest oxygen in our incubations. A possible cause for the higher MOx rates at low oxygen is the absence of grazers that were found to control the community size of MOB in shallow Finnish lakes (Devlin et al., 2015). For our incubations, we purged the water with N_2 for 30 min and only subsequently re-adjusted oxygen concentration. This may have led to the death of all grazers, or at least has limited their metabolic functions in the low oxygen incubations. Opposing this theory, we also found these trends of highest MOx at low oxygen levels in incubations with originally hypoxic waters (June 2014; Fig. 3b), where grazers were probably absent from the beginning of the incubations. The reason for the obvious boost of MOx rates at low oxygen levels thus seems to be at the cellular or biochemical level. Indeed, in our incubations with ^{14}C-CH_4 tracer, we detected differences in the metabolic functioning of cells at low and high oxygen concentration. Although MOx rates were faster at low oxygen concentration, the fraction of ^{14}C incorporated into biomass was higher at elevated oxygen concentration when compared to low oxygen concentrations. It thus seems possible that aerobic methanotrophs need to oxidise methane at higher rates in low oxygen environments in order to keep up their metabolism under oxygen-deficiency stress, similar as for e.g., low temperature stress (Price and Sowers, 2004). The partitioning between catabolic and anabolic

processes tended towards an increase of metabolic processes at low oxygen concentration at the cost of anabolic investment. Another possibility for the observation of high MOx at low oxygen is a switch to a fermentation-based metabolism as was found in culture-based experiments (Kalyuzhnaya et al., 2013). Kalyuzhnaya et al. showed that methane assimilation in *Methylomicrobium alcaliphylum* 20Z switched to a fermentation-based metabolism under oxygen-limiting conditions (ca. ~10 μmol l^{-1}). However, additional biochemical investigations are necessary to constrain this aspect further. We can also not rule out that different MOB species are active at differential O_2-concentrations at Boknis Eck, which may also lead to the observed differences. However, the incubation period in our experiment was rather low at 6-10 hours. With respect to the relatively slow doubling time of marine methanotrophic bacteria estimated at ~3.5 d (Kessler et al., 2011), a major community shift during the short incubation time thus seems unlikely.

4.3. Perturbations: North-Sea water inflow changes MOx community

The MOx community at Boknis Eck generally showed a mesophilic temperature optimum between 10°C and 37 °C, both at 5 mbsl (Supplementary Fig. 2) and at 20 mbsl (Fig. 5), which is typical for most cultured aerobic methanotrophs (Hanson and Hanson 1996; Murrell 2010). The temperature optimum was ~5-20°C higher than the in situ temperature (at the time of sampling), which is typical for many microorganisms (Price and Sowers 2004). Hence the observed increase in yearly (bottom) water temperatures (Lennartz et al., 2014) and the anticipated further increase in response to global warming could lead to an increased MOx activity in the future. However, how much change elevated atmospheric temperatures of up to several °C by the end of the century (IPCC, 2013) will cause in the composition of the methanotrophic community at Boknis Eck remains speculative.

Contrary to the general mesophilic behaviour of the MOx community at Boknis Eck, incubations with waters sampled in Nov. 2013 (Fig. 5b) revealed a psychrophilic temperature optimum between 0°C and 20°C. This difference strongly suggests the presence of a different microbial MOx community at Boknis Eck in Nov. 2013 contrasting all other sampling times. Compared to all other samplings, maximum k and r_{MOx} were detected at 15 mbsl and not in bottom waters. The sampling took place on 8th Nov, about a week after a large October 2013-inflow of oxygen-rich, salty North Sea water (Naumann and Nausch, 2015). At Boknis Eck, the unusual oxygen profile with a distinct minimum at 15 mbsl and increasing O_2 concentrations in bottom waters attest to this inflow (M. Naumann, pers. comm.). The North Sea is characterised by numerous seabed features associated to methane emission (Judd and Hovland, 2007). In addition, water column methane concentrations are typically elevated in the North Sea (Rehder et al., 1998) and water column MOx activity was detected at several sites in the North Sea (Mau et al., 2015; Osudar et al., 2015; Steinle et al., subm.). It thus

seems possible that the MOB community of the inflowing North Sea water replaced the previously prevailing MOB community at Boknis Eck, leading to the observed shift from a mesophilic to a psychrophilic community.

4.4 Significant methane removal by MOx

The calculated median methane efflux from our measurements (5.1 or 11.9 μmol m^{-2} d^{-1}, considering min. and max. k, respectively) was very similar to the previous data of a monthly sampling campaign at Boknis Eck from 2006 to 2008 (6.3 – 14.7 μmol m^{-2} d^{-1}; Bange et al., 2010). Average surface saturation (447% with respect to atmospheric equilibrium) at Boknis Eck was at the lower end of European estuarine systems and river plumes, but clearly higher than values determined for European shelf waters (Upstill-Goddard et al., 2000; Bange, 2006; Schubert et al., 2006; Grunwald et al., 2009; Ferrón et al., 2010; Schmale et al., 2010; Osudar et al., 2015; Upstill-Goddard and Barnes, 2016).

Table 2. Integrated methane oxidation rates (F_{MOx}) and methane flux into the atmosphere (F_{atm}) in comparison to stratification (indicated by the buoyancy frequency N). F_{atm} was calculated with a min and max k_w-value. $F_{tot} = F_{MOx} + F_{atm-avg.}$. N is given as the average for 10 – 20 mbsl. A water column with N values >120 is considered stratified.

sampling	F_{MOx} [μmol l^{-1} d^{-1}]	F_{atm} - min k_w [μmol l^{-1} d^{-1}]	F_{atm} - max k_w [μmol l^{-1} d^{-1}]	F_{atm} - avg. [μmol l^{-1} d^{-1}]	F_{MOx}/F_{tot} [%]	N [rad s^{-1}]	stratification
Oct. 2012	29.6	12.4	31.1	21.7	58	91	weak/mixed
Mar. 2013	11.7	10.5	26.4	18.5	39	59	weak/mixed
June 2013	27.3	3.2	7.9	5.5	83	241	strong
Sept. 2013	33.0	3.4	8.5	5.9	85	229	strong
Nov. 2013	28.0	6.3	15.8	11.0	72	216	strong
Feb. 2014	14.5	7.0	17.6	12.3	54	114	weak/mixed
June 2014	12.7	2.9	7.4	5.2	71	201	strong
Sept. 2014	82.3	2.5	6.2	4.3	95	245	strong

At Boknis Eck, methane originates from sedimentary methanogenesis (Whiticar 2002; Treude et al., 2005; Maltby et al., in prep.), which can enter the water column either by diffusion of by bubble transport in this system. The amplitudes of methanogenesis and AOM were found to show strong spatiotemporal heterogeneity and flux estimates are difficult from these measurements (Treude et al, 2005; Maltby et al., in prep.). Additionally, methane input into the water column via bubble transport has not been quantified at Boknis Eck. A survey with an echosounder system in September 2014 did not reveal the presence of bubbles at Boknis Eck (unpubl. data), but temporal and spatial variability are very likely. Ebullition of methane was nevertheless observed in the vicinity of Boknis Eck (Jackson et al., 1998). As a result, we can only speculate on the relative importance of methane release from sediments by diffusion or ebullition and on the absolute methane flux. We hence assume that the release

of methane from sediments to the water column equals the total flux of methane ($F_{sed} = F_{tot}$), i.e., the sum of methane oxidized via MOx and the evasion of the remaining methane to the atmosphere ($F_{atm} + F_{MOx} = F_{tot}$). Possible effects of advection on the methane concentration and MOx, and other possible sources of methane are ignored (e.g., from groundwater seepage; Bussmann and Suess, 1998). Thus, we can estimate how much of the water column methane is removed by MOx before its potential emission into the atmosphere. Our depth integrated rates and the average of our minimum and maximum estimates of methane efflux to the atmosphere indicate that 71 – 95% of methane released from the sediment to the water column is oxidized during stratified conditions (Tab. 2). In contrast, only 39 – 58% is oxidized during mixed conditions. Our F_{MOx} estimates are probably conservative as our deepest sampling depth was 25 mbsl and we always measured maximum r_{MOx} in this depth (except for Nov. 2013; see 4.3.). This could mean that actual r_{MOx} between 25 and 28 mbsl (water depth at Boknis Eck) might be higher.

5. Conclusions

Extensive research efforts have been directed at quantifying methane fluxes from coastal environments but only a few studies cover different seasons and hence the majority cannot account for differences between fully mixed and stratified conditions (Bange, 2006; Bange et al., 2010; Bakker et al., 2014). Furthermore, to the best of our knowledge, this is the first long-term (>2 years) seasonal study on MOx activity in coastal environments. The results from our study are thus important for the understanding of the efficiency of MOx as the pelagic microbial filter, which counteracts methane evasion to the atmosphere from these systems. Trends at Boknis Eck and in large parts of other coastal systems indicate warmer temperatures in the future, and thus an earlier onset of stratification (e.g., Lennartz et al., 2014). Together with an increased organic matter/nutrient input, these factors will cause the expansion of hypoxic zones. In our seasonal study, we observed positive and negative feedback mechanisms of these environmental controls on MOx, which can be used to estimated how the predicated changes may affect MOx activity.

The predicted lower average oxygen concentrations should intuitively lead to aerobic methane oxidation rates. However, in our field and laboratory investigations we observed highest MOx activity at lowest oxygen concentrations, providing evidence that an increase in the length of hypoxic periods, at least at Boknis Eck, will most likely not lead to a decreased MOx potential. The increasing length of the hypoxic period caused by an earlier onset of stratification may furthermore be an important control of the MOx community growth since our data suggest that the MOx community experiences growth restrictions under oxygen-deficiency stress. However, a longer stratification period might also be favourable for MOx: Not only does the methanotrophic community have more stability for development under

stratified conditions (vertical methane transport is also slowed down by the presence of a thermocline, which limits turbulent diffusion, allowing more time for MOx to proceed. The predicted increasing temperatures and/or potentially enhanced mineralisation in bottom waters will likely lead to elevated methane production. On the other hand, higher temperatures will also cause an increase in MOx rates due to the mesophilic behaviour of the MOx community. Additionally, the MOx community at Boknis Eck can be disturbed in case of large North Sea inflows, leading to shifts in the MOx community, and underscoring the importance of currents in modulating water column MOx (Steinle et al., 2015). The frequency of these events is hard to predict but they will probably not impact the MOx potential greatly at Boknis Eck. Overall, the net effect of these positive and negative feedback mechanisms cannot be quantified, but the results from this study greatly enhance current knowledge on MOx in coastal systems.

Acknowledgements

We thank the captains and crews of R/V Alkor, RC Littorina and RB Polarfuchs, and the staff of the GEOMAR's Technology and Logistics Centre for the excellent support at sea and onshore during our sampling campaigns. Additional thanks go to G. Schüssler, F. Wulff, P. Wefers, A. Petersen, M. Lange, and F. Evers for help with the field work. We also thank F. Malien, X. Ma, A. Kock, S. Lennartz and T. Baustian for the regular calibration of the CTD and CH_4 analysis. This work received financial support through a D-A-CH project funded by the Swiss National Science Foundation and the German Research foundation (grant no. 200021L_138057, 200020_159878/1), and through the Cluster of Excellence "The Future Ocean" funded by the German Research Foundation. Further support was provided through the EU COST Action PERGAMON (ESSEM 0902).

Supplementary Figures

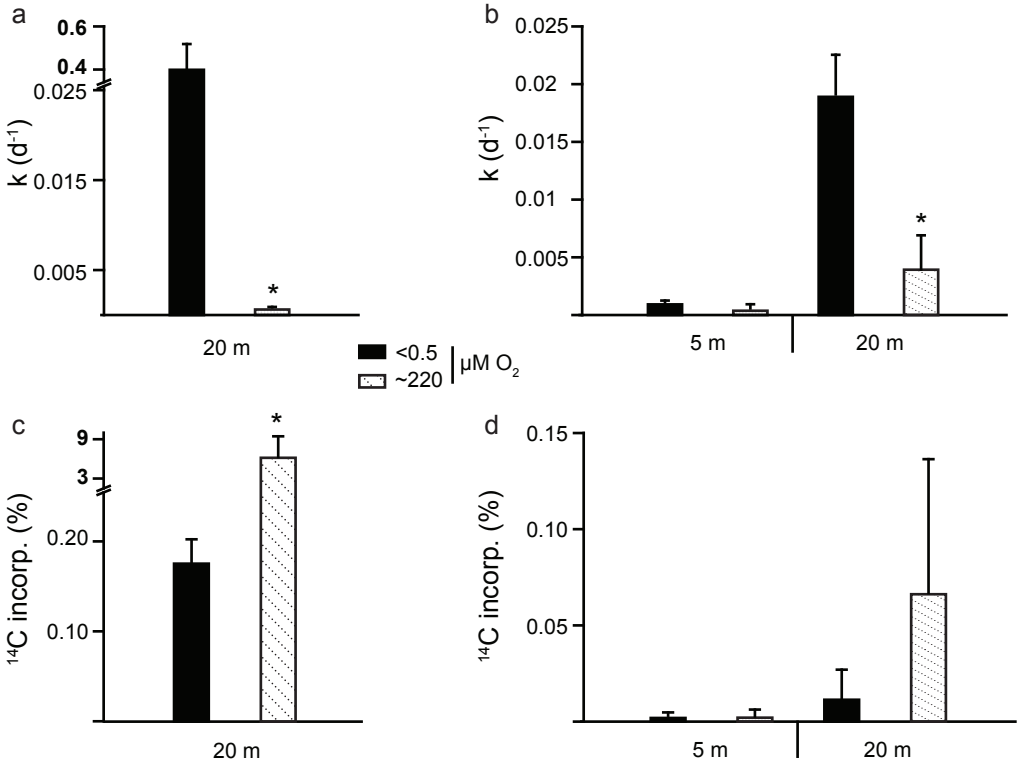

Supplementary Figure 1. *Methane-carbon assimilation in relation to oxygen concentration*. Methane-carbon assimilation was determined from incubations amended with ^{14}C-CH_4 at saturated (~220 μmol l^{-1}, shaded bars) or low oxygen concentrations (<0.5 μmol l^{-1}, black bars) of water recovered in Nov. 2013 at 20 mbsl (a, c) and in Feb. 2014 at 5 and 20 mbsl (b, d). Incubations were performed in triplicates and standard deviations are indicated. (a, b) First-order rate constant (*k*). (c, d) Fraction of oxidized methane incorporated into biomass. * indicates a p-value <0.05 of a two-tailed, two-sample t-test assuming equal variance between the samples at low and high oxygen concentrations.

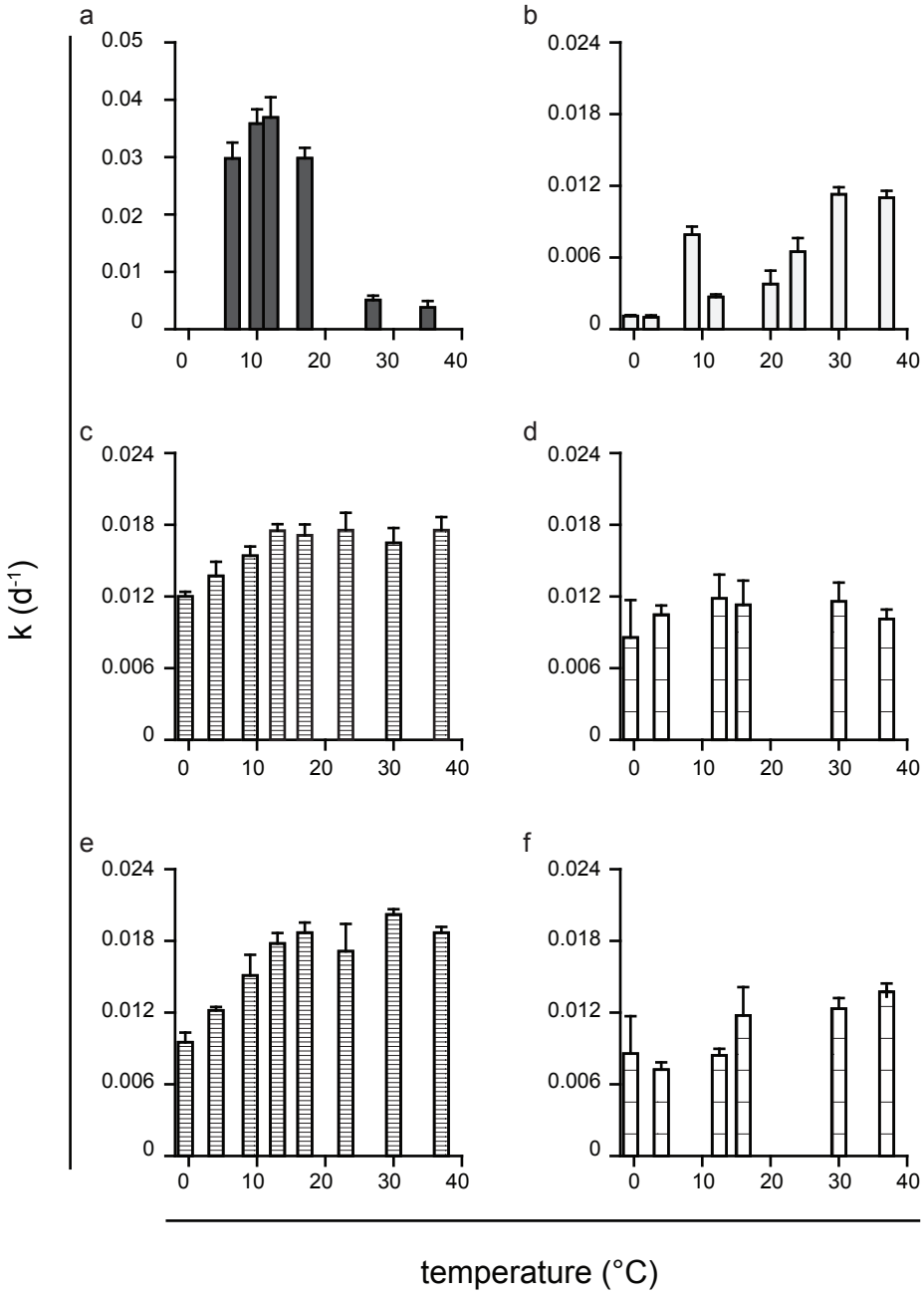

Supplementary Figure 2. *MOx first order rate constants (k) at different temperatures*. First order rate constants of MOx were determined with $^{3}H\text{-}CH_4$ amendments in triplicated incubations of water from 5 mbsl (a-d) and 20 mbsl (e, f), recovered in Nov. 2013 (a), Feb. 2014 (b), June 2014 (c, e), and Sept. 2014 (d, f).

References

Abril, G., and Iversen, N. (2002). Methane dynamics in a shallow non-tidal estuary(Randers Fjord, Denmark). Marine ecology progress series 230: 171-181.

Bakker, D.C., Bange, H.W., Gruber, N., Johannessen, T., Upstill-Goddard, R.C., Borges, A.V., et al. (2014). Air-sea interactions of natural long-lived greenhouse gases (CO2, N2O, CH4) in a changing climate, p. 113-169. In P.S. Liss, and M.T. Johnson (eds), Ocean-Atmosphere Interactions of Gases and Particles. Springer Verlag.

Bange, H.W (2006). Nitrous oxide and methane in European coastal waters. Estuarine, Coastal and Shelf Science 70: 361-374.

Bange, H. W., Hansen, H.P., Malien, F., Laß, K., Dale, A.W., Karstensen, J., et al. (2011). Boknis Eck time series station (SW Baltic Sea): measurements from 1957 to 2010. LOICZ inprint 2011: 16-22.

Bange, H.W., Bergmann, K., Hansen, H.P., Kock, A., Koppe, R., Malien, F., and Ostrau, C. (2010). Dissolved methane during hypoxic events at the Boknis Eck time series station (Eckernförde Bay, SW Baltic Sea). Biogeosciences 7: 1279-1284.

Bange, H.W., Bartell, U.H., Rapsomanikis, S., and Andreae, M.O. (1994). Methane in the Baltic and North Seas and a reassessment of the marine emissions of methane. Global Biogeochemical Cycles 8: 465-480.

Blees, J., Niemann, H., Wenk, C.B., Zopfi, J., Schubert, C.J., Kirf, M.K., et al. (2014). Micro-aerobic bacterial methane oxidation in the chemocline and anoxic water column of deep south-Alpine Lake Lugano (Switzerland). Limnology and oceanography 59: 311-324.

Bussmann, I., and Suess, E. (1998). Groundwater seepage in Eckernförde Bay (Western Baltic Sea): Effect on methane and salinity distribution of the water column. *Continental Shelf Research* 18: 1795-1806.

Canfield, D.E. and Thamdrup, B. (2009). Towards a consistent classification scheme for geochemical environments, or, why we wish the term suboxic would go away. Geobiology 7: 385-392.

Carini, S., Bano, N., LeCleir, G., and Joye, S.B. (2005). Aerobic methane oxidation and methanotroph community composition during seasonal stratification in Mono Lake, California (USA). Environ Microbiol 7: 1127-1138.

Devlin, S.P., Saarenheimo, J., Syväranta, J., and Jones, R.I. (2015). Top consumer abundance influences lake methane efflux. Nat Commun 6: 8787.

Diaz, R.J. and Rosenberg, R. (2008). Spreading dead zones and consequences for marine ecosystems. Science 321: 926-929.

Elliott, S., Maltrud, M., Reagan, M., Moridis, G., and Cameron-Smith, P. (2011). Marine methane cycle simulations for the period of early global warming. Journal of Geophysical Research: Biogeosciences 116: G01010, doi:10.1029/2010JG001300.

Ferrón, S., Ortega, T., and Forja, J.M. (2010). Temporal and spatial variability of methane in the north-eastern shelf of the Gulf of Cádiz (SW Iberian Peninsula). Journal of Sea Research 64: 213-223.

Grunwald, M., Dellwig, O., Beck, M., Dippner, J.W., Freund, J.A., Kohlmeier, C., et al. (2009). Methane in the southern North Sea: Sources, spatial distribution and budgets. Estuarine, Coastal and Shelf Science 81: 445-456.

Hansen, H.P., Giesenhagen, H.C. and Behrends, G. (1999). Seasonal and long-term control of bottom-water oxygen deficiency in a stratified shallow-water coastal system. ICES Journal of Marine Science 56: 65-71.

Hanson, R. S. and Hanson, T.E. (1996). Methanotrophic bacteria. Microbiological reviews 60: 439-471.

Heintz, M.B., Mau, S., and Valentine, D.L. (2012). Physical control on methanotrophic potential in waters of the Santa Monica Basin, Southern California. Limnology and oceanography 57: 420-432.

HELCOM: (2009). Eutrophication in the Baltic Sea - an integrated assessment of the effects of nutrient enrichment in the Baltic Sea region. Baltic Sea Environ. Proc. 115: 1-145.

Hoppe, H.-G., Giesenhagen, H.C., Koppe, R., Hansen, H.-P., and Gocke, K. (2013).Impact of change in climate and policy from 1988 to 2007 on environmental and microbial variables at the time series station Boknis Eck, Baltic Sea. Biogeosciences 10: 4529-4546.

IPCC, 2013. Stocker, T.F., Qin, D., Plattner, G., Tignor, M., Allen, S., Boschung, J., et al. (eds). Climate Change 2013 - The Physical Science Basis. Contribution of Working Group I to the Fifth Assessment Report of the Intergovernmental Panel on Climate Change. Cambridge University Press.

Jackson, D.R., Williams, K.L., Wever, T.F., Friedrichs, C.T., and Wright, L.D. (1998).Sonar evidence for methane ebullition in Eckernförde Bay. Continental Shelf Research 18: 1893-1915.

Jähne, B., Heinz, G., and Dietrich, W. (1987). Measurement of the diffusion coefficients of sparingly soluble gases in water. Journal of Geophysical Research: Oceans 92: 10767-10776.

Judd, A. and Hovland, M. (2007). Seabed Fluid Flow: The impact of geology, biology and the marine environment. Cambridge University Press.

Kalyuzhnaya, M.G., Yang, S., Rozova, O.N., Smalley, N.E., Clubb, J., Lamb, A., et al. (2013). Highly efficient methane biocatalysis revealed in a methanotrophic bacterium. Nat Commun 4: 2785.

Kessler, J.D., Valentine, D.L., Redmond, M.C., Du, M., Chan, E.W., Mendes, S.D., et al. (2011). A persistent Oxygen Anomaly Reveals the Fate of Spilled Methane in the Deep Gulf of Mexico. Science 331: 312-315.

Kirschke, S., Bousquet, P., Ciais, P., Saunois, M., Canadell, J.G., Dlugokencky, E.J., et al. (2013). Three decades of global methane sources and sinks. Nature Geoscience 6: 813-823.

Knittel, K. and Boetius, A. (2009). Anaerobic Oxidation of Methane: Progress with an Unknown Process. Annual Review of Microbiology 63: 311-334.

Lennartz, S.T., Lehmann, A., Herrford, J., Malien, F., Hansen, H.-P., Biester, H., and Bange, H.W. (2014). Long-term trends at the Boknis Eck time series station (Baltic Sea), 1957-2013: does climate change counteract the decline in eutrophication? Biogeosciences 11: 6323-6339.

Madigan, Q.D., Martinko, J., Bender, K., Buckley, D., and Stahl, D. (2015). Brock Biology of Microorganisms. Boston.

Maltby, J., Steinle, L., Bange, H.W., Löscher, C.R., Fischer, M.A., Schmidt, M., and Treude, T. Microbial methanogenesis in the sulfate-reducing zone in sediments from Eckernförde Bay, SW Baltic Sea. Geochemica Cosmochimica et Acta: **in preparation**.

Mau, S., Körber, J.-H., Torres, M.E., Römer, M., Sahling, H., Wintersteller, P., et al. (2015). Seasonal methane accumulation and release from a gas emission site in the central North Sea. Biogeosciences 12: 5261-5276.

Mau, S., Blees, J., Helmke, E., Niemann, H., and Damm, E. (2013). Vertical distribution of methane oxidation and methanotrophic response to elevated methane concentrations in stratified waters of the Arctic fjord Storfjorden (Svalbard, Norway). Biogeosciences 10: 6267-6278.

Mau, S., Heintz, M.B., and Valentine, D.L. (2012). Quantification of CH4-loss and transport in dissolved plumes of the Santa Barbara Channel, California. Continental Shelf Research 32: 110-120.

Middelburg, J.J., and Levin, L.A. (2009). Coastal hypoxia and sediment biogeochemistry. Biogeosciences 6: 1273–1293.

Milucka, J., Kirf, M., Lu, L., Krupke, A., Lam, P., Littmann, S., et al. (2015). Methane oxidation coupled to oxygenic photosynthesis in anoxic waters. ISME J 9: 1991-2002.

Mohrholz, V., Naumann, M., Nausch, G., Krüger, S., and Gräwe, U. (2015). Freshoxygen for the Baltic SeaAn exceptional saline inflow after a decade of stagnation. Journal of Marine Systems 148: 152-166.

Murrell, J C. (2010). The Aerobic Methane Oxidizing Bacteria (Methanotrophs), p. 1953-1966. In K.N. Timmis (eds), 3.26. Springer Berlin Heidelberg.

Naqvi, S. W. A., Bange, H.W., Far\'\ias, L., Monteiro, P.M.S., Scranton, M.I. and Zhang, J. (2010). Marine hypoxia/anoxia as a source of CH4 and N2O. Biogeosciences 7: 2159-2190.

Nauw, J., Haas, H.D., and Rehder, G. (2015). A review of oceanographic andmeteorological controls on the North Sea circulation and hydrodynamics with a view to the fate of North Sea methane from well site 22 / 4b and other seabed sources. Marine and Petroleum Geology 68: 861-882.

Niemann, H., Steinle, L.I., Blees, J., Krause, S., Bussmann, I., Treude, T., et al. (2015). Toxic effects of butyl elastomers on aerobic methane oxidation. Limnology and Oceanography: Methods 13: 40-52.

Osudar, R., Matoušů, A., Alawi, M., Wagner, D., and Bussmann, I. (2015). Environmental factors affecting methane distribution and bacterial methane oxidation in the German Bight (North Sea). Estuarine, Coastal and Shelf Science 160: 10-21.

Oswald, K., Milucka, J., Brand, A., Littmann, S., Wehrli, B., Kuypers, M.M., and Schubert, C.J. (2015). Light-Dependent Aerobic Methane Oxidation Reduces Methane Emissions from Seasonally Stratified Lakes. PLoS One 10: e0132574.

Price, P.B., and Sowers, T. (2004). Temperature dependence of metabolic rates formicrobial growth, maintenance, and survival. Proc Natl Acad Sci U S A 101: 4631-4636.

Rabalais, N.N., Cai, W.-J., Carstensen, J., Conley, D.J., Fry, B., Hu, X., et al. (2014). Eutrophication-driven deoxygenation in the coastal ocean. Oceanography 27: 172-183.

Raymond, P.A., and Cole, J.J. (2001). Gas exchange in rivers and estuaries: Choosing a gas transfer velocity. Estuaries and Coasts 24: 312-317.

Reeburgh, W.S. (2007). Oceanic methane biogeochemistry. CHEMICAL REVIEWS 107: 486-513.

Reeburgh, W.S., Ward, B.B., Whalen, S.C., Sandbeck, K.A., Kilpatrickt, K.A., and Kerkhof, L.J. (1991). Black Sea methane geochemistry. Deep Sea Research Part A. Oceanographic Research Papers 38: S1189-S1210.

Rehder, G., Keir, R.S., Suess, E., and Pohlmann, T. (1998). The multiple sources and patterns of methane in North Sea waters. Aquatic Geochemistry 4: 403-427.

Rhein, G., Rintoul, D., Aoki, F., Campos, W., Chambers, J., Feely, J., et al. (2013). Observations: Oceans, p. 255-316. In I.P.O.C. Change (eds), Climate Change 2013 - The Physical Science Basis. Cambridge University Press.

Naumann, M. and Nausch, G. (2015). Salzwassereinstrom 2014. Die Ostsee atmet auf. *Chemie unserer Zeit* 49, 76 – 80.

Schmale, O., Schneider von Deimling, J., Gülzow, W., Nausch, G., Waniek, J.J., and Rehder, G. (2010). Distribution of methane in the water column of the Baltic Sea. GEOPHYSICAL RESEARCH LETTERS 37: DOI: 10.1029/2010GL043115.

Schubert, C. J., Coolen, M.J., Neretin, L.N., Schippers, A., Abbas, B., Durisch-Kaiser, E., et al. (2006). Aerobic and anaerobic methanotrophs in the Black Sea water column. Environ Microbiol 8: 1844-1856.

Siedler, P. and Peters, H. (1986). Properties of sea water, Physical properties (general), p. 233-264. In J. Sündermann (eds), LANDOLT-BÖRNSTEIN, Numerical Data and Functional Relationships in Science and Technology, New Series, Oceanography. Springer Verlag.

Smetacek, V. (1985). The annual cycle of Kiel Bight plankton: a long-term analysis. Estuaries 8: 145-157.

Smetacek, V., von Bodungen, B., Knoppers, B., Peinert, R., Pollehne, F., Stegmann, P., and Zeitzschel, B. (1984). Seasonal stages characterizing the annual cycle of an inshore pelagic system. Rapports et Proces-Verbaux des Reunions Conseil International pour l'Exploration de la Mer 183: 126-135.

Steinle, L., Graves, C.A., Treude, T., Ferré, B., Biastoch, A., Bussmann, I., et al. (2015). Water column methanotrophy controlled by a rapid oceanographic switch. Nature Geoscience 8: 378-382.

Steinle, L., Schmidt, M., Bryant, L., Haeckel, M., Linke, P., Sommer, S., et al. Linked sediment and water column methanotrophy at a man-made gas blowout in the North Sea: Implications for methane budgeting in seasonally stratified shallow seas. Limnology and Oceanography: **submitted.**

Treude, T., Krüger, K., Boetius, A., and Jørgensen, B.B. (2005). Environmental control on anaerobic oxidation of methane in gassy sediments of Eckernförde Bay (German Baltic). Limnology and Oceanography 50: 1771-1786.

Upstill-Goddard, R. C. and Barnes, J. (2016). Methane emissions from UK estuaries: Re-evaluating the estuarine source of tropospheric methane from Europe. Marine Chemistry 180: 14-23.

Upstill-Goddard, R. C., Barnes, J., Frost, T., Punshon, S., and Owens, N.J. (2000). Methane in the southern North Sea: Low-salinity inputs, estuarine removal, and atmospheric flux. Global Biogeochemical Cycles 14: 1205-1217.

Whiticar, M. J. (2002). Diagenetic relationships of methanogenesis, nutrients, acoustic turbidity, pockmarks and freshwater seepages in Eckernförde Bay. Marine Geology 182: 29-53.

Wiesenburg, D. A. and N.L. Guinasso Jr., N.L. (1979). Equilibrium solubilities of methane, carbon monoxide, and hydrogen in water and sea water. Journal of Chemical and Engineering Data 24: 356-360.

Micro-aerophilic methanotrophy and sulfate reduction in the Kryos brine basin: evidence for microbial activity at 4 M $MgCl_2$

Lea Steinle[1,2], Nicole Felber[1], Claudia Casalino[3], Chiara Tessarolo[4], Gert de Lange[3], Alina Stadniskaia[5], Jaap S. Sinninghe Damste[5], Moritz Lehmann[1], Tina Treude[2,a], Helge Niemann[1,6]

in preparation for *Environmental Microbiology*.

[1] Department of Environmental Sciences, University of Basel, Basel, Switzerland

[2] GEOMAR, Helmholtz Centre for Ocean Research, Kiel, Germany

[3] Geosciences, Utrecht University, Utrecht, Netherlands

[4] Department of Earth and Environmental Sciences, University of Milano-Bicocca, Milan, Italy

[5] NIOZ, Royal Netherlands Institute for Sea Research, Texel, Netherlands

[6] CAGE – Centre for Arctic Gas Hydrate, Environment and Climate, Department of Geology, UiT the Arctic University of Norway, 9037 Tromsø, Norway

[a] Present address: Department of Earth, Planetary & Space Sciences and Atmospheric & Oceanic Sciences, University of Los Angeles, Los Angeles, California, USA

*Corresponding author: lea.steinle@unibas.ch

Abstract

The Kryos brine basin is located at ~3300 m water depth in the Eastern Mediterranean Sea (~34.95°N; 22.02°E). The anoxic brine originates from redissolved subsurface late-stage Messinian evaporites, and contains near-saturation concentrations of $MgCl_2$-equivalents (3.9 mol kg^{-1}), which makes this environment extremely challenging for life. The strong density difference between the brine and the overlying Mediterranean seawater impedes mixing and leads to a narrow (<3 m) chemocline at the seawater-brine interface. Concentrations of sulfate, sulfide and methane sharply increased across the chemocline from seawater background values to 144 mmol kg^{-1}, 150 μmol kg^{-1} and 20 μmol kg^{-1}, respectively, in the anoxic brine. Radiotracer-based ex situ measurements revealed aerobic methane oxidation (MOx) at micro-oxic conditions within the interface (up to 60 nmol kg^{-1} d^{-1}). In line with elevated MOx rates, the residual methane within the interface became ^{13}C-enriched when compared to the brine, and we found diagnostic ^{13}C-depleted lipid biomarkers (e.g., diplopterol, -46.6‰), which can be attributed to aerobic methanotrophs. Additionally, we detected relatively ^{13}C-enriched fatty acids (up to -18‰) in the lower interface, which likely originated from organisms fixing carbon via the reverse tri-carboxylic acid (rTCA) cycle, such as sulfur-oxidizing Epsilonproteobacteria. Within the brine, we could not find evidence for anaerobic oxidation of methane (AOM), despite thermodynamically favorable conditions for AOM in this environment. Sulfate reduction rates, in contrast, were high within the brine (up to 430 μmol kg^{-1} d^{-1}) providing evidence that sulfate reducers are active at nearly saturated Mg^{2+} concentrations. Our results underscore that microbial life has adapted to the extremely harsh conditions in $MgCl_2$-rich environments.

1. Introduction

Environments characterized by salt concentrations higher than 5% (w/v) are considered hypersaline (Capece et al., 2013). These environments are challenging for life due to the high energetic costs for osmotic adaptation (Boetius and Joye, 2009), and the additional limitation of available water (Stevenson et al., 2015). Hypersaline environments are found in terrestrial settings (e.g., lakes, salt flats, salterns), but they are also encountered in the marine environment (e.g., mud volcanoes, sea-ice brine channels or brine basins); and microbial life was found in many of these systems (Boetius and Joye, 2009). Finally, hypersaline environments were also discovered on extraterrestrial objects (Hansen et al., 2006; McEwen et al., 2014; Hsu et al., 2015; Martín-Torres et al., 2015), raising the possibility that terrestrial, hypersaline environments are an example of how life could exist in an extraterrestrial environment (Preston and Dartnell, 2014). On Earth, brine basins were discovered at the seafloor of the Gulf of Mexico, the Red-, Black- and Eastern Mediterranean

Sea (see Stock et al., 2013, for a review). In the Mediterranean Sea, brine basins are located in bathymetric depressions at the Mediterranean Ridge and Strabo Trench south of Crete at water depths >3000 meters below sea level (mbsl). These lake-like features in the deep sea are up to several kilometers long and more than hundred meters deep (Stock et al., 2013). Mediterranean brines originate from the re-dissolution of evaporites deposited during the Messinian salinity crisis (5-6 million years ago), a time period during which the Eastern Mediterranean Sea evaporated almost completely on several occasions (Hsü et al., 1973; Camerlenghi, 1990). During evaporation, different salts/minerals precipitate in the order of their solubility products: Calcium minerals form the first evaporites, followed by halite, potash salts, and finally bischofite ($MgCl_2 \times 6H_2O$; De Lange et al., 1990). After burial by newly formed sediment, tectonic activity may re-expose these salt layers to seawater, which leads to re-dissolution of the precipitates, thereby forming brine (Wallmann et al., 1997). As the brines have a higher density than seawater, they accumulate in seafloor depressions, which are then referred to as brine basins (Camerlenghi, 1990). Even though many Mediterranean brine basins are in close proximity, the geochemical composition of the brine can differ strongly depending on the source evaporite (Stock et al., 2013). Most basins contain thalassohaline brines, i.e., the brine contains a multiple of seawater ion concentrations (i.e., the l'Atalante, Bannock, Thetis, Tyro and Urania basins; van der Wielen et al., 2005; La Cono et al., 2011). The Discovery basin and the much larger Kryos basin, however, are dominated by secondary $MgCl_2$ athalassohaline brines (Wallmann et al., 1997; Yakimov et al., 2015). Thus, they contain lower Na^+ concentrations than seawater but very high concentrations of Mg^{2+}.

The density difference between the brines and the overlying seawater results in reduced mixing. Since the seawater and brines differ in their electron donor and acceptor concentrations, a narrow (1-3 m) chemocline forms between the two liquids, referred to as the "interface" (Stock et al., 2013). Brine-seawater interfaces were found to be a hotspot for biological activity (Sass et al., 2001; van der Wielen et al., 2005; Daffonchio et al., 2006; Yakimov et al., 2007; Boetius and Joye, 2009; Yakimov et al., 2015), but microbial activity was even detected within the highly saline and anoxic brine basins (van der Wielen et al., 2005; Daffonchio et al., 2006). In contrast to the overlying seawater, no oxygen is present within the brines but alternative electron acceptors are plentiful, most importantly SO_4^{2-} (Stock et al., 2013). Previous studies provided evidence for sulfate reduction, methanogenesis and heterotrophic activity in most Mediterranean brine systems and their associated seawater-brine interfaces (van der Wielen et al., 2005; Daffonchio et al., 2015, LaCono et al., 2011), but not in the Kryos basin (Yakimov et al., 2015). Methane is a ubiquitous electron donor in these Mediterranean brines (van der Wielen et al., 2005; Cita, 2006; Borin et al., 2009). At

the interface, where oxygen is still available, aerobic oxidation of methane (MOx) can thus take place. MOx is mediated by methane-oxidizing bacteria (MOB) according to *Eq. 1*:

$$CH_4 + 2O_2 \rightarrow CO_2 + 2H_2O \qquad (Eq.\ 1)$$

MOB generally belong to the Type I- or Type II MOB within the Gamma- or Alphaproteobacteria, respectively. Once oxygen is depleted, methane can also be oxidized via anaerobic oxidation of methane (AOM). AOM is typically mediated by consortia of anaerobic methanotrophic archaea (ANME) and sulfate-reducing bacteria (SRB), according to *Eq. 2* (Boetius et al., 2000; Orphan et al., 2001; Niemann et al., 2006):

$$CH_4 + SO_4^{2-} \rightarrow HCO_3^- + HS^- + H_2O \qquad (Eq.\ 2)$$

Three main groups of ANME exist (ANME-1, -2, and -3), all of which are most closely related to methanogenic archaea (Knittel and Boetius, 2009). Recent findings demonstrated that ANME may also mediate AOM without partner bacteria (Milucka et al., 2012). Additionally, ANMEs and/or bacteria can oxidize methane with alternative electron acceptors, i.e., iron, manganese (Beal et al., 2009; Wankel et al., 2010; Egger et al., 2015), or nitrate (Haroon et al., 2013), but the environmental importance of these processes is not well constrained. Recent studies also identified freshwater bacteria that can oxidize methane anaerobically with nitrite (e.g., Ettwig et al., 2010), but this process has not yet been detected in marine environments.

However, neither MOx nor AOM has been investigated in the Mediterranean brine systems. Furthermore, an exception to the detection of widespread microbial activity within Mediterranean brines is Kryos, where microbial activity (mRNA of sulfate reducers and methanogens) has only been confirmed in the lower interface, but is regarded as impossible in the brine itself (Yakimov et al., 2015). Similarly, the presence of active microbes in the brine of the nearby Discovery Basin, which also contains nearly saturated $MgCl_2$ concentrations, has been discussed controversially (van der Wielen et al., 2005; Hallsworth et al., 2007; Oren, 2013). Major challenges for microbial life in bischofite-dominated environments, in addition to osmotic stress, are exceptional high levels of chaotropicity and very low water availability (a_W; Stevenson et al., 2015). Chaotropicity is an empiric measure of the effect of ions on the water hydrogen bounds (Cray et al., 2013). High chaotropicity, for instance, leads to the denaturation of proteins (Cray et al., 2013). Water availability, on the other hand, is a relative value of the vapor pressure of a solution relative to distilled water, and a key parameter used to determine limits of life (Stevenson et al., 2015).

In the present study, we investigate microbial processes at the Kryos brine basin across the seawater-brine interface into the brine itself using an interdisciplinary approach that included geochemical measurements of major ion concentrations, sulfate, sulfide, methane, methane-isotopic composition ($\delta^{13}C$, δD), and direct measurements of microbial methane oxidation and sulfate reduction with radio-tracer assays. Finally, we detected microbial communities with the aid of lipid biomarker analyses.

2. Methods

2.1 Study site

Kryos is one of eight deep hypersaline anoxic brine basins located at the bottom of the Eastern Mediterranean Sea (Fig. 1). It was discovered in 2008 during the MIDDLE08 cruise with R/V Urania (Yakimov et al., 2015), and is a north-south elongated basin (22°02′E 35°02′N – 22°04′E 34.93 N) with a brine volume of almost 10 km^3. The brine originates from secondary late-stage evaporites, dominated by bischofite (Yakimov et al., 2015). Its composition is similar to the of the Discovery brine (Wallmann et al., 1997; Wallmann et al., 2002), with the exception of higher concentrations of Na^+ and SO_4^{2-} (Yakimov et al., 2015). Samples presented in this study were collected on the Ristretto&Lungo Cruise (2010/2011) with R/V Meteor in the frame-work of the Moccha project (Eurodeep-Middle Program of the European Science Foundation).

2.2 Bathymetric mapping

Morphobathymetric data were collected with the Simrad EM122 Multibeam Echosounder (12kHz) of R/V Meteor. Due to its low frequency, the EM122 maintains a resolution of ~0.4% of the investigated depths (>3000 m). The systems was connected to the SIS Navigation System in order to define acquisition parameters and plan the navigation, as well as for visualizing collected data in realtime. Geophysical data were acquired in geographic coordinates (Lat/Long, datum WGS84) and the grid model was projected in UTM (WGS84, 34N). Data processing and export of the base XYZ coordinates was realized with the CARIS HIPS and SIPS and subsequently mapped using the Surfer and Global Mapper software packages.

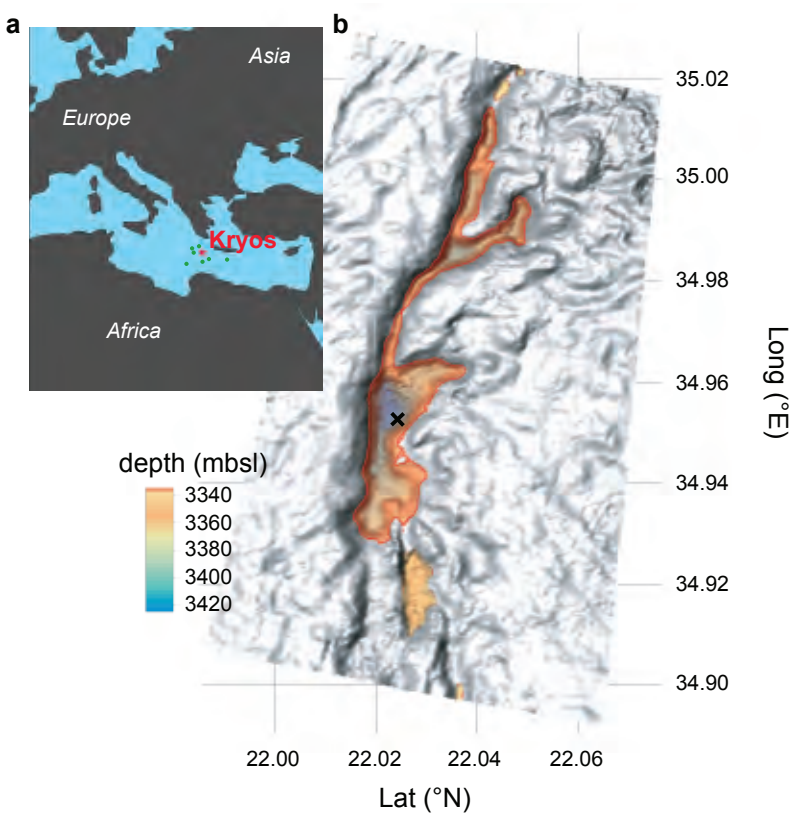

Figure 1. Overview map and bathymetry of the Kryos brine basin in the Eastern Mediterranean. a, Overview map of the brine basins of the Eastern Mediterranean. Kryos is indicated with a red star, the other basins with green dots. b, Bathymetry of the Kryos brine basin (resolution: 30 m). The extent of the basin is delimited with a dark orange line and the depth of the basin is indicated by the colored scale bar.

2.3 Sampling

Water samples were recovered with a rosette sampler equipped with 12 × 10 L Niskin bottles and probes for continuous measurements of conductivity, temperature and density (CTD; Seabird SBE9) in the deepest part of the Kryos basin (34.952°N; 22.025°E; Fig. 1). We sampled the water column just above the seawater-brine interface, within the interface and in the brine. To detect the exact position of the interface (IF), the conductivity sensor (mounted at the lower part of the rosette sampler frame) was monitored online. For IF sampling, we fired several bottles in quick succession immediately after a conductivity increase was detected, while slowly lowering the sampler through the IF. This way, each bottle contained a sample collected in a different section of the IF (Fig. 2). During recovery, the strong density difference impeded vertical mixing within the bottle, preserving the in situ stratified conditions. Upon retrieval, each bottle was sampled successively (~2 L per interval, which corresponds to ~20 cm vertical extension of the IF); first for volatiles (CH_4, HS^-) and dissolved O_2, then for microbial rate measurements, and finally for additional geochemical analyses (major elements, SO_4^{2-}). The relative position of the different Niskin Bottles (Fig. 2)

was aligned using Cl^- concentrations as a conservative tracer as described previously (e.g., Yakimov et al., 2015). CH_4, HS^- and dissolved O_2 concentrations were measured onboard, whereas SO_4^{2-} concentration and stable isotope measurements ($\delta^{13}C$-CH_4, δD-CH_4) were determined onshore.

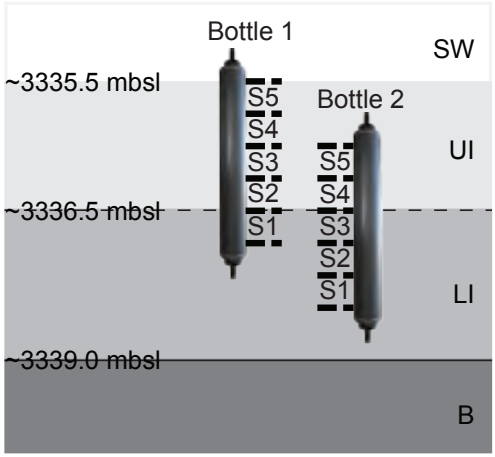

Figure 2. Sampling scheme. For the Niskin bottles closed at the interface, 5 (-7) cycles of sampling of different parameters were performed resulting in a vertical resolution of the water column of ca. 20 cm. Different bottles were aligned with respect to chlorinities.

2.4 Geochemical analyses

Onboard measurements

Oxygen concentrations were measured by Winkler titrations of ~115 ml water/brine sample (Grasshoff et al., 1999). Samples were analysed in triplicate, yielding an analytical error of <0.5% (stdev. between replicates).

HS^--analyses were carried out with a TRAACS800 continuous flow analyzer, using colorimetric methods (after Grasshoff et al., 1999). The standard deviation of all measurements was <2%. Similarly, DIC analyses were, after appropriate dilution, also made with the TRAACS800 continuous flow analyzer (Stoll et al., 2001), with an analytical error <0.5%.

CH_4 and higher hydrocarbon (i.e., C_2, C_3 and C_4) concentrations were determined on board by headspace measurements (Grasshoff et al., 1999) of 1 mL gas sample with a gas chromatograph (GC; Shimadzu GC-14B) equipped with a 250 µL sample loop, a capillary column (Valco-plot-HayeSep D: 30 m, 0.53 mm i.d., 20 µm d.f.) and a flame ionization detector. GC conditions were as described previously (Mastalerz et al., 2009).

Onshore analyses

Water samples for SO_4^{2-}-measurements were acidified onboard and subsequently stripped with N_2-gas inside an anoxic glovebox in order to remove all H_2S. Total SO_4^{2-} was then

measured onshore using an ICP-AES after appropriate dilutions so that concentrations were ~ 3.5 mg L^{-1} ionic strength (Stefansson et al., 2007).

The stable carbon and hydrogen isotope composition of CH_4 was analyzed at Utrecht University using a Gas Chromatograph–Isotope Ratio Mass Spectrometer (GC–IRMS) system consisting of an Agilent HP 6890 gas chromatograph connected to a Finnigan Deltaplus XP IRMS with a combustion interface (Luong et al., 2013). Prior to IRMS, gaseous compounds were separated on a HPPLOT column (D: 32 m, 0.32 mm i.d. 10 µm d.f.), using the following temperature program: 2 min hold time at 40°C, followed by a temperature ramp (12°C min^{-1} to 140°C), and a final hold time of 3 min.

2.5 Methane oxidation and sulfate reduction rate measurements

Water samples for methane oxidation- and sulfate reduction rate measurements were filled bubble-free into 20 mL glass vials and closed with bromobutyl stoppers (Niemann et al., 2015). They were incubated in quadruplicates for 72 h at in-situ T in the dark, with trace amounts of ^{14}C-labelled aqueous methane solution (10 μl, 4 kBq, ~150 nmol CH_4, American Radiolabeled Chemicals, USA) and ^{35}S-labelled sulfate (25 μl, 20 kBq, American Radiolabeled Chemicals, USA), respectively (Jørgensen, 1977; Treude et al., 2003; Niemann et al., 2005). Incubations were stopped by fixing samples in ~1 g of solid sodium hydroxide (methane oxidation), or in 20 ml 20% zinc acetate (sulfate reduction) in butyl-rubber sealed 100 mL glass bottles. The bottles were stored cool and upside down until determination of SRR and MOx/AOM in the home laboratory. Methane oxidation rates were assessed by $^{14}CH_4$ combustion (Iversen and Blackburn, 1981; Treude et al., 2003) and $^{14}CO_2$ acidification (Blees et al., 2014). The first order rate constant (k) was calculated from the fractional tracer turnover with consideration of ^{14}C-label transfer into biomass (Eq. 3; Blees et al., 2014; Steinle et al., subm.):

$$k = \frac{(A_{CO_2} + A_R)}{(A_{CH_4} + A_{CO_2} + A_R)} \times \frac{1}{t} \qquad \text{(Eq. 3)}$$

where A_{CH_4} is the activity of remaining ^{14}C-methane after incubation, A_{CO_2} is the activity of the generated CO_2, A_R is the left-over activity after purging and acidification, and t is the incubation time. The determination of A_R allows estimation of the fractional incorporation of oxidized CH_4 into biomass ($C_{incorp.}$), which was calculated according to Eq. 4:

$$C_{incorp.} = \frac{A_R}{A_{CO_2} + A_R} \qquad \text{(Eq. 4)}$$

Sulfate reduction rates were determined with the cold-chromium distillation method (Kallmeyer et al., 2004) to separate total reduced inorganic sulphur species (TRIS) from unreacted SO_4^{2-}. Similar to AOM, the first order rate constant of SR (k_{SRR}) was then determined from the fractional tracer turnover (Eq. 5):

$$k_{SRR} = \frac{A_{TRIS}}{\left(A_{TRIS} + A_{SO_4^{2-}}\right)} \times \frac{1}{t} \times 1.06 \quad \text{(Eq. 5)}$$

where $A_{SO_4^{2-}}$ is the remaining activity in the sulfate pool after incubation, A_{TRIS} is the activity of the generated sulfide and associated sulphur species, t is the incubation time and 1.06 is the correction factor for the expected isotopic fractionation (Jørgensen and Fenchel, 1974).

Rates of AOM/MOx (Eq. 6) and SR (Eq. 7) were then calculated as

$$r_{AOM/MOx} = k \times \left[CH_4\right] \quad \text{(Eq. 6)}$$

$$SRR = k_{SRR} \times \left[SO_4^{2-}\right] \quad \text{(Eq. 7)}$$

where $[CH_4]$ and $[SO_4^{2-}]$ are the concentration of methane or sulfate at the beginning of the incubations. All rate measurements were corrected for abiotic tracer turnover (which was insignificant) in killed controls using the same matrix (i.e., seawater, interface water or brine) as investigated for methane oxidation or sulfate reduction.

2.6 Biomarker analyses

For lipid biomarker analyses, 20 L of water/brine (combined from 2 - 3 Niskin bottles) from each layer (seawater, upper and lower IF, brine) was filtered on GF/F filters and stored at -20°C until extraction in the home laboratory. Lipid biomarkers were extracted from 7/8th of each filter according to Elvert et al. (Elvert et al., 2003) with small modifications. Briefly, filter samples were ultrasonicated in four steps with solvents of decreasing polarity. (1) dichloromethane (DCM) : methanol (MeOH) 1 : 2; (2) DCM:MeOH 2 : 1; (3) and (4) DCM. In order to extract compounds not soluble in solvents, we performed an additional ultrasonication with (5) MeOH:H_2O 1:3. The resulting total lipid extract was then separated into a polar fatty acid- and a neutral fraction, and the fatty acid fraction was derivatized to fatty-acid methyl-esters (Elvert et al., 2003; Niemann et al., 2005). The neutral fraction was separated on a SPE silica glass cartridge into hydrocarbons (I), ketones (II) and alcohols (III) with solvent mixtures of increasing polarity (I: n-hexane:DCM 95:5, II: n-hexane:DCM 2:1; III: DCM:acetone 9:1; Niemann et al., 2005). Alcohols were analyzed as trimethylsilyl-ethers. Double-bond positions of monoenoic fatty acids were determined by analyzing fatty acid dimethyl-disulfide derivatives (Nichols et al., 1986; Moss and Lambert-Fair, 1989).

Concentrations, identities and stable carbon isotope ratios of individual compounds were determined by GC, GC-MS and GC-IRMS, respectively with instrument specifications and operation modes described previously (Blees et al., 2014).

3. Results

3.1 Geochemical composition

In the following, based on conductivity gradients and O_2 concentration levels, we will refer to the upper interface (IF) as the depth layer between 3335.5 - 3336.5 mbsl where O_2 was still detectable, but HS^- was below the detection limit and could not be smelled. The lower IF is the depth layer between 3336.5 – 3337.5 mbsl, where O_2 concentrations were below the detection limit (<1μM) and increasing levels of HS^- were detectable.

Concentration levels of SO_4^{2-}, Cl^- and Mg^{2+} increased from seawater background values through the upper IF towards the brine to 167 mmol kg^{-1}, 6.55 mol kg^{-1}, and 3.94 mol kg^{-1}, respectively (Fig. 3a, b). In contrast, Na^+ concentrations decreased from 510 to 75 mmol kg^{-1} (Fig. 3b). CH_4 and HS^- levels were low or below detection limit in the upper interface but both compounds increased sharply in the lower IF towards the brine to maximum concentrations of 20 μmol kg^{-1} and 150 μmol kg^{-1}, respectively (Fig. 3c, d). The $\delta^{13}C$- and δD values of CH_4 exhibited a distinct maximum in the lower IF (Fig. 3f). While δD-CH_4 could not be determined in the upper IF, $\delta^{13}C$-CH_4 shifted towards lighter values from the lower to the upper interface. $\delta^{13}C$-DIC values were ~0‰ (±2‰, data not shown) both within the brine and the interface and no consistent trends were observed. C_2 concentrations were 1.3 μmol kg^{-1} within the brine, and below the detection limit within the interface, while C_3 and C_4 concentrations were always below the detection limit (Tab. 1). C_{2+} concentrations thus accounted for ~4% of total alkane concentrations. O_2 sharply decreased in the upper IF to values below the detection limit in the lower IF (Fig. 3d).

3.2 Sulfate reduction and methane oxidation

Sulfate reduction rates (SRR) increased from about 4 μmol kg^{-1} d^{-1} in the upper IF up to 460 μmol kg^{-1} d^{-1} within the brine (Fig. 3g). In contrast, MOx rates increased from ~0.2 nmol kg^{-1} d^{-1} in the upper IF to a maximum of 58 nmol kg^{-1} d^{-1} in the lower IF (i.e., three orders of magnitude lower than SRR), and sharply decreased in the brine (Fig. 3h). Incorporation of methane-carbon into biomass during MOx followed an opposite trend to MOx rates, with the highest incorporation at the top of the upper IF and no detectable incorporation into biomass in the lower IF or the brine (Fig. 3i).

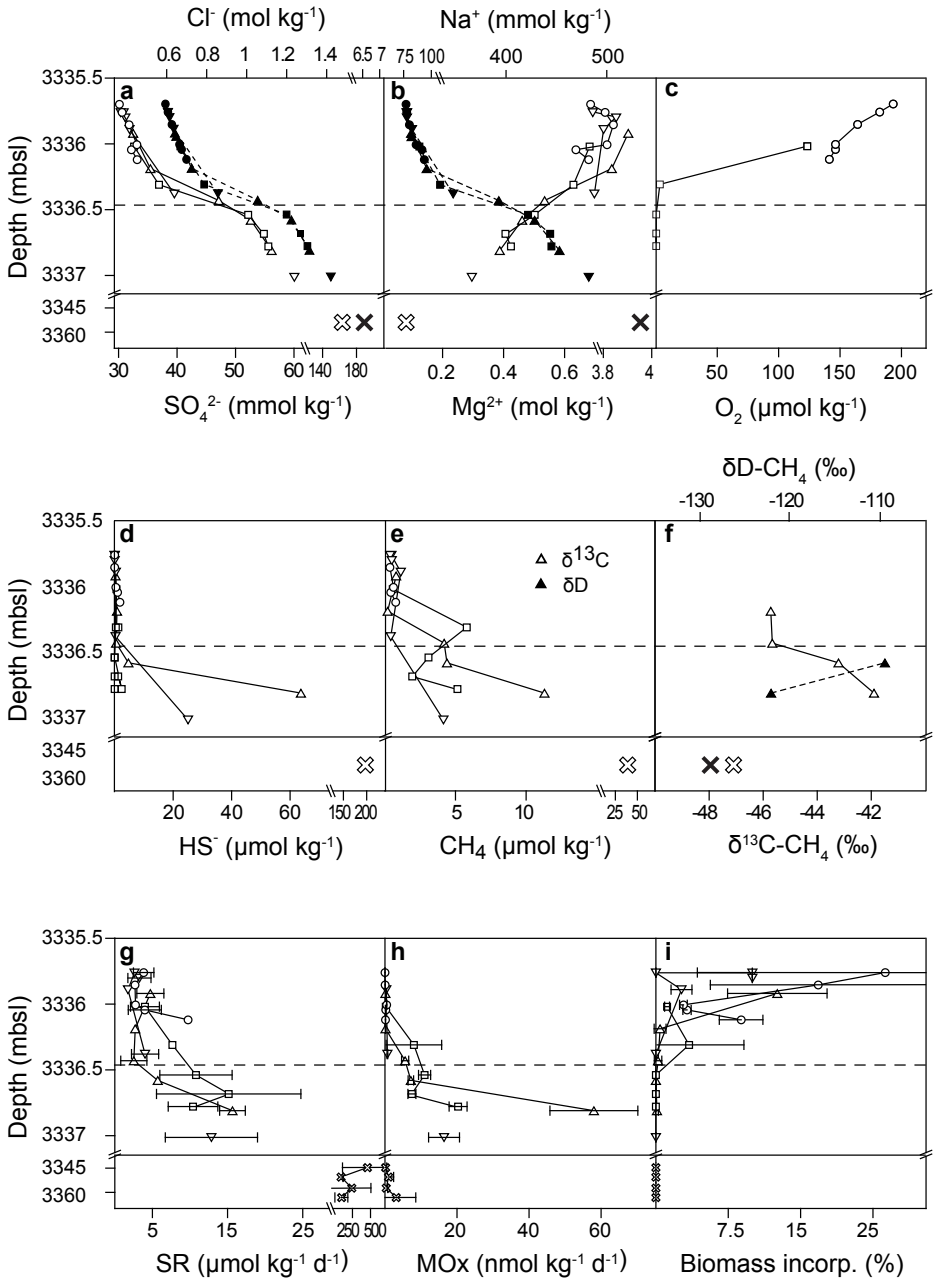

Figure 3. Geochemical profiles and rate measurements across the seawater-brine interface. a-e, Concentrations of a, chloride (filled symbols) and sulfate (open symbols), b, sodium (filled symbols) and magnesium (open symbols), c, oxygen, d, sulfide, and e, methane. f, Isotopic composition of methane - $\delta^{13}C$ (open symbols) and δD (filled symbols). Rates of g, sulfate reduction (SR), and h, methane oxidation (MOx). i, Methane-C incorporated into biomass during methane oxidation. Rates and incorporation into biomass were determined in quadruplicates. Error bars represent standard deviations. The dashed horizontal line indicates the border between upper and lower interface, and the continuous horizontal line the beginning of the brine. Please note the y-axis break. Different symbols (regardless of filling) represent different Niskin bottles.

Table 1. Table with geochemical parameters and rate measurements of the Kryos brine basin and interface. For the upper and lower interface, the value on the left represents the value for the lowest sample, the value on the right the value for the shallowest sample. ns: not sampled.

	unit	brine	lower interface		upper interface	
depth	mbsl	>3344	3337	3336.5	3336.4	3335.7
Cl^-	mmol kg^{-1}	**6545**	1421	1200	1055	594
Na^+	mmol kg^{-1}	**75**	366	428	483	521
Mg^{2+}	mmol kg^{-1}	**3936**	665	466	221	83
SO_4^{2-}	mmol kg^{-1}	144.2	61	52	40	30
O_2	µmol kg^{-1}	*ns*	0	0	3	193
HS^-	µmol kg^{-1}	150	64	0	0.8	0
CH_4	µmol kg^{-1}	20	11	2	4	0.2
C_2	µmol kg^{-1}	1.25	bd	bd	bd	bd
DIC	µmol kg^{-1}	4150	4060	3704	3747	2406

3.3 Lipid biomarker composition

Diagnostic alcohols and hydrocarbons

We detected traces of the bacterial hopanoid diplopterol in the seawater directly overlying the upper interface, but could not find diploptene. Both compounds were quantifiable in the upper IF (6 and 1.6 ng L^{-1}, respectively; Fig. 4a, b) and their concentrations increased towards the brine to 49 ng L^{-1} (diplopterol), and 9 ng L^{-1} (diploptene). They were both depleted in ^{13}C, with the most negative $\delta^{13}C$-values reaching -50‰ (diplopterol) and -47‰ (diploptene) in the lower IF.

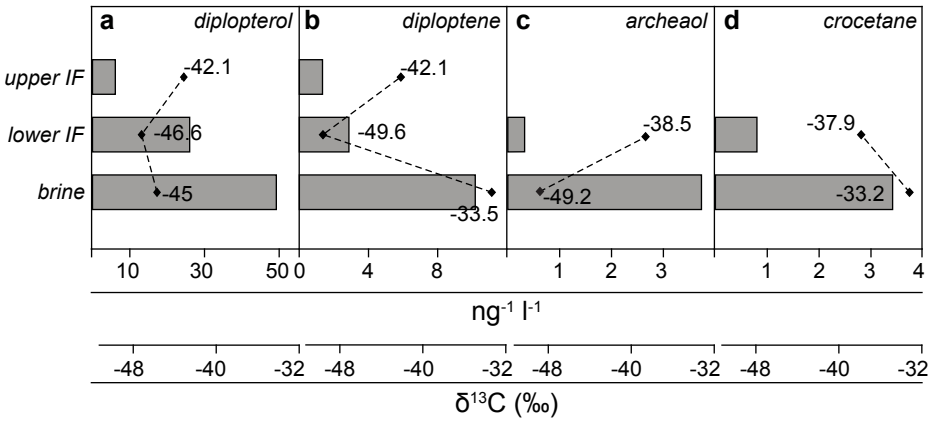

Figure 4. Concentrations and stable carbon isotope ratios of specific alcohols and hydrocarbons. a, Diplopterol. b, Diploptene. c, Archaeol. d, Crocetane. Numeric carbon isotope values are indicated in the plots. In the seawater fraction, only traces of Diplopterol were detected, but none of the other compounds was present.

In contrast, neither the archaeal di-ether archaeol nor the archaeal isoprenoid hydrocarbon crocetane were present in the seawater or in the upper IF (Fig. 4c, d). Small amounts of archaeol and crocetane were detected in the lower IF (both ~0.5 ng L^{-1}) and much higher concentrations in the brine (3.8 ng L^{-1} and 3.2 ng L^{-1}, respectively). Archaeol was more

depleted in ^{13}C with $\delta^{13}C$-values as low as -49‰ in the brine compared to crocetane, whose lowest $\delta^{13}C$-value (-38‰) was detected in the lower IF.

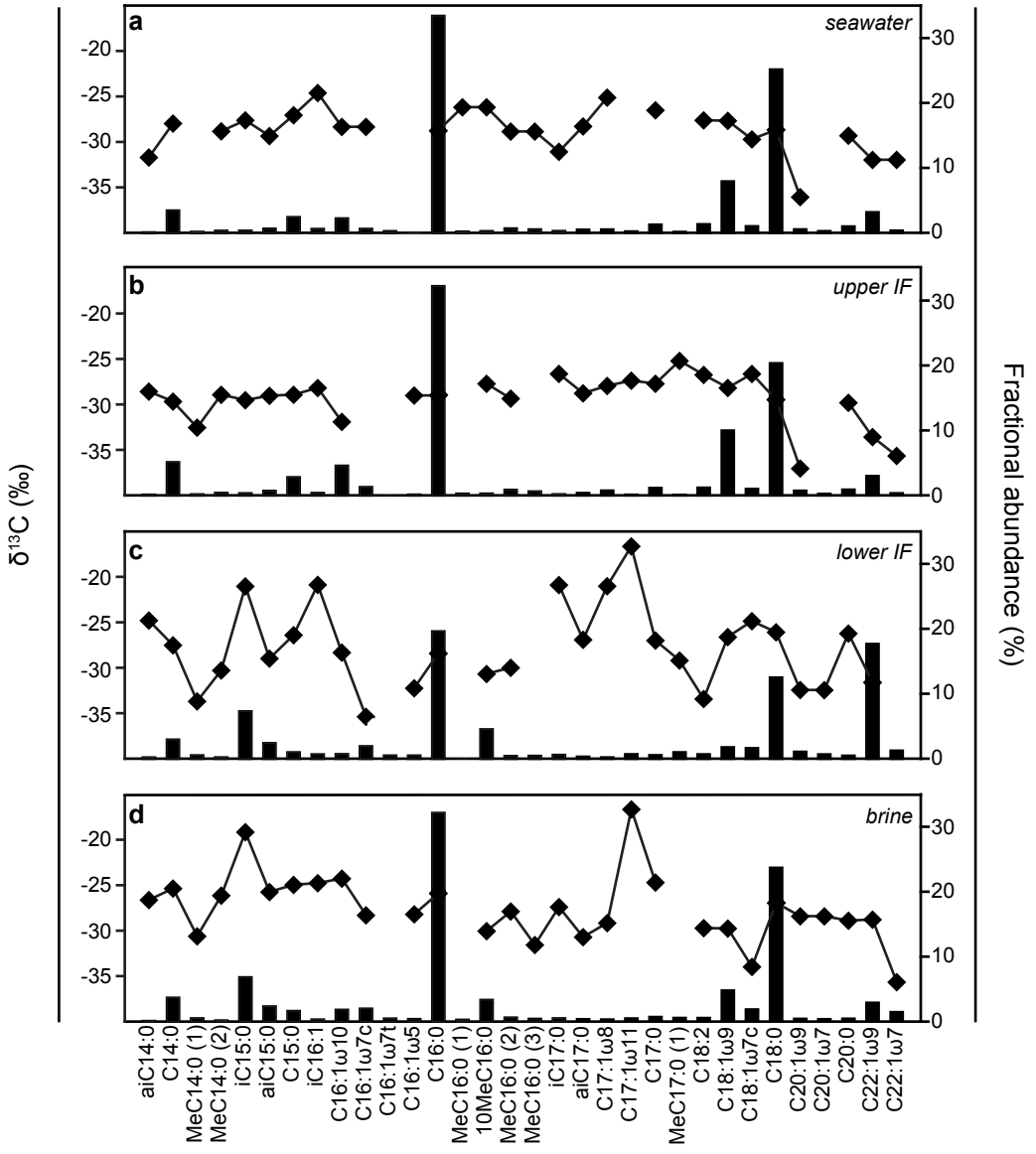

Figure 5. *Fractional abundance and $\delta^{13}C$-value of different fatty acids.* Fractional abundance (bars) and compound-specific $\delta^{13}C$-value (diamonds) of fatty acids (C14 - C22) from the seawater (a), the upper interface (b), the lower interface (c), and the brine (d). Mass traces of C16:1ω8 were detected in DMDS-derivates from the upper and lower interface, as well as the brine.

Fatty acids

The distribution of fatty acids in the seawater sample and the upper IF was very similar (Fig. 5a, b). In contrast, the distribution differed in the lower IF, where the fractional abundances of iC15:0, aiC15:0, 10MeC16:0, C17:1ω11, and C22:1ω9 increased, and the abundances of C16:1ω10 and C18:1ω9 strongly decreased when compared to the upper IF (Fig. 5b, c). Mass

traces of C16:1ω8 were detected in DMDS derivatives of the upper and lower IF samples, as well as the brine samples. In general, we found several methylated fatty acids (e.g. MeC14:0, 10MeC16:0), which were more abundant within the lower IF and the brine than within the upper IF or the seawater. The fatty acid distribution pattern in the brine strongly resembled the one of the lower IF, though we found a much lower abundance of C22:1ω9 (Fig. 5c, d).

The total fatty acid concentration (C14-C22) was highest in the brine (73.7 μg L^{-1}), intermediate in seawater and the upper IF, at 23.4 and 24.5 μg L^{-1}, respectively, and lowest in the lower IF (16.5 μg L^{-1}).

Next to fatty acid abundance, the fatty acid isotope signatures were also alike in the seawater and the upper IF sample. In general, low variability in the $\delta^{13}C$-values of different fatty acids was observed (Fig. 5a, b), with the exception of two fatty acids (C20:1ω9 and C22:1ω7) that had depleted $\delta^{13}C$-values (~-35‰). In contrast, the isotopic signature showed high variability in the lower IF where $\delta^{13}C$-values were as low as -36‰ (i.e., C16:1ω7c), and as high as -18‰ (i.e., C17:1ω11, Fig. 5c). In the brine, isotopic signatures were similar to the lower IF but fewer compounds were enriched in ^{13}C (Fig. 5d).

4. Discussion

4.1 Geochemical indications for methane and sulfide elimination within the interface

The Kryos basin is filled with athalassohaline brine, dominated by a near-saturated concentrations of $MgCl_2$-equivalents (3.9 mol kg^{-1}). In brine systems, chloride can be used as an inert tracer for mixing of the brine and seawater, since chloride contributions from sources other than brine or seawater are negligible and its concentration hence increases linearly with depth (van der Wielen et al., 2005; Yakimov et al., 2015). Other brine end-members should behave similarly unless there is an additional source or sink, which is evidenced as a deviation from a linear correlation of a specific solute with chloride. For magnesium, for instance, a clear linear relationship with chloride is observed (i.e., R^2 = 0.99). Methane, however, shows a relatively strong deviation (R^2 = 0.95) suggesting net methane removal within the interface. Indeed, methane concentrations sharply decrease within the lower interface indicating that methane oxidation is likely proceeding in this layer. Furthermore, $\delta^{13}C$- and δD-CH_4 values of the lowest interface sample are clearly enriched in ^{13}C ($d^{13}C$ = 5.2‰) and D (dD = 6.7‰) with respect to the methane isotope signature of the brine (Fig. 3f). This is consistent with methane oxidation in the lower interface because methane oxidation (both aerobically and anaerobically) is associated with a strong kinetic isotope effect (Whiticar, 1999; see section 4.2 for further discussion on the mode of methane oxidation, i.e., aerobic or anaerobic). Methane oxidation at brine-seawater interfaces was

previously detected in three halite brine basins (Red Sea: Atlantis II, Schmidt et al., 2003; Abdallah et al., 2014, and Kebrit, Abdallah et al., 2014; Gulf of Mexico brine pool, Wankel et al., 2010), but has not been studied in athalassohaline brine systems. The origin of methane potentially fueling methane oxidation at the interface is likely of thermogenic origin as indicated by the isotopic composition of brine-CH_4 ($\delta^{13}C$ = -47.1‰, δD = -128.9‰; Whiticar, 1999). The presence of substantial amounts of higher hydrocarbons (CH_4:C_{2+} = 24) also attests to this (Bernard et al., 1978).

Like methane, hydrogen sulfide concentrations also deviate from a linear correlation with chloride (R^2 = 0.92), indicating sulfide elimination in the interface. Indeed, sulfide sharply decreased to values below the detection limit at the boundary between the upper- and lower interface, indicating sulfide consumption within this zone (see section 4.4 for further discussion on potential sulfide oxidizing microbial communities). Other studies found potentially sulfide-oxidizing bacteria at the interface of the Thetis brine basin (Pachiadaki et al., 2014) and at the interface of the Urania basin (Borin et al., 2009).

4.2 Mode of methane oxidation in the interface

In our study, we found clear signals of methane oxidation in the interace of the Kryos brine basin. We detected elevated rates in the upper and, more importantly, in the lower interface, i.e., in a zone where oxygen disappeared and hydrogen sulfide started to accumulate. In these layers, oxygen (though at very low concentrations), as well as sulfate may serve as potential electron acceptors. This means that both aerobic- and anaerobic oxidation of methane are thermodynamically feasible, and hence both processes could account for the observed methane oxidation activity. MOx is mediated by Gamma- or Alphaproteobacteria (Hanson and Hanson, 1996). Bacterial membrane lipids typically include fatty acids as well as hopanoids (Peters et al., 2007). Previous studies found that ^{13}C-depleted C16:1ω5c, C16:1ω7c or C16:1ω8c as well as the C30-hopanoids diplopterol and diploptene can be used as diagnostic biomarkers for tracing MOB in aquatic environments (Hanson and Hanson, 1996; Elvert et al., 2001; Hinrichs et al., 2003; Schubert et al., 2006; Niemann et al., 2006; Elvert and Niemann, 2008; Blees et al., 2014).

The $\delta^{13}C$-values of diplopterol (-46.6‰) and diploptene (-49.6‰), which we detected in the lower interface of the Kryos basin, are in a similar range as diplopterol (-40.1‰) and diploptene (-40‰) found in the oxicline of the Black Sea (Wakeham et al., 2003; Schubert et al., 2006). At Kryos, these two compounds were about 5‰-depleted compared to methane (-42‰), whereas this factor cannot be clearly determined for the Black Sea since methane $\delta^{13}C$-values varied between -20‰ and -50‰ at the oxicline (Schubert et al., 2006). The presence of depleted diplopterol and diploptene in the Kryos interface are thus a strong indication of aerobic methane oxidation. The second set of methanotrophic biomarkers (i.e.,

specific fatty acids) also suggest aerobic methanotrophy: we found clearly depleted C16:1ω7c (-35.5‰) and moderately depleted C16:1ω5 (-32.5‰) compared to the bulk isotopic fatty acid value (~-30‰), and we additionally detected traces of C16:1ω8. These results suggest that the biomass from non-methanotrophic organisms masks the MOB fatty-acid signature to some extent. Compared to SR, MOx rates are much lower, indicating that MOx is a relatively minor process in the interface at Kryos. Nevertheless, the presence of the above-mentioned unsaturated fatty acids (though at low concentrations) suggests that Type I MOB mediate MOx in the Kryos interface (Hanson and Hanson, 1996). Further chemotaxonomic identification was not possible because of the rather weak MOB-derived lipid signal and the absence of other diagnostic compounds (e.g., 4α-methyl steroids, Elvert and Niemann, 2008).

AOM, on the other hand, is mediated by ANME archaea that are most closely related to methanogenic archaea (Knittel and Boetius, 2009). Unlike bacteria, ANME synthesize a suite of ^{13}C-depleted membrane lipids, typically isoprenoids, such as the glycerol-ethers archaeol and *sn2*-hydroxyarchaeol or the isoprenoid-hydrocarbon crocetane (see Niemann and Elvert, 2008, for a review). The presence of these lipids in anoxic aquatic environments, for example in the Black Sea (Schubert et al., 2006; Blumenberg et al., 2007), has been used to trace AOM-mediating communities. We could detect traces of archaeol in the upper interface, and both archaeol and crocetane in the lower interface, but they were only slightly ^{13}C-depleted (-38.5‰ and -37.9‰, respectively). If these compounds would originate from ANME, much more depleted δ^{13}C-values of about -65‰ could be expected since they were generally found to be ca. 20‰ depleted compared to the methane source (Niemann and Elvert, 2008). Hence, archaeol and crocetane were likely not produced by ANME, but by other organisms, such as methanogenic archaea (see section 4.4; Jahnke et al., 2008). Moreover, we could not find methanotrophic activity in the brine, despite high levels of methane and sulfate, indicating that ANME cannot thrive under such high salt conditions. Similar absence or inhibition of AOM in hypersaline environments was observed in a brine pool and a mud volcano in the Gulf of Mexico (Joye et al., 2009) and at the Mercator mud volcano in the Mediterranean Sea (Maignien et al., 2013). For the particular case of Kryos, it was argued that water availability and chaotropicity were too high to sustain microbial life (Yakimov et al., 2015), which, at least for AOM, seems to hold true.

Other modes of anaeraobic methane oxidation include oxidation with NO_3^-/NO_2^-, Fe^{3+} and Mn^{5+} as electron acceptors. The N-AOM mediating bacteria belong to the NC10 clade including the species Candidatus Methylomirabilis oxyfera (Ettwig et al., 2010; Kool et al., 2012) and synthesize an unusual suite of fatty acids such as 10MeC16:0, 10MeC16:1ω7 and cyC19:0. Of these, we only found 10MeC16:0 but not its ω7-unsaturated homologue. 10MeC16:0 was also found in other bacteria, for instance in members of the

Desulfobacteriacea (Taylor and Parkes, 1983; Dowling et al., 1988; Frostegård et al., 1993; Rütters et al., 2002). An origin of 10MeC16:0 from M. oxyfera thus remains unlikely. Furthermore, M. oxyfera was found to incorporate DIC- rather than CH_4-derived carbon, so that lipids from this organism may not be ^{13}C-depleted since $\delta^{13}C$-DIC-values were 0 (±2‰), which makes it even less probably that 10MeC16:0 originates from these species (Kool et al., 2012). No lipid biomarker data are available for organisms mediating Fe/Mn dependent modes of AOM.

In conclusion, the presence of ^{13}C-depleted diplopterol and diploptene as well as traces of C16:1ω8 along with the apparent absence of (S- and N-dependent) AOM-derived compounds indicates that measured methanotrophic activity in the seawater-brine interface of the Kryos basin is the result of an aerobic mode of methane oxidation mediated by Type I MOB.

4.3 Methanotrophy and sulfate reduction at the Kryos brine basin: life on the edge

Methanotrophy in the lower interface

Several studies at oxic/anoxic interfaces reported that aerobic MOx proceeds at high rates in micro-oxic conditions in different marine (Schubert et al., 2006; Jakobs et al., 2013; Steinle et al., subm.), as well as lacustrine environments (Rudd et al., 1976; Blees et al., 2014; Blees et al., 2014). Furthermore, evidence for aerobic methane oxidation within the interface of a thalassohaline brine basin in the Red Sea (methane isotope shifts, Schmidt et al., 2003; pmoA, Abdallah et al., 2014) and the Gulf of Mexico (rate measurements, Wankel et al., 2010), provides evidence that some aerobic methanotrophs are adapted to extremely high salinity levels encountered in NaCl-dominated brines. With this study we demonstrated that they are also adapted to micro-oxic conditions in a $MgCl_2$-dominated brine, and are even more active (up to 60 nmol kg^{-1} d^{-1}) than in the halite brine pool in the Gulf of Mexico (only up to 130 pmol l^{-1} d^{-1}). Previous studies suggested that avoidance of grazing pressure (Blees et al., 2014; Devlin et al., 2015), and it was also suggested that MOx activity might be impeded on an organismic level under oxygen replete conditions (Steinle et al., subm.) could drive MOB to inhabit micro-oxic environments. The Kryos brine contains a high diversity of dissolved organic carbon and sulphur-containing compounds (Yakimov et al., 2015), which may be oxidized with oxygen as the terminal electron acceptor. Adaptation of MOB to micro-oxic conditions may consequently be a strategy of MOB to avoid competition for oxygen with other microbes. However, although rates of MOx were highest in the lower interface, the higher fractional incorporation of methane-carbon into biomass in the upper interface (Fig. 3h, i) suggests that MOx-mediating organisms appear to be living at the edge of their optimum conditions in the lower interface. In a recent study, Steinle et al. (subm.) reported a similar behavior: In the water column of a coastal inlet, the overall methanotrophic activity

was higher under hypoxic conditions but the fractional incorporation of methane-carbon into biomass was lower. Although conditions encountered in the lower interface apparently provide some advantage for MOB, the low oxygen content (Steinle et al., subm.) and high salinity level most likely also lead to cellular stress (Oren, 2013; Yakimov et al., 2015), which hampers growth of the MOB community in the lower interface. Similarly, the absence of growth under sub-optimal conditions was reported for other organisms, for example sulfate reducers, while high substrate-turnover rates were measured (Cypionka, 2000).

Sulfate reduction in brine at nearly saturated $MgCl_2$ concentrations

Sulfate reduction was already detected within the upper interface and strongly increased by two orders of magnitude across the seawater-brine interface, reaching maximum values of up to 460 μmol kg^{-1} d^{-1} within the brine at $MgCl_2$-equivalent concentrations of 3.9 mol kg^{-1}. The maximum rates were ~5-20 times higher than highest rates at most other Mediterranean brine basins (van der Wielen et al., 2005; Borin et al., 2009), and about 10 times lower than SRR at the Bannock brine basin (Daffonchio et al., 2006). They were clearly higher (about three orders of magnitude) than SRR in brine systems in the Gulf of Mexico (Joye et al., 2009; Wankel et al., 2010) or at the Mediterranean Mercator mud volcano (Maignien et al., 2013). Like methane oxidation, we measured SRR directly using radio-tracer assays that have been proven useful in a variety of marine environments (e.g., Jørgensen and Fenchel, 1974; van der Wielen et al., 2005; Niemann et al., 2006; Glombitza et al., 2013). We monitored potential, abiotic tracer turnover in killed controls, which (in the brine) was <1% in comparison to live controls. Conservatively, we only considered tracer turnover as 'real' SRR and different from killed controls if it was at least as great as the mean tracer turnover in killed controls plus three standard deviations of the killed control value (Grasshoff et al., 1999). With the exception of the effect of lower pressure during ex situ incubations, we can thus, with confidence, exclude a methodological artifact potentially biasing our rate measurements. Our measurements consequently provide evidence for a very active sulfate reducing microbial community in the Kryos basin. Sulfate reducers can hence be active in an environment, where water activity is ca. 0.42 a_w and which is, next to the Discovery basin, one of the most chaotropic systems on earth (>300 kJ kg^{-1}; Yakimov et al., 2015). Our results are in good agreement with investigations at the Discovery brine basin, which is also dominated by $MgCl_2$ (~5 M; van der Wielen et al., 2005), and where high sulfate reduction and methanogenesis rates were detected within the brine. Our results, however, stand in contrast to recent publications arguing against the possibility of microbial life in the Kryos brine (Hallsworth et al., 2007; Oren, 2013; Yakimov et al., 2015). These authors base their argumentation on biophysical constraints of low water activity and chaotropicity, and on the absence of detectable mRNA of sulfate reducers and methanogenic archaea in the Discovery (Hallsworth et al., 2007), and the Kryos brine (Yakimov et al., 2015). The authors thus

suggested that the limit for microbial life in the Kryos basin was at 3.03 M $MgCl_2$ concentrations, i.e., within the lower interface from where mRNA was still recovered. Potential explanations for the negative results of mRNA detection within the Kryos and Discovery brine, despite the high sulfate reduction rates detected there, include potentially different enzymes involved in sulfate reduction and methanogenesis, which are not detectable with conventional primers, and also processing/extraction artifacts that interfere with mRNA analyses.

We can only speculate about the phylogenetic identity of sulfate reducers within the brine. The detection of the unusual fatty acid 10MeC16:0 in the lower interface and within the brine corresponds to layers characterized by elevated SRR. This compound has previously been detected in sulfate reducers, mostly belonging to the genus *Desulfobacter* (Taylor and Parkes, 1983; Dowling et al., 1988; Frostegård et al., 1993; Rütters et al., 2002), which also includes known halophiles (Ollivier et al., 1994). The fatty acid cyC17:0 is usually also present in *Desulfobacter*, but was not detected in the Kryos brine and, therefore, further characterization of the sulfate reducing organisms is not possible. In line with our biomarker analysis, Yakimov et al. (2015) detected sequences related to members of the family *Desulfobacteriaceae*, to which the genus *Desulfobacter* belongs.

4.4 Indications for specific carbon acquisition pathways

In addition to aerobic methanotrophy and sulfate reduction at the Kryos brine basin, we also found indications of (i) methanogenesis and (ii) sulfide oxidation.

(i) methanogenesis. We detected a light $\delta^{13}C$-methane signature in the upper interface when compared with the lower interface, which is not consistent with ongoing methane oxidation throughout the interface (see section 4.2). To some degree, mixing of interface methane and atmospheric methane ($\delta^{13}C$: ~-47‰; Dlugokencky et al., 2011) dissolved in the overlying seawater may account for the isotope depletion. Yet, background methane concentrations in the overlying Mediterranean seawater are in the nanomolar range, while we found micromolar methane concentrations in the upper interface, so that mixing alone cannot account for this isotopic shift. Alternatively, secondary admixture of microbial methane in the interface could explain this trend, since methanogenesis, like microbial methanotrophy, is associated with a strong kinetic isotopic fractionation (Whiticar, 1999). An additional line of evidence for the presence of methanogens is provided by our biomarker analyses: We detected moderately depleted archaeal lipid biomarkers with a rather non-depleted $\delta^{13}C$-signature (i.e., archaeol, -49.2‰; crocetane, -37.9‰; see section 4.2). Archaeol is not only a biomarker for ANMEs, which mediate AOM, but was found in a variety of other archaea (Koga and Morii, 2005), but crocetane is generally only produced by members of the ANME-2 group (Niemann and Elvert, 2008). However, in one study large amounts of crocetane were

detected in the absence of 16S-RNA from ANME co-occurring with high methane production rates (Orphan et al., 2008), and the authors proposed methanogenic archaea as the source of this compound (Jahnke et al., 2008). The observed archaeol and crocetane at Kryos could hence originate from other non-ANME archaea, most likely methanogens. Indeed, Yakimov et al. (2015) found sequences related to methanogenic archaea in the lower interface. However, as we did not measure methanogenesis rates, we can only speculate as to how much methane originates from biogenic methanogenesis produced within the interface and how the usually anaerobic methanogens (Madigan et al., 2015) can withstand potentially present oxygen.

ii) Sulfide oxidation. Sulfide concentration profiles indicate that sulfide elimination occurs within the interface, a process that was already observed at other seawater-brine interfaces (e.g., Pachiadaki et al., 2014; Borin et al., 2009), and which is mediated by a diversity of bacteria, including members of the Delta- and Epsilonproteobacteria. Our lipid analysis revealed several unusual fatty acids enriched in ^{13}C in the lower interface and the brine with $\delta^{13}C$-values as high as -18‰ (Fig. 5). It is unlikely that these fatty acids originate from the overlying seawater, as these compounds did not have such enriched $\delta^{13}C$-values in the seawater or upper interface samples, which indicates that in situ production occurred in the lower interface and/or brine. Similarly conspicuous isotope signatures were measured at hydrothermal vents, where biomass had two distinct isotopic compositions, one of which was ^{13}C-enriched ($\delta^{13}C$ = -10 to -15‰) relative to the other ($\delta^{13}C$ = -20 to -30‰; see Hügler and Sievert, 2011, for a review). The lighter values can be readily explained by isotopic fractionation during carbon fixation via the Calvin Benson Cycle, which is the most common pathway in the bacterial realm (Hügler and Sievert, 2011). The heavier values likely originate from different carbon fixation pathways, such as the reductive Tri-Carboxylic Acid Cycle (rTCA), which is characterized by an isotope enrichment factor (ε) of about 2-13‰ (Preuß et al., 1989), and is mostly found in micro-aerophilic and anaeraobic organisms (Hügler and Sievert, 2011). The isotope-enrichment factor is hence substantially lower than the observed ε of the Calvin Benson Cycle (up to 30‰; Preuß et al., 1989; House et al., 2003; Hügler and Sievert, 2011). In the lower interface, where sulfide is sharply decreasing, the observed $\delta^{13}C$-values of the heavy fatty acids and $\delta^{13}C$-DIC values of ~0‰ (±2‰) are hence consistent with carbon fixation via the rTCA cycle, rather than the Calvin Benson Cycle. The heavy fatty acids iC15:0, iC16:0 and iC17:0 are clearly of bacterial origin (Peters et al., 2007) but are not diagnostic for any specific strains, whereas the source organisms of the other two heavy fatty acids (17:1ω8 and 17:1ω11) remain unknown. Most known sulfide oxidizers belong to Epsilon- or Gammaproteobacteria, and most Epsilonproteobacteria fix carbon via the rTCA cycle (Hügler and Sievert, 2011). Additionally, Magnetococcus marinus of the Alphaproteobacteria has also been found to oxidize sulfide and fix carbon via the rTCA

pathway (Bazylinski et al., 2013). Yakimov et al. (2015) detected several sequences closely related to known sulfur-oxidizing Epsilonproteobacteria (i.e., Sulfurovum sp.), and others to Magnetococcus sp., indicating that the heavy fatty acids detected in our study could indeed originate from sulfide oxidizing Epsilonproteobacteria and/or Alphaproteobacteria.

5. Summary and conclusions

Geochemical analyses, rate measurements and lipid biomarker analyses across the seawater-brine interface at the Kryos brine basin revealed that methane is oxidized aerobically in the micro-oxic layer of the interface. This process is most likely mediated by Type I methane-oxidizing bacteria. We also found indications of sulfide oxidizers, possibly fixing carbon via the rTCA cycle, and not via the most commonly encountered Calvin-Benson Bassham cycle. Additionally, methanogenesis might proceed in the interface and/or the brine. Within the brine, at nearly saturated magnesium concentrations, high sulfate-reduction rates within the brine were. This study thus adds to a growing body of studies showing that brines and the brine/seawater interfaces are microbial hot spots. We also provide further evidence that microbial activity is possible in extreme environments characterized by a high degree of chaotropicity and low water activity (just as in Discovery basin). One implication of this finding is that the search for a niche where extraterrestrial life could develop should include environments with water activities even lower than previously suggested.

Acknowledgements

We thank Captain Schneider and the crew of R/V Pelagia, and the scientific party for the excellent support at sea. Special thanks go to E. vanWeerlee and K. Bakker for help with DIC and HS^- analysis, to D. Gallego-Torres for CH_4 measurements, to C. Stalder for Winkler titrations, to V. Darakchieva for Cl^- determination, to R. Groenewegen for help with CTD deployment, and to M. L. Goudeau for additional analytical support. This work received financial support through a D-A-CH project funded by the Swiss National Science Foundation and the German Research foundation (grant no. 200021L_138057, 200020_159878/1). Further support was provided through the EU COST Action PERGAMON (ESSEM 0902).

References

Abdallah, R.Z., Adel, M., Ouf, A., Sayed, A., Ghazy, M.A., Alam, I., et al. (2014) Aerobic methanotrophic communities at the Red Sea brine-seawater interface. *Frontiers in microbiology* 5: doi: 10.3389/fmicb.2014.00487.

Bazylinski, D.A., Williams, T.J., Lefèvre, C.T., Berg, R.J., Zhang, C.L., Bowser, S.S., et al. (2013) Magnetococcus marinus gen. nov., sp. nov., a marine, magnetotactic bacterium that represents a novel lineage (Magnetococcaceae fam. nov., Magnetococcales ord. nov.) at the base of the Alphaproteobacteria. *Int J Syst Evol Microbiol* 63: 801-808.

Beal, E.J., House, C.H., and Orphan, V.J. (2009) Manganese- and iron-dependent marine methane oxidation. *Science* 325: 184-187.

Bernard, B.B., Brooks, J.M., and Sackett, W.M. (1978) Light hydrocarbons in recent Texas continental shelf and slope sediments. *Journal of Geophysical Research: Oceans* 83: 4053-4061.

Blees, J., Niemann, H., Wenk, C.B., Zopfi, J., Schubert, C.J., Jenzer, J.S., et al. (2014) Bacterial methanotrophs drive the formation of a seasonal anoxic benthic nepheloid layer in an alpine lake. *Limnology and Oceanography* 59: 1410-1420.

Blees, J., Niemann, H., Wenk, C.B., Zopfi, J., Schubert, C.J., Kirf, M.K., et al. (2014) Micro-aerobic bacterial methane oxidation in the chemocline and anoxic water column of deep south-Alpine Lake Lugano (Switzerland). *Limnology and oceanography* 59: 311-324.

Blumenberg, M., Seifert, R., and Michaelis, W. (2007) Aerobic methanotrophy in the oxic--anoxic transition zone of the Black Sea water column. *Organic Geochemistry* 38: 84-91.

Boetius, A., and Joye, S. (2009) Thriving in salt. *Science* 324: 1523-1525.

Boetius, A., Ravenschlag, K., Schubert, C.J., Rickert, D., Widdel, F., Gieseke, A., et al. (2000) A marine microbial consortium apparently mediating anaerobic oxidation of methane. *Nature* 407: 623-626.

Borin, S., Brusetti, L., Mapelli, F., D'Auria, G., Brusa, T., Marzorati, M., et al. (2009) Sulfur cycling and methanogenesis primarily drive microbial colonization of the highly sulfidic Urania deep hypersaline basin. *Proc Natl Acad Sci U S A* 106: 9151-9156.

Camerlenghi, A. (1990) Anoxic basins of the eastern Mediterranean: geological framework. *Marine chemistry* 31: 1-19.

Capece, M.C., Clark, E., Saleh, J., Halford, D., Heinl, N., Hoskins, S., and Rothschild, L. (2013) Part I: General aspects, In *Polyextremophiles. Life under multiple forms of stress*. Seckbach, J., Oren, A., and Stan-Lotter, H. (eds). Dordrecht: Springer, pp. 3-60.

Cita, M.B. (2006) Exhumation of Messinian evaporites in the deep-sea and creation of deep anoxic brine-filled collapsed basins. *Sedimentary Geology* 188: 357-378.

Cypionka, H. (2000) Oxygen Respiration by Desulfovibrio Species 1. *Annual Reviews in Microbiology* 54: 827-848.

Daffonchio, D., Borin, S., Brusa, T., Brusetti, L., van der Wielen, P.W., Bolhuis, H., et al. (2006) Stratified prokaryote network in the oxic-anoxic transition of a deep-sea halocline. *Nature* 440: 203-207.

Devlin, S.P., Saarenheimo, J., Syväranta, J., and Jones, R.I. (2015) Top consumer abundance influences lake methane efflux. *Nat Commun* 6: 8787.

Dowling, N.J., Nichols, P.D., and White, D.C. (1988) Phospholipid fatty acid and infra-red spectroscopic analysis of a sulphate-reducing consortium. *FEMS microbiology letters* 53: 325-333.

Eder, W., Jahnke, L.L., Schmidt, M., and Huber, R. (2001) Microbial diversity of the brine-seawater interface of the Kebrit Deep, Red Sea, studied via 16S rRNA gene sequences and cultivation methods. *Appl Environ Microbiol* 67: 3077-3085.

Egger, M., Rasigraf, O., Sapart, C.J., Jilbert, T., Jetten, M.S., Röckmann, T., et al. (2015) Iron-mediated anaerobic oxidation of methane in brackish coastal sediments. *Environ Sci Technol* 49: 277-283.

Elvert, M., and Niemann, H. (2008) Occurrence of unusual steroids and hopanoids derived from aerobic methanotrophs at an active marine mud volcano. *Organic Geochemistry* 39: 167-177.

Elvert, M., Boetius, A., Knittel, K., and Jørgensen, B.B. (2003) Characterization of specific membrane fatty acids as chemotaxonomic markers for sulfate-reducing bacteria involved in anaerobic oxidation of methane. *Geomicrobiology Journal* 20: 403-419.

Elvert, M., Whiticar, M.J., and Suess, E. (2001) Diploptene in varved sediments of Saanich Inlet: indicator of increasing bacterial activity under anaerobic conditions during the Holocene. *Marine Geology* 174: 371-383.

Ettwig, K.F., Butler, M.K., Le Paslier, D., Pelletier, E., Mangenot, S., Kuypers, M.M., et al. (2010) Nitrite-driven anaerobic methane oxidation by oxygenic bacteria. *Nature* 464: 543-548.

Frostegård, A., Tunlid, A., and Bååth, E. (1993) Phospholipid Fatty Acid composition, biomass, and activity of microbial communities from two soil types experimentally exposed to different heavy metals. *Appl Environ Microbiol* 59: 3605-3617.

Grasshoff, K., Kremling K., and Ehrhardt, M. (1999) *Methods of Seawater Analysis*. Weinheim: Wiley-VCH.

Glombitza, C., Stockhecke, M., Schubert, C.J., Vetter, A., and Kallmeyer, J. (2013) Sulfate reduction controlled by organic matter availability in deep sediment cores from the saline, alkaline Lake Van (Eastern Anatolia, Turkey). *Front Microbiol* 4: 209.

Hallsworth, J.E., Yakimov, M.M., Golyshin, P.N., Gillion, J.L., D'Auria, G., de Lima Alves, F., et al. (2007) Limits of life in MgCl2-containing environments: chaotropicity defines the window. *Environ Microbiol* 9: 801-813.

Hansen, C.J., Esposito, L., Stewart, A.I., Colwell, J., Hendrix, A., Pryor, W., et al. (2006) Enceladus' water vapor plume. *Science* 311: 1422-1425.

Hanson, R.S., and Hanson, T.E. (1996) Methanotrophic bacteria. *Microbiological reviews* 60: 439-471.

Haroon, M.F., Hu, S., Shi, Y., Imelfort, M., Keller, J., Hugenholtz, P., et al. (2013) Anaerobic oxidation of methane coupled to nitrate reduction in a novel archaeal lineage. *Nature* 500: 567-570.

Hinrichs, K.U., Hmelo, L.R., and Sylva, S.P. (2003) Molecular fossil record of elevated methane levels in late Pleistocene coastal waters. *Science* 299: 1214-1217.

House, C.H., Schopf, J.W., and Stetter, K.O. (2003) Carbon isotopic fractionation by Archaeans and other thermophilic prokaryotes. *Organic Geochemistry* 34: 345-356.

Hsü, K.J., Ryan, W.B.F., and Cita, M.B. (1973) Late Miocene desiccation of the Mediterranean. *Nature* 242: 240-244.

Hügler, M., and Sievert, S.M. (2011) Beyond the Calvin cycle: autotrophic carbon fixation in the ocean. *Ann Rev Mar Sci* 3: 261-289.

Iversen, N., and Blackburn, T.H. (1981) Seasonal Rates of Methane Oxidation in Anoxic Marine Sediments. *Applied & Environmental Microbiology* 41: 1295-1300.

Jahnke, L.L., Orphan, V.J., Embaye, T., Turk, K.A., Kubo, M.D., Summons, R.E., and DES Marais, D.J. (2008) Lipid biomarker and phylogenetic analyses to reveal archaeal biodiversity and distribution in hypersaline microbial mat and underlying sediment. *Geobiology* 6: 394-410.

Jakobs, G., Rehder, G., Jost, G., Kießlich, K., Labrenz, M., and Schmale, O. (2013) Comparative studies of pelagic microbial methane oxidation within the redox zones of the Gotland Deep and Landsort Deep (central Baltic Sea). *Biogeosciences* 10: 7863-7875.

Joye, S.B., Samarkin, V.A., MacDonald, I.R., Hinrichs, K.-U., Elvert, M., Teske, A.P., et al. (2009) Metabolic variability in seafloor brines revealed by carbon and sulphur dynamics. *Nature Geoscience* 2: 349-354.

Jørgensen, B.B. (1977) The Sulfur Cycle of a Coastal Marine Sediment (Limfjorden , Denmark). *Limnology and Oceanography* 22: 814-832.

Jørgensen, B.B., and Fenchel, T. (1974) The sulfur cycle of a marine sediment model system. *Marine Biology* 24: 189-201.

Kallmeyer, J., Ferdelman, T.G., Weber, A., Fossing, H., and Jørgensen, B.B. (2004) A cold chromium distillation procedure for radiolabeled sulfide applied to sulfate reduction measurements. *Limonolgy and Oceanography: Methods* : 171-180.

Knittel, K., and Boetius, A. (2009) Anaerobic Oxidation of Methane: Progress with an Unknown Process. *Annual Review of Microbiology* 63: 311-334.

Koga, Y., and Morii, H. (2005) Recent advances in structural research on ether lipids from archaea including comparative and physiological aspects. *Biosci Biotechnol Biochem* 69: 2019-2034.

Kool, D.M., Zhu, B., Rijpstra, W.I., Jetten, M.S., Ettwig, K.F., and Sinninghe Damsté, J.S. (2012) Rare branched fatty acids characterize the lipid composition of the intra-aerobic methane oxidizer "Candidatus Methylomirabilis oxyfera". *Appl Environ Microbiol* 78: 8650-8656.

La Cono, V., Smedile, F., Bortoluzzi, G., Arcadi, E., Maimone, G., Messina, E., et al. (2011) Unveiling microbial life in new deep-sea hypersaline Lake Thetis. Part I: Prokaryotes and environmental settings. *Environ Microbiol* 13: 2250-2268.

De Lange, G.J., Middelburg, J.J., Van der Weijden, C.H., Catalano, G., Luther, G.W., Hydes, D.J., et al. (1990) Composition of anoxic hypersaline brines in the Tyro and Bannock Basins, eastern Mediterranean. *Marine Chemistry* 31: 63-88.

Luong, J., Gras, R., Cortes, H.J., and Shellie, R.A. (2013) Determination of trace ethylene glycol in industrial solvents and lubricants using phenyl boronic acid derivatization and multidimensional gas chromatography. *Analytica chimica acta* 805: 101-106.

Madigan, Q.D., Martinko, J., Bender, K., Buckley, D., and Stahl, D. (2015) *Brock Biology of Microorganisms*. Person: Boston.

Maignien, L., Parkes, R.J., Cragg, B., Niemann, H., Knittel, K., Coulon, S., et al. (2013) Anaerobic oxidation of methane in hypersaline cold seep sediments. *FEMS Microbiol Ecol* 83: 214-231.

Martín-Torres, F.J., Zorzano, M.-P., Valentín-Serrano, P., Harri, A.-M., Genzer, M., Kemppinen, O., et al. (2015) Transient liquid water and water activity at Gale crater on Mars. *Nature Geoscience* .

Mastalerz, V., De Lange, G.J., and Dählmann, A. (2009) Differential aerobic and anaerobic oxidation of hydrocarbon gases discharged at mud volcanoes in the Nile deep-sea fan. *Geochimica Et Cosmochimica Acta* 73: 3849-3863.

McEwen, A.S., Dundas, C.M., Mattson, S.S., Toigo, A.D., Ojha, L., Wray, J.J., et al. (2014) Recurring slope lineae in equatorial regions of Mars. *Nature Geoscience* 7: 53-58.

Milucka, J., Ferdelman, T.G., Polerecky, L., Franzke, D., Wegener, G., Schmid, M., et al. (2012) Zero-valent sulphur is a key intermediate in marine methane oxidation. *Nature* 491: 541-546.

Moss, C.W., and Lambert-Fair, M.A. (1989) Location of double bonds in monounsaturated fatty acids of Campylobacter cryaerophila with dimethyl disulfide derivatives and combined gas chromatography-mass spectrometry. *Journal of clinical microbiology* 27: 1467-1470.

Nichols, P.D., Guckert, J.B., and White, D.C. (1986) Determination of monosaturated fatty acid double-bond position and geometry for microbial monocultures and complex consortia by capillary GC-MS of their dimethyl disulphide adducts. *Journal of Microbiological Methods* 5: 49-55.

Niemann, H., and Elvert, M. (2008) Diagnostic lipid biomarker and stable carbon isotope signatures of microbial communities mediating the anaerobic oxidation of methane with sulphate. *Organic Geochemistry* 39: 1668-1677.

Niemann, H., Elvert, M., Hovland, M., Orcutt, B., Judd, A., Suck, I., et al. (2005) Methane emission and consumption at a North Sea gas seep (Tommeliten area). *Biogeosciences* 2: 335-351.

Niemann, H., Lösekann, T., de Beer, D., Elvert, M., Nadalig, T., Knittel, K., et al. (2006) Novel microbial communities of the Haakon Mosby mud volcano and their role as a methane sink. *Nature* 443: 854-858.

Niemann, H., Steinle, L.I., Blees, J., Krause, S., Bussmann, I., Treude, T., et al. (2015) Toxic effects of butyl elastomers on aerobic methane oxidation. *Limnology and Oceanography: Methods* 13: 40-52.

Ollivier, B., Caumette, P., Garcia, J.-L., and Mah, R.A. (1994) Anaerobic bacteria from hypersaline environments. *Microbiological reviews* 58: 27-38.

Oren, a. (2013) Life in magnesium- and calcium-rich hypersaline environments: salt stress by chaotropic ions, In *Polyextremophiles. Life under multiple forms of stress*. Seckbach, J., Oren, A., and Stan-Lotter, H. (eds). Dordrecht: Springer, pp. 215-232.

Orphan, V.J., House, C.H., Hinrichs, K.-U.H., McKeegan, K.D., and Delong, E.F. (2001) Methane-consuming archaea revealed by directly coupled isotopic and phylogenetic analysis. *Science* 293: 484-487.

Orphan, V.J., Jahnke, L.L., Embaye, T., Turk, K.A., Pernthaler, A., Summons, R.E., and DES Marais, D.J. (2008) Characterization and spatial distribution of methanogens and methanogenic biosignatures in hypersaline microbial mats of Baja California. *Geobiology* 6: 376-393.

Pachiadaki, M.G., Yakimov, M.M., LaCono, V., Leadbetter, E., and Edgcomb, V. (2014) Unveiling microbial activities along the halocline of Thetis, a deep-sea hypersaline anoxic basin. *ISME J* 8: 2478-2489.

Peters, K., Walters, C., and Moldowan, J. (2007) The Biomarker Guide: Biomarkers and Isotopes in the Environment and Human History. Cambridge.

Preston, L.J., and Dartnell, L.R. (2014) Planetary habitability: lessons learned from terrestrial analogues. *International Journal of Astrobiology* 13: 81-98.

Preuß, A., Schauder, R., Fuchs, G., and Stichler, W. (1989) Carbon isotope fractionation by autotrophic bacteria with three different C02 fixation pathways. *Zeitschrift für Naturforschung C* 44: 397-402.

Rudd, J.W., Furutani, A., Flett, R.J., and Hamilton, R.D. (1976) Factors controlling methane oxidation in shield lakes: the role of nitrogen fixation and oxygen concentration. *Limnology and Oceanography* 21: 357-364.

Rütters, H., Sass, H., Cypionka, H., and Rullkötter, J. (2002) Phospholipid analysis as a tool to study complex microbial communities in marine sediments. *J Microbiol Methods* 48: 149-160.

Rütters, H., Sass, H., Cypionka, H., and Rullkötter, J. (2002) Phospholipid analysis as a tool to study complex microbial communities in marine sediments. *J Microbiol Methods* 48: 149-160.

Sass, A.M., Sass, H., Coolen, M.J., Cypionka, H., and Overmann, J. (2001) Microbial communities in the chemocline of a hypersaline deep-sea basin (Urania basin, Mediterranean Sea). *Appl Environ Microbiol* 67: 5392-5402.

Schmidt, M., Botz, R., Faber, E., Schmitt, M., Poggenburg, J., Garbe-Schönberg, D., and Stoffers, P. (2003) High-resolution methane profiles across anoxic brine--seawater boundaries in the Atlantis-II, Discovery, and Kebrit Deeps (Red Sea). *Chemical geology* 200: 359-375.

Schubert, C.J., Coolen, M.J., Neretin, L.N., Schippers, A., Abbas, B., Durisch-Kaiser, E., et al. (2006) Aerobic and anaerobic methanotrophs in the Black Sea water column. *Environmental microbiology* 8: 1844-1856.

Sivan, O., Adler, M., Pearson, A., Gelman, F., Bar-Or, I., John, S.G., and Eckert, W. (2011) Geochemical evidence for iron-mediated anaerobic oxidation of methane. *Limnology and Oceanography* 56: 1536-1544.

Stefansson, A., Gunnarsson, I., and Giroud, N. (2007) New methods for the direct determination of dissolved inorganic, organic and total carbon in natural waters by Reagent-Free Ion Chromatography and inductively coupled plasma atomic emission spectrometry. *Analytica chimica acta* 582: 69-74.

Steinle, L., Schmidt, M., Bryant, L., Haeckel, M., Linke, P., Sommer, S., et al. Linked sediment and water-column methanotrophy at a man-made gas blowout in the North Sea: Implications for methane budgeting in seasonally stratified shallow seas. *Limnology and Oceanography:* **submitted**.

Stevenson, A., Burkhardt, J., Cockell, C.S., Cray, J.A., Dijksterhuis, J., Fox-Powell, M., et al. (2015) Multiplication of microbes below 0.690 water activity: implications for terrestrial and extraterrestrial life. *Environ Microbiol* 17: 257-277.

Stock, a., Filker, s., Yakimov, M., and Stoeck, T. (2013) Deep hypersaline anoxic basins as model systems for environmental selection of microbial plankton, In *Polyextremophiles. Life under multiple forms of stress*. Seckbach, J., Oren, A., and Stan-Lotter, H. (eds). Dordrecht: Springer, pp. 499-516.

Stoll, M.H., Bakker, K., Nobbe, G.H., and Haese, R.R. (2001) Continuous-flow analysis of dissolved inorganic carbon content in seawater. *Anal Chem* 73: 4111-4116.

Taylor, J., and Parkes, R.J. (1983) The cellular fatty acids of the sulphate-reducing bacteria, Desulfobacter sp., Desulfobulbus sp. and Desulfovibrio desulfuricans. *Microbiology* 129: 3303-3309.

Treude, T., Boetius, A., Knittel, K., Wallmann, K., and Barker Jørgensen, B. (2003) Anaerobic oxidation of methane above gas hydrates at Hydrate Ridge, NE Pacific Ocean. *Marine Ecology Progress Series* 264: 1-14.

van der Wielen, P.W., Bolhuis, H., Borin, S., Daffonchio, D., Corselli, C., Giuliano, L., et al. (2005) The enigma of prokaryotic life in deep hypersaline anoxic basins. *Science* 307: 121-123.

Wakeham, S.G., Lewis, C.M., Hopmans, E.C., Schouten, S., and Sinninghe Damsté, J.S. (2003) Archaea mediate anaerobic oxidation of methane in deep euxinic waters of the Black Sea. *Geochimica et Cosmochimica Acta* 67: 1359-1374.

Wallmann, K., Aghib, F.S., Castradori, D., Cita, M.B., Suess, E., Greinert, J., and Rickert, D. (2002) Sedimentation and formation of secondary minerals in the hypersaline Discovery Basin, eastern Mediterranean. *Marine geology* 186: 9-28.

Wallmann, K., Suess, E., Westbrook, G., Winckler, G., Cita, M., and and the Medriff consortium (1997) Salty brines on the mediterranean seafloor. *Science* 387: 31-32.

Wankel, S.D., Joye, S.B., Samarkin, V.A., Shah, S.R., Friederich, G., Melas-Kyriazi, J., and Girguis, P.R. (2010) New constraints on methane fluxes and rates of anaerobic methane oxidation in a Gulf of Mexico brine pool via in situ mass spectrometry. *Deep Sea Research Part II: Topical Studies in Oceanography* 57: 2022-2029.

Whiticar, M.J. (1999) Carbon and hydrogen isotope systematics of bacterial formation and oxidation of methane. *Chemical Geology* 161: 291-314.

Yakimov, M.M., La Cono, V., Denaro, R., D'Auria, G., Decembrini, F., Timmis, K.N., et al. (2007) Primary producing prokaryotic communities of brine, interface and seawater above the halocline of deep anoxic lake L'Atalante, Eastern Mediterranean Sea. *The ISME journal* 1: 743-755.

Yakimov, M.M., La Cono, V., Spada, G.L., Bortoluzzi, G., Messina, E., Smedile, F., et al. (2015) Microbial community of the deep-sea brine Lake Kryos seawater-brine interface is active below the chaotropicity limit of life as revealed by recovery of mRNA. *Environ Microbiol* 17: 364-382.

Final discussion and outlook

In this dissertation, aerobic methane oxidation (MOx) was investigated in the water column at four different types of methane-rich habitats where MOx had not yet been studied. By applying an interdisciplinary approach using biogeochemical and molecular tools, complemented by experimental and modeling work, methane turnover was investigated in a system-oriented study. The high spatial and/or temporal coverage during sampling of the water column above these systems allowed determination of environmental factors controlling MOx. Moreover, estimates of the filter efficiency of this process and identification of bacterial groups mediating MOx were possible in several systems. The water column/brine at the following methane-rich sediments was studied:

- gas-hydrate associated methane seeps at the continental margin offshore Svalbard
- a highly active gas blowout – initiated by industrial drilling activities on the North Sea shelf
- gassy sediments of a shallow coastal inlet in the southern Baltic Sea (Eckernförde Bay)
- the athalassohaline, anoxic deep-sea brine basin "Kryos" in the eastern Mediterranean Sea

Table 6.1 provides an overview of the main characteristics of these four habitats. In the following, the magnitude and spatial extent of MOx in all habitats will be summarized and discussed. Within the context of reviewing the environmental controls shown to impact MOx in each of the four study sites, additional preliminary results are presented, along with a short excursion into the methodology of MOx rate measurements. Last, future research questions will be proposed.

Table 6.1: Overview of the main characteristics of the methane-rich environments presented in Chapter 2 – 5. A definition of "Vertical extent of MOx" is provided in section 6.1.2.

Location	**Type**	**Methane origin**	**Methane transport in sediments**	**Water depth**	**Avg. [CH_4] in surface water**	**Vertical extent of elevated MOx rates**	**Efficiency of MOx filter (% CH_4 removal)**	**predominant MOB Type**
Eckernförde Bay	gassy coastal sediments	in situ production	diffusive/ advective	28 m	14.8 (1 mbsl)	5-10 m	40-95%	Type I ^
North Sea	blowout gas seep	fossil (biogenic) gas reservoir	advective	98 m	11.5 (11 mbsl)	~78 m	~25%	Type II (Type I)
Svalbard continental margin	hydrate associated gas seep	mixed	advective	~400 m	11 (1-12 mbsl)	100-150 m	~60%*	Type I
Kryos basin	anoxic brine basin	fossil thermogenic gas (and in situ production?)	diffusive (?)	3334 m	nd	1-2 m	nd	Type I**

*from Graves et al., 2015

**based on biomarker evidence

^ unpubl. Results

6.1 Summary and short comparison of MOx rates in the studied habitats

6.1.1 Magnitude of aerobic MOx

Figure 6.1 summarizes average MOx rates in all sampled habitats during this PhD project. Rates were generally split into two groups, one containing the rates from the area with clearly elevated rates (see section 6.1.2), and the second containing all other rates. Overall, maximum averages rates covered a wide range, from 498 nM d^{-1} within the Blowout crater to 0.01 nM d^{-1} in the Irish Sea. Higher rates were generally observed if methane concentrations were higher.

At both the Kryos brine basin and the Blowout, methane concentrations were found to be in the μM-range. At the Kryos basin, however, maximum MOx rates were clearly lower than at the Blowout (20 nM d^{-1} compared to 498 nM d^{-1}), but still higher than in the other studied habitats. The high salinity encountered in this habitat, which exerts high energetic costs on cells, is a possible explanation for the lower rates despite high methane concentrations.

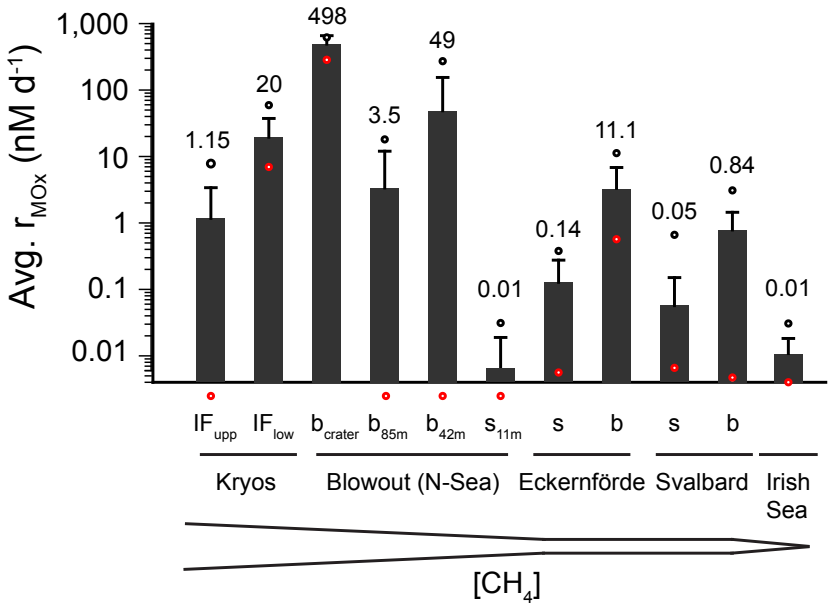

Figure 6.1. Average MOx rates in all habitats sampled. Kryos: IF_{upp}=upper interface, IF_{upp}=lower interface; Blowout: b_{crater}=bottom water within the Blowout crater, b_{85m}=bottom water at 85 m below sea level (mbsl), b_{43m} =bottom water at 42 mbsl (lower part of the thermocline), s_{11m}=surface waters at 11 mbsl; Eckernförde: s=surface waters (1 – 10 mbsl), b=bottom waters (15 – 25 mbsl). Error bars represent standard deviation (Kryos: IF_{upp} – n=9, IF_{upp} – n=6; Blowout: b_{crater} – n=4, b_{85m} – n=46, b_{43m} – n=42, s_{11m} – n=40; Eckernförde: s – n=84, b – n=84; Svalbard: s – n=368, b – n=412; Irish Sea: n=24)

MOx rates measured at the Blowout are among the highest ever reported for the ocean, falling in the same order of magnitude the ones measured in the water column after an accidental large-scale industrial methane release in the Gulf of Mexico (Deepwater Horizon oil spill; Kessler et al., 2011; Crespo-Medina et al., 2014), and in anoxic basins (Reeburgh et al., 1991). The Blowout system is more comparable to the Deepwater Horizon oil spill environment since large amount of methane are being/or were, injected into the water column in both systems. Hence, these environments can be regarded as model systems for potential rapid large-scale release of permafrost- or hydrate-bound methane in the Arctic region (Wilfert et al., 2015). The results presented by Kessler et al. (2011) indicate that MOB are able to respond quickly to sudden inputs of large amounts of methane and the results presented in this thesis show that a strongly elevated MOx potential can be encountered in such high-flux systems. Both of these factors point at a quick and effective response of MOB to very high methane concentrations. However, temperatures are generally lower in Arctic waters, and aerobic methane oxidizing bacteria (MOB) might not be able to sustain such high rates in these regions (Brocks 2015).

Rates in Eckernförde Bay and in waters above the Svalbard seeps were in the lower nM per day-range (0.1 - 3 nM d^{-1}). These rates lie within a typical range for continental shelf seep habitats and coastal systems (Gentz et al., 2014; Heintz et al., 2012; Mau et al., 2013; Reeburgh, 2007; Ward et al., 1989). In both of these systems, methane concentrations never exceeded 1,000 nM (max. concentrations Svalbard: 825 nM; Eckernförde Bay: 425 nM).

Samples from the water column above the croker slabs in the Irish Sea determined with ^{14}C-CH_4 were very low (unpubl. data) and were, for instance, comparable to the upper mixed layer in the North Sea. In situ methane concentrations were around 5 nM in that environment (Van Landeghem et al., 2015).

6.1.2 Spatial extent of the MOx zone

Visual examination of the MOx profiles allows estimation of the vertical extent of elevated MOx rates (Tab. 6.1). The extent of this zone ranged from ~1 m at the Kryos interface, 6 - 12 m in Eckernförde Bay (Fig. 6.2a), and ~80 m above the Blowout up to 100 - 150 m above the Svalbard seeps (Fig. 6.2b).

Figure 6.2: Vertical extent of the zone with elevated MOx rates exemplified at selected vertical profiles from a), Eckernförde Bay, and b), Svalbard. This zone ranged between 6 – 12 m in Eckernförde Bay (a), and between 100 – 150 m in Svalbard (b), as indicated with a dark and light grey bar. Error bars represent standard deviation of quadruplicates.

At Kryos, the niche is most likely constrained to a small vertical extent by the steep redoxcline at the interface, which limits the availability of oxygen from the seawater and methane and nutrients from the brine. Similarly, maximum MOx rates were detected at the

relatively sharp oxicline of the Gotland and Landsort deep (Baltic Sea; Jakobs et al., 2013) and the Black Sea (Schubert et al., 2006).

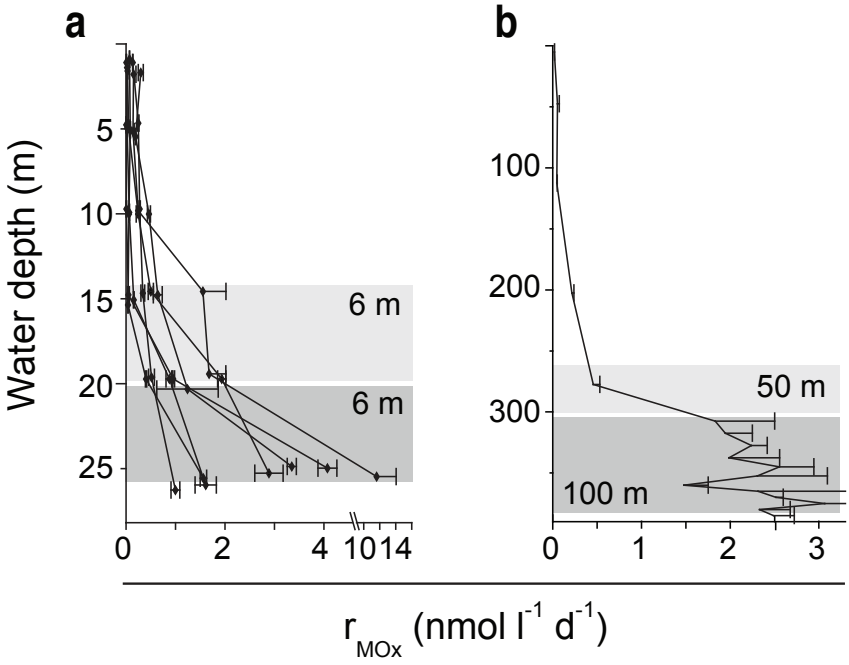

The vertical extent of the ecological niche for MOx is thus highly variable in these systems and seems, in general, to be related to the steepness of the chemical gradients:

In Eckernförde Bay, MOx rates generally increased sharply in the deepest sample (~25 mbsl; Fig. 6.2a), and were possibly even higher closer to the seafloor (28 mbsl). We showed that the MOx community is well adapted to sub-micromolar oxygen concentrations, which could explain the prevalence of highest rates in the lowest sample. Mixing processes are not as limited as in the Kryos brine basin and, as evidenced by CTD-profiles, the oxicline shows a larger vertical extent. Despite high methane availability in surface waters (up to 27 nM), MOx rates were not elevated. Preliminary experiments conducted under light/dark conditions in order to investigate the possibility of light inhibition in surface waters do not support his mechanism (see section 1.5). It is however still possible that the growth of MOB is inhibited by UV light (Madigan et al., 2015), which could hinder the establishment of a large methanotrophic community in surface waters. Other explanations include grazing (Devlin et al., 2015) or competition with heterotrophic bacteria (Murrell, 2010), but we did not investigate these processes.

In the North Sea, elevated MOx rates extended throughout the whole bottom-water mixed layer up to the thermocline. This is likely explained by the high methane supply and seeding of sedimentary methanotrophs into the water column. The rates in the bottom mixed layer were, however, highly variable with depth, i.e., highest rates were detected within the crater, as well as at the thermocline, but lower rates were measured in between these two depth intervals (~15 m above the seafloor). An elevated water column stability within the crater and at the thermocline is potentially the reason for this observation (see section 1.3.1). MOx rates at the Blowout are not limited to low oxygen environments (see section 6.5.3).

Above the Svalbard seeps, the vertical extent of MOx was large (100-150 m). Reasons for the high vertical extent of MOx could be that methane input is very widespread in this area (seep area at the continental shelf ~25 km long; Berndt et al., 2014). Additional methane input comes from seeps on the shelf and from close-by fjords (Graves et al., 2015). In a study including data from this thesis, we also reported indications for seepage ~30 km further south of the known seepage area (Supplementary Fig. S3; Graves et al., 2015). Similar to the water column above the Blowout, the MOx community seems to be adapted to near-saturated oxygen concentrations in the Svalbard area (see section 6.5.3).

Sediment-water interface

The water layer immediately above the sediments including the first 1 cm of sediments is referred to as the sediment-water interface, and several studies have found high vertical variability and high bacterial diversity in this 'sediment slurry interface' (see Turley, 2000, for a review). It is a layer where the "good stuff" from both seawater and sediments is available, i.e., nutrients, electron acceptors (oxygen) and trace metals. The bottom boundary layer and especially the sediment-water interface are hence potentially areas that may account for a high percentage of total water column methane removal potential if the cell density is similar to surface sediments (generally about 10^3 cells more than in seawater in the same volume). Indeed, in both the North Sea and Eckernförde Bay, rates were extremely elevated very close to the seafloor, which might be due to a shielding from currents or the above-mentioned higher bacterial density (confirmed for the Blowout). In contrast to these findings, we did not detect highest rates immediately (~20 cm) above the seafloor at the Svalbard seeps (sampled with the submarine JAGO, unpubl. data). Abril and Ino (2007) found, for instance, that clay particles were enhancing MOx, which are likely to more abundant in the sediment-water interface.

6.2 Environmental controls on MOx

Our investigations of water-column MOx in diverse marine environments led us to identify several environmental factors that can control the size of the MOx community and the magnitude of MOx rates:

1) Physical processes

1.4. advective processes (e.g., currents) [Chapters 2, 3, 4]

1.5. stratification [Chapters 3, 4, 5]

1.6. gas/fluid-flow mediated seeding of methanotrophs from sediments into the water column [Chapter 3]

1. Substrate and temperature dependency

1.7. oxygen [Chapter 3, 4]

1.8. methane [all Chapters to some extent]

1.9. temperature [Chapter 4]

(Chapter 2: Svalbard; Chapter 3: Blowout (North Sea); Chapter 4: Eckernförde Bay; Chapter 5: Kryos brine basin)

6.2.1 Physical processes

Advective processes

Above the Svalbard seeps, we observed that cold bottom water containing a large number of aerobic methanotrophs (MOB) was rapidly displaced by warmer water carrying a considerably smaller methanotrophic community. The warmer water we observed was the core of the West Spitsbergen Current, which flows northwards along the Spitsbergen continental margin, whereas the colder water originated from the shelf. The observed water mass exchange is hence caused by short-term variations of the West Spitsbergen Current and constitutes an oceanographic switch, which significantly reduces methanotrophic activity in the water column. At Boknis Eck, we most likely observed a similar exchange of the MOx community due to a large inflow of salty North Sea water, which replaces bottom Baltic Sea water. Similarly, at the Blowout, we observed strong horizontal heterogeneity of rate distributions, which we hypothesized to result from rapid advective exchanges caused by the strong tidal currents in the North Sea. Our observations that advective currents can impact MOx in a variety of shallow ocean systems are in line with model analyses of global shelf bottom currents (presented in Chapter 2), which revealed that strong and fluctuating currents are widespread oceanographic features common at many methane seep systems and led us to hypothesize that they are likely to globally affect methane oxidation in the ocean water column.

Stratification of the water column

The investigations of aerobic MOx above the Blowout and in Eckernförde Bay both led to the conclusion that stratification is an important factor controlling the size and/or the efficiency of the MOx community. Above the Blowout, rates were on average an order of magnitude higher in the thermocline than in waters below the thermocline (i.e., 15 m above the sediments). The reason for this observation may be that the lower vertical turbulence encountered at the thermocline not only leads to trapping of methane at the thermocline, but also to stable conditions favorable for MOB community development. In the coastal environment studied in this thesis (Eckernförde Bay), MOx was a lot less efficient under (almost) fully mixed than stratified conditions. In this setting, however, the higher efficiency was probably not caused by a larger community present at thermocline under stratified conditions, since maximum MOx rates were not detected at the thermocline but in bottom waters. The cause for the lower efficiency under weak stratification conditions was also not because of overall lower methane removal, but more likely caused by increased losses by seawater-atmosphere exchange (see section 1.4). These effects of stratification on the size and/or the efficiency of MOx community are likely also encountered in other shallow, (temporarily) stratified environments (i.e., coastal environments, continental shelves).

Bubble transport of sedimentary MOB

At the Blowout, gas-seepage associated transport of methanotrophic sedimentary bacteria is taking place, thereby providing MOB inocula to the water column. On a smaller scale (up to ~15 cm over the seafloor), this bubble-mediated transport was also demonstrated at the Rostocker seeps offshore California (Schmale et al., 2015). Since bubble emission is a widespread feature at cold seeps, it might be an important vector for the transport of sediment-borne microbial inocula, aiding in the rapid colonization of the water column by methanotrophic communities and promoting their persistence close to highly active methane point sources.

6.2.2 Substrate and temperature dependency

Oxygen

In both the Kryos interface and Eckernförde Bay, MOx was detected at sub-micromolar oxygen concentrations. Experiments with adjusted oxygen concentrations in the range of 0.2 – 220 μmol l^{-1} confirmed this micro-aerophilic behaviour of MOB in Eckernförde Bay waters and, together with other results presented in Chapter 4, this indicates an adaptation on the organismic level of the water column methanotrophs to hypoxic conditions. The determination of MOx rates in environmental samples at different oxygen concentrations showed that the K_m for MOx in this system is below 0.1 µM, which also constitutes the first extensive experimental evidence to support the observation of micro-aerophilic behaviour of

MOB observed in several other marine studies (Abdallah et al., 2014; Jakobs et al., 2013; Sansone & Martens, 1978; Schubert et al., 2006).

Additionally, in both the Kryos interface and in Eckernförde Bay, we detected limited incorporation of methane-carbon (and thus presumably lower growth) but higher rates at low oxygen concentrations (<10 μM). Microbial cells require a certain amount of energy to maintain their basic functions, and need even more energy if they want to replicate cellular material (i.e., growth; Valentine, 2007). The presented results in this dissertation hence indicate that cells were stressed under low oxygen (and elevated salt) concentrations, and could not generate enough energy for replication/growth (i.e., for anabolic functions; Fig. 6.3). Possibly, a switch to a fermentative metabolism was observed as has been reported previously for oxygen concentrations <10 μM (Kalyuzhnaya et al., 2013). Physiological studies targeting the fate of carbon at such low concentrations are required to systematically investigate these processes, for instance by tracking the potential production of volatile fatty acids.

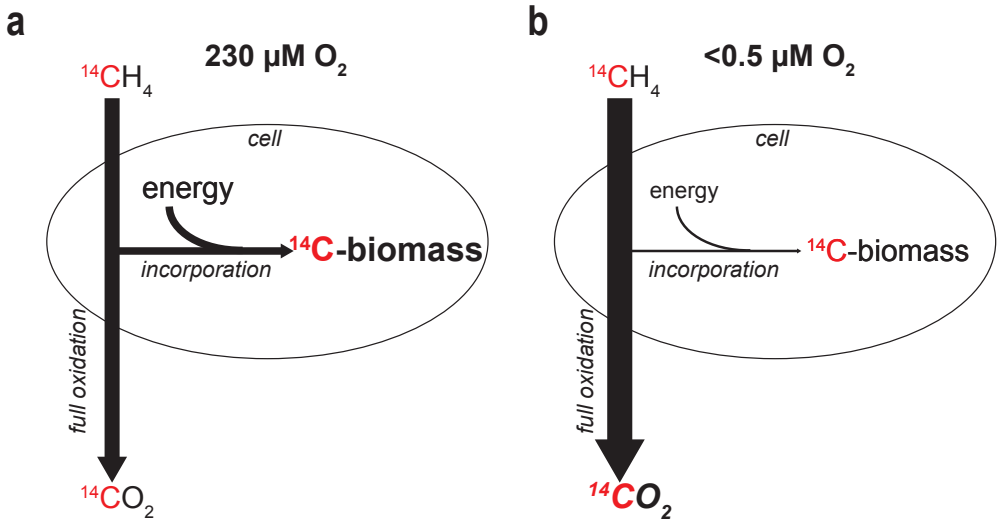

Figure 6.3. Schematic of relative importance of metabolic (i.e., full oxidation of methane), and anabolic (i.e., incorporation of methane-carbon into biomass) at saturated (a) and sub-micromolar (b) oxygen concentrations, as proposed in Chapter 4.

Methane

Several authors have proposed that methane concentrations in a specific environment can be used as a predictor to estimate the turnover time (Elliott et al., 2011; Nauw et al., 2015; Osudar et al., 2015), i.e., the time needed to completely oxidize the available methane (turnover time=$1/k$, where *k*=first order rate constant of MOx). Plotting of all the data acquired in this dissertation (Fig. 6.4) on a double-log plot shows that while this may hold true on a very general scale (mostly for methane concentrations below 100 nM), a clear offset can be observed for MOx turnover times measured in environments with very high methane concentrations (i.e., at Blowout and Kryos). As will be elaborated in section 6.6, the method used to determine MOx rates can additionally influence turnover constants (i.e., $^{3}H\text{-}CH_4$ or $^{14}C\text{-}CH_4$). Moreover, no correlation between methane concentration and *k* was observed for rate measurements in a specific environment, i.e., in Svalbard, at the Blowout or in Eckernförde Bay (see Chapters 2 – 4). On a very broad scale, the inverse linear relationship between methane concentration and turnover time might hold true, but cannot be used as sole predictor for MOx rates.

Temperature

Experimental work with Eckernförde Bay waters showed that the MOB community was generally composed of mesophilic bacteria with a temperature optimum between 20 - 40°C. These temperatures are above in situ temperatures, as is commonly observed in bacteria (Madigan et al., 2015). However, in one month a psychrophilic optimum of the MOx community was observed. The change of the MOB temperature optimum was likely caused by an inflow of North Sea water, which would have simultaneously replaced the normally present MOx community with a community adapted to different in situ temperature conditions. This change of the methanotrophic community was also observed in preliminary phylogenetic analyses (unpubl. data). Hence, MOx communities in the marine systems are diverse and may be adapted to different in situ temperatures.

Figure 6.4 (next page). Compilation of methane turnover time versus dissolved methane concentrations for a), the data acquired during the course of this dissertation, and b), for a variety of other studies. Panel b) was adapted from Nauw et al., 2015. Note the logarithmic scale, which cover different ranges in a) and b). Rates were determined with 3H-CH4 tracer in a), Svalbard and Eckernförde Bay and b), Valentine et al., 2001, with 14C-CH4-tracer in a), Kryos, Irish Sea, North Sea and b), Ward et al., 1987, 1989, Kadko et al., 1990, De Angelis et al., 1993, Jones and Amador, 1993, or inferred from tracer/tracer relations in Rehder et al., 1999 and Scranton and Brewer, 1978. Kadko et al., 1990, and De Angelis et al., 1993, measured MOx rates in hydrothermal systems.

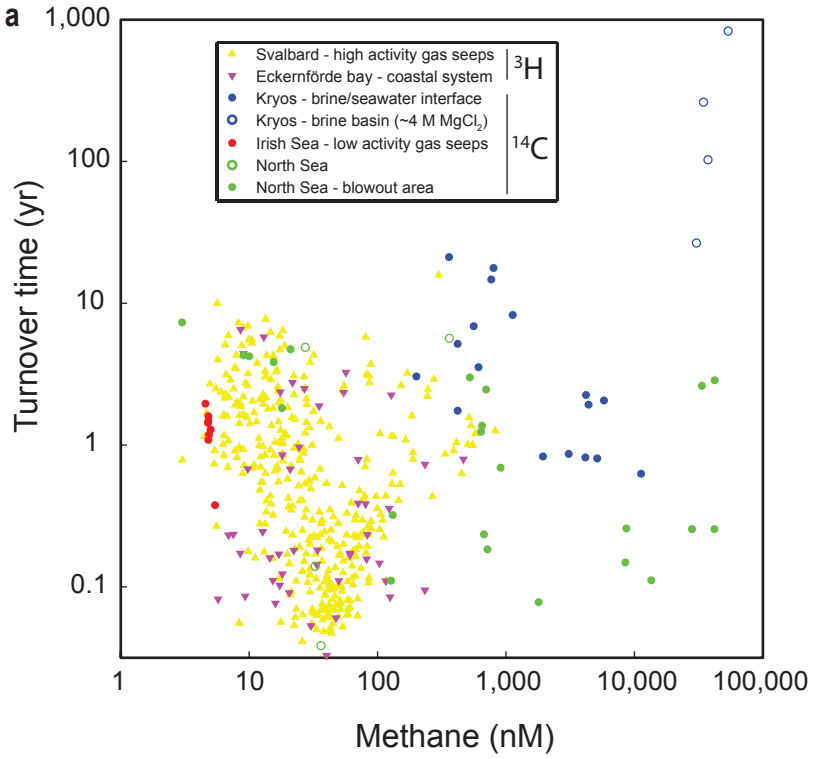
a
Svalbard - high activity gas seeps
Eckernförde bay - coastal system
Kryos - brine/seawater interface
Kryos - brine basin (~4 M MgCl2)
Irish Sea - low activity gas seeps
North Sea
North Sea - blowout area
3H
14C
Turnover time (yr)
1,000
100
10
1
0.1
1
10
100
1,000
10,000
100,000
Methane (nM)

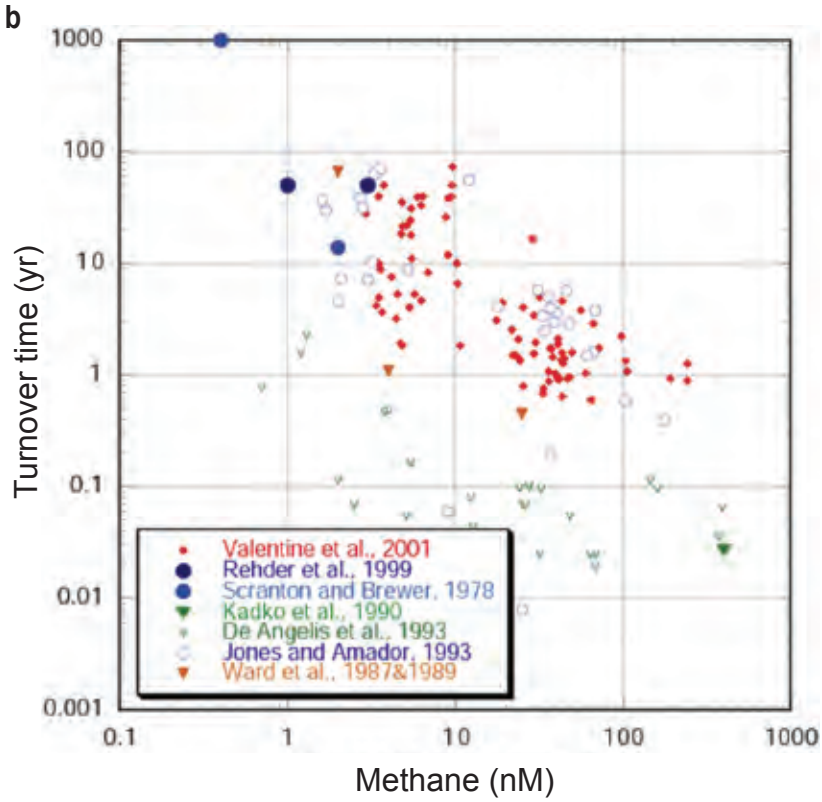
b
Valentine et al., 2001
Rehder et al., 1999
Scranton and Brewer, 1978
Kadko et al., 1990
De Angelis et al., 1993
Jones and Amador, 1993
Ward et al., 1987&1989
Turnover time (yr)
1000
100
10
1
0.1
0.01
0.001
0.1
1
10
100
1000
Methane (nM)

6.3 Filter efficiency

In Eckernförde Bay, 40 - 95% of methane released from sediments is consumed, depending on stratification regime and wind-speed parameterization of the gas transfer coefficient. In Svalbard, model results predicted (using the MOx rates presented in Chapter 2) that MOx removes ~60% of methane released into the hydrosphere (Graves et al., 2015). Estimates at the Blowout indicate that about 25% of methane is consumed by MOx before it can be emitted into the atmosphere. MOx is thus an important biological filter in all of these systems. These estimates, however, contain still large uncertainties due to the high spatial and temporal variability of methane emissions and consumption (MOx), as well as often poorly constrained sediment-hydrosphere and seawater-atmosphere methane fluxes and future efforts should aim at better constraining these parameters (see section 6.7).

6.4 Bacteria mediating marine MOx

Previous studies targeting pelagic MOB diversity found exclusively Type I MOB (e.g., Tavormina et al., 2008; Tavormina et al., 2010). Confirming these findings, Type I MOB were detected in the water column of the Svalbard-, the Blowout- and the Eckernförde Bay area using (CARD-)FISH (Tab. 6.1; data from Eckernförde Bay are unpubl.). Additionally, indications from biomarker analyses point toward the presence of Type I MOB within the Kryos brine interface. This group hence seems to be adapted to a wide range of habitats with salinities of ~20 - 55 g kg^{-1}, sub-micromolar and saturated oxygen concentrations, and methane concentrations from nM to mM. However, in this dissertation, the first occurrence of Type II MOB in the pelagic zone was reported, observed in the water column above the Blowout. The extremely high methane concentrations together with constant seeding of sedimentary MOB into the water column, or trace-metal replete concentrations are possible factors explaining the abundant occurrence of Type II MOB (Hanson & Hanson, 1996). Our additional, unpublished, FISH analysis results from Eckernförde Bay indicate the presence of Type II MOB in the water column, suggesting that this group of MOB may be more common in the marine environment than previously thought.

More specifically, phylogenetic analyses of DGGE bands showed that Type I MOB in Blowout sediments and the water column were most closely related to known MOB of the 'Marine Methanotrophic Group I' or 'deep-sea clade 1' (Ruff et al., 2013; Tavormina et al., 2008). Type II MOB sequences were most similar to obligate methanotrophic *Methylocapsa sp*. (Marín & Ruiz Arahal, 2014), and others to *Hyphomicrobium sp.,* a group of which members are known to be methylotrophic and not obligate methanotrophs (Urakami et al., 1995). Additionally, several sequences of both Type I and II MOB were related to sequences found in other methane-rich environments, but of which no close cultivated relatives are known (i.e., less than ~90% similarity to cultivated organisms; Tavormina et al., 2008;

Tavormina et al., 2010). Very similar sequences were also detected in Eckernförde Bay (phylogenetic analyses of DGGE bands, unpubl. data), which emphasizes the need to expand molecular knowledge on MOx communities in the marine environment.

The water column above the Svalbard seeps was also extensively screened for MOB with a lipid biomarker approach, but the bulk analysis of fatty acids did not lead to detection of MOB-derived fatty acids (unpubl. data). Nevertheless, distinctly different fatty acid signatures were observed related to the different water masses (see Chapter 2) present above the Svalbard seeps (unpubl. data). The reason for the inconclusiveness of this analysis with respect to MOB is likely the low cell numbers compared to the rest of the microbial community (ca. 100x lower). The lipid biomarker approach is thus better adapted to lake systems (e.g., Blees et al., 2014a, 2014b), sediments (e.g., Niemann et al., 2006), or the interface of anoxic (brine) basins such as Kryos (Chapter 5) or the Black Sea (Schubert et al., 2006), where the cell density of MOB and the corresponding biomass is higher. Alternatively, very large amounts of water should be filtered (> 100 L).

6.5 Additional aspects of MOx

6.5.1 Light

Incubations under light and dark conditions with surface (5 mbsl) and bottom water (25 mbsl) from Boknis Eck in Eckernförde Bay indicate that MOx rates are enhanced in surface waters but inhibited in bottom waters in light conditions (Fig. 6.5). Incubations with addition of the standard photosynthetic inhibitor (DCMU; 3-(3,4-dichlorophenyl)-1,1-dimethylurea; e.g., Milucka et al., 2015) dissolved in seawater did show similar results as incubations without DCMU. Hence, the differences observed in incubations under light and dark conditions are not caused by the oxygen production of phytoplankton, which was previously reported in lakes (Milucka et al., 2015; Oswald et al., 2015). The surface MOB community seems to be adapted to light since MOx rates were higher under light compared to dark conditions, whereas the bottom water community was hampered by light. The latter community is not exposed to high light intensities in situ since the Secchi depth always lies between 5-7 m at Boknis Eck (Bange et al., 2010), and light might have initiated photo-destruction of cells or production of oxygen radicals, which may have led to the observed drop in rates (Madigan et al., 2015)

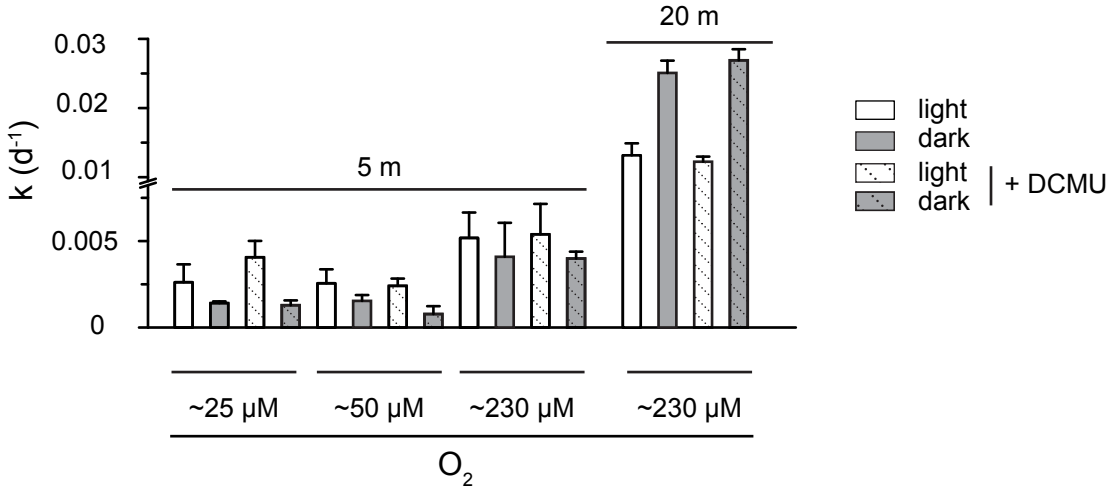

Figure 6.5: First order rate constant of MOx for light (white bars) and dark (grey bars) incubations of surface- (5 mbsl) and bottom (20 mbsl) waters sampled at Boknis Eck in February 2014, with (shaded bars) or without (plain bars) DCMU addition. Surface samples were incubated at three different oxygen concentrations. Error bars represent standard deviation of quadruplicates. Oxygen adjustments were performed as described in Chapter 4.

6.5.2 Physiology of MOB aggregates

CARD-FISH analyses of MOB from the water column above both the Svalbard seeps and the North Sea Blowout revealed loose aggregates of MOB cells (Fig. 6.6), which were connected by a matrix most likely consisting of extrapolymeric substances (EPS; a mixture of exuded polysaccharides, proteins and/or lipids by microbial cells; see Tourney and Ngwenya, 2014, for a review). In contrast, no such aggregates were observed in Eckernförde Bay water (unpubl. data). “Slimy” layers around aggregates of MOB were observed in several studies (Wilshusen et al., 2004; Wise et al., 2001). The reasons why EPS production can be favorable for bacteria are diverse (Tourney and Ngwenya, 2014). For instance, the presence of EPS can lead to bio-sorption of metals. In the marine water column more specifically, it is suggested that EPS exerts a major control on the biogeochemical cycling of trace metals. Studies with phytoplankton suggested that EPS can enhance bioavailability of trace metals, e.g. Fe(III), by keeping them in their soluble complexed form (Tourney and Ngweny, 2014). In marine system, MOB were found to be limited by the concentrations of copper and iron (Crespo-Medina et al., 2014); and the expression of genes that encode the soluble or particulate form of MMO is also controlled by the levels of trace metals (Semrau et al., 2010). It would thus be interesting to investigate the composition of these extracellular matrices and the distribution of trace metals, for instance by mapping them using metal-selective fluorescent probes and confocal laser scanning microscopy (Hao et al., 2013). Alternatively, these aggregates could also serve the purpose of creating a low oxygen environment (Wilshusen et al., 2004). Oxygen was replete in the water column above both the Svalbard margin and the

Blowout. In Eckernförde Bay, however, bottom waters turned regularly hypoxic. The presence of EPS in Svalbard and Blowout samples where oxygen was abundant, but not in Eckernförde Bay where bottom waters are often hypoxic, is therefore consistent with the hypothesis that EPS creates a low oxygen environment favorable for MOB. Indeed, a study on the relationship of oxygen concentrations and EPS production by Type I and II MOB showed that EPS production increased by 250% under high oxygen conditions (Wilshusen et al., 2004).

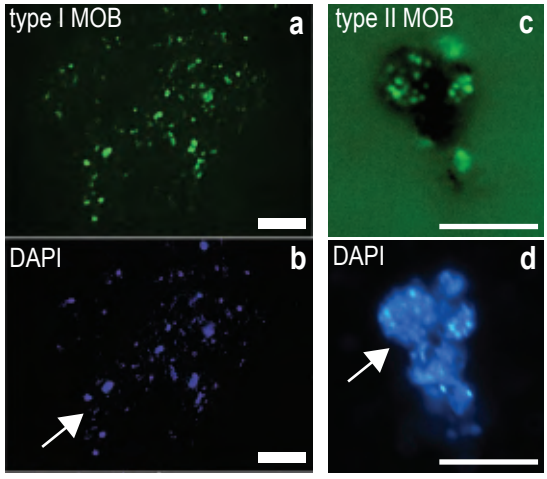

Figure 6.6: Epifluorescence micrographs from water samples from Svalbard (a, b) and the Blowout (c, d). Images a) and c) are stained with Alexa488 for CARD-FISH using a), probe Mγ705 and Mγ84 targeting Type I MOB or b), probe Mα450 targeting Type II MOB, and images b) and d), are stained with DAPI for total cell counts. Scale bars represent 10 μm. Arrows indicate potential extrapolymeric substances (EPS).

6.5.3 Interplay between methane and nitrogen transformations

An aspect not studied in this dissertation is the interplay between methane and nitrogen transformations. Nitrogen fixation, for instance, has been documented in a large variety of methanotrophs (Hanson and Hanson, 1996). Recent studies have shown that methanotrophs can also use nitrate as electron acceptor in the absence of oxygen, and produce N_2O (Kits et al., 2015). Some nitrifying bacteria, on the other hand, have the ability to oxidize methane but generally much less effectively than methanotrophs (Sansone and Martens, 1978). In order to further explore these interactions, an experimental study (e.g., with Eckernförde Bay waters) could be initiated to probe the interplay between nitrogen and methane transformations, including the ability of nitrate to act as an alternative electron acceptor.

6.6 Methodology of rate measurements

6.6.1 Choice of radiotracer: ^{3}H-CH_4 versus ^{14}C-CH_4

In this dissertation, methane oxidation rates were determined by adding radioactively-labeled methane (^{14}C-CH_4 or ^{3}H-CH_4) and subsequent tracking of the radio-activity in product pools. Radiotracer-based rate measurements are advantageous for determining rates directly ex situ and for the detection of very low rates (Reeburgh, 2007). There are, however, important differences between the two radiotracers.

In case of in situ methane concentrations in the nM-range, ^{3}H-CH_4 tracer is preferable to ^{14}C-CH_4 because of its high specific activity. As a result, only a few nmol of additional methane are added to the samples compared to 100 - 1,000 nmol if ^{14}C-tracer is used. Simultaneous incubations of Svalbard water samples with both tracers provide an example of tracer-dependent results: first order rate constants were ~85% lower if ^{14}C-tracer was used (Fig. 6.7a). Final rates could be corrected to within 10% of each other when the additional methane concentration due to the tracer addition in ^{14}C-incubations was taken into account (generally multiplying in situ concentrations by a factor of 10; Fig. 6.7b). In this case, the MOB community was not adapted to such high methane concentrations and could not increase its activity in the short time-period of the incubation (i.e., *k*; see also Mau et al., 2013). The comparison of *k* and thus also of turnover times (1/*k*) between different studies employing different tracers should thus be done with care. An additional advantage of the use of ^{3}H-CH_4 is that a higher number of incubations and the subsequent rate measurements can be performed in the same time as for ^{14}C-CH_4. Moreover, results of the incubations can directly be obtained onboard if a scintillation counting device is available.

In contrast, ^{3}H-CH_4 tracer is not suitable to anoxic environments, i.e., where sulfide is present, since other members of my working group at the Aquatic and Isotope Biogeochemistry Group (University of Basel) observed a strong isotope exchange between ^{3}H from the radiotracer and sulfide, making it hard to obtain reliable MOx rate measurements. This means that rate measurements with ^{14}C-tracer should be envisioned in anoxic environments. ^{14}C-CH_4 has the additional advantage that alongside the determination of the MOx rates, the incorporation of methane-carbon into biomass can be tracked (White, 2000), and the percentage of incorporated methane relative to methane turned over to CO_2 (Fig. 6.3) can then be used as an indicator for the metabolic state of a MOx community (see section 6.2.2). In contrast, this is not possible when using ^{3}H-CH_4 since the incorporation of methane-hydrogen into biomass is much more complex and less direct (Sessions et al., 2002). However, in incubations with water from Eckernförde Bay we detected clear differences in the percentage of ^{3}H-incorporation for different incubation parameters (i.e., temperature, oxygen concentrations, dark/light; unpubl. data). Not much is known about the pathways

leading to, and the parameters controlling, the incorporation of methane-hydrogen into biomass: Sessions et al., (2002), for instance, proposed that the percentage of methane-derived hydrogen incorporated into biomass was determined by the exchange of intracellular water with extracellular oxygen relative to the MOx rate. The preliminary results obtained during this dissertation would hence be a good basis to initiate more thorough studies about the pathway of water in MOB under different conditions.

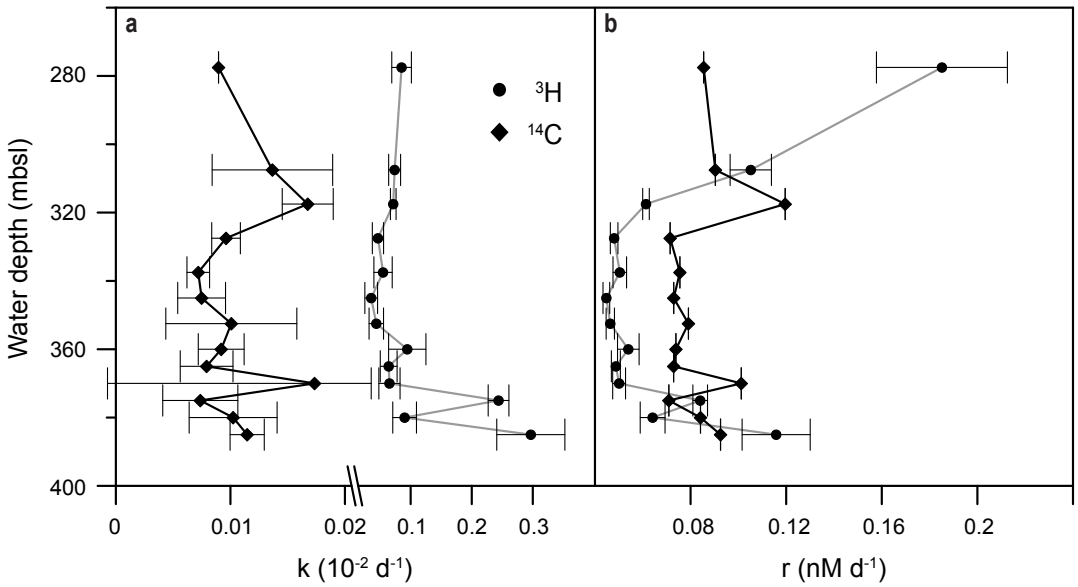

Figure 6.7: Results of parallel incubations of Svalbard water samples using either ^{3}H- or ^{14}C-CH_4-tracer for determining MOx rates. a) First order rate constant (*k*), and b) MOx rate (*r*) calculated considering methane addition if using ^{14}C-CH_4. Error bars represent standard deviation of quadruplicates.

6.6.2 Use of specific stoppers

A side-project of this thesis included the study of the effects on MOx if different rubber stoppers were used to close the water-column incubation vials (published in Niemann et al, 2015). A high variety of stoppers were tested and we found that only halogenated stoppers did not hamper MOx, whereas most non-halogenated stoppers exuded various compounds that strongly impeded MOx activity. The effect of rubber stoppers must thus be carefully tested before using them for MOx incubations. Additional tests with liquid media containing variable densities of pure MOB cultures (*Methylosinus trichosporium* and *Methylococcus capsulatus*) showed that the stoppers only inhibited activity at lower cell densities (Fig. 6.8). The effect of using non-halogenated stoppers on pure cultures or sedimentary incubations is hence most likely minor due to the lower mixing of pore-water, and thus of extracted (toxic) chemicals, as well as the higher cell density.

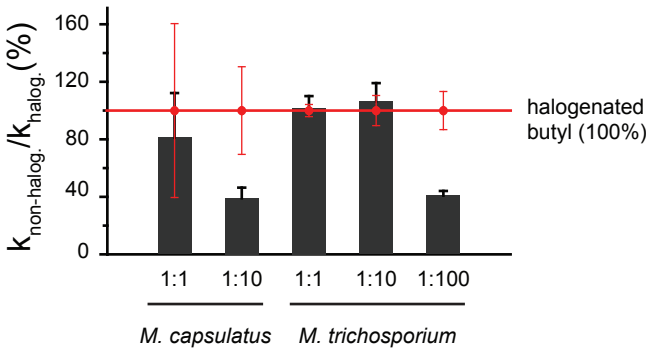

Figure 6.8: First order rate constant of incubations sealed with black bromobutyl stoppers (black bars) normalized to incubations sealed with halogenated grey butyl rubber stoppers (Helvoet Pharma, Belgium) indicated with red dots. 1:10 and 1:100 indicate a dilution of the original cell culture (~10^9 cell ml^{-1}) by a factor of 10 or 100, respectively. Error bars represent standard deviation of triplicates.

6.7 Future research suggestions

Several research questions emerged during this thesis, which have already been introduced in the final discussion, and which are listed below:

1. How widespread is bubble-mediated transport of MOB (and other bacteria)?
2. What are the MOx rates immediately at the sediment-water interface?
3. Is there a fermentative mode of MOB present in marine waters?
4. Are there unknown phylogenetic groups mediating MOx?
5. What is the role of the matrix (presumably EPS) holding together MOB aggregates?
6. What are the effects of light on surface- and bottom water MOB communities?
7. What are the connections between methane and nitrogen transformations?
8. What are the pathways and controls on the percentage of incorporated methane-hydrogen into biomass?

Next to these specific questions, I would like to suggest three main points that should be considered for the investigation of MOx in a system-wide approach, especially for studies aiming to determine the fate of methane and the biological filter efficiency.

1) Studying the fate of the MOB community downstream of methane point sources - In strong contrast to lake systems, the water column in marine systems is rarely stable over long time periods (e.g., weeks to months). Tidal- and other ocean currents advect water quickly away from methane point sources. Water containing methane but also MOB will thus be transported away from the immediate seep area. As a result of mixing with seawater, which has not come in contact with methane seep areas, methane and the MOx community will be diluted. Several model studies indicate that MOx is likely to play an important part in the removal of this advectively transported methane from the water column (Mau et al., 2012; Wåhlström and Meier, 2014), including a model study of the Svalbard seep area, which incorporated MOx rates obtained in this thesis (Graves et al., 2015). However, thus far, measurements of MOx rates and MOB communities have focused exclusively on the methane seepage sites themselves; no study has investigated how the MOx rates and the MOB community change following advection.

2) Combined studies of biogeochemistry and oceanography - As a direct result of the above mentioned hydrodynamics of the water column in most marine systems, projects aiming at studying microbial biogeochemical processes in the ocean should more frequently include collaboration with physical oceanographers. Thus, currents can be recorded while sampling and/or the system can be modeled before sampling takes place to design efficient and focused sampling strategies, and also to enable a broader, multidisciplinary understanding of observations after sampling. Small-scale ocean models, for instance, carry the possibility to insert tracer particles at a certain location and track their paths both forward and backwards in time (A. Biastoch, pers. comm.). Since planktonic bacteria behave more or less like particles, this approach would be suitable to answer questions such as those introduced in point 1).

3) Importance of spatial and temporal resolution of observations – The results of MOx rate measurements presented in Chapter 2-4 highlight their high spatial heterogeneity, and Chapters 2 and 4 additionally emphasize the temporal variability of this microbial process. In addition, methane seepage into the water column is also often highly variable in time. Most importantly, seasonal and short-time (hours to weeks) changes in the structure of the water column stability are large (i.e., strength of West Spitsbergen Current meandering over the Svalbard seeps or stratification regimes at the North Sea Blowout and in Eckernförde Bay). In order to get a more complete and representative picture of such systems, it would be better to combine different approaches, i.e., to extend the spatial and temporal coverage but also to aim at identifying key environmental controls on MOx and use this information to estimate the MOx potential in a specific environment via small-scale ocean models.

References

Abdallah, R.Z., Adel, M., Ouf, A., Sayed, A., Ghazy, M. A., Alam, I., et al. (2014). Aerobic methanotrophic communities at the Red Sea brine-seawater interface. *Front Microbiol* **5:** doi: 10.3389/fmicb.2014.00487

Abril, G., Commarieu, M.-V., & Guérin, F. (2007). Enhanced methane oxidation in an estuarine turbidity maximum. *Limnology and oceanography* **52**: 470-475.

Bange, H.W., K. Bergmann, K., Hansen, H.P., Kock, A., Koppe, R., Malien, F., and Ostrau, C. 2010). Dissolved methane during hypoxic events at the Boknis Eck time series station (Eckernförde Bay, SW Baltic Sea). *Biogeosciences* **7**: 1279-1284.

Berndt, C., Feseker, T., Treude, T., Krastel, S., Liebetrau, V., Niemann, H., et al. (2014). Temporal Constraints on Hydrate-Controlled Methane Seepage off Svalbard. *Science* **343**: 284-287.

Blees, J., Niemann, H., Wenk, C.B., Zopfi, J., Schubert, C.J., Jenzer, J.S., et al. (2014a). Bacterial methanotrophs drive the formation of a seasonal anoxic benthic nepheloid layer in an alpine lake. *Limnology and Oceanography* **59**: 1410-1420.

Blees, J., Niemann, H., Wenk, C.B., Zopfi, J., Schubert, C.J., Kirf, M.K, et al. (2014b). Micro-aerobic bacterial methane oxidation in the chemocline and anoxic water column of deep south-Alpine Lake Lugano (Switzerland). *Limnology and oceanography* **59**: 311-324.

Crespo-Medina, M., Meile, C.D., Hunter, K.S., Diercks, A., Asper, V.L., Orphan, V.J., et al. (2014). The rise and fall of methanotrophy following a deepwater oil-well blowout. *Nature Geoscience* **7**: 423-427.

Devlin, S.P., Saarenheimo, J., Syväranta, J., and Jones, R.I. (2015). Top consumer abundance influences lake methane efflux. *Nat Commun* **6**: 8787.

Elliott, S., Maltrud, M., Reagan, M., Moridis, G., and Cameron-Smith, P. (2011). Marine methane cycle simulations for the period of early global warming. *Journal of Geophysical Research: Biogeosciences* **116**: G01010, doi:10.1029/2010JG001300.

Gentz, T., Damm, E., Schneider von Deimling, J., Mau, S., McGinnis, D. F., and Schlüter, M. (2014). A water column study of methane around gas flares located at the West Spitsbergen continental margin. *Continental Shelf Research* **72**: 107-118.

Graves, C. A., Steinle, L., Rehder, G., Niemann, H., Connelly, D. P., Lowry, D., et al. (2015). Fluxes and fate of dissolved methane released at the seafloor at the landward limit of the gas hydrate stability zone offshore western Svalbard. *Journal of Geophysical Research: Oceans* **120**: 6185-6201.

Hanson, R.S. and Hanson, T.S. (1996). Methanotrophic bacteria. *Microbiological reviews* **60**: 439-471.

Hao, L., Li, J., Kappler, A., and Obst, M. (2013). Mapping of heavy metal ion sorption to cell-extracellular polymeric substance-mineral aggregates by using metal-selective fluorescent probes and confocal laser scanning microscopy. *Appl Environ Microbiol* **79**: 6524-6534.

Heintz, M.B., Mau, S. and Valentine, D.L. (2012). Physical control on methanotrophic potential in waters of the Santa Monica Basin, Southern California. *Limnology and oceanography* **57**: 420-432.

Jakobs, G., Rehder, G., Jost, G., Kießlich, K., Labrenz, M., and Schmale, O. (2013). Comparative studies of pelagic microbial methane oxidation within the redox zones of the Gotland Deep and Landsort Deep (central Baltic Sea). *Biogeosciences* **10**: 7863-7875.

Kalyuzhnaya, M.G., Yang, S., Rozova, O.N., Smalley, N.E., Clubb, J., Lamb, A., et al. (2013). Highly efficient methane biocatalysis revealed in a methanotrophic bacterium. *Nat Commun* **4**: 2785.

Kessler, J.D., Valentine, D.L., Redmond, M.C., Du, M., Chan, E.W., Mendes, S.D., et al. (2011). A persistent Oxygen Anomaly Reveals the Fate of Spilled Methane in the Deep Gulf of Mexico. *Science* **331**: 312-315.

Kits, K.D., Klotz, M.G. and Stein, L.Y. (2015). Methane oxidation coupled to nitrate reduction under hypoxia by the Gammaproteobacterium Methylomonas denitrificans, sp. nov. type strain FJG1. *Environ Microbiol* **17**: 3219-3232.

Madigan, Q.D., Martinko, J., Bender, K., Buckley, D., and Stahl, D. (2015). Brock Biology of Microorganisms. Boston.

Marín, I. and Ruiz Arahal, D. (2014). The Family Beijerinckiaceae, p. 263-282. *In* E. Rosenberg, E.F. DeLong, S. Lory, E. Stackebrandt, and F. Thompson (eds), 4. Springer Berlin Heidelberg.

Mau, S., Blees, J., Helmke, E., Niemann, H., and Damm, E. (2013). Vertical distribution of methane oxidation and methanotrophic response to elevated methane concentrations in stratified waters of the Arctic fjord Storfjorden (Svalbard, Norway). *Biogeosciences* **10**: 6267-6278.

Mau, S., Heintz, M.B. and Valentine, D.L. (2012). Quantification of CH backslashn 4 loss and transport in dissolved plumes of the Santa Barbara Channel, California. *Continental Shelf Research* **32**: 110-120.

Milucka, J., Kirf, M., Lu, L., Krupke, A., Lam, P., Littmann, S., et al. (2015). Methane oxidation coupled to oxygenic photosynthesis in anoxic waters. *ISME J* **9**: 1991-2002.

Murrell, J.C (2010). The Aerobic Methane Oxidizing Bacteria (Methanotrophs), p. 1953-1966. *In* K.N. Timmis (eds), Handbook of Hydrocarbon and Lipid Microbiology. Springer Berlin Heidelberg.

Nauw, J., Haas, H.D. and Rehder, G. (2015). A review of oceanographic and meteorological controls on the North Sea circulation and hydrodynamics with a view to the fate of North Sea methane from well site 22 / 4b and other seabed sources. *Marine and Petroleum Geology*. **68**: 861-882.

Niemann, H., Lösekann, T., de Beer, D., Elvert, M., Nadalig, T., Knittel, K., et al. (2006). Novel microbial communities of the Haakon Mosby mud volcano and their role as a methane sink. *Nature* **443**: 854-858.

Niemann, H., Steinle, L.I., Blees, J., Krause, S., Bussmann, I., Treude, T., et al. (2015) Toxic effects of butyl elastomers on aerobic methane oxidation. *Limnology and Oceanography: Methods* **13**: 40-52.

Osudar, R., Matoušů, A., Alawi, M., Wagner, D., and Bussmann, I. (2015). Environmental factors affecting methane distribution and bacterial methane oxidation in the German Bight (North Sea). Estuarine, *Coastal and Shelf Science* **160**: 10-21.

Oswald, K., Milucka, J., Brand, A., Littmann, S., Wehrli, B., Kuypers, M.M., and Schubert, C.J (2015). Light-Dependent Aerobic Methane Oxidation Reduces Methane Emissions from Seasonally Stratified Lakes. *PLoS One* **10**: e0132574.

Reeburgh, W.S. (2007). Oceanic methane biogeochemistry. *CHEMICAL REVIEWS* **107**: 486-513.

Reeburgh, W.S., Ward, B.B., Whalen, S.C., Sandbeck, K.A., Kilpatrickt, K.A., and Kerkhof, L.J. (1991). Black Sea methane geochemistry. Deep Sea Research Part A. *Oceanographic Research Papers* **38**: S1189-S1210.

Ruff, S.E., Arnds, J., Knittel, K., Amann, R., Wegener, G., Ramette, A., and Boetius, A. (2013). Microbial communities of deep-sea methane seeps at Hikurangi continental margin (New Zealand). *PLoS One* **8**: e72627.

Sansone, F.J. and Martens, C.S (1978). Methane oxidation in Cape Lookout Bight, North Carolina. *Limnology and Oceanography* **23**: 349-355.

Schmale, O., Leifer, I., Schneider VanDeimling, J., Stolle, C., Krause, S., Kießlich, K., et al. (2015). Bubble Transport Mechanism: Indications for a gas bubble-mediated inoculation of benthic methanotrophs into the water column. *Continental Shelf Research* **103**: 70-78.

Schubert, C. J., M.J. Coolen, L.N. Neretin, A. Schippers, B. Abbas, E. Durisch-Kaiser, B. Wehrli, E.C. Hopmans, J.S.S. Damsté and S. Wakeham (2006). Aerobic and anaerobic methanotrophs in the Black Sea water column. *Environ Microbiol* **8**: 1844-1856.

Semrau, J.D., DiSpirito, A.A. and Yoon, S. (2010). Methanotrophs and copper. *FEMS Microbiology Reviews* **34**: 496-531.

Sessions, A.L., Jahnke, L.L., Schimmelmann, A., and Hayes, J.M. (2002). Hydrogen isotope fractionation in lipids of the methane-oxidizing bacterium Methylococcus capsulatus. *Geochimica et Cosmochimica Acta* **66**: 3955-3969.

Tavormina, P.L., Ussler, W., and Orphan, V.J. (2008). Planktonic and Sediment-Associated Aerobic Methanotrophs in Two Seep Systems along the North American Margin. *Appl Environ Microbiol* **74**: 3985-3995.

Tavormina, P.L., Ussler, W., Joye, S.B., Harrison, B.K., and Orphan, V.J. (2010). Distributions of putative aerobic methanotrophs in diverse pelagic marine environments. *ISME J* **4**: 700-710.

Tourney, J. and Ngwenya, B.T. (2014). The role of bacterial extracellular polymeric substances in geomicrobiology. *Chemical Geology* **386**: 115-132.

Turley, C. (2000). Bacteria in the cold deep-sea benthic boundary layer and sediment-water interface of the NE Atlantic. *FEMS Microbiol Ecol* **33**: 89-99.

Urakami, T., Sasaki, J., Suzuki, K.-I., and Komagata, K (1995). Characterization and Description of Hyphomicrobium denitrificans sp. nov. *International journal of systematic bacteriology* **45**: 528-532.

Valentine, D.L. 2007. Adaptations to energy stress dictate the ecology and evolution of the Archaea. *Nature Reviews Microbiology* **5**: 316-323.

Van Landeghem, K.J., Niemann, H., Steinle, L.I., OReilly, S.S., Huws, D.G., and Croker, P.F (2015). Geological settings and seafloor morphodynamic evolution linked to methane seepage. *Geo-Marine Letters* **15**: DOI 10.1007/s00367-015-0407-5.

Ward, B.B., Kilpatrick, K.A., Wopat, A.E., Minnich, E.C., and Lidstrom, M.E. (1989). Methane oxidation in Saanich Inlet during summer stratification. *Continental Shelf Research* **9**: 65-75.

Wåhlström, I. and Meier, H.E.M. (2014). A model sensitivity study for the sea-air exchange of methane in the Laptev Sea, Arctic Ocean. *Tellus B* **66**: 24174, http://dx.doi.org/10.3402/tellusb.v66.24174.

White, D. (2000). Prokaryotes Vol. 3. Oxford University Press.

Wilshusen, J.H., Hettiaratchi, J.P.A., De Visscher, A., and Saint-Fort, R. (2004). Methane oxidation and formation of EPS in compost: effect of oxygen concentration. *Environmental Pollution* **129**: 305-314.

Wise, M. G., McArthur, J.V. and Shimkets, L.J. (2001). Methylosarcina quisquiliarum sp. nov., novel type I methanotrophs. *Int J Syst Evol Microbiol* **51**: 611-62

Acknowledgements

Acknowledgments

This dissertation could not have come together without the support and help of many people that I have worked with over the last years.

First, I would like to thank my main supervisor, Helge Niemann, for his patience in teaching me and trying to understand my thoughts, very often successfully. Thank you, Helge for letting me do what I wanted and to provide guidance if needed. Thank you both, Helge and Moritz Lehmann, for pushing me to be exact in my writing and ordered in my thoughts. Thank you, Moritz, for providing a stimulating and uncomplicated work environment in the Aquatic and Isotope Biogeochemistry group in Basel. A big thank you also to my second supervisor, Tina Treude, who taught me foremost how to collaborate with other scientists, and also hosted me countless times in her Marine Geobiology group at the GEOMAR in Kiel. I always felt supported and so warmly welcomed by you, Tina, and everybody else in the group. I would also like Gregor Rehder for being part of my panel chair.

Many collaborators enabled big parts of the work presented in this thesis: Carolyn Graves and Johanna Schweers, for the sampling and discussion about data and also for your friendship and the support during the last week of writing my thesis; Arne Biastoch for an interesting, uncomplicated, and productive exchange resulting in Chapter 2 of this thesis; Célia Sapart for her efforts with isotope analysis and many wonderful meals shared at conferences; Peter Linke, Mark Schmidt, Matthias Haeckel, Lee Bryant, Jens Greinert, Lisa Vielstädte and Stefan Sommer for a lively exchange about data and for helping me with sampling at sea; Hermann Bange and Annette Kock for methane analysis and input to the manuscript about Boknis Eck; and Gert de Lange, Alina Stadnitskaia and Chiara Tessarolo for their efforts in our joint Kryos basin project. I also want to thank the principal scientists of the research cruises that I took place in: thank you Katrien vanLandeghem, Christian Berndt and Peter Linke for providing an organized framework, in which scientific work seemed easy.

An enormous thank you to the research groups in Basel and Kiel, especially to Jakob Zopfi for his help with molecular analyses, and Stefan Krause for discussion about science and for hosting me so many times (thank you Elina und Lili!). It was wonderful being supported by Gabi Schüssler, Peggy Wefers, Karin Liesenfeld, Marion Liebetrau, Thomas Kuhn, Axel Birkholz, Judith Kobler Waldis, Katharina Blaurock, and Kerstin Kretschmer, in the lab, onboard and with administrative problems. Without all of my fellow Phd students, Philip, Jan, Yuki, Sonakshi, Jessi, Skadi, Christine, Adéline, Jana, Guangy, Stefan, Jan Paul, Emiliano, Laura, Simon, Matthias, my working days would have been much more boring. I would also like to thank all the people working and dancing with me on the research cruises, especially Felix, Gero, Kerstin, and Tom for their friendship. To the students I helped

supervise, Irina, Nicole, Nadine, Chrstina and Dominik: thank you for the work together. I actually also learned a lot.

Numerous other people made life good during these last years, cooking meals for me during the last weeks of writing, singing, spending lot's of time in the "time zone", etc. Thank you for being my friends. Eric, thank you for all your support and for reading through parts of my thesis. A very warm thank you goes to my parents and brothers who provided me with the necessary strength for this project and life in general. Thank you, Johannes, for the support during these last months.

Other publications during my dissertation:

2014

Berndt, Christian, Tom Feseker, Tina Treude, Sebastian Krastel, Volker Liebetrau, Helge Niemann, Victoria J. Bertics, Ines Dumke, Karolyn Dünnbier, Bénédicte Ferré, Carolyn Graves, Felix Gross, Karen Hissmann, Veit Hühnerbach, Stefan Krause, Kathrin Lieser, Jürgen Schauer, and Lea Steinle. (2014). Temporal Constraints on Hydrate-Controlled Methane Seepage off Svalbard. *Science* **343**: 284-287.

2015

Graves, Carolyn A., Lea Steinle, Gregor Rehder, Helge Niemann, Douglas P. Connelly, David Lowry, Rebecca E. Fisher, Andrew W. Stott, Heiko Sahling, Rachael H. James. 2015. Fluxes and fate of dissolved methane released at the seafloor at the landward limit of the gas hydrate stability zone offshore western Svalbard. *J Geophys. Res.-Oceans* 120: 6185-6201.

Katrien J. J. Van Landeghem, Helge Niemann, Lea I. Steinle, Shane S. O'Reilly, Dei G. Huws, Peter F. Croker. (2015). Geological settings and seafloor morphodynamic evolution linked to methane seepage. *Geo. Mar. Lett.* **35(4):** 289-304.

Niemann, Helge, Lea I. Steinle, Jan H. Blees, Ingeborg Bussmann, Tina Treude, Stefan Krause, Marcus Elvert, and Moritz F. Lehmann. 2015. Toxic effects of lab grade butyl rubber stoppers on aerobic methane oxidation. *Limnol. Oceanogr.: Methods* **13**, 2015, 40–52

Soon to be submitted:

Maltby, Johanna, Lea Steinle, Hermann W. Bange, Carolin R. Löscher, Martin A. Fischer, Mark Schmidt, and Tina Treude. Microbial methanogenesis in the sulfate-reducing zone in sediments from Eckernförde Bay, SW Baltic Sea. (to be submitted to GCA)

Vielstaedte, Lisa, Matthias Haeckel, Jens Karstens, Peter Linke, Mark Schmidt, Lea Steinle, and Klaus Wallmann. Drilling-induced methane leakage into the North Sea. (to be submitted to PNAS)